



HAL
open science

Role of the actomyosin cytoskeleton on the synaptic effects of the type-1 cannabinoid receptor (CB1R)

Maureen Mcfadden

► **To cite this version:**

Maureen Mcfadden. Role of the actomyosin cytoskeleton on the synaptic effects of the type-1 cannabinoid receptor (CB1R). *Neurons and Cognition [q-bio.NC]*. Université Paris sciences et lettres, 2018. English. NNT : 2018PSLET006 . tel-02518809

HAL Id: tel-02518809

<https://pastel.hal.science/tel-02518809>

Submitted on 25 Mar 2020

HAL is a multi-disciplinary open access archive for the deposit and dissemination of scientific research documents, whether they are published or not. The documents may come from teaching and research institutions in France or abroad, or from public or private research centers.

L'archive ouverte pluridisciplinaire **HAL**, est destinée au dépôt et à la diffusion de documents scientifiques de niveau recherche, publiés ou non, émanant des établissements d'enseignement et de recherche français ou étrangers, des laboratoires publics ou privés.

THÈSE DE DOCTORAT

de l'Université de recherche Paris Sciences et Lettres
PSL Research University

Préparée à l'Ecole Supérieure de Physique et de
Chimie Industrielles de la ville de Paris (ESPCI PARIS)

Role of the actomyosin cytoskeleton in the synaptic effects of the type- 1 cannabinoid receptor (CB1R)

Ecole doctorale n°158

Cerveau, Cognition, Comportement (ED3C)

Spécialité Neurosciences

**Soutenue par Maureen
McFADDEN**

le 20 avril 2018

Dirigée par **Zsolt LENKEI**

COMPOSITION DU JURY :

Dr. DIGREGORIO David
UPMC, Président du jury

Dr. ANDRIEUX Annie
CHU de Grenoble, Rapporteur

Pr. KATONA István
Hungarian Academy of Sciences (MTA),
Rapporteur

Dr. LEBRETON Stéphanie
Paris XI, Membre du jury

Dr. IZEDDIN Ignacio
ESPCI-PSL, Membre du jury

Dr. LENKEI Zsolt
Paris V, Membre du jury

Acknowledgments

*First and foremost, I would like to thank my jury members **Annie Andrieux**, **István Katona**, **David DiGregorio**, **Ignacio Izeddin**, and **Stephanie Lebreton** for accepting to take part in my thesis defense and for their time and expertise in examining my work. I hope my thesis will be as enjoyable to read as it was to produce.*

*To my supervisor **Zsolt Lenkei**, I would like to thank you for accepting me within your team. Your open-mindedness and breadth of expertise has been an inspiration, and allowed me to develop both technically and personally. You have challenged me never to rest on my past knowledge and abilities but to develop new skills and expand my understanding, all the while remaining supportive and optimistic when things weren't seeming too bright. For this and much more, I am very grateful to you.*

*To my team colleagues, I would like to thank you for your support and advice. Seeing you at the lab has always been a highlight of my day and has made my 4 years within the team a memorable experience I shall treasure. **Diana Zala**, you have been my mentor/ surrogate mother. Although you have been quite severe and harsh in your judgment at times, it has always been truthful and sometimes necessary to counteract my stubbornness, for which I apologize. Your integrity both in science and in life has truly been a great influence and an inspiration to me. To **Jeremy Ferrier**, my surrogate big brother, thank you for being my balcony/gym buddy. You were always happy to offer constructive criticism, even unrequested, which, when serious, has always been helpful. You have never hesitated to help me when you saw me struggling. Thank you for your patience and advice. To **Sergio Leite**, my evening buddy, you're the only team member that had a time schedule similar to mine. You too have never hesitated to help in times of moral and/or technical need. Thank you for making the long nights and weekends at the lab so much brighter.*

*Thank you to all team members past and new: **Ana Ricobaraza**, for training me during my Masters internship and easing my entry into the team; **Delphine Ladarre**, for her advice in videomicroscopy; **Sophie Pezet**, for her experienced advice and support in all matters, **Julie Nguyen**, for taking the cell culture off my shoulders, and her positive and sunny disposition; **Michael Salerno**, for being my go to reference for all English language and American culture questions without complaint; **Renata Santos**, for helping me figure out my life plan. Thank you to the students for their positive attitude and great work. Particularly I would like to thank **Lea Anselin** for helping me out with my project and for our insightful conversations on culture and ethics; and **Navid Barakzoy** for taking on the continuation of my project and for his constant smile.*

*Thank you to all the members of my old lab unit 'Plasticité du Cerveau', where I spent 4 years, and its director **Thomas Preat**, for accepting me within the unit. My interactions there have always been pleasant and insightful, be it with the team leaders, researchers, postdocs*

*or students. I would also like to thank our new unit at the CPN and its director **Thierry Galli** for welcoming us in, and allowing me to defend my thesis there.*

Last but certainly not least, I would like to thank my family and friends for their support and for generally making my life all the brighter even in hard times. In particular I would like to thank my mother, for always believing in me, even in the face of my undying pessimism, and my father, for his experience and advice in life, but especially in all things academic, statistics and programming. Your crash course in R programming has been a life saver.

Table of Contents

<u>1 THE CHEMICAL SYNAPSE: A COMPUTATIONALLY AND PHYSIOLOGICALLY PLASTIC UNIT.....</u>	<u>7</u>
1.1 BRAIN WIRING: A LIFELONG PLASTIC PROCESS.....	7
1.2 SYNAPTIC STRUCTURE AND FUNCTION.....	8
1.2.1 PRESYNAPTIC STRUCTURE	9
1.2.2 PRESYNAPTIC FUNCTION: SYNAPTIC VESICLE RECYCLING.....	12
1.3 SYNAPTIC PLASTICITY	15
1.3.1 Ca^{2+} LEVEL REGULATION.....	16
1.3.2 KINASE RECRUITMENT AS A BIDIRECTIONAL SWITCH	16
1.3.3 PROTEIN SYNTHESIS	17
1.3.4 RELEASE MACHINERY MODULATION.....	17
1.3.5 SYNAPTIC VESICLE POOL MODULATION	18
1.3.6 STRUCTURAL MODULATION	18
<u>2 THESIS AIM</u>	<u>20</u>
<u>3 THE ACTOMYOSIN CYTOSKELETON AND SYNAPTIC ACTIVITY</u>	<u>22</u>
3.1 THE ACTOMYOSIN CYTOSKELETON.....	23
3.1.1 ACTIN FILAMENTS	23
3.1.2 NON-MUSCULAR MYOSIN II.....	24
3.1.3 ACTOMYOSIN UPSTREAM SIGNALING PATHWAYS	26
3.2 ACTOMYOSIN AT THE SYNAPSE.....	28
3.2.1 ACTIN IN THE AZ.....	29
3.2.2 ACTIN AND SYNAPTIC VESICLE POOLS	29
3.2.3 ACTOMYOSIN AND SYNAPTIC FUNCTION.....	31
<u>4 CB1R AND THE ENDOCANNABINOID SYSTEM</u>	<u>35</u>
4.1 RECEPTORS, LIGANDS, ET AL.: PROPERTIES OF THE ENDOCANNABINOID NEUROTRANSMITTER SYSTEM.....	36
4.1.1 RECEPTORS	36
4.1.2 LIGANDS	39
4.1.3 EXTRACELLULAR LIGAND RELEASE	40
4.2 CB1R DOWNSTREAM SIGNALING.....	41
4.2.2 GB/T SIGNALING	43
4.2.3 $G_{i/o}$ SIGNALING.....	43
4.2.4 G_s SIGNALING	44
4.2.5 $G_{12/13}$ SIGNALING.....	44
4.2.6 $G_{q/11}$ TYPE SIGNALING.....	44
4.3 CB1R-MEDIATED SYNAPTIC PLASTICITY	45
4.3.1 SHORT-TERM DEPRESSION (STD).....	47

4.3.2	LONG-TERM DEPRESSION (LTD)	47
4.4	CB1R IN NEURAL DEVELOPMENT	49
4.4.1	CB1R EXPRESSION IN DEVELOPMENT	50
4.4.2	CB1R IN NEURONAL MORPHOGENESIS.....	50
 <u>ARTICLE 1 (PUBLISHED): CANNABINOID-INDUCED ACTOMYOSIN CONTRACTILITY SHAPES NEURONAL MORPHOLOGY AND GROWTH</u>		<u>53</u>
 <u>5 RESULTS PART1: ACTOMYOSIN DYNAMICS MEDIATE CB1R-INDUCED INHIBITION OF VESICLE RELEASE IN CULTURE.....</u>		<u>77</u>
5.1	IMAGING EXOCYTOSIS IN CULTURE WITH SYNAPTOPHLUORIN.....	78
5.2	CB1R-ACTIVATION INDUCES A DECREASE IN SYNAPTIC VESICLE EXOCYTOSIS	79
5.3	ACTOMYOSIN CONTRACTILITY THROUGH ROCK MEDIATES THE EFFECTS OF CB1R ON VESICLE EXOCYTOSIS	81
 <u>6 RESULTS PART2: STORM IMAGING REVEALS ACTOMYOSIN-INDUCED SYNAPTIC VESICLE REDISTRIBUTION UNDER CB1R ACTIVATION.....</u>		<u>83</u>
6.1	STOCHASTIC OPTICAL RECONSTRUCTION MICROSCOPY (STORM)	84
6.2	CLUSTERING ANALYSIS FOR STORM IMAGES	86
6.3	PREDICTING THE ACTIVE ZONE LOCATION FROM THE POST SYNAPTIC DENSITY.....	89
6.3.1	PROPERTIES OF HOMER1 AND BASSOON APPPOSITIONS	89
6.3.2	PREDICTING THE AZ.....	89
6.4	SYNAPTIC VESICLE IDENTIFICATION	91
6.4.1	IDENTIFYING SYNAPTIC VESICLES	91
 <u>7 RESULTS PART 3: THESIS ARTICLE</u>		<u>97</u>
 <u>ARTICLE 2 (IN SUBMISSION): ACTOMYOSIN-MEDIATED NANOSTRUCTURAL REMODELING OF THE PRESYNAPTIC VESICLE POOL BY CANNABINOIDS INDUCES LONG-TERM DEPRESSION</u>		<u>98</u>
 <u>8 DISCUSSION: ACTOMYOSIN CONTRACTILITY THROUGH ROCK MEDIATES CB1R INDUCED LTD</u>		<u>121</u>
8.1	ACTOMYOSIN IN LTD VERSUS DSI/DSE	121
8.2	SIGNALING PATHWAY TO ACTOMYOSIN CONTRACTILITY IN CB1R-LTD.....	122
8.3	ACTOMYOSIN AND VESICLE RECYCLING UNDER CB1R	124
 <u>PERSPECTIVES.....</u>		<u>125</u>
 <u>ANNEXES: R SCRIPTS.....</u>		<u>127</u>
 <u>BIBLIOGRAPHY</u>		<u>148</u>

Abbreviations

2AG:	2-Arachidonyl glycerol
ABP:	Actin Binding Protein
ADP:	Adenosine Diphosphate
AEA:	Anandamide
ATP:	Adenosine triphosphate
AZ:	Active Zone
CB1R:	Cannabinoid type-1 Receptor
CB2R:	Cannabinoid type-2 Receptor
DBSCAN:	Density-Based Spatial Clustering of Applications with Noise
eCB:	endocannabinoid
ELC :	Essential Light Chain
EM:	Electron Microscopy
GTP:	Guanosine Triphosphate
LTD:	Long-Term Depression
LTP:	Long-term Potentiation
MLC:	Myosin Light Chain
MLCK:	Myosin Light Chain Kinase
MLCP:	Myosin Light Chain Phosphatase
MYH:	Myosin Heavy Chain
NMII:	Non-Muscle Myosin II
OPTICS:	Ordering Points to Identify the Clustering Structure

PALM: Photo-Activated Localization Microscopy

PSD: Post-Synaptic Density

RLC: Regulatory Light Chain

ROCK: Rho-associated, coiled-coil-containing protein kinase

STD: Short-Term Depression

STORM: Stochastic Optical Reconstruction Microscopy

SV: Synaptic Vesicle

Figures

Figure 1: Synaptic Structures

Figure 2: Synaptic vesicle Pools and Recycling

Figure 3: Synaptic plasticity and its potential mechanisms

Figure 4: Actin cytoskeleton formations and binding proteins

Figure 5: Non-Muscle Myosin II (NMII) activation and filament formation

Figure 6: Rho-GTPase downstream effectors in cytoskeletal modulation

Figure 7: Actin at the synapse

Figure 8: Actin-like filament polymerisation at endocytic zone during synaptic activity

Figure 9: Preferential signaling pathways of G-protein subunits

Figure 10: Mechanisms of CB1R-induced synaptic plasticity

Figure 11: Function of the synaptophysin-pHluorin probe in reporting exocytosis

Figure 12: CB1R inhibits exocytosis at axonal boutons in hippocampal cultures

Figure 13: Actomyosin contractility mediates CB1R-induced reduction in exocytosis.

Figure 14: Novel discoveries accomplished through STORM imaging

Figure 15: Principles of DBSCAN and OPTICS.

Figure 16: Effect of parameter p on protein localisation clustering

Figure 17: Homer1 and Bassoon apposition properties in control and under CB1R activation

Figure 18: Distribution of Vamp2 within the presynaptic compartment and at synaptic vesicles

Figure 19: Effect of nested p value in the identification of clusters in randomized distributions

Figure 20: p value effect on simulated spheres of different densities

Figure 21: Nested cluster diameters and axonal bouton properties

Introduction

1 The chemical synapse: a computationally and physiologically plastic unit

1.1 Brain wiring: a lifelong plastic process

Animal behavior is inextricably linked to brain wiring. The brain regulates such basic but vital processes as breathing, heart rhythm, and stimuli perception to higher order processes such as learning and decision-making. The regulation of these processes ultimately depends on the activity of distinct neural networks. The great bulk of these networks is genetically programmed, forming distinct brain regions that are well conserved between members of a same species, and even between different phylum classes. However, in order to adapt to a constantly changing environment, the brain needs to conserve a certain deal of plasticity. Memory, for example, essentially depends on the capacity of rewiring neural networks to retain new information.

We now know that a great deal of plastic processes thought to stop after development remain in adulthood. Neurogenesis, for example, was found to occur throughout life both in the hippocampus and in the olfactory bulb. These newly formed neurons grow out and integrate into pre-formed neural networks by forming new connections to regulate network activity (Aimone et al. 2014). Beyond neurogenesis, the majority of neurons formed early in development can change their activity throughout life to adapt to changing requirements. This adaptation can be done either by increasing or decreasing the number of synapses a neuron will make onto other neurons within the network, or by changing the strength of the synapse itself, in a process known as synaptic plasticity.

This section will outline the structure and function of the synapse before introducing different forms of synaptic plasticity, focusing on presynaptically-induced plasticity and known mechanisms of action.

1.2 Synaptic structure and function

The synapse is a highly compartmentalized structure whose primary function is in intercellular signaling. Within the brain, it is typically formed between the axon of one neuron and the dendrite of a second neuron. While the main inputs to synapses are changes in the electrical potential of the membrane, the signal transduction that occurs at a neuronal synapse is principally chemical. The most widely accepted model of synaptic transmission goes as follows: An action potential arriving at a synapse will trigger the activation of voltage gated calcium channels (VGCCs), inducing Ca^{2+} entry into the presynaptic compartment. This presynaptic Ca^{2+} rise initiates synaptic vesicle fusion to the presynaptic membrane and the release of the neurotransmitters contained within into the synaptic cleft (**Figure 1**). These neurotransmitters go on to activate specific receptors at the post-synaptic membrane, where activation of ionotropic receptors leads to ion exchange with the extracellular medium. Depending on the neurotransmitter released and receptor activated, this process leads to depolarization or hyperpolarization of the postsynaptic membrane, corresponding to excitatory or inhibitory transmission, respectively.

These steps occur through highly regulated processes and specified structures contained within each compartment (**Figure 1**). At the synaptic cleft the postsynaptic and presynaptic sites are mirrored by the post synaptic density (PSD) and presynaptic active zone (AZ) respectively. These densely packed structures are easily identifiable by electron microscopy and are essential to evoked synaptic transmission (**Figure 1B**). The AZ docks and primes vesicles for fusion, and the postsynaptic density docks neurotransmitter receptors at the membrane. Furthermore, the presynaptic site contains a number of synaptic vesicles (SVs) separated into different functional pools, which can be tapped on depending on synaptic activity (**Figure 1B**).

This section will briefly review some of the steps and structures important in synaptic signaling with regards to the presynaptic compartment.

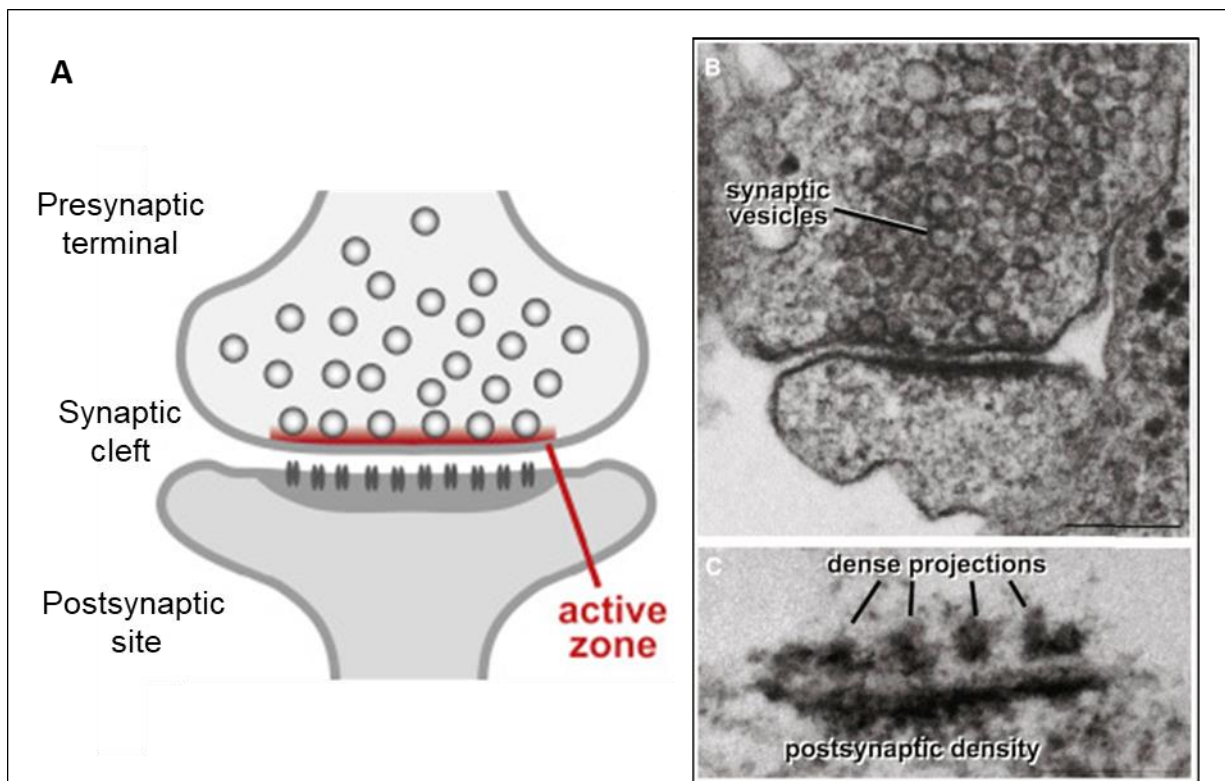


Figure 1. Synaptic Structures

(A) Schematic drawing of a synapse. (B) Electron micrograph of a conventionally fixed and stained synapse in a cultured hippocampal neuron. (C) Electron micrograph of a phosphotungstic acid stained synapse in a cultured hippocampal neuron to visualize pre- and postsynaptic specializations. (B) and (C) are reproduced from Kaeser et al. (2011). (Figure adapted from Sudhof et al. (2012))

1.2.1 Presynaptic Structure

1.2.1.1.1 The Active Zone

Similarly to the post-synaptic density (PSD), the active zone (AZ) is the “site of action” of the presynaptic compartment, where SVs are docked and primed for fusion. It is precisely aligned to the postsynaptic density in order to ensure precise targeting of neurotransmitters to postsynaptic receptors and thus ensure fast and efficient signal transmission. Recent studies, using superresolution microscopy, have even observed what the authors call nanocolumns, a trans-synaptic alignment of AZ and PSD scaffolding proteins into virtual columns, the integrity of which affects synaptic efficacy (Tang et al. 2016).

The majority of the active zone is composed of scaffolding proteins, which help anchor and prime synaptic vesicles ready to be released (**Figure 2**), or the readily releasable pool (RRP). The precise function of all of these still remains to be fully understood, however a number of

them are known to interact directly with proteins of the synaptic vesicle membrane (Südhof 2012). For example, the AZ scaffolding protein Rim1 α is known to interact directly with the SV protein Rab3A, docking the vesicles at the AZ (Haucke, Neher, and Sigrist 2011). Other known proteins such as bassoon and piccolo are also thought to play a role, if not in directly docking vesicles, at least in the maintenance of the AZ structure. It is further suspected that some of these proteins help prime vesicle for fusion with the plasma membrane, such as Munc-13 found to catalyze the SNARE complex essential for membrane fusion (Südhof 2012).

1.2.1.2 Synaptic Vesicle Pools

While a great number of synaptic vesicles are present at the presynaptic bouton, around 200 at hippocampal synapses as observed through electron microscopy (EM) (Harris and Sultan 1995; Schikorski and Stevens 1997), not all of them are competent for membrane fusion. A great majority of them are clustered within the bouton, bound by proteins such as synapsins which immobilize them by tethering them to each other and to the actin cytoskeleton (Siksoo et al. 2007; Fornasiero et al. 2012). This observation among others has led to the categorization of different synaptic vesicle pools depending on their fusion-competence (**Figure 2**).

1.2.1.2.1 The readily releasable pool (RRP)

The readily releasable pool indicates the synaptic vesicles ready to be released upon evoked stimulation. It is typically qualified as the pool released upon low frequency stimulation, or when exposed to hypertonic sucrose solutions (Rosenmund and Stevens 1996). The RRP has typically been identified as the vesicles docked at the active zone, although it was found that certain docked vesicles do not undergo fusion (Darcy et al. 2006; Harata et al. 2001; Marra et al. 2012; Ratnayaka et al. 2012). Nonetheless, it has been shown that the number of docked vesicles correlates positively with the probability of release (Branco, Marra, and Staras 2010), as well as AZ and PSD sizes (Rosenmund and Stevens 1996). It contains on average between 5 and 15 synaptic vesicles at small hippocampal synapses (Harris and Sultan 1995; Schikorski et al. 1997).

1.2.1.2.2 The reserve pool, or recycling pool

The reserve pool indicates the synaptic vesicles that are recruited for release once the RRP is depleted. This recruitment typically occurs upon strong stimulation, or upon exposure to high concentrations of extracellular K^+ (50-90mM). It is also typically thought to comprise mainly recently endocytosed vesicles. Indeed, studies find that RRP refilling during sustained stimulation will preferentially occur through newly recycled vesicles, which are more mobile (Gaffield, Rizzoli, and Betz 2006; Kamin et al. 2010) and preferentially relocate close to the active zone (Marra et al. 2012; Schikorski et al. 1997). This property has also given the reserve pool the name of ‘recycling pool’. It includes approximately 20-30% of the total pool, although this can vary greatly up to 70% depending on the synapse and stimulation paradigm (Annette Denker and Rizzoli 2010). Similarly to the RRP, its size has been found to correlate positively with probability of release (Murthy and Stevens 1998; Waters and Smith 2002).

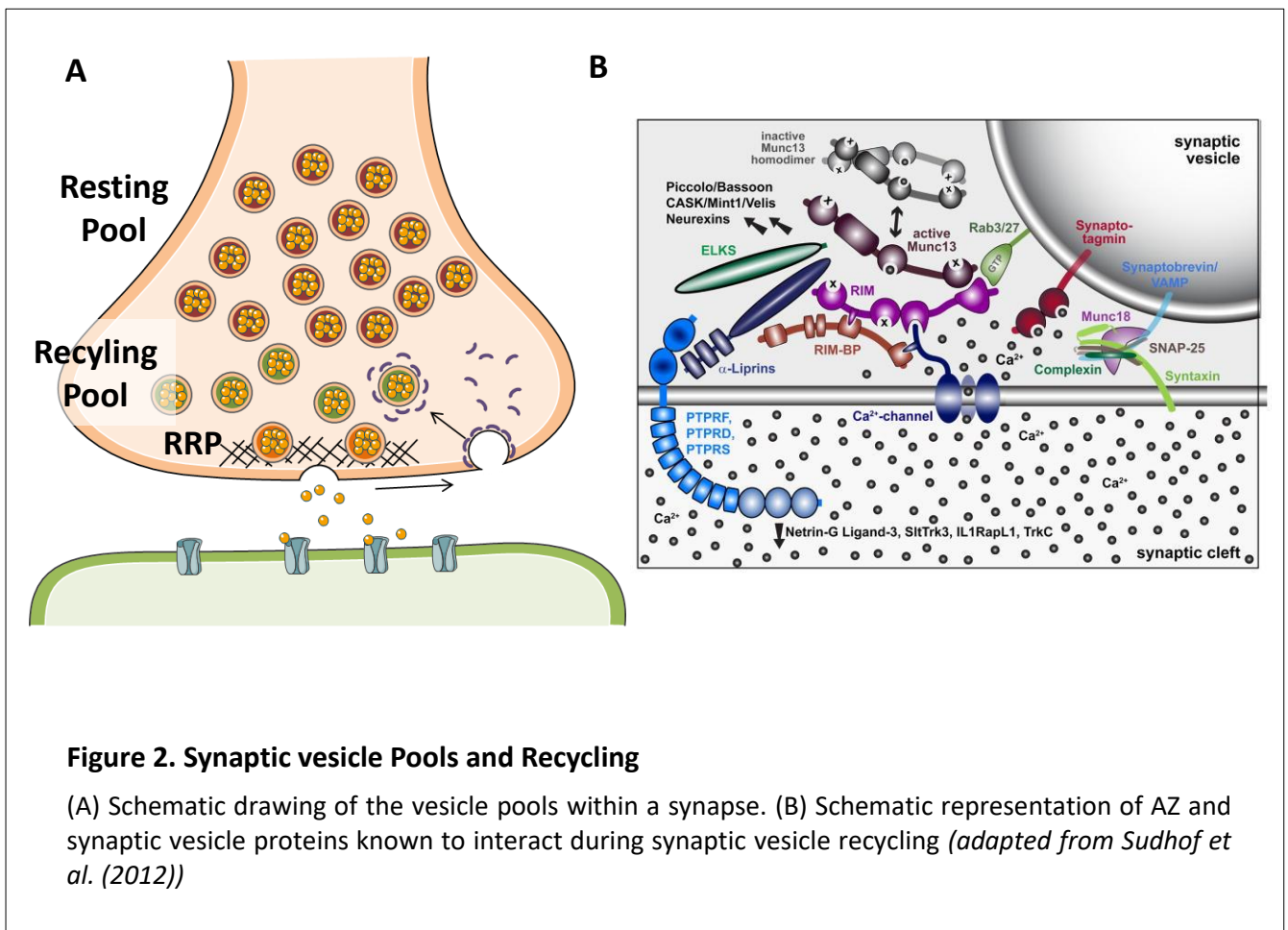


Figure 2. Synaptic vesicle Pools and Recycling

(A) Schematic drawing of the vesicle pools within a synapse. (B) Schematic representation of AZ and synaptic vesicle proteins known to interact during synaptic vesicle recycling (adapted from Sudhof et al. (2012))

1.2.1.2.3 The resting pool

The resting pool indicates the synaptic vesicles which are not recruited upon evoked stimulation and it typically comprises a majority of the synaptic vesicles of the total pool. It is relatively unknown why such a large quantity of supposedly fusion incompetent vesicles resides within the bouton. One suggestion is that a portion of these vesicles may be precursor vesicles which are not neurotransmitter filled, but act as a buffer for proteins involved in vesicle recycling (Shupliakov 2009; A. Denker, Bethani, et al. 2011; A. Denker, Krohnert, et al. 2011). Furthermore, there is evidence of SV trading between the recycling pool and the resting pool (Kim and Ryan 2010; Ratnayaka et al. 2012), and certain forms of synaptic modulation have been found to recruit SVs from the resting pool as a form of potentiation (Tyler et al. 2006; J. Jung et al. 2014), suggesting that the resting pool may act as a resource in the modulation of synaptic activity.

Although the spatial distribution of vesicles within the presynaptic compartment appears to have a lot to do with their assignment to one of the pools, this does not appear to be a consistent rule as docked vesicles are not necessarily fusion competent and recycling vesicles can be found intermixed within the resting pool (Fowler and Staras 2015a). Some have therefore suggested there may be molecular markers distinguishing the different pools. SNARE proteins have been suggested to be good candidates, as it was found that VAMP7 is more present in resting vesicles, whereas VAMP2 may be preferentially located to the recycling pool (Hua et al. 2011), for example. Others have suggested that vesicle mobility within the presynaptic bouton may be a better indicator of pool assignment. Indeed, as mentioned previously, recycling vesicles are more mobile than resting pool vesicles (Gaffield, Rizzoli, and Betz 2006; Kamin et al. 2010). One reason for this may be the tethering of resting pool vesicles to the actomyosin cytoskeleton through synapsins, as inhibition of synapsin, either through genetic deletion or phosphorylation, increases mobility of vesicles within the presynaptic compartment (Orenbuch et al. 2012; Gaffield, Rizzoli, and Betz 2006).

1.2.2 Presynaptic function: synaptic vesicle recycling

While the basic principles underlying synaptic vesicle release upon stimulation have been known for some time, the knowledge concerning the different steps of synaptic vesicle recruitment, priming and recycling is relatively poor. One main reason for this paucity is the small size of the presynaptic compartment, especially at central small synapses, as well as the

minute size of its composing elements. Indeed, axonal boutons are on average around $1\mu\text{m}^3$ in volume, with synaptic vesicles being around 30-50nm in diameter, approximately 4x smaller than the resolution of conventional microscopy techniques. While this discrepancy can be overcome with electron microscopy (EM), EM does not lend itself well to studying the highly dynamic processes involved in synaptic vesicle cycling, which occur within a couple of seconds.

This section will briefly review what is known of the essential steps of the synaptic vesicle cycle within the presynaptic terminal.

1.2.2.1 Synaptic vesicle docking and priming

In order to rapidly respond to arriving stimuli, synaptic vesicles need to be positioned close to the presynaptic membrane and ready to be released. This is made possible by the docking of synaptic vesicles at the active zone (AZ). Although the specific mechanisms inducing SV docking are poorly understood, Rab3-interacting molecules (RIMs) are thought to play an important role. Indeed, RIM proteins are known to bind to SV membrane proteins such as Rab3 (Haucke, Neher, and Sigrist 2011), by which they may tether SVs to the AZ. RIMs have also been found to interact with VGCCs (Deng et al. 2011; Han et al. 2011; Kaeser et al. 2011; K. S. Y. Liu et al. 2011). This interaction may allow them to dock SVs close to VGCCs, which would accelerate SV/membrane fusion initiation upon depolarization.

1.2.2.2 Exocytosis

The release of vesicle contents into the extracellular medium, known as exocytosis, occurs upon SV fusion to the presynaptic membrane. This reaction is known to occur through the formation of a SNARE complex between SNARE proteins of the SV membrane, such as VAMP2, and SNARE proteins of the plasma membrane, such as SNAP25. Formation of a complex between these proteins draws the two membranes together, forcing their fusion (Fasshauer et al. 1998).

While it is clear that Ca^{2+} entry upon depolarization initiates the fusion of synaptic vesicles, how this initiates the formation of the SNARE complex is relatively unclear. Synaptotagmin has been posited as a candidate as its calcium binding form is known to interact both with SNAREs and the plasma membrane, which may allow it to catalyze complex formation upon depolarization-induced Ca^{2+} entry (Chapman 2008).

1.2.2.3 Endocytosis

Endocytosis, or vesicle formation from the plasma membrane, is an important step of the synaptic vesicle cycle as it both compensates for the increase in membrane surface induced by exocytosis as well as replenishing the depleted synaptic vesicle pool. Importantly, endocytosis is often triggered by exocytosis, although the extent to which these mechanisms are linked is still under debate (Rizzoli 2014).

Upon SV fusion to the plasma membrane, the resulting SV membrane protein pool clusters and diffuses along the plasma membrane (Willig et al. 2006; Hoopmann et al. 2010; Opazo et al. 2010), clearing out of the synaptic cleft (Z. Li and Murthy 2001; Fernández-Alfonso, Kwan, and Ryan 2006; Wienisch and Klingauf 2006). There, these protein clusters are taken up through invagination of the plasma membrane to form novel synaptic vesicles.

Arguably the most widespread form of endocytosis is clathrin-dependent endocytosis. This process is relatively slow compared to exocytosis, causing a bottleneck for vesicle pool replenishment upon strong stimulations (Miller and Heuser 1984; Heuser et al. 1979; Heuser and Reese 1981). Initiation of the endocytotic process is elusive. Once plasma membrane invagination has started, clathrin-chain assemblies known as “triskelia” coat the forming vesicle. The vesicle is then detached from plasma membrane, through the action of ring-like dynamin assemblies, released of clathrin and refilled with neurotransmitter through specific transporters (Rizzoli 2014).

Other known forms of endocytosis have been described. One such form is bulk endocytosis, a process by which excessive exocytosis, for example under strong and repetitive stimulation, causes the presynaptic membrane to fold in onto itself. The resulting endosome is then budded off through clathrin-mediated endocytosis within the presynaptic terminal (Rizzoli 2014).

Another form of vesicle recycling is performed through a process termed ‘kiss and run’. SVs undergoing this process do not completely fuse with the plasma membrane, but are opened just enough to release part of their content before reforming. This form of recycling has an advantage over conventional recycling as it is much faster than clathrin-mediated endocytosis (Q. Zhang, Li, and Tsien 2009; Park, Li, and Tsien 2012), meaning vesicle pools can be replenished more quickly. The relative part of ‘kiss and run’ events as compared to conventional SV recycling in synaptic signaling remains to be established however (Granseth et al. 2006; Granseth et al. 2009).

1.3 Synaptic plasticity

A great number of behavioral functions rely on the plasticity of neural systems. Arguably one of the simplest ways of regulating this is by modifying the activity of different neurons by modifying the activity of different synapses at different points in time, a phenomenon known as synaptic plasticity. While the difficulty of correlating synaptic plasticity with behavioral outputs in the past had struck a debate as to the *in vivo* relevance of known forms of plasticity (Malenka and Bear 2004), advances in the past decade have overcome these doubts, with a number of studies showing the direct involvement of synaptic plasticity in a number of behavioral processes, including monocular deprivation, reward seeking, and fear conditioning (reviews in (Malenka and Bear 2004) and (Monday and Castillo 2017)).

Synaptic plasticity is the process by which the output of a synapse to depolarizing stimuli is changed. An increase in the output is termed a potentiation, while a decrease is named a depression. The induction of these changes typically occurs through activation of G-protein coupled receptors (GPCRs). Indeed, forms of plasticity have been described for GPCR activation of most of the major neurotransmitter systems, including dopaminergic, serotonergic, glutamatergic and GABAergic. Indeed, GPCR-induced plasticity englobes most forms of plasticity described, with one major exception being NMDA-induced forms (Atwood, Lovinger, and Mathur 2014).

The induction of synaptic plasticity has been described both at presynaptic and postsynaptic compartments. Postsynaptically-induced plasticity results in decreases or increases in postsynaptic ionic currents in response to neurotransmitter release. Presynaptically-induced plasticity results in an increase or decrease in the probability of neurotransmitter release.

Synaptic plasticity can be transient, occurring on a timescale of milliseconds to a couple of minutes, in which case it is termed short-term plasticity. Changes can further persist from 30min to several weeks (Malenka and Bear 2004), in which case it is known as long-term plasticity (**Figure 3A**). Importantly, a number of GPCRs known to induce plasticity are known to enact both short- and long-term forms (Atwood, Lovinger, and Mathur 2014). What mediates the induction of a short term rather than a long-term form of plasticity in these cases is unknown, although it is suggested that previous synaptic activity and duration of GPCR activation may be mediating factors (Atwood, Lovinger, and Mathur 2014).

Indeed, the mechanisms underlying short-term forms of plasticity are often tied to relatively simple molecular cascades, such as the direct modulation of ion channels, regulating membrane excitability. Long-term forms of plasticity however recruit complex signaling cascades and the mechanisms regulating their long-term maintenance remain often unknown, particularly concerning the presynaptic forms (**Figure 3B**). This section will focus on long-term forms of presynaptic plasticity, looking at what is known of the common molecular or structural mechanisms they induce that ultimately lead to changes in synaptic strength.

1.3.1 Ca²⁺ level regulation

As opposed to short-term forms of plasticity, it would appear that both long-term potentiation (LTP) and long-term depression (LTD) depend on increases in presynaptic Ca²⁺ levels (Lüscher and Malenka 2012). However, studies have suggested that the magnitude of the increase determines the orientation of the plasticity, towards depression or potentiation. This was found to be the case in at hippocampal mossyfiber/CA3 synapses, where strong or weak activity would induce LTP or LTD respectively presumably by modulating the level of presynaptic Ca²⁺ (Tzounopoulos et al. 1998). This necessity for Ca²⁺ holds true when considering that both LTP and LTD have been found to recruit kinases and phosphatases for induction and/or maintenance, which either directly depend on Ca²⁺ for activation or recruit calcium dependent processes.

1.3.2 Kinase recruitment as a bidirectional switch

One of the most observed mediators of long-term plasticity is the cAMP/PKA signaling pathway, although the specific mechanisms underlying its effect on neurotransmitter release remains elusive. Indeed, increases and decreases of cAMP/PKA signaling have been reported in LTP and LTD respectively (Ying Yang and Calakos 2013). Many forms of LTP and LTD are dependent on GPCRs most often coupled to G_s and G_{i/o} type proteins, respectively, both of which have opposite effects on cAMP/PKA signaling. Thus, G_s coupled GPCRs such as the dopamine-1 receptor (D1R) are found to induce LTP in a PKA-dependent manner (C. Li and Rainnie 2014), whereas G_{i/o} coupled receptors such as mGluR2/3, D2R or CB1R are found to induce LTD through PKA (Ying Yang and Calakos 2013). This model favors a common target mechanism in the bidirectional regulation of synaptic plasticity at the synapse, although the nature of this mechanism remains to be determined.

Other kinases found to affect presynaptic forms of plasticity are mitogen-activated protein kinases, found downstream of LTD induction (Morrison and Davis 2003). Their downstream

mechanisms in plasticity are poorly understood, however these kinases have been known to be involved in the expression of immediate early genes, which may help to induce protein synthesis for long-term maintenance.

1.3.3 Protein synthesis

Protein synthesis has long been established as essential in a number of postsynaptic forms of synaptic plasticity (Santini, Huynh, and Klann 2014), and has therefore been postulated as a potential mediator of presynaptic forms. Indeed, some forms of presynaptic plasticity have been found to rely on protein synthesis (Yin et al. 2006; Y. Y. Huang, Li, and Kandel 1994; Calixto et al. 2003; Younts et al. 2016). Similarly to Ca^{2+} -dependence however this does not appear to be bidirectional as both LTP and LTD forms have been found to depend on protein synthesis.

While the proteins synthesized are most likely different for both LTP and LTD their nature in both cases is as of yet unknown, but may include the production of kinases or phosphatases necessary for LTP/LTD maintenance, as well as certain structural proteins such as AZ or vesicle proteins that could be used to strengthen the synapse.

1.3.4 Release machinery modulation

One of the most promising candidates suggested to be the substrate of long-term plasticity is the AZ protein RIM1 α . Among its several known functions, RIM1 α is known to bind to the SV Rab3 proteins, docking them to the AZ, as well as to VGCCs, bringing them closer to the AZ and synaptic vesicles (Deng et al. 2011; Han et al. 2011; Kaeser et al. 2011; K. S. Y. Liu et al. 2011). Rim1 α is also known to interact with a number of other AZ scaffolding proteins, such as Munc-13, which may help it catalyze vesicle priming (Südhof 2012). As such, RIM1 α appears to be a good target to regulate synaptic plasticity and indeed, with its interacting proteins Munc13 and Rab3A, it was found to be necessary for a number of forms of presynaptic LTP and LTD (Ying Yang and Calakos 2013).

Although PKA is known to be able to phosphorylate RIM1 α , which would elegantly link the cAMP/PKA and Rim1 α dependence of many of these forms of plasticity, attempts to show an interaction between the two pathways has been relatively mixed (Lonart et al. 2003; Simsek-Duran, Linden, and Lonart 2004; Kaeser et al. 2008; Y. Yang and Calakos 2010; Castillo et al. 2002).

1.3.5 Synaptic vesicle pool modulation

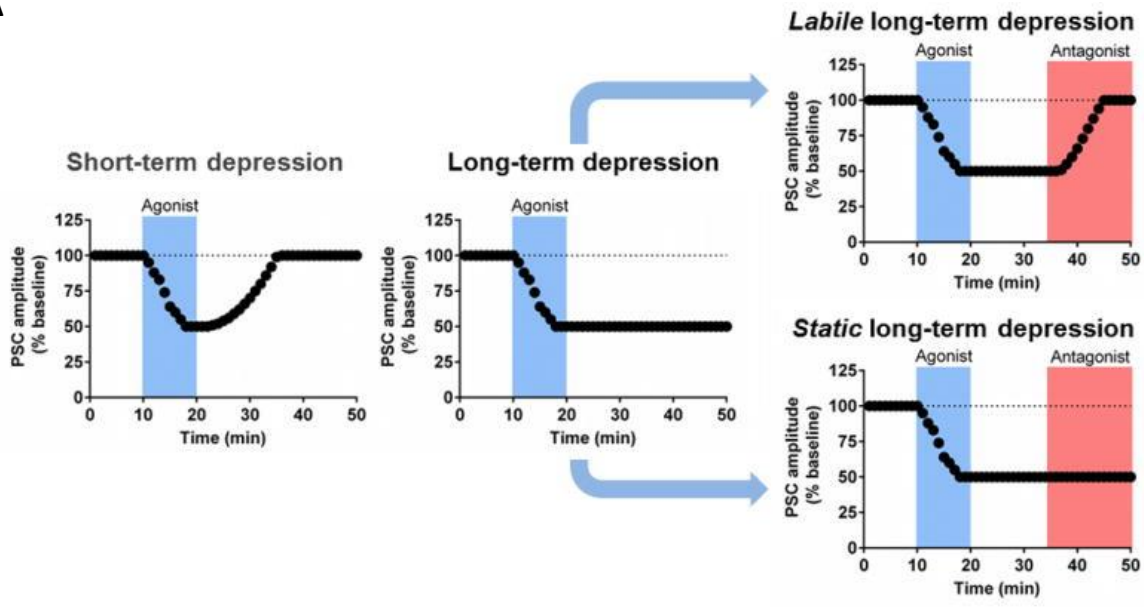
Another candidate target for bidirectional long-term plasticity is in the recruitment/depletion of the synaptic vesicles from different SV pools. Although findings in this area are relatively scarce, an increase/reduction in RRP size has been found to mediate certain forms of LTP and LTD respectively (Fowler and Staras 2015b). Furthermore, bidirectional recruitment of SVs to and from the resting pool was found to mediate plasticity, with CDK5- dependent recruitment of SVs from the resting pool thought to mediate NMDA-dependent LTP (Fowler and Staras 2015b). Conversely, eCB-LTD was found to require calcineurin (Heifets, Chevaleyre, and Castillo 2008), which has been found to mediate the transfer of vesicles from the recycling pool to the resting pool (Marra et al. 2012).

1.3.6 Structural modulation

Much like postsynaptic spines, a number of studies have shown that presynaptic sites can show extensive structural modulation. Indeed it has been shown that, while a majority of axonal boutons will remain stable over the course of weeks to months, particularly in adulthood (De Paola et al. 2006; Qiao et al. 2016), bouton turnover can occur on a timescale of minutes to hours at certain neurons (Kuhlman and Huang 2008; Marik et al. 2010; Keck et al. 2011; Fu et al. 2012; Schuemann et al. 2013), often in an activity dependent manner (Fu et al. 2012; Kuriu, Yanagawa, and Konishi 2012; Schuemann et al. 2013).

Furthermore, axonal boutons have been shown to change size in an activity-dependent manner. Stimulation of individual boutons through glutamate uncaging was found to increase bouton volume along with spine size, although the change occurred relatively slowly, increasing by 45% over 3 hours, difference to control only becoming significant after 130min (Meyer, Bonhoeffer, and Scheuss 2014). Given the relatively slow time course described, it could be suggested that structural changes may start to occur upon plasticity induction, but may occur on a nanoscopic scale. This hypothesis needs further research.

A



B

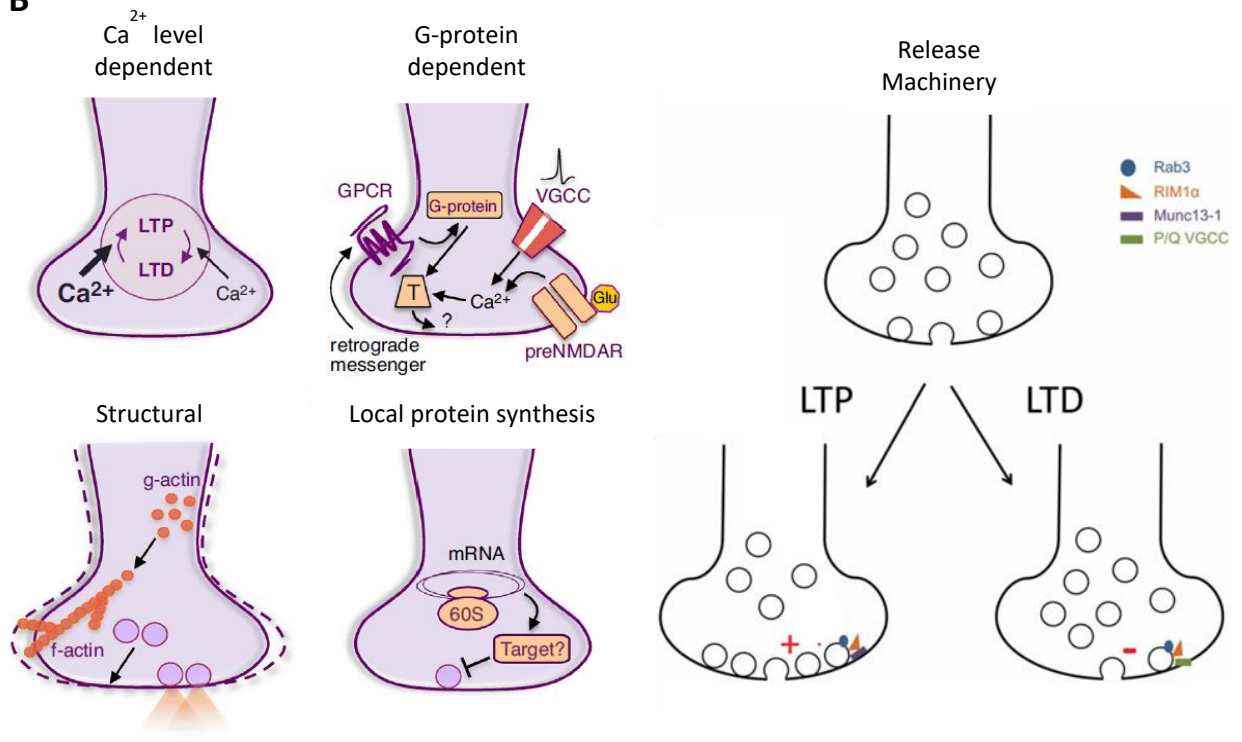


Figure 3. Synaptic plasticity and its potential mechanisms

(A) Operational definitions for distinct forms of synaptic depression (*adapted from Atwood et al. (2014)*) (B) Potential mechanisms of presynaptic plasticity. Both LTP and LTD have been found to occur through mediated changes in Ca²⁺, G-protein recruitment, protein synthesis, changes in release machinery and structural changes, potentially occurring through actin cytoskeleton modulation. (*adapted from Monday and Castillo (2012) and Yang and Calakos (2013)*)

2 Thesis Aim

While there is little information on presynaptically induced synaptic plasticity, that is not to say that it does not hold importance within behavior. Indeed, the cannabinoid type-1 receptor (CB1R) is one known presynaptically located modulator of synaptic plasticity, and is one of the most abundant transmembrane receptors in the brain. It has long been known to affect both short-term forms of synaptic plasticity as well as long-term forms, and its activity has been tied to a number of behavioral correlates, including effects on memory, mood, motor-activity and perception . Nonetheless, although the mechanisms driving short-term effects of CB1R induced plasticity are well established, those mediating its long-term effects remain poorly understood, with a number of candidate mechanisms having been suggested but none properly confirmed.

In parallel, CB1R has been found to affect neural development. Early studies, including one issued by my hosting team, have shown CB1R to be highly expressed in the axons of developing projection neurons (Romero et al. 1997; Berghuis et al. 2007; Vitalis et al. 2008). Looking further into individual neuron development in cultures, studies showed that modulation of CB1R activity had a significant effect on neuronal morphology, including axon and dendrite length, as well as dendrite number (Berghuis et al. 2005; Berghuis et al. 2007; Vitalis et al. 2008). Furthermore, a number of studies would specifically find CB1R-activation to have a repulsive effect on axonal growth cone pathfinding (Berghuis et al. 2007; Argaw et al. 2011). Combined, these findings would point towards a downstream effect of CB1R activation on the actomyosin cytoskeleton (Berghuis et al. 2007), known effector of axonal outgrowth (Dent, Gupton, and Gertler 2011), although the specific molecular pathway employed had yet to be determined.

When I arrived within the hosting team at the start of my thesis, the team held important results showing a downstream pathway linking CB1R activation to contraction of the actomyosin cytoskeleton and growth cone retraction, results to which I contributed to before publishing (Roland et al., 2014). Importantly, these results provided a novel effector pathway downstream of neuronal CB1R through RhoA/ ROCK activation and phosphorylation of the cytoskeletal motor non-muscle myosin II.

Given the elusive nature of CB1R-induced plasticity and the molecular pathway described in our article, one obvious question given these results was whether CB1R-activation might recruit actomyosin contractility to induce long-term plasticity. The aim of my thesis has therefore been in providing answers to this question.

To start providing answers, two initial questions were formulated:

- (1) Is there evidence that the actomyosin cytoskeleton may play a role in synaptic plasticity?
- (2) Is there evidence that CB1R may recruit the actomyosin cytoskeleton at synapses?

The following sections will explore evidence that provides answers to these questions before arriving at the main results obtained during my thesis.

3 The Actomyosin Cytoskeleton and Synaptic Activity

Cells hold a plethora of different proteins allowing them to perform essential functions for organism survival. These functions could not be carried out however without a specific structural organization allowing them both to quickly and efficiently cycle essential proteins to their necessary locations (a process more efficient than random diffusion) as well as a core structure allowing them to hold or adapt depending on the necessities of the organism. Cells are therefore composed of a cytoskeleton which gives them structure. This cytoskeleton is composed of different types of filaments which hold both similar and different roles. These are mainly microfilaments, or filamentous actin (F-actin) composed of actin, microtubules composed of α - and β - tubulin, and intermediate filaments, which may be composed of various different proteins including formin.

Focusing on the two best described components, actin filaments and microtubules vary in their filament structure and dynamics. While actin filaments are relatively thin, around 7nm in diameter, microtubules are larger, around 25nm. Given their simple structure, actin filaments are therefore more adapted to mediate processes requiring fast assembly and disassembly, while the more stable nature of microtubules is more adapted to providing structural stability, a property which is reflected in their preferential location within cell processes. Indeed, while microtubules are more prominent in the cell body and at the dendritic shaft of polarized dendrites, actin filaments are often preferentially located in dynamic processes, such as migration rings in endothelial cells or growth cones in neurons. This is further reflected at the synapse, with one study revealing actin to be twice more prevalent than tubulin in synaptosomes (Wilhelm et al., 2014). By this logic, synapses are structurally dynamic compartments, requiring actin dynamics in their functions (Kevenaar and Hoogenraad 2015).

This chapter will introduce the fundamentals of actin and myosin in the composition of the actomyosin cytoskeleton before outlining the importance of actomyosin dynamics in synaptic structure and function, with a particular focus on what is known of presynaptic actomyosin and how it may contribute to presynaptically-induced synaptic plasticity.

3.1 The actomyosin cytoskeleton

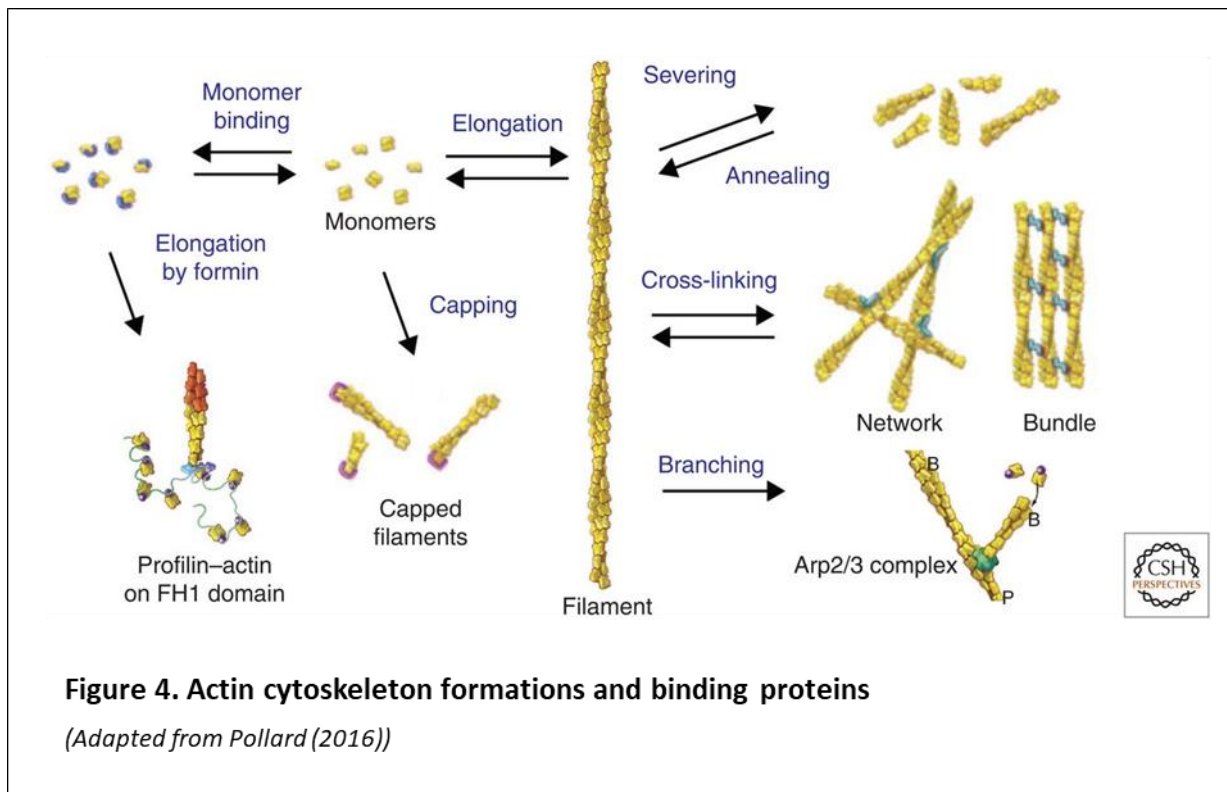
3.1.1 Actin filaments

An actin filament (F-actin) is composed of 2 chains intertwined in a helical structure. These chains are composed of monomeric G-actin, the asymmetric structure of which endows a polarized nature to actin filaments, of which a barbed, or (+), end and a (-) end can be distinguished. F-actin formation starts with the nucleation of G-actin monomers into dimers and trimers. G-actin coupling to ATP induces the polymerization of G-actin monomers, upon which the actin-coupled ATP is hydrolyzed to ADP. ADP release leads to depolymerization of actin, which must be recharged with ATP in order to polymerize once again.

While polymerization of the actin filaments is possible at both (+) and (-) ends, polymerization occurs 10 times faster at the barbed end (T. D. Pollard and Mooseker 1981; Thomas D. Pollard 1986), with depolymerization of the filaments occurring preferentially at the (-) end. G-actin will therefore preferentially travel back to the barbed end of the filament before polymerizing once again. This polar property of F-actin polymerization/depolymerization has given the name of “treadmilling” to F-actin dynamics (Wegner 1976).

F-actin formation occurs intrinsically in a buffered solution of G-actin and ATP, an assay often used to study F-actin targeted signaling and dynamics in vitro. Nonetheless, a number of proteins are capable of binding to actin in order to regulate this treadmilling process, either by catalyzing or stabilizing the polymerization/depolymerization reaction. Indeed, while the F-actin filament is relatively stable, G-actin dimers and trimers are relatively unstable. A number of actin binding proteins (ABP) are available therefore to bind these assemblies and connect them to the F-actin filament before denucleation. Some ABPs may also block the reaction depending on the cell's needs. For example, cofilin promotes G-actin nucleation, thus catalyzing F-actin polymerization, while thymosine- β 4 capping of G-actin monomers abates polymerization (**Figure 4**) (Thomas D. Pollard 2016).

Furthermore, certain proteins allow the formation of specific F-actin structures that would be impossible with F-actin filaments alone. For example, Arp2/3 allows new F-actin filaments to branch out from pre-existing filaments (**Figure 4**), creating F-actin networks necessary for the fast trafficking of a number of proteins within the cell, or for the development of filopodia necessary for cell motility (Thomas D. Pollard and Cooper 2009). Myosin II also confers



specific architecture to actin filaments within cells. A good example of this is the sarcomere, the basic unit of striated muscle fibers, whose actomyosin organization gives the muscle its fibrous appearance. This property of myosin II as well as its contractile functions will be expanded upon below.

3.1.2 Non-muscular myosin II

Myosins are a eukaryotic superfamily of actin-binding molecular motors, of which 18 classes have been established. Of these, 11 classes have been identified in humans (Richards and Cavalier-Smith 2005). Phylogenetically related to kinesins, the microtubule-binding motor proteins, many of the myosin classes function as cargo trafficking motors, with their C-terminal binding cargo vesicles, while their N-terminals transiently bind to F-actin in an ATP dependent manner, conferring them a ‘walking’ mechanism along F-actin tracts. The myosin II class differs from these, as, while its N-terminal maintains actin binding properties, its C-terminal mostly binds other myosin II motors, forming thick myosin filaments capable of contracting the actin cytoskeleton. Nonetheless, myosin II is the most common class of myosin found in eukaryotic cells, responsible for generating most cellular contractile forces (Vicente-Manzanares et al. 2009).

The myosin II class can further be separated into muscle and non-muscle (NMII) myosin II subtypes. While the muscular subtype is mostly restricted to striated muscle, where it is responsible for muscle tone and contraction, NMII is found in all eukaryotic cells, contributing to fundamental cellular functions, such as maintaining cellular tension, adhesion and migration during development (Vicente-Manzanares et al. 2009).

Like muscle myosin, NMII is formed by the dimerization of two chain units, each composed of a globular head and three peptide chains: a heavy chain, a regulatory light chain (RLC) and an essential light chain (ELC) (see Fig). Dimerization into NMII occurs through the helical intertwining of the heavy chains. At the resting state this heavy chain helix folds onto itself in an incompetent formation. Phosphorylation of the RLC is then necessary to unfold the dimer and render the myosin functional (**Figure 5A**). Once unfolded, the heavy chain domains of NMII units can self-associate to form isoform-specific, anti-parallel myosin filaments (**Figure 5B**) (Vicente-Manzanares et al. 2009), which can contain up to 20 NMII copies. These filaments crosslink actin filaments, forming the actomyosin cytoskeleton, and translocate them towards each other upon motor activity (Kneussel and Wagner 2013). These properties

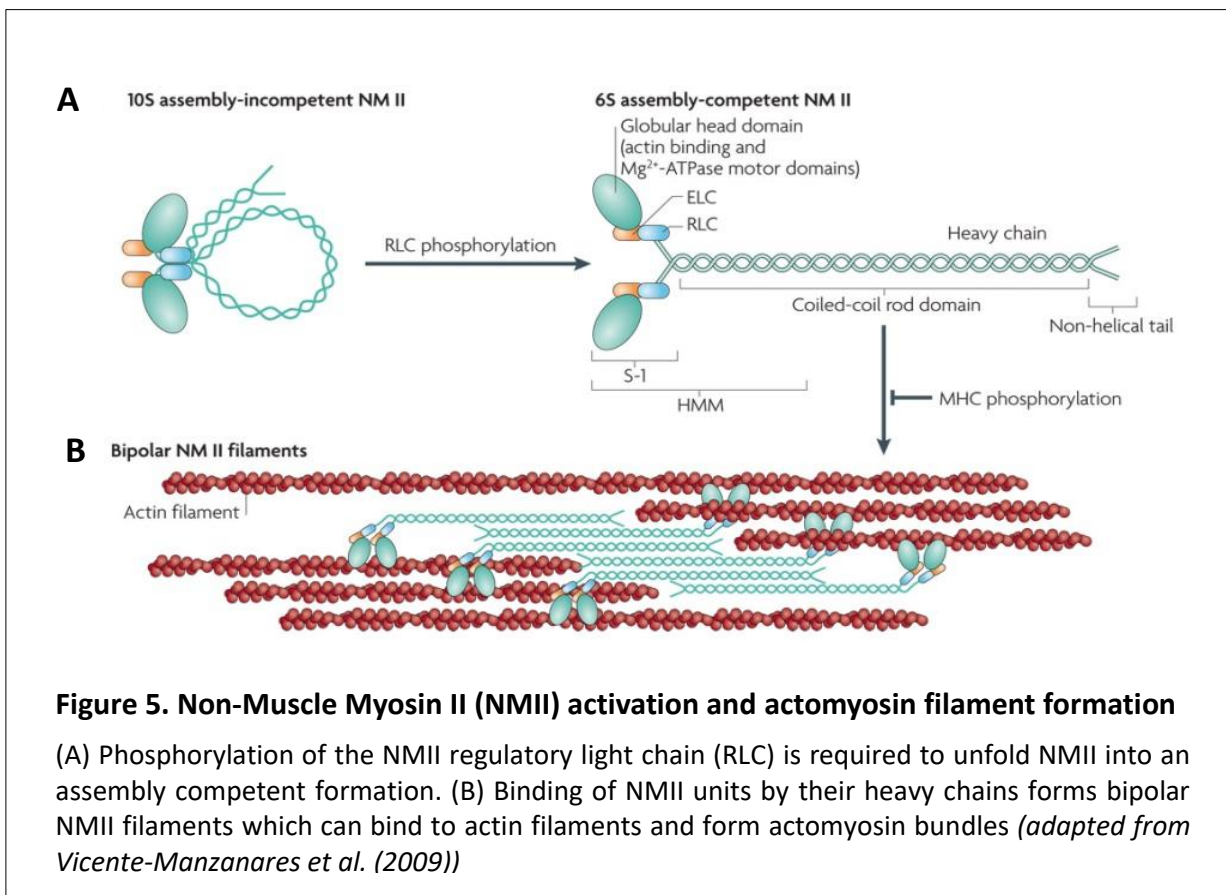


Figure 5. Non-Muscle Myosin II (NMII) activation and actomyosin filament formation

(A) Phosphorylation of the NMII regulatory light chain (RLC) is required to unfold NMII into an assembly competent formation. (B) Binding of NMII units by their heavy chains forms bipolar NMII filaments which can bind to actin filaments and form actomyosin bundles (*adapted from Vicente-Manzanares et al. (2009)*)

can be regulated by phosphorylation of the NMII heavy chains, leading to dissociation of the filaments or preventing their formation.

Actin binding occurs at the globular head domain, where an Mg^{2+} -ATPase unit is also located. Actin binding occurs with high affinity while in an ADP bound state. Upon ADP release and ATP binding, actin unbinds from the head. ATP hydrolysis then leads to conformational change of the myosin head and light chains, which, upon P_i release and actin binding, leads to a lever-like power stroke of the myosin head towards the barbed end of the actin filament. This motor activity can further be regulated by phosphorylation of the RLC, which increases myosin head ATPase activity by controlling myosin head conformation (Kneussel and Wagner 2013; Vicente-Manzanares et al. 2009).

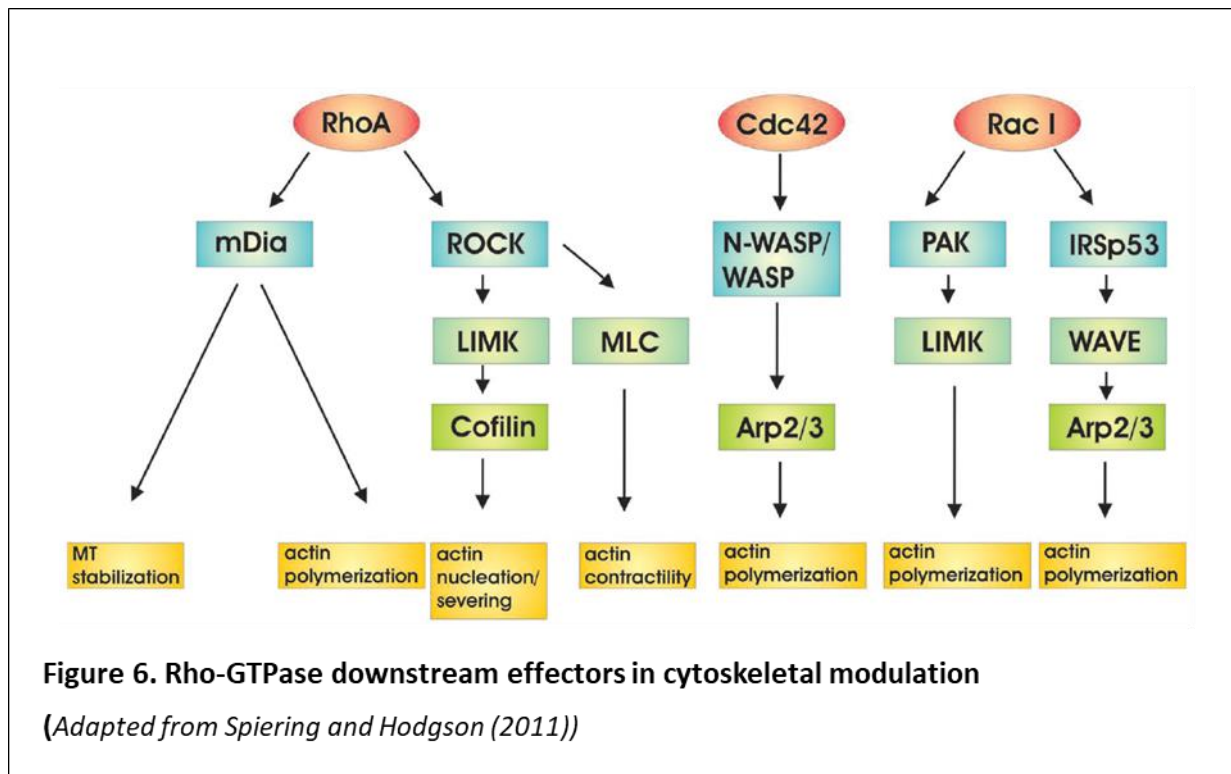
In mammals, three NMII isoforms have been identified, NMIIA, NMIIB and NMIIC, distinguished uniquely by their heavy chains, and encoded by the MYH9, MYH10 and MYH14 genes, respectively. These isoforms differ in cellular distribution, Mg^{2+} -ATPase activity, and actin affinity. All three isoforms have been found to be expressed in the brain, although their preferential expression patterns appear to differ between cell type, with NMIIA and NMIIB being the most expressed in neurons (Y. Zhang et al. 2014).

3.1.3 Actomyosin upstream signaling pathways

A number of signaling pathways have been described that lead to regulation of actomyosin formation and activity.

3.1.3.1 Small GTPases

Small GTPases are the best known regulators of the actomyosin cytoskeleton. They are a superfamily composed of around 200 proteins which can be further separated into 6 subcategories: Rho, Ras, Rab, Arf, Sar and Ran (Colicelli 2004). Their activation is dependent on their specific binding to GTP. Among these subcategories, Rho-GTPases are known to regulate a number of cytoskeletal processes (Spiering and Hodgson 2011). Specifically, Rho-GTPase subfamilies are known to conduct opposite effects on the actomyosin cytoskeleton (**Figure 6**). RhoA proteins are generally associated with negative growth (Luo 2002), particularly through the action of ROCK and phosphorylation of the myosin light chain. Rac and Cdc42 generally promote growth (Albertinazzi et al. 1998; Albertinazzi et al. 2003; Hall and Lalli 2010), by catalyzing actin polymerization and inhibiting NMII, for example.



3.1.3.2 Myosin Kinases

Regulation of NMII phosphorylation is an important target in the regulation of actomyosin cytoskeleton crosslinking and contraction. This can be achieved through the phosphorylation/hydrolysis of the myosin light chain (MLC).

Over a dozen kinases have been reported to phosphorylate NMII RLC isoforms. These include myosin light chain kinase (MLCK), Rho-associated, coiled coil-containing kinase (ROCK), citron kinase, leucine zipper interacting kinase (ZIPK; also known as DAPK3) and myotonic dystrophy kinase-related CDC42-binding kinase (MRCK; also known as CDC42BP). Both ROCK and ZIPK are activated by RhoA while MLCK is activated by Ca²⁺-calmodulin. ROCK can also increase MLC activity by inhibiting its two principal phosphatases, protein phosphatase 1 (PP1) and myosin light chain phosphatase (MLCP) (Vicente-Manzanares et al. 2009).

3.1.3.3 G-proteins coupled receptors (GPCRs)

Although a direct link between GPCRs and recruitment of the actomyosin cytoskeleton has not consistently been shown, a number of GPCRs have been found to induce structural effects known to depend on actomyosin contraction. One such assay is in the study of changes in cell

morphology such as cell rounding and process outgrowth, which are critically dependent on actomyosin dynamics.

Globally, $G_{i/o}$ coupled receptors have been found to produce negative effects on cell outgrowth. In neurons, axonal growth cone retraction can be inhibited by activation of GABAB (Xiang et al. 2002) and somatostatin type-1 receptor (SST1) (Cai et al., 2008). Neurite branching has also been found to be inhibited by activation of dopamine 2 receptors (D2R) and serotonin 5-HT_{1B} receptors (Parish et al. 2001; Parish et al. 2002; Gaspar, Cases, and Maroteaux 2003), as well as activation of the chemokine receptor type 4 (CXCR4) (Lysko, Putt, and Golden 2011).

3.1.3.4 cAMP/PKA

In neurons, cAMP/ PKA has been found to induce the attractive cues for axonal outgrowth induced by BDNF and netrin-1 (De La Torre et al. 1997; Ming et al. 1997; Song, Ming, and Poo 1997). While the link to actomyosin is not described in these studies, studies in non-neuronal cells find that cAMP//PKA activity can induce morphological changes through inhibition of RhoA (Aburima et al. 2013; Oishi et al. 2012). In particular, one study shows platelet shape change through phosphorylation of RhoGDI α by PKA, and subsequent sequestration of RhoA into RhoA-RhoGDI α complexes (Oishi et al. 2012).

3.2 Actomyosin at the synapse

The actin cytoskeleton is a predominant component of the synaptic cytoskeleton at both pre- and postsynaptic compartments (**Figure 7A**) (Cingolani and Goda 2008). At the presynaptic compartment, it has been found to compose 2% of protein content (Wilhelm et al. 2014).

Despite a number of efforts from studies using electron microscopy, the specific structure of the actomyosin cytoskeleton at the presynaptic compartment remains under debate. Part of the reason for this might be that as the actin cytoskeleton is highly dynamic in nature, its specific structure may vary widely depending on experimental conditions, such as stages of synaptic vesicle recycling or synapse maturity. Furthermore, sample preparation may further affect the cytoskeleton, with different fixation protocols potentially producing different effects. Nonetheless, several studies seem to corroborate the presence of actin both at the active zone and within the synaptic vesicle pool.

3.2.1 Actin in the AZ

Direct evidence for actin filaments at the AZ is relatively scarce. GFP- β actin was found to colocalize well with Bassoon, as observed with conventional microscope (Miguel Morales, Colicos, and Goda 2000) and immunogold staining of actin shows actin staining of the AZ in electron micrographs (**Figure7C**) (Bloom et al. 2003).

Nonetheless, a number of reports have been produced of different filaments connecting synaptic vesicles to the AZ (Landis et al. 1988; Hirokawa et al. 1989). Some of these filaments were found to be short, interconnecting docked vesicles or directly docking vesicles at the AZ (Landis et al. 1988; A. A. Cole, Chen, and Reese 2016). Furthermore, short filaments extending from the active zone are found to tether vesicles (Cole, Chen, and Reese 2016; Hirokawa et al. 1989) most likely to facilitate vesicle replenishment during synaptic activity. However, the morphological identification of these filaments is difficult, with some studies suggesting these filaments might be composed of fodrin, rather than actin (Hirokawa et al. 1989).

3.2.2 Actin and Synaptic vesicle pools

A number of EM studies show long filaments extending either from the active zone or plasma membrane into the central synaptic vesicle pool (Hirokawa et al. 1989; Landis et al. 1988; Perkins et al. 2010; A. A. Cole, Chen, and Reese 2016). Although their nature is not specifically analyzed, they can be morphologically identified due to their helical structure (**Figure7B**) (Hirokawa et al. 1989).

Within the vesicle pool, actin is known to interact with a number of vesicle binding proteins including β -catenin and synapsin, among others (Bamji et al. 2003; Takamori et al. 2006; Fernández-Busnadiego et al. 2010). Although the specific function of this tethering remains under debate, a number of reports suggest their importance in keeping synaptic vesicles within the presynaptic bouton as well as immobilizing diffusing vesicles to restrain vesicle recycling (T A Ryan et al. 1996; Siksou et al. 2007; Fornasiero et al. 2012). Furthermore, functional studies have provided evidence for a role of actin itself in vesicle recycling. These functions will be reviewed in later sections.

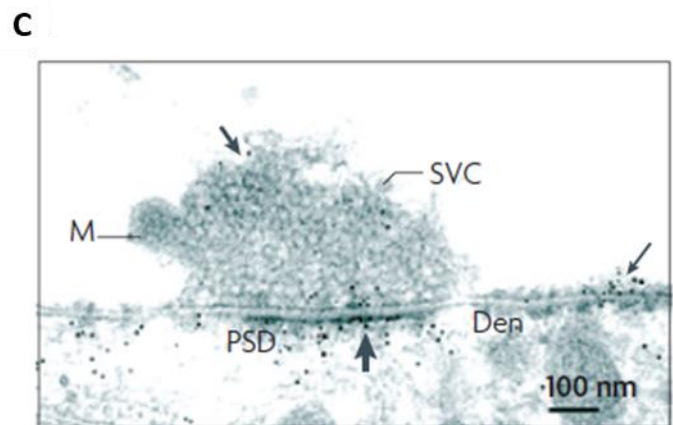
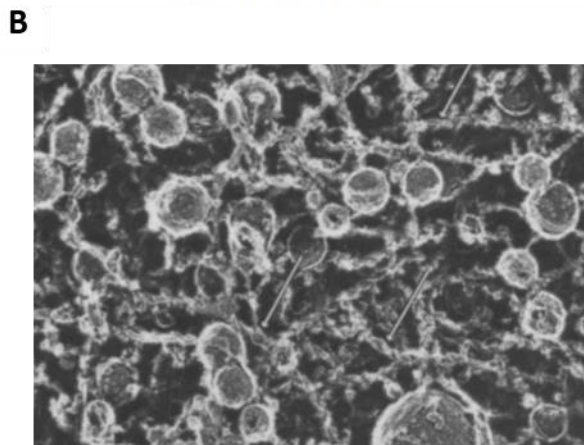
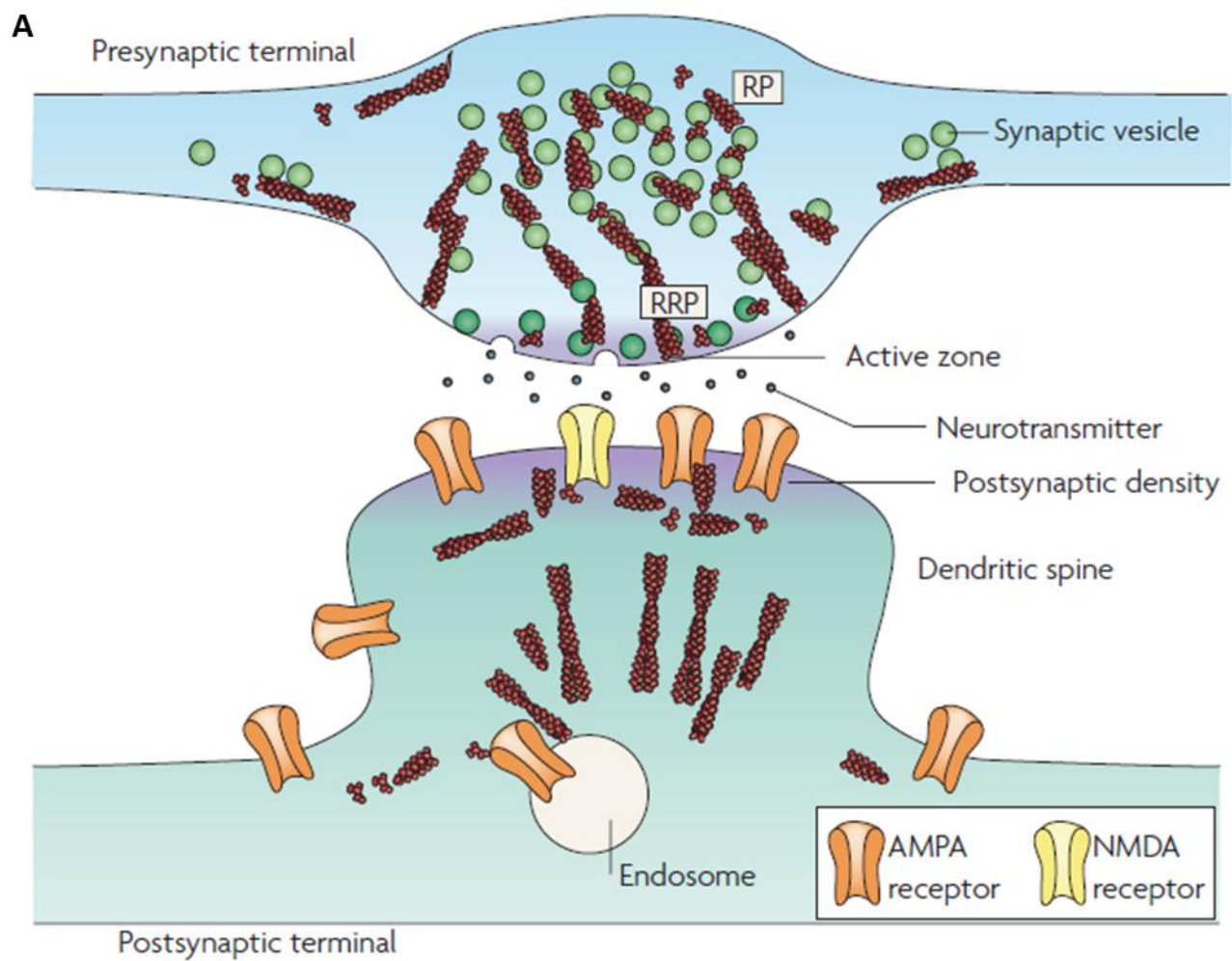


Figure 7. Actin at the synapse

(A) Schematic representation of the potential structure of the actin cytoskeleton at the synapse (*from Cingolani and Goda (2008)*). (B) Electron micrograph of synaptic vesicles tether to actin-like filaments (*adapted from Hirokawa et al. (1989)*). (C) Electron micrograph of a lamprey reticulospinal synapse with immunogold actin staining (arrows). Staining is present both the PSD and AZ, but also within the synaptic vesicle pool (*adapted from Bloom et al. (2003)*).

3.2.2.1 Presynaptic NMII

Direct evidence of the presence of non-muscle myosin II in presynaptic terminals is scarce. It has been shown that the NMIIB isoform is present in presynaptic sites at superior cervical ganglion neurons (SCGNs) (Takagishi et al. 2005), and both NMIIA and NMIIB isoforms have been found at mouse neuromuscular junctions (Vega-Riveroll et al. 2005). Blocking NMII activity has been found to affect vesicle recycling in certain models. These functions will be explored further below.

3.2.3 Actomyosin and synaptic function

Due to the difficulty of access of the presynaptic compartment, particularly at small central synapses, a consensus concerning the specific roles of the actomyosin cytoskeleton in neurotransmitter release remains to be reached. Part of the reason for this might be the diversity of models used to study presynaptic function, which include studies at hippocampal cultures, calyx of Held, neuromuscular junctions, and the lamprey reticulospinal synapse.

3.2.3.1 Actin cytoskeleton and endocytosis

A number of reports indicate activity-induced polymerization of the actin cytoskeleton (Bernstein, DeWit, and Bamberg 1998; Shupliakov et al. 2002; Trifaró et al. 2002; Bloom et al. 2003; Sankaranarayanan, Atluri, and Ryan 2003). The most coherent role suggested for this has been in endocytosis. In lamprey synapses, stabilization of actin filaments with phalloidin blocks vesicle recycling as observed through FM1-43 dye uptake (Bleckert, Photowala, and Alford 2012). Furthermore, at both the Calyx of Held and snake neuromuscular junctions, disruption of the actin cytoskeleton was found to inhibit RRP recovery under high frequency stimulation, without affecting low frequency evoked transmission (Kuromi and Kidokoro 1998; J. C. Cole, Villa, and Wilkinson 2000; Sakaba and Neher 2003; Lee et al. 2013; Miki et al. 2016). As RRP refilling is strongly dependent on the recycling pool, which principally arises from evoked endocytosis, these studies strongly suggest a role for actin filaments in vesicle endocytosis during recycling. Indeed, in *drosophila* expressing the *shibire* mutation, a temperature sensitive dynamin homolog, it was found that disruption of actin polymerization with cytochalasin D did not have a direct effect on the RRP but rather on the size of the recycling pool (Kuromi and Kidokoro 1998). While studies at central synapses are ambivalent, there is evidence that actin polymerization might

mediate certain types of endocytosis at hippocampal synapses, specifically compensatory endocytosis (Watanabe et al. 2013).

Furthermore, certain EM studies find the formation of elongated filaments in endocytic zones after stimulation (**Figure 8**) (Shupliakov et al. 2002; Bloom et al. 2003), and stabilization of the actin cytoskeleton was found to cause changes in the structure of clathrin-coated pits (Shupliakov et al. 2002). In addition, it was found in hippocampal synapses that, while recycling vesicles preferentially relocate close to the active zone, stabilization of the actin cytoskeleton prevented this relocation, and slowed sustained exocytosis during prolonged stimulation (Marra et al. 2012). These results strongly suggest a role for actin in redistributing vesicles to the recycling vesicle pool after endocytosis.

3.2.3.2 Actomyosin and synaptic vesicle tethering

Going seemingly against the studies reported above, certain studies have found facilitation of transmission upon actin filament disruption. In cultured chick sympathetic neurons it was found that actin depolymerization occurs in presynaptic terminal after prolonged stimulation, and preventing this depolymerization with phalloidin significantly reduced sustained release (Bernstein, DeWit, and Bamberg 1998). In hippocampal cultures, inducing depolymerization with latrunculin A was found to increase the frequency of small neurotransmitter induced currents (Miguel Morales, Colicos, and Goda 2000). Furthermore, at cultured frog neuromuscular junctions, it was found that depression of transmission induced by prolonged stimulation was prevented by latrunculin A, which was accompanied by microfilament disruption (Wang, Zheng, and Poo 1996). Taken together these studies suggest a second role for actin at the presynaptic compartment in what has been called a ‘barrier’ model, preventing excessive depletion of the vesicle pool upon sustained stimulation.

Several other trails of evidence support this role. A number of studies show that a majority of synaptic vesicles are immobile at the synapse, with recycling vesicles showing the most mobility (Gaffield, Rizzoli, and Betz 2006; Kamin et al. 2010). Depolymerization of the actin cytoskeleton has been found to increase the mobility of vesicles (Shtrahman et al. 2005; R. Jordan, Lemke, and Klingauf 2005), suggesting the integrity of the cytoskeleton at rest might restricts vesicle movement.

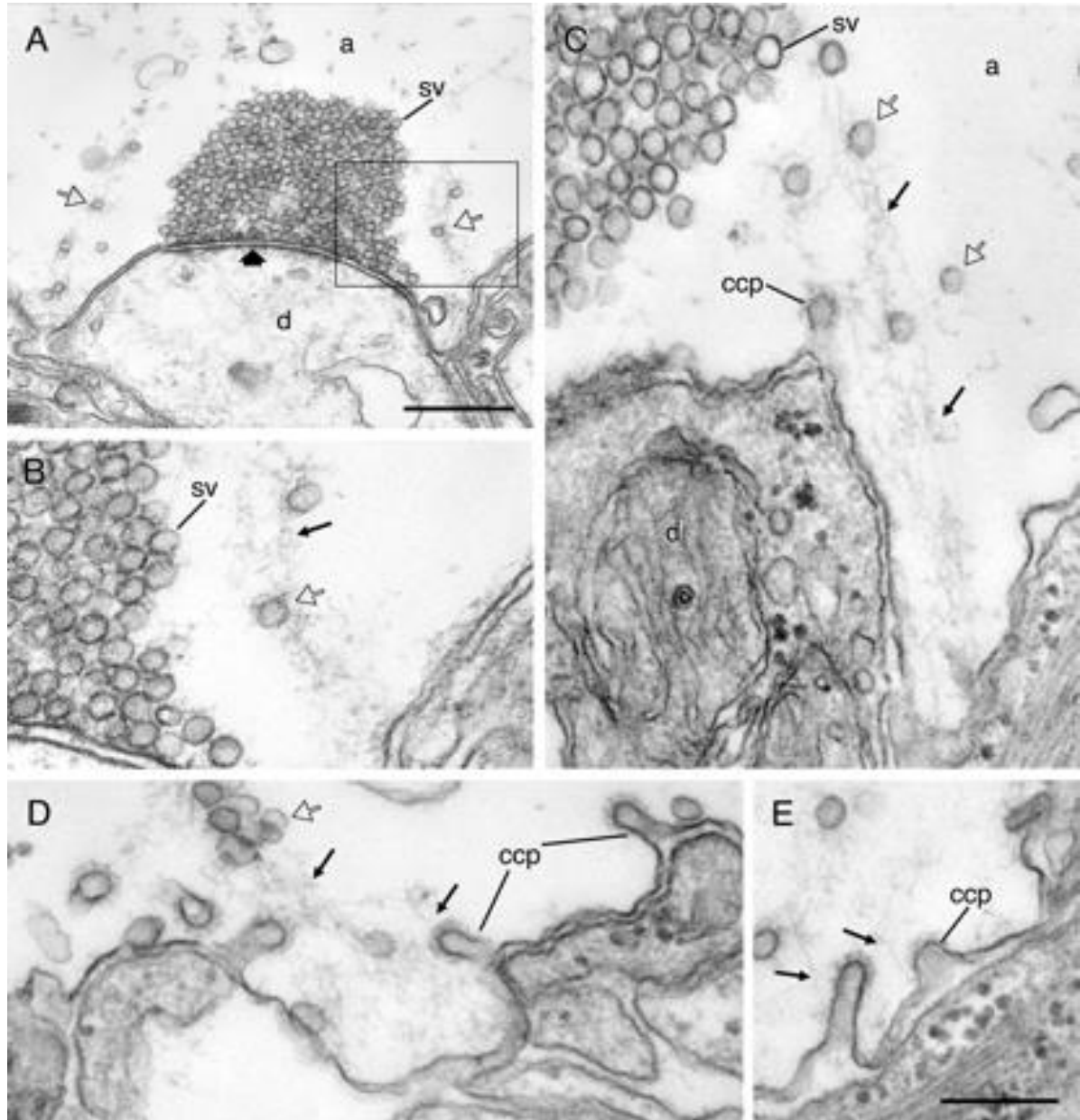


Figure 8. Actin-like filament polymerization at endocytic zone during synaptic activity

(A–C) Electron micrographs from two different synapses in axons that were microinjected with phalloidin and stimulated before fixation. Synaptic vesicles (open arrows) are tethered along filaments (thin arrows) extending from the endocytic zone toward the margin of the vesicle cluster. (D and E) Clathrin-coated pits (ccp) at the plasma membrane of the endocytic zone are attached by the neck to actin-like filaments (thin arrows). (Scale bars: A, 0.5 μm ; B–E, 0.2 μm .) (*adapted from Shupliakov et al. (2002)*)

As mentioned previously, the actomyosin cytoskeleton is known to bind to a number of vesicle binding proteins, which tether vesicles to each other as well as to the cytoskeleton (Landis et al. 1988; Hirokawa et al. 1989). One such binding protein that has been extensively studied is synapsin, which forms short filaments of 30-40nm long (Hirokawa et al. 1989), which tether vesicles together and to the actin cytoskeleton (Peters and Kaiserman-Abramof 1970; Landis et al. 1988; Hirokawa et al. 1989). Deletion of synapsin was found to reduce vesicle pool clustering (T A Ryan et al. 1996; Siksou et al. 2007; Fornasiero et al. 2012), with vesicles spreading out to extrasynaptic areas. Furthermore, synapsin deletion or phosphorylation has been found to increase vesicle mobility (Orenbuch et al. 2012; Gaffield, Rizzoli, and Betz 2006). Although changes in synapsin tethering do not necessarily indicate a similar role for actin, it could be inferred that disruption of the cytoskeleton integrity might unbind synapsin bound vesicles and therefore produce similar results.

3.2.3.3 Presynaptic NMII function

Much like the actin cytoskeleton, evidence for a role of non-muscle myosin II at the synapse is scarce and contradictory. At the Calyx of Held, inhibition of MLCK leads to increase in RRP size (Srinivasan, Kim, and von Gersdorff 2008). Conversely, at motorneuron excitatory synapses, activation of MLCK through LPA/LPA1 leads to decrease in transmission and reduces the number of vesicles in the RRP, observed through EM (García-Morales et al. 2015).

Alternatively, inhibition of NMII ATPase activity with the selective inhibitor blebbistatin was found to decrease transmission during prolonged activity in hippocampal cultures (Peng et al. 2012), as well as inhibit facilitation of transmission at cerebellar parallel fiber to MFI synapses (Miki et al. 2016). Furthermore, various MLCK inhibitors have been shown to inhibit transmission, particularly during sustained transmission both at hippocampal cultures (Timothy A. Ryan 1999; Yue and Xu 2014; L. Li et al. 2016) and SCGN cholinergic synapses (Mochida et al. 1994).

These studies also show contradiction with some showing preferential effects on exocytosis (Timothy A. Ryan 1999), while others show effects on endocytosis (Yue and Xu 2014). Furthermore, some studies show that the inhibitors used might not be specific to MLCK, with one study showing an effect of ML-7 produced through VGCCs rather than MLCK (Tokuoka and Goda 2006).

4 CB1R and the endocannabinoid system

While the psychoactive and therapeutic effects of cannabinoids have been known and exploited for thousands of years, the physiological mechanisms underlying these effects have only truly started to unravel in the past 20 years. With the main psychotropic compound of the cannabis plant, (-)- Δ^9 -tetrahydrocannabinol (Δ^9 -THC), being discovered in the mid-1960s ((Gaoni and Mechoulam 1964; Mechoulam and Gaoni 1967), it would be another 20 years before the necessary technological advancements could bring us the cloning and molecular identification of THC's main psychotropic agent in the brain, the cannabinoid-type 1 receptor (CB1R) (W. A. Devane et al. 1988; Bidaut-Russell, Devane, and Howlett 1990; Lisa A. Matsuda et al. 1990). Later research would identify this receptor not only as one of the most abundant transmembrane proteins in the brain (Y. Zhang et al. 2014), but as a major regulator of neuronal function through the endocannabinoid neurotransmitter system.

The endocannabinoid system is highly conserved throughout vertebrate species, especially among mammals. This is especially true when looking at the properties of CB1R expression and distribution. Not only is there 97-99% homology in the *cnr1* gene amino acid identity between mammals, but CB1R concentrations between brain areas is also well conserved between rodents (immunostaining) and humans (PET imaging). Furthermore, intracellular distributions of endocannabinoid metabolic enzymes has also been well conserved between rodents and humans (Ludányi et al. 2011). What these findings point to is not only a conserved evolutionary function for endocannabinoid signaling in vertebrates, but furthermore, they suggest a primary role for the ECS in fundamental brain function.

This chapter will introduce the components of the endocannabinoid system, its receptors, ligands and metabolic pathways, before focusing on the known functions of CB1R in development and synaptic transmission, and the known and putative signaling pathways mediating these functions.

4.1 Receptors, ligands, et al.: Properties of the endocannabinoid neurotransmitter system

Two phylogenetically similar receptors have been identified in mediating the majority of known physiological effects of cannabinoids, the cannabinoid-type 1 receptor (CB1R) and the cannabinoid-type 2 receptor (CB2R). Genetic sequencing and cloning has shown that both are seven transmembrane spanning class A G-protein coupled receptors (GPCRs), sharing 44% amino acid homology in humans (Munro, Thomas, and Abu-Shaar 1993). Identified, first through the binding of the phytocannabinoid Δ 9-THC, CB1R and CB2R remain the most established receptors of the ECS, answering for most of the reported effects of the recognized endocannabinoids, anandamide and 2AG. Nonetheless, as with other known neurotransmitter system, there is a certain degree of cross-talk between different systems, with endocannabinoids binding other known receptors, and receptors responding to other known ligands. Furthermore, an additional number of candidate orphan receptors and ligands have been suggested for incorporation under the ECS umbrella.

This section will review the properties of the main cannabinoid elements within the endocannabinoid system as well as briefly review their potential crosstalk with other systems and the novel ECS candidates suggested.

4.1.1 Receptors

4.1.1.1 CB2R expression and location

The CB2R receptor is encoded by the single-exon CNR2 gene located on the human chromosome 1, and on chromosomes 4 and 5 of mice and rats respectively. The receptor is highly conserved between species with an 82% sequence identity between human and mouse and an 81% sequence identity between human and rat (Munro, Thomas, and Abu-Shaar 1993; Shire et al. 1996).

The CB2 receptor is mostly expressed in the periphery, particularly within immune cells (Munro et al., 1993; Shire et al., 1996), with a higher concentration in B cells, NK cells and macrophages, respectively (Bouaboula et al. 1993; Galiègue et al. 1995). As such it is thought to mediate a number of the non-psychoactive effects of cannabinoids, such as their anti-inflammatory and analgesic effects. Immunoreactivity and ligand binding studies have also reported CB2R presence in a number of other tissue types, including pulmonary, bone, and gastrointestinal cells (Atwood and Mackie 2010).

Although initial Northern blotting and in situ hybridization studies did not report any significant expression in the brain (Munro, Thomas, and Abu-Shaar 1993; Schatz et al. 1997), later studies, using the more sensitive PCR method, would find low levels of CNS expression, then attributed to activated microglial cells (Carlisle et al. 2002; Walter et al. 2003; Stella 2004). An RNA sequencing study of mouse cortex cell types would later find highest expressions in endothelial cortical cells, closely followed by microglia, with low but non-negligible amounts expressed in neurons (Y. Zhang et al. 2014). Several studies have reported immunoreactivity of CB2R in various brain regions (Atwood and Mackie 2010), including in granule and hippocampal neuronal cultures, supporting a neuronal locus for CB2R. However, there remains skepticism towards a neuronal CB2R, opponents putting forth the non-specificity of CB2R antibodies and ligands as well as the mixed results from mRNA detection studies as confounding factors.

4.1.1.2 CB1R expression and location

CB1R is a 472 amino acid receptor coded by the *cnr1* gene, located on chromosome 6 in humans. It is highly conserved between vertebrates, with 98% sequence identity between rats and humans (Lisa A. Matsuda et al. 1990; Gerard et al. 1991).

With CB2R mainly considered the ‘peripheral’ cannabinoid receptor, CB1R is unequivocally the ‘brain’ cannabinoid receptor (Lisa A. Matsuda et al. 1990; Galiègue et al. 1995), with highest expression levels in the brain as compared to the periphery (Galiègue et al. 1995). Nonetheless, CB1R expression is also present at lower levels in a number of peripheral tissues, namely hepatic, adipose, vascular, cardiac, reproductive, skeletal, and cutaneous tissues (Galiègue et al. 1995).

In the brain, CB1R has been reported as one of the most abundant GPCRs (L A Matsuda, Bonner, and Lolait 1993). Namely, CB1R has been identified as the 6th most abundantly expressed transmembrane receptor in cortical neurons, after protein tyrosine phosphatase receptor, AMPA and NMDA subunits (Y. Zhang et al. 2014). Radioligand binding assays have shown highest concentrations in the basal ganglia, the granular layer of the cerebellum, the dentate gyrus and CA3 regions of the hippocampus and the inner layers of the olfactory bulb. Lowest binding was found in the brain stem and spinal cord (Herkenham et al. 1991). This distribution was found to be conserved across mammalian species (Herkenham et al. 1990), however, there is evidence of a discrepancy in cell-type expression between species. Namely, it was found that while CB1R is most highly expressed in neurons as compared to

non-neuronal brain cells (10-fold higher in humans and 4-fold higher in mice), mice show a higher expression in astrocytes as compared to humans (Y. Zhang et al. 2014).

CB1R localization has further been found to differ between neuronal types. Immunoreactivity studies of CB1R found it is expressed at much higher densities in GABAergic neurons than glutamatergic neurons in the hippocampus (Katona et al. 1999), amygdala (Katona et al. 2001), and cortex (M Morales et al. 2004; Hill et al. 2007; Bodor et al. 2005; Vitalis et al. 2008). Furthermore, these studies show a strikingly preferential immunoreactivity of CB1R in cholecystokinin (CCK)-positive interneurons as compared to parvalbumin-positive interneurons. Nonetheless, CB1Rs are indeed found to be expressed in glutamatergic neurons (Marsicano and Lutz 1999; Kawamura 2006; Katona 2006), albeit at a much lower level, where they mediate a number of forms of synaptic plasticity. Furthermore, one striking study has found that glutamatergic CB1Rs bind more readily to GTP γ S when stimulated than GABAergic CB1Rs (Steindel et al. 2013). Although a mechanism for this discrepancy in binding properties is not put forth, these findings suggest that while CB1R is less concentrated in glutamatergic than GABAergic neurons, glutamatergic CB1Rs may be more active.

A discrepancy in the location of CB1R can also be found within the individual neuron. Both immunoreactivity and EM studies find that surface expression of CB1R is highly polarized to the axonal membrane both *in vitro* (Coutts et al. 2001; Leterrier et al. 2006; McDonald et al. 2007) (Coutts et al. 2001; Leterrier et al. 2006; McDonald et al. 2007) and *in vivo* (Katona et al. 1999; Katona et al. 2001; Pickel et al. 2004; Nyíri et al. 2005; Bodor et al. 2005; Kawamura 2006; Mátyás et al. 2006; Thibault et al. 2013). Nonetheless, a great majority of receptors are located to intracellular endosomes in the somatodendritic compartment of both mature (Katona et al. 2001; Bodor et al. 2005; Coutts et al. 2001; Leterrier et al. 2006; Thibault et al. 2013) and embryonic neurons (Vitalis et al. 2008). Furthermore, the size of this endosomal pool was found to increase after *in vivo* treatment with CB1R agonists, both in somatodendritic compartments as well as in axon terminals (Thibault et al. 2013). This endosomal pool is was found to be especially important in the axonal targeting and recycling of CB1R (Leterrier et al. 2006; McDonald et al. 2007).

4.1.1.3 Other putative receptors

Of all the suggested putative endocannabinoid receptors, the GPR55 orphan receptor is the most likely candidate, as it has been found to mediate many of the non-CB1R/CB2R effects induced by cannabinoids (Baker et al. 2006).

4.1.2 Ligands

Two major endocannabinoids were the first to be discovered and remain the most established as part of the endocannabinoid system. First, N-arachidonylethanolamide (AEA), also known as anandamide, was extracted from lipid soluble brain fractions (W. Devane et al. 1992). Second, 2-arachidonoylglycerol (2-AG) was identified (Mechoulam et al. 1995; Sugiura et al. 1995). Both these endocannabinoids are lipid-based molecules of the eicosanoid family of poly-unsaturated fatty acids, and hold a similar molecular structure both to each other but also to certain phytocannabinoids such as delta-9-THC, which is what initially led to their isolation from lipid brain fractions. Due to their lipophilic nature, they are mainly found at the plasma membrane, where they are synthesized through multiple biosynthetic pathways in response to elevated intracellular Ca^{2+} levels or $G_{q/11}$ protein activation. Other molecules interacting with the endocannabinoid receptors have since been described.

4.1.2.1 Anandamide

Anandamide is a partial agonist to both CB1R and CB2R, as well as being an agonist of the transient receptor potential cation channel V1 (TRPV1). It has also been found to activate the GPR55 orphan receptor, as well as certain ion channels.

Several pathways have been described in the synthesis of anandamide (G. M. Simon and Cravatt 2010). The most characterized involves the hydrolysis of N-acyl-phosphatidylethanolamines (NAPEs) by NAPE-hydrolyzing phospholipase D (NAPE-PLD). Its main degradation enzyme is fatty-acid amine hydrolase (FAAH) (Kano et al. 2009), although other degradation pathways have been also been described, such as anandamide oxidation through cyclooxygenase-2 (COX-2).

4.1.2.2 2AG

2AG is a full agonist of both CB1R and CB2R. It has also been found to bind to other receptors however, including putative orphan receptors of the ECS, as well as other GPCRs.

The most described pathway in 2AG synthesis involves the enzyme sn-1-diacylglycerol lipases (DAGL) α and β , which catalyzes a Ca^{2+} -dependent hydrolysis of arachidonic acid-containing diacylglycerols (DAGs) among other membrane phospholipids. Other reported synthetic pathways include sequential reactions by phospholipase A1 and lysophosphatidylinositol-specific phospholipase C (lyso-PLC), and phosphatase-mediated conversion of 2-arachidonoyl lysophosphatidic acid to 2-AG (Kano et al. 2009).

Importantly, the Ca^{2+} -sensitivity of DAGL and the PLC sensitivity of other synthetic reactions means many of these synthetic reactions can be initiated either through Ca^{2+} increases, as through entry through Ca^{2+} -permeable channels such as NMDA, or through Gq/11 activation by different GPCRs, such as metabotropic glutamate, GABA, acetylcholine, dopamine or serotonin receptors.

2AG degradation is mainly catalyzed by monoacylglycerol lipase (MAGL). Other pathways include the hydrolases α/β -hydrolase domain-containing 6 and 12 (ABHD6, ABHD12) (Marrs et al. 2010), and, like anandamide, it has been found to be degraded by FAAH and COX-2 (Kano et al. 2009); however the contribution of these pathways relative to MAGL-induced degradation is thought to be negligible.

4.1.2.3 Other endocannabinoids

Other members of the eicosanoid family found in neurons have also been found to activate CB1R. These include dihomi- γ -linolenoyl ethanolamide and docosatetraenylethanolamide. This is also the case for several other arachidonic-acid derived molecules, including 2-arachidonoylglyceryl ether (noladin ether), O-arachidonoylethanolamine (virhodmaine) and N-arachidonoyldopamine (NADA) (Bisogno, Ligresti, and Di Marzo 2005).

Of these, most have been associated with the CB1R receptor, with noladine ether being the only one to show full agonism at CB2R (Shoemaker 2005).

4.1.3 Extracellular ligand release

The lipophilic nature of endocannabinoids restricts them to lipid membranes within the cell, preventing them from being released and diffused freely in the extracellular medium as other neurotransmitters. While it has been shown that endocannabinoids will diffuse 2 dimensionally along membranes to constitutively activate CB1Rs, there is also strong evidence that intercellular signaling does occur, the retrograde nature of eCB- induced synaptic plasticity, as detailed in future sections, being one of several examples. Several

methods, including the existence of an eCB lipid transporter or exosomal signalling, have thus been postulated to help the intercellular signaling of endocannabinoids. The nature of this mechanism remains to be determined (Alger and Kim 2011).

4.2 CB1R downstream signaling

CB1R was found to recruit similar pathways in both neuronal cells and non-polarized cells (Glass and Felder 1997; Childers and Deadwyler 1996; Pan, Ikeda, and Lewis 1996). As with other GPCRS, CB1R typically exposes a preferential coupling to one type of G-protein heterotrimer, namely $G_{i/o}$, and a majority of the synaptic effects of CB1R are thought to occur through $G_{i/o}$ signaling. Nonetheless, GPCRS are known to be able to couple to different $G\alpha$ subunits depending on the cellular environment, although the specific conditions mediating these differences are not properly understood. Indeed, there are reports of CB1R coupling to G-protein signaling pathways other than that attributed to $G_{i/o}$. These reports either provide direct evidence of G-protein coupling or show recruitment of downstream proteins known to be preferentially activated by specific G-proteins. Furthermore, non G-protein related signaling has also been reported. This section will briefly describe the canonical $G_{i/o}$ signaling recruitment under CB1R, as well as other non-conventional pathways that have been attributed to it.

4.2.1.1 Fundamentals of G-protein coupled receptors (GPCRs)

G-protein coupled receptors (GPCRs) are membrane receptors which share a common 7 transmembrane domain structure (Pierce et al., 2002). Over 1000 GPCRS have been identified in the human genome (Foord et al. 2005; Wettschureck and Offermanns 2005), and it has been estimated that 80% of hormones and neurotransmitters can act through them to mediate signal transduction (Birnbaumer, Abramowitz, and Brown 1990). Despite the wide diversity of GPCRS, it would appear that they share a common mechanism of activation through their intracellular C-terminal coupling to heterotrimeric G-proteins (Lebon et al. 2011). Indeed, the vast majority of signal transduction conducted by GPCRS is undertaken by these G-proteins.

Heterotrimeric G-proteins are composed of three subunits, α , β , and γ . The α subunit is an enzyme capable of hydrolysing guanosyl triphosphate (GTP) (John K Northup et al. 1980; J. K. Northup, Sternweis, and Gilman 1983), a property which gave the G-protein its name. Binding of the α subunit to GDP allows the binding of α to $\beta\gamma$ subunit dimers, conferring the ability of the newly formed heterotrimer to bind to ligand-activated or constitutionally activated GPCRS. Their coupling allows the release of GDP and its replacement by GTP. This

exchange uncouples the G-protein from the receptor and the release of the $\beta\gamma$ dimer, which goes on to induce various signaling pathways, while the now activated α subunit may itself engage with its own downstream effectors (McCudden et al. 2005).

The specific effectors recruited downstream of G-protein activation depends on the subunit variant activated. Heterotrimeric G-proteins have been classified in 4 wider families based on the degree of similarity of their α subunit sequences: G_s , $G_{i/o}$, $G_{q/11}$, and $G_{12/13}$ (M. I. Simon, Strathmann, and Gautam 1991). Their main established signaling pathways are summarized in **(Figure 9)**. Furthermore, $\beta\gamma$ subunits have their own signaling pathways, although these do not seem to differ between G-protein families. They include the activation of PLC- β , PI3K and GIRK channels, and the inhibition of P/Q-type and N-type Ca^{2+} channels (Wettschureck and Offermanns 2005). Of interest, $G\beta\gamma$ has also been found to interact with vesicle fusion machinery, including certain SNAREs (Betke, Wells, and Hamm 2012).

Furthermore, while GPCRs display a preference for certain types of $G\alpha$ subunits, they have

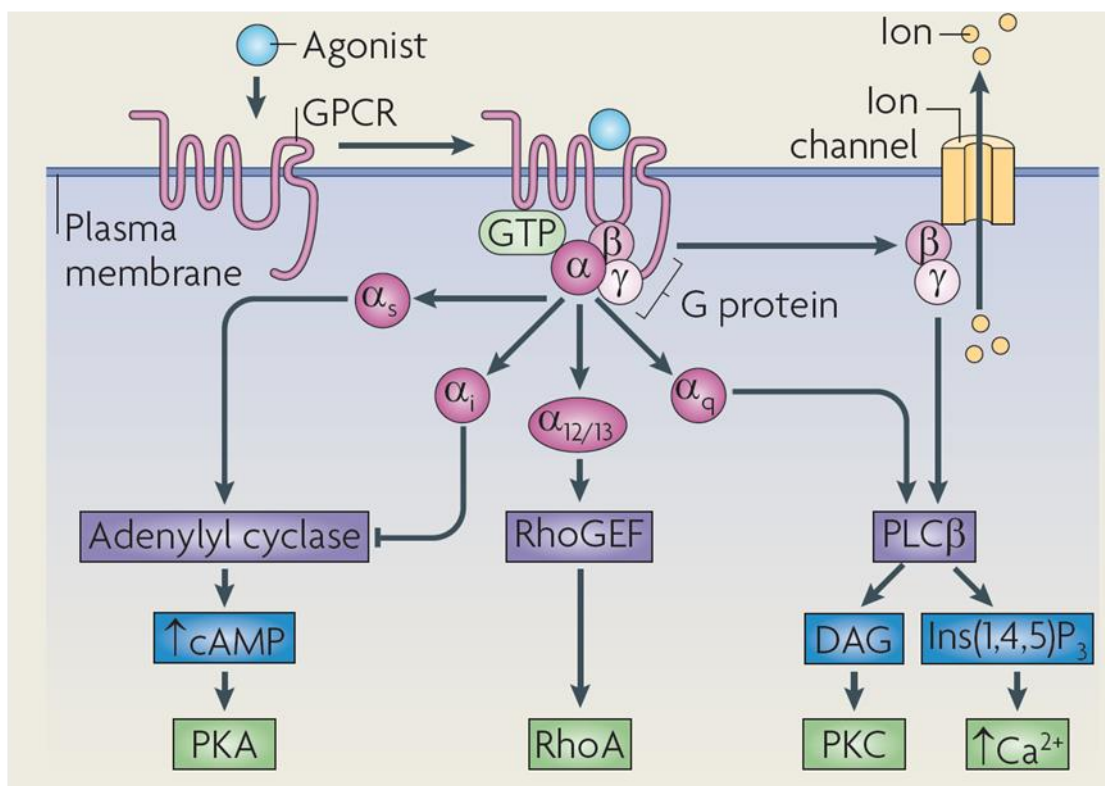


Figure 9. Preferential signaling pathways of G-protein subunits

(adapted from Riter and Hall (2009))

been found to recruit different downstream signaling pathways in different contexts. The specific reasons affecting preference for different G-proteins in different cellular environments is relatively unknown, with conditions on a GPCR's active state and the local membrane lipid composition having been suggested (Goddard and Watts 2012).

Taking this into account, CB1R signaling has also been found to be mediated by various pathways associated to different G-proteins.

4.2.2 G β / γ signaling

Recruitment of the β/γ signaling pathway was found under CB1R activation. Namely, CB1R activation was found to inhibit L- (Gebremedhin et al. 1999), Q- (Mackie et al. 1995), and N-type VGCCs (Mackie and Hille 1992; Pan, Ikeda, and Lewis 1996; Wilson and Nicoll 2001b) as well as activating G-protein-coupled inwardly rectifying potassium channels (GIRKS) (Mackie et al. 1995; Bacci, Huguenard, and Prince 2004; Luján, Maylie, and Adelman 2009). This pathway is particularly thought to mediate the short-term forms of CB1R induced synaptic plasticity.

The PLC β /PKC signaling branch of the G β/γ pathway was also found to be recruited under CB1R activation. Namely 2AG was found to activate phospholipase C β (PLC β) and subsequent IP3 production in neuroblastomas (Allyn C. Howlett and Mukhopadhyay 2000). Furthermore, anandamide was found to affect reserve pool access in neuronal synaptosomes through a PKC-dependent mechanism (Cannizzaro et al. 2006).

CB1R-activation was also found to recruit mitogen-activated protein kinase (MAPK) through activation of phosphoinositide 3-kinase (PI3K) (Greenhough et al. 2007; López-Cardona et al. 2017) as well as c-Jun N-terminal kinase (JNK) (Derkinderen et al. 2001; J. Liu et al. 2000; Rueda et al. 2000), both known effectors downstream of G β/γ .

4.2.3 G $_{i/o}$ signaling

CB1Rs have predominantly been found to couple to G $_{i/o}$ proteins. Indeed, one of the first studies to identify CB1R found it to inhibit adenylate cyclase activity, a telltale sign of G $_{ai/o}$ recruitment. Indeed this effect was blocked by pertussis toxin, a selective G $_{ai/o}$ inhibitor (Lisa A. Matsuda et al. 1990; A C Howlett and Fleming 1984). A number of studies since have found CB1R-induced effects to be pertussis toxin sensitive, both in neurons and non-polarized cells. Specifically, in neuroblastoma cells, it was found that CB1R could couple to all three

G α i subtypes (Mukhopadhyay and Howlett 2001). Importantly, however, this preference was found to change depending on the CB1R-agonist employed (Bonhaus et al. 1998).

Furthermore, a number of accounts report that activation of CB1R leads to the inhibition of the cAMP/PKA pathway (Childers and Deadwyler 1996) the best known effectors of adenylate cyclase. This pathway is known to regulate a number of different effectors including the phosphorylation of synaptic vesicle interacting proteins such as synapsins, as well as various actin binding proteins, among others. The specific effectors affected by CB1R-induced cAMP/PKA inhibition are poorly characterized although several of them have been described. For example, PKA inhibition through CB1R was found to increase ERK1/2 activity (Davis, Ronesi, and Lovinger 2003).

4.2.4 G_s signaling

Several studies have found that CB1R activation can activate the cAMP/PKA pathway, seemingly through G_s recruitment. Specifically, it has been shown that exacerbating G_{i/o} availability, either by co-activating CB1R with another G_{i/o} coupled receptor, D2R, or through pertussis toxin, CB1R activation would induce activation of cAMP (Glass and Felder 1997). Furthermore, it was found that recruitment of this pathway under CB1R was agonist-sensitive (Bonhaus et al. 1998).

4.2.5 G_{12/13} signaling

Although direct recruitment of G_{12/13} under CB1R has not been shown, several accounts report the recruitment of the RhoA/ROCK signaling pathway, the principal effector pathway of the G_{12/13} protein. Indeed, RhoA/ROCK activation under CB1R was found in both cultured neurons and neuroblastoma cells (Berghuis et al. 2007; Ishii and Chun 2002). This does not necessarily imply the recruitment of G_{12/13}, however, as RhoA recruitment under CB1R was found to be pertussis toxin-sensitive in macrophages (Mai et al. 2015). Furthermore, in platelets, exposure to 2-AG was found to activate ROCK through PI3K and AKT (Signorello and Leoncini 2014), a preferential pathway of the G-protein $\beta\gamma$ subunits.

4.2.6 G_{q/11} type signaling

CB1Rs in astrocytes have been found to couple to G_{q/11} (Navarrete and Araque 2008). Furthermore, transfected CB1R was found to couple to G_{q/11} and PLC β signaling in HEK-293 cells (Lauckner, Hille, and Mackie 2005).

4.2.6.1 Other pathways

CB1R also can dimerize with itself as well as form heterodimers with other receptors, such as the dopamine D2 receptor or the orexin 1 receptor (OX1R) (Hudson, Hébert, and Kelly 2010). Although the effects of these interactions aren't clear, the resulting dimerization might facilitate the combination of different signaling pathways.

4.3 CB1R-mediated synaptic plasticity

In the early 1990's, it was discovered that electrical depolarization of postsynaptic neurons prevented the release of neurotransmitter from presynaptic sites (Llano, Leresche, and Marty 1991; Pitler and Alger 1992). These findings suggested a retrograde feedback mechanism by which postsynaptic activity could regulate presynaptic inputs. A decade later, studies using specific agonists and antagonists would find that this phenomenon was mediated by CB1R activation (Wilson and Nicoll 2001a; Ohno-Shosaku, Maejima, and Kano 2001).

Although retrograde eCB signaling is not the only form of retrograde synaptic plasticity in the brain, nitric oxide (NO) and BDNF induced synaptic plasticity being two others, it is, if not the most ubiquitous, the most commonly reported. A substantial number of studies reporting this retrograde nature of CB1R-induced synaptic modulation have since both confirmed and detailed this mechanism. Firstly, it was found that CB1R is principally located at the axon, where it is ideally located to modulate presynaptic activity. Secondly, it was found that the main synthetic enzyme of 2-AG, DAGL α , is mainly located postsynaptically (**Figure 10 BC**) (Bisogno et al. 2003; Ludányi et al. 2011) where it is anchored by PSD proteins (Roloff et al. 2010), and activated by elevated Ca²⁺ levels and G_{q/11} recruitment (**Figure 10B**), an ideal configuration for on demand synthesis and retrograde release of 2AG. Indeed, retrograde CB1R-induced synaptic signaling is abolished in DAGL α 1a KO mice (Tanimura et al. 2010; Gao et al. 2010).

Different forms of CB1R-induced plasticity have been identified, although their specific induction and maintenance parameters have been found to differ depending on the brain area and cell type affected. Importantly, while the endogenous regulation of endocannabinoid-mediated synaptic plasticity is mainly retrograde, the retrograde component of this plasticity can be bypassed through direct activation of CB1R although certain induction parameters have to be conserved. Some rare non-retrograde forms of CB1R induced plasticity have been also been observed (reviewed in (Chevalleyre, Takahashi, and Castillo 2006; Castillo et al.

2012)). This section will outline the main forms of CB1R-induced plasticity and their known mechanisms of action.

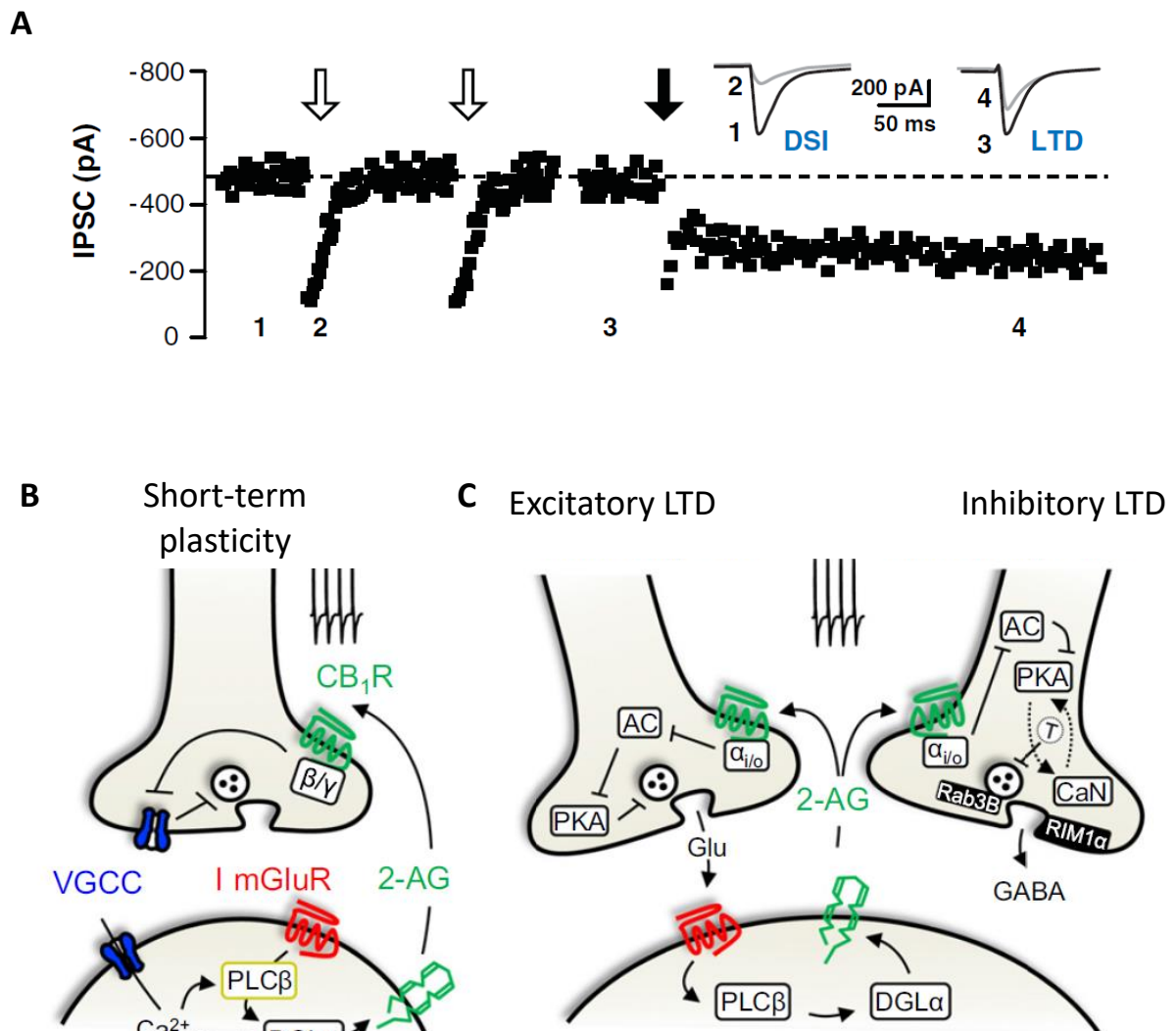


Figure 10. Mechanisms of CB1R-induced synaptic plasticity

(A) Example traces of electrophysiological recordings from an inhibitory afferent in the hippocampus, under induction of short-term plasticity (DSI; open arrows) and long-term plasticity (I-LTD; full arrows). While DSI is very short, lasting no longer than a minute, LTD is prolonged over 30 minutes after induction. (*adapted from Chevaleyre et al. (2006)*). (B) CB1R induced short term depression. Retrograde activation of CB1R through 2-AG induces inhibition of presynaptic VGCCs through $G_{\beta\gamma}$. (C) Retrograde activation of CB1R induces long-term depression (LTD) at both inhibitory and excitatory synapses. Activation of the $G_{\alpha_{i/o}}$ subunit through CB1R induces inhibition of the AC/cAMP/PKA pathway leading to long-term inhibition of neurotransmitter release through unknown targets (T). At inhibitory synapses, potential targets include calcineurin (CaN) and RIM1 α . (*adapted from Castillo et al. (2012)*).

4.3.1 Short-term depression (STD)

Found at both excitatory and inhibitory synapses. The most common forms found are depolarization-induced suppression of inhibition (DSI) and depolarization-induced suppression of excitation (DSE). These are differentiated only by the type of neurotransmitter release affected, i.e. inhibition of GABA or glycine release for DSI and inhibition of glutamate release for DSE. Accounts of both have been reported in most all CB1R-concentrated brain areas, including the hippocampus, cerebellum, corticostriatal projections...

As mentioned previously, these modes of plasticity occur endogenously through retrograde endocannabinoid signaling and activation of presynaptic CB1R receptors. They can be reproduced exogenously however, through phytocannabinoid or synthetic CB1R-agonist application. As opposed to long-term plasticity, these forms of plasticity occur on the timescale of milliseconds to 1 or 2 minutes. Release inhibition is mainly thought to occur through $G\beta/\gamma$ signaling, through inhibition of Q- and N-type VGCCs (Wilson, Kunos, and Nicoll 2001; Varma et al. 2002) and activation of GIRK channels, thus inhibiting SV Ca^{2+} dependent priming and hyperpolarizing the presynaptic membrane, respectively.

4.3.2 Long-term depression (LTD)

As with short-term forms, CB1R-induced long-term suppression of neurotransmitter release is found to occur through retrograde eCB signaling both at inhibitory (I-LTD) and excitatory (E-LTD) synapses. Both are found to occur ubiquitously throughout the brain.

4.3.2.1 Induction, maintenance and calcium regulation

Long-term forms of CB1R-induced synaptic plasticity differ from short-term forms by their duration, induction and maintenance, and signaling pathways. LTD can occur from 30 minutes to several hours. Furthermore, LTD induction was found to depend on a prolonged activation of CB1R receptors ($>10\text{min}$) (Chevalleyre and Castillo 2003; Ronesi 2004) as well as an increase in presynaptic Ca^{2+} (Singla, Kreitzer, and Malenka 2007), as opposed to eCB-STD. Importantly, CB1R activation was only found to be necessary for the induction of LTD, as agonist washout or antagonist application after induction does not reverse the depression. In addition, although it was found that LTD could be induced exogenously through CB1R agonists, CB1R activation was not always found to be sufficient in LTD induction (Chevalleyre, Takahashi, and Castillo 2006). The specific reason for this is unclear, although it has been speculated that an increase in presynaptic Ca^{2+} might be necessary for LTD

induction, as would occur during presynaptic depolarization in retrograde eCB signaling paradigms. Indeed, at GABAergic synapses, it was found that regulating presynaptic activity with TTX, a Ca^{2+} channel inhibitor, would determine whether CB1R-activation would induce a STD or a LTD (Singla, Kreitzer, and Malenka 2007). It was found however that this Ca^{2+} dependence might differ between synapses (Adermark, Talani, and Lovinger 2009; Nahir, Lindsly, and Frazier 2010).

The dependence on Ca^{2+} holds weight as many signalling elements necessary for long-term plasticity are Ca^{2+} -dependent, such as certain kinases. For example, calcineurin, a Ca^{2+} -activated phosphatase, was found to be necessary for eCB-LTD at hippocampal synapses (Heifets, Chevaleyre, and Castillo 2008).

4.3.2.2 cAMP/PKA

Finally, as with other forms of presynaptic long-term plasticity, the specific mechanisms employed in maintaining LTD remain elusive. Several studies have found CB1R-dependent LTD to be pertussis toxin sensitive and cAMP/PKA-dependent (Chevaleyre et al. 2007), implying activation of the $G_{i/o}$ signaling pathway. However, previous studies had suggested that CB1R agonists suppress action-potential driven synaptic responses independently of PKA (Azad et al. 2003; Daniel, Rancillac, and Crepel 2004; Robbe et al. 2002).

4.3.2.3 Protein synthesis

Supporting the protein synthesis model of long-term plasticity mentioned in the previous chapter, one recent study has further shown that hippocampal iLTD was dependent on local axonal protein synthesis (Younts et al. 2016). In accordance, previous studies had found that protein translation was necessary for CB1R-LTD (Yin et al. 2006; Kellogg, Mackie, and Straiker 2009; Yuan and Burrell 2013), although their results suggest it may be more necessary for the maintenance rather than the induction phase (Yin et al. 2006). However, other studies did not find eCB-LTD to be affected by protein synthesis inhibitors in the nucleus accumbens (Kwang Mook Jung et al. 2012), although their methods may have only affected post-synaptic synthesis. Importantly, none of these studies specify a mechanism by which neurotransmitter release may be affected under eCB-LTD.

4.3.2.4 Vesicle release machinery

Several studies have reported the importance of the AZ protein RIM1 α in LTD induction. Indeed, I-LTD was found to be abolished in RIM1 α KO mice in both the hippocampus and

the nucleus accumbens (Chevaleyre et al. 2007; Grueter, Brasnjo, and Malenka 2010), suggesting a direct effect of CB1R-activation on synaptic vesicle docking . Authors suggest a model by which a decrease in PKA activation under CB1R activation and $G_{i/o}$ recruitment may lead to a dephosphorylation of RIM1 α , inhibiting its vesicle docking properties.

4.3.2.5 Vesicle pool distribution

Interestingly, several reports both in slices and hippocampal cultures have found an effect of synaptic vesicle distribution and recycling under prolonged CB1R activation, although they were not reported in typical LTD induction paradigms. Several studies report that prolonged CB1R activation suppresses vesicle exocytosis under strong stimulation as imaged through FM1-43 or pHluorin markers (Ramírez-Franco et al. 2014). One study also shows that endocytosis is reduced upon prolonged CB1R activation in cultured hippocampal neurons (Ramírez-Franco et al. 2014). Furthermore, two independent reports have found a reduced number of synaptic vesicles located near the AZ under CB1R activation both at cerebellar granule neurons (Ramírez-Franco et al. 2014) and motoneurons (García-Morales, Montero, and Moreno-López 2015), suggesting a reduced RRP size. Conversely, shorter CB1R activation periods (0.5-3min) were not found to affect RRP size in cultured hippocampal neurons (Sullivan 1999), suggesting that CB1R activation has a direct effect on synaptic vesicle recycling under conditions suitable for LTD induction but not STD induction. The specific mechanisms linking CB1R activation to RRP depletion are not explored, however.

4.4 CB1R in neural development

In the past decade, a novel function of CB1R in different stages of neural development has come to light, highlighting the importance of the ECS not only in synaptic plasticity but in general neural plasticity throughout life. Indeed, not only is CB1R a preferentially neural marker at adulthood, as mentioned previously, it's expression pattern further follows neuronal differentiation and polarization steps during neural development (Galve-Roperh et al. 2013). This expression is found to have functional consequences on neurogenesis, neurite polarization, axonal guidance and synaptogenesis, the essential stages of brain wiring. This section will review some of these properties and what is known of the signaling mechanisms underlying them.

4.4.1 CB1R expression in development

CB1R expression is already present at early fetal stages in a number of brain areas (Fernández-Ruiz et al. 1999; Vitalis et al. 2008). Furthermore, while CB1R expression is relatively low in neuroepithelial progenitor cells in early embryonic stages, levels increase along neural differentiation stages (Galve-Roperh et al. 2013). This is particularly true of the GABAergic neurons within the hippocampus, cerebellum, caudate putamen and cortex, where CB1R gradually increases throughout embryonic development before reaching peak levels in adulthood (Romero et al. 1998; Berghuis et al. 2007; Vitalis et al. 2008). A similar gradual increase throughout neural development is also seen in white matter areas, however peak levels are reached earlier and then decline before reaching stable levels during adulthood (Romero et al. 1997; Berghuis et al. 2007; Vitalis et al. 2008; Mulder et al. 2008). Indeed, contrarily to mature neurons, CB1R is highly expressed in glutamatergic neurons such as the projection neurons found in white matter areas during development. Glutamatergic expression then decreases after birth (Romero et al. 1997; Berghuis et al. 2007; Vitalis et al. 2008; Mulder et al. 2008), explaining its preferential expression in GABAergic neurons in adulthood.

4.4.2 CB1R in neuronal morphogenesis

As its progressive expression throughout neuronal development would suggest (Galve-Roperh et al. 2013), CB1R is expected to play an especially important role in the later stages of neuron growth. While certain studies have found a role for CB1R in early stages such as neural progenitor proliferation and differentiation, these findings are often controversial with different studies showing different effects depending on the treatment type and duration, as well as the cellular model used (Gaffuri, Ladarre, and Lenkei 2012; Galve-Roperh et al. 2013). Studies looking at CB1R function in neurite development however tend to confirm a generally negative role in outgrowth. Indeed, in cultured neuroblastoma cells several studies have found cell rounding and neurite retraction induced by CB1R agonists (Cabral, McNerney, and Mishkin 1987; Zhou and Song 2001; Chemin, Nargeot, and Lory 2002). One study further showed a similar effect under CB1R overexpression, which they found to be both pertussis toxin (PTX) sensitive, suggesting involvement of $G_{i/o}$, and dependent on ROCK (Ishii and Chun 2002). On the other hand one group has found an increase in growth under CB1R agonism (He et al. 2005; J. D. Jordan et al. 2005; K M Jung et al. 2011), although it has been argued that this effect could be due to the high agonist concentrations used and the prolonged duration of treatment (Gaffuri, Ladarre, and Lenkei 2012).

In cultured neurons, it was found that CB1R activation through eCBs inhibits neurite extension in developing interneurons, through modulation of TrkB receptor signaling and Src and MAPK activity (Berghuis et al. 2005). Furthermore, a study issued from our group found that activation of CB1R inversely correlates with dendrite and axon length, as well as dendrite number (Vitalis et al. 2008). Although, certain studies have contradicted these results, showing a positive effect of CB1R agonism on neurite outgrowth (Bisogno et al. 2003; Williams, Walsh, and Doherty 2003), it was found that the generally negative effects of CB1R activation could produce a dual, seemingly contradictory effect in neurites, where the negative effect on neurite branching would induce a positive effect on general neurite length (Mulder et al. 2008; Oudin, Hobbs, and Doherty 2011).

This negative effect is further evidenced in axonal pathfinding both *in vivo* and *in vitro*. Indeed, a number of studies have found that inhibition of CB1R activity *in vivo*, either through pharmacological or genetic means, induces de-fasciculation and mistargeting of axonal tracts (Watson et al., 2008; Mulder et al., 2008; Gomez et al., 2008; Wu et al., 2010). This effect is confirmed *in vitro* where it was found that acute activation of CB1R induces axonal growth cone collapse (Berghuis et al. 2007; Argaw et al. 2011). These studies did suggest different activation pathways however, with one putting forth the importance of PKA inhibition and diminished surface expression of deleted in colorectal cancer receptor (DCC) (Argaw et al. 2011), while the second put forth the importance of RhoA/ROCK activation downstream of CB1R (Berghuis et al. 2007).

Initial Thesis Results

The following study in which I collaborated at the start of my thesis provided some consensus towards this mechanism. In this study, we find as previously that disruption of CB1R activity in embryonic development impairs fasciculation and targeting of corticofugal tracts. Importantly, we provide some evidence that these effects are dependent on non-muscle myosin II contractility *in vivo*, *through* in utero application of the selective NMII inhibitor blebbistatin. Furthermore, in cultured hippocampal neurons, we show that the growth cone repulsion induced by CB1R activation is produced through recruitment of the G_{12/13}/RhoA/ROCK pathway, providing a direct molecular linkage between CB1R activation and NMII-mediated growth cone retraction. My contribution to this study included helping in the setup and analysis of G_{12/13} siRNA experiments, as well as the analysis of phospho-NMII immunocytochemistry timelapse experiments.

Article 1 (published): Cannabinoid-induced actomyosin contractility shapes neuronal morphology and growth

Cannabinoid-induced actomyosin contractility shapes neuronal morphology and growth

Alexandre B Roland^{1,2†}, Ana Ricobaraza^{1†}, Damien Carrel^{1†‡}, Benjamin M Jordan³, Felix Rico⁴, Anne Simon¹, Marie Humbert-Claude¹, Jeremy Ferrier¹, Maureen H McFadden¹, Simon Scheuring⁴, Zsolt Lenkei^{1*}

¹Brain Plasticity Unit, ESPCI-ParisTech, CNRS UMR8249, Paris, France; ²FAS Center for Systems Biology, Harvard University, Cambridge, United States; ³Department of Organismic and Evolutionary Biology, Harvard University, Cambridge, United States; ⁴U1006 INSERM, Aix-Marseille Université, Parc Scientifique et Technologique de Luminy, Marseille, France

Abstract Endocannabinoids are recently recognized regulators of brain development, but molecular effectors downstream of type-1 cannabinoid receptor (CB1R)-activation remain incompletely understood. We report atypical coupling of neuronal CB1Rs, after activation by endo- or exocannabinoids such as the marijuana component Δ^9 -tetrahydrocannabinol, to heterotrimeric G₁₂/G₁₃ proteins that triggers rapid and reversible non-muscle myosin II (NM II) dependent contraction of the actomyosin cytoskeleton, through a Rho-GTPase and Rho-associated kinase (ROCK). This induces rapid neuronal remodeling, such as retraction of neurites and axonal growth cones, elevated neuronal rigidity, and reshaping of somatodendritic morphology. Chronic pharmacological inhibition of NM II prevents cannabinoid-induced reduction of dendritic development in vitro and leads, similarly to blockade of endocannabinoid action, to excessive growth of corticofugal axons into the sub-ventricular zone in vivo. Our results suggest that CB1R can rapidly transform the neuronal cytoskeleton through actomyosin contractility, resulting in cellular remodeling events ultimately able to affect the brain architecture and wiring.

DOI: [10.7554/eLife.03159.001](https://doi.org/10.7554/eLife.03159.001)

*For correspondence: zsolt.lenkei@espci.fr

†These authors contributed equally to this work

Present address: [†]Université Paris Descartes, Sorbonne Paris Cité, CNRS UMR8250, Paris, France

Competing interests: The authors declare that no competing interests exist.

Funding: See page 20

Received: 22 April 2014

Accepted: 09 September 2014

Published: 15 September 2014

Reviewing editor: Franck Polleux, Columbia University, United States

© Copyright Roland et al. This article is distributed under the terms of the [Creative Commons Attribution License](https://creativecommons.org/licenses/by/4.0/), which permits unrestricted use and redistribution provided that the original author and source are credited.

Introduction

The endocannabinoid (eCB) system is emerging as an important regulator of brain wiring during development with a variety of functions, ranging from lineage segregation of stem cells to refinement of synaptic functions in complex neuronal networks (*Williams et al., 2003; Berghuis et al., 2007; Harkany et al., 2008; Mulder et al., 2008; Vitalis et al., 2008; Watson et al., 2008; Wu et al., 2010*). In both the embryonic and adult brains, eCB action is predominantly mediated by CB1 cannabinoid receptors (CB1Rs), which is one of the most highly expressed neuronal G-protein-coupled receptors (GPCRs), known to couple to G₁₀ heterotrimeric proteins (*Howlett, 2005*), but the molecular mechanisms by which CB1R shapes developing neurons remain mostly unknown. The exact role of eCBs in shaping the neuronal architecture is also under debate, since several reports indicate neurite retraction, while others found the induction of neurite outgrowth following CB1R activation (review in *Gaffuri et al., 2012*). Likewise, currently it is difficult to reconcile the locally repulsive effects of eCBs, reported at axonal growth cones (*Berghuis et al., 2007; Argaw et al., 2011*), and their role of mediating efficient directional axonal growth and shaping well-fasciculated axonal tracts (*Mulder et al., 2008; Vitalis et al., 2008; Watson et al., 2008*).

During neuronal development, an elaborate balance of positive and negative regulators is necessary to establish precise neuronal structure. This structure is stabilized by the cytoskeleton, which, similar

eLife digest Our brains are full of cells called neurons, which are connected to each other in complex networks that send messages around the brain. The way the neurons connect to each other, known as brain wiring, differs widely between individuals. Moreover, our brain wiring changes in response to our environment and experiences throughout our lives, from developing embryo to old age.

One way this happens is through the action of chemicals called cannabinoids. Produced naturally in the body, cannabinoids are also found in the popular recreational drug cannabis that is increasingly being used in medicine to treat chronic pain and other conditions. However, cannabis misuse can have negative side effects on the brain leading to memory loss and mental illness, especially in young people.

Cannabinoids can be detected by a group of proteins called cannabinoid receptors, but it is not clear how this leads to changes in brain wiring. Roland et al. now show that detection of cannabinoids by a type-1 cannabinoid receptor triggers a series of events that change how neurons grow and connect with each other.

Detection of the cannabinoid by the receptor leads to the activation of an enzyme called ROCK. This, in turn, activates a motor protein called non-muscle myosin II that inhibits the growth of neurons. Roland et al. suggest that this prevents the neurons from reaching their neighbors and forming new connections. Investigating how this works in individuals with medical conditions that alter brain function could help inform us how cannabis could be used more safely.

DOI: [10.7554/eLife.03159.002](https://doi.org/10.7554/eLife.03159.002)

to non-neuronal cells, is composed of two major polymers, the highly plastic filamentous-actin (F-actin) and the more stable microtubule (MT) networks. Actin filaments are often cross-linked to a molecular motor protein, the non-muscle myosin II (NM II), whose contractile properties further endow the actomyosin network with highly dynamic control of cell behavior and architecture (*Vicente-Manzanares et al., 2009*). The cytoskeleton is mainly regulated by Rho-like GTPases that control a wide variety of effector mechanisms such as actin polymerization and branching, actomyosin contractility, focal adhesions, microtubule dynamics, and membrane transport (*Kaibuchi et al., 1999; Etienne-Manneville and Hall, 2002; Hall and Lalli, 2010*). Downstream protein kinases such as the Rho-associated, coiled coil-containing kinase (ROCK) are the key activator proteins of these convergent-signaling pathways. Interestingly, ROCK is associated with particular CB1R-induced phenotypes. In CB1R-over-expressing B103 cells, the endocannabinoid anandamide induces cell rounding via ROCK (*Ishii and Chun, 2002*), and CB1R activation results in RhoA- and ROCK-dependent repulsion of growth cones of cultured hippocampal neurons (*Berghuis et al., 2007*), but neither the coupling mechanism of CB1R to ROCK nor the cytoskeletal targets downstream of CB1R-activated ROCK are identified yet. Since Rho-activated effectors operate over a large range of spatial and temporal scales, understanding of eCB-mediated structural plasticity requires the identification of the precise spatial and temporal dynamics of CB1R-mediated cytoskeletal modifications.

In this study, by using highly resolved live imaging approaches, we report that CB1R-activation rapidly and reversibly contracts the neuronal actomyosin cytoskeleton through an unusual coupling to G₁₂/G₁₃ proteins that produce Rho- and ROCK-mediated NM II activation. In addition, we show that chronic CB1R-mediated activation of actomyosin contractility may mediate lasting changes in neuronal and cerebral morphology.

Results

CB1R-activation results in rapid retraction of actin-rich growth cones

In order to investigate the spatio-temporal dynamics of cannabinoid-induced cytoskeletal modifications, we have established a sensitive, specific, and highly accessible experimental assay system to study neuronal remodeling downstream of CB1R activation. We have visualized highly dynamic neuronal growth cones in cultured hippocampal neurons, where the activation of endogenous CB1Rs results in repulsion (*Berghuis et al., 2007*), by labeling endogenous F-actin with fluorescent LifeAct. This actin-binding peptide allows observation of the dynamic actin network without perturbing natural reorganization kinetics (*Riedl et al., 2008*).

Time-lapse microscopy of live neurons, expressing Flag-CB1R-eGFP and LifeAct-mCherry, showed numerous F-actin-rich dynamic growth cones (**Figure 1A**) advancing at individually variable velocities (**Figure 1A,B**), but yielding a fairly constant mean growth rate of 20–30 $\mu\text{m/hr}$ (**Figure 1D**). In addition

to growth cones, axonal F-actin was also present in filopodia and in isolated patches on the shaft of the distal axonal region (**Figure 1—figure supplement 1**). Strikingly, bath application of 100 nM WIN 55,212-2 (WIN), a synthetic cannabinoid agonist, led to a rapid retraction of the F-actin-rich domain (**Figure 1A**), with mean retraction amplitude of $62.2 \mu\text{m} \pm 5.2$ (**Figure 1C–E**). Retraction was already detectable at 2 min after agonist exposure and typically reached a plateau between 10 and 20 min (**Figure 1C,D**). The morphology of retracted axons was characterized by an F-actin-rich retraction bulb (arrowheads on **Figure 1A** and **Figure 1—figure supplement 1**) and a thin membranous trailing remnant (open arrowheads on **Figure 1A** and **Figure 1—figure supplement 1**), the latter of which was not included in the length measurement. Pre-treatment with the CB1R selective antagonist/inverse agonist AM281 (AM) (1 μM) inhibited retraction (**Figure 1D,E**).

Further pharmacological characterization showed that several other chemically distinct CB1R agonists, the endocannabinoid 2-arachidonoylglycerol (2-AG) (1 μM), the principal psychoactive marijuana constituent Δ^9 -tetrahydrocannabinol (Δ^9 -THC) (1 μM) and the synthetic agonists CP55,940 (100 nM) and HU-210 (100 nM) also produced significant retraction (**Figure 1E**). The retraction was saturable and concentration-dependent with a half-maximal effective concentration (EC_{50}) value of around 20 nM for WIN (**Figure 1F**). When treatment with 25 nM WIN was followed by ligand-free wash-out, growth cone progression resumed normally showing the reversibility of cannabinoid-induced growth cone retraction (**Figure 1G**). Finally, this retraction was not a result of CB1R over-expression since treatment with 100 nM WIN or 1 μM 2-AG induced significant retraction with similar kinetics in neurons transfected only with LifeAct-mCherry (**Figure 1H–I**). However, the mean amplitude of retraction was lower and responses were more variable than in Flag-CB1R-eGFP-expressing neurons (compare **Figure 1C,D** with **Figure 1H,I**), as expected in a heterogeneous neuronal population expressing endogenous CB1Rs at highly variable levels (**Letierrier et al., 2006**). In addition, growth cone advance rapidly resumed even in the continued presence of 100 nM WIN (**Figure 1H**).

In conclusion, our results show that cannabinoids trigger a rapid, saturable, and reversible retraction of actin-rich growth cones downstream of both endogenous and overexpressed CB1Rs.

G₁₂/G₁₃ heterotrimeric proteins, Rho GTPase, ROCK, myosin II, and F-actin microfilaments mediate CB1R-induced rapid growth cone retraction

First, we investigated which cytoskeletal elements act downstream of CB1Rs to induce rapid growth cone retraction. We expressed, in addition to LifeAct-mCherry, a GFP-tagged version of End-binding protein 3 (EB3-eGFP), which binds to endogenous microtubule (MT) plus ends without changing MT growth parameters and thus allows the visualization of MT structure and dynamics (**Stepanova et al., 2003**). Indeed, MTs in the entire neuron were labeled in green, with many bright comet-like fluorescent dashes in all the neuronal compartments, moving randomly in the cell body and directionally in axons and distal dendrites, representing dynamic MT plus ends (**Stepanova et al., 2003**). During 100 nM WIN-induced retraction the dynamics of the two main cytoskeletal polymers, F-actin and MTs, was remarkably different (**Figure 2A**). A significant portion of F-actin redistributed in the first 2–4 min after stimulation from its original location in growth cones into a more homogenous cable-like pattern on the distal axonal shaft (**Figure 2B** and **Figure 2—figure supplement 1**). In contrast, MTs bent during the same time frame forming periodic local loops (**Figure 2A,A',B** and **Video 1**) before finally consolidating into a homogeneously labeled retraction bulb. The F-actin cables (bundles of F-actin filaments, which are not separately resolved here by diffraction-limited microscopy), often co-localized with regions displaying periodic bends in MTs (**Figure 2B'**), suggesting that an F-actin-related force pulls strongly enough to bend MTs. This effect was not the result of the over-expression of the cytoskeletal markers EB3-eGFP or LifeAct-mCherry, since we could observe similar periodic MT bends, detected by post hoc immunohistochemistry, in neurons not expressing these markers (**Figure 2—figure supplement 2**).

To investigate the requirement for polymerized actin microfilaments and MTs in these retractions, we depolymerized MTs with nocodazole (10 μM) and F-actin with cytochalasin D (1 μM) (**Forscher and Smith, 1988**). Nocodazole pre-treatment stopped growth cone advance but WIN still induced significant retraction (**Figure 2C,D**, **Figure 3E** and **Video 2**). In contrast, cytochalasin D inhibited both growth cone advance and WIN-induced retraction (**Figure 2E,F**, **Figure 3E** and **Video 3**) showing that while the presence of both F-actin and MTs is necessary for growth cone advance, as reported previously (**Dent et al., 2003**), only F-actin is necessary for CB1R-induced retraction.

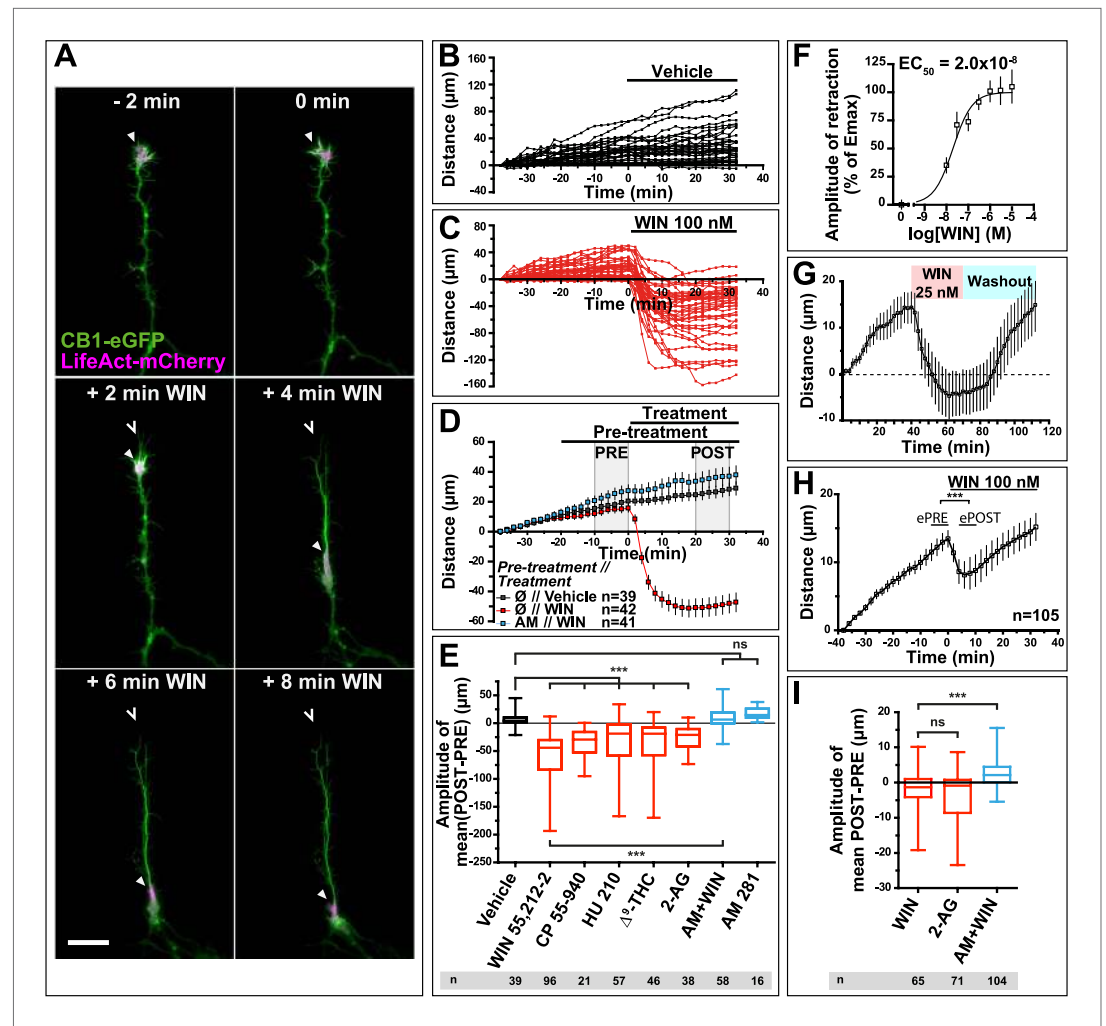


Figure 1. CB1R activation induces retraction of actin-rich growth cones. Cultured DIV8 hippocampal neurons co-expressing Flag-CB1R-eGFP and LifeAct-mCherry on (A–G) and LifeAct-mCherry only on (H and I). (A) Treatment with CB1R agonist WIN55,212-2 (WIN, 100 nM, added at 0 min) induces rapid retraction of the F-actin-rich domain (arrowheads). Open arrowheads: growth cone position at 0 min. (B) Progression of individual growth cones in control conditions. (C) WIN-induced retraction of individual growth cones. (D) Mean values of growth cone progression in control condition or after treatment with WIN with or without pre-treatment with the CB1R-specific antagonist AM281 (AM, 1 μ M). WIN-induced growth cone retraction is effectively abolished by AM. (E) Amplitudes of growth cone retraction induced by different exo- and endocannabinoids, calculated as the net difference of mean growth cone position in the pre-treatment (PRE on D) and post-treatment (POST on D) time intervals from at least three independent experiments. (F) Concentration-response curve of WIN-induced retraction, 9 to 27 neurons per concentration from two independent experiments expressed as percentage of maximal retraction, $E_{50} = 52.2 \mu\text{m}$. (G) WIN-induced retraction (25 nM at 40 min) is fully reversible after WIN-washout (at 70 min), $n = 9$. (H) Mean values of growth cone retraction downstream of endogenous CB1R activation, from four pooled independent experiments, outliers were removed in accordance with the Grubb's test. (I) Amplitudes of growth cone retraction downstream of endogenous CB1R activation after treatment with WIN (100 nM), 2-AG (1 μ M), or with WIN (100 nM) after pre-treatment with the CB1R-specific antagonist AM281 (AM, 1 μ M). WIN-induced growth cone retraction is effectively abolished by AM. Values in D, F, G, and H are mean \pm SEM; values in E and I are presented as boxplots; $n.s. = p > 0.05$, $***p < 0.001$, calculated using Kruskal–Wallis one-way ANOVA followed by Dunn's post-tests on (E and I) and paired t-test on (H). Scale bar: 20 μm . DOI: 10.7554/eLife.03159.003

The following figure supplement is available for figure 1:

Figure supplement 1. mCherry-LifeAct label (red channel) from Figure 1A. Scale bar: 20 μm . DOI: 10.7554/eLife.03159.004

A likely candidate for the generation of such rapid F-actin-related force, which is capable of bending microtubules, is non-muscle myosin II (NM II), an ATPase protein with actin cross-linking and contractile properties, which is activated by the phosphorylation of its regulatory light chain. The two main activators of NM II are myosin light chain kinase (MLCK) and ROCK, the latter being already known to participate in CB1R-induced cytoskeletal modifications (Ishii and Chun, 2002; Berghuis et al., 2007). This raises the possibility that ROCK- and/or MLCK-induced NM II contractility is responsible for the force-generation reported above. In order to directly investigate the implication of NM II, we pre-incubated neurons, for 20 min before WIN stimulation, with the highly selective NM II ATPase inhibitor blebbistatin (25 μ M) that blocks NM II in an actin-detached state without perturbing F-actin polymerization (Kovacs et al., 2004). Blebbistatin pre-treatment induced substantial morphological changes of the growth cone, which continued to move forward in a rather disorganized fashion (Figure 2G and Video 4), typically transforming the growth cone lamellipodia into several dynamically advancing filopodia, as reported previously (Rosner et al., 2007). Remarkably, blebbistatin completely abolished WIN-mediated retraction of these dynamically advancing F-actin-rich structures (Figure 2G,H, Figure 3E and Video 4), suggesting that the main force-generating factor downstream of CB1R activation is actomyosin contractility. This inhibitory effect of blebbistatin was concentration dependent with half-maximal value of inhibition (EC_{50}) of 116 nM (Figure 2—figure supplement 3). Immunocytochemical analysis of WIN-treated F-actin-rich growth cones at 2 min after the addition of WIN strikingly showed rapid and strong up-regulation of myosin light chain phosphorylation in the distal axon, adjacent to the F-actin-rich growth cone (Figure 3A–C and Figure 3—figure supplement 1), at the right place for the subsequent NMII-dependent contraction, both in neurons transfected only with LifeAct-mCherry (Figure 3A–C) and with Flag-CB1R-eCFP and LifeAct-mCherry (Figure 3C).

Next, we investigated the mechanism coupling CB1R to the ROCK/NM II pathway. First, we showed that NMII-dependent growth cone contraction is not a result of CB1R over-expression, since treatment with blebbistatin (25 μ M) or the ROCK inhibitor Y-27632 (10 μ M) (Figure 3D) significantly inhibited endogenous CB1R-induced retraction of growth cones, previously presented on Figure 1I, in neurons transfected only with LifeAct-mCherry and EB3-eGFP. Then we used neurons expressing Flag-CB1R-eCFP, LifeAct-mCherry, and EB3-eGFP, our high-throughput experimental read-out, to characterize in detail the molecular mechanism of CB1R-induced actomyosin contractility. The amplitude of WIN-mediated retraction was significantly reduced by pre-treatment with the Rho inhibitor C3 transferase (1 μ g/ml, Figure 3—figure supplement 2), the ROCK inhibitor Y-27632 (10 μ M) (Figure 3E), but not by the MLCK-specific inhibitor ML-7 (30 μ M) (Figure 3E). Treatment with the inactive (R)-(+)-blebbistatin (25 μ M) stereoisomer was ineffective (data not shown). The implication of neuronal NM II was further confirmed by siRNA knock-down of endogenous NM IIA and NM IIB (Miserey-Lenkei et al., 2010), which resulted in significant reduction of WIN-mediated contractility as compared to control (anti-luciferase) siRNA (Figure 3F).

Next, we investigated which heterotrimeric G-protein family couples CB1Rs to Rho activation. Notably, treatment with pertussis toxin (100 ng/ μ l), a specific inhibitor of $G_{i/o}$ heterotrimeric proteins, which are generally considered as the main signaling pathway of CB1Rs (Howlett, 2005), did not decrease significantly cannabinoid-induced growth cone retraction (Figure 3E), similarly to a previously reported finding for ROCK-mediated induced cell rounding after anandamide treatment (Ishii and Chun, 2002). Another family of heterotrimeric G-proteins, G_{12}/G_{13} , may mediate rapid growth cone collapse, neurite retraction, and cell rounding in neuronal cell lines in response to certain GPCR agonists such as lysophosphatidic acid (LPA) (Kato et al., 1998; Kranenburg et al., 1999). Therefore, we inactivated endogenous G_{12}/G_{13} proteins in our hippocampal neuronal cultures by using two pools of 4 different siRNAs directed against rat G_{12} - or G_{13} -alpha proteins, respectively. Used separately, neither pool decreased WIN-induced growth cone retraction as compared to control (anti-luciferase) siRNA (Figure 3F). However, when we combined together 2 siRNAs of each pool, each resulting mixed pools efficiently inhibited WIN-mediated contractility (Figure 3F). These results show that the presence of either G_{12} or G_{13} is necessary and sufficient for CB1R-induced actomyosin contraction.

Finally, to verify that CB1R-induced retraction is not an artifact of altered adhesion properties of growth cones in vitro, we co-transfected Flag-CB1R-eCFP, EB3-eGFP, and LifeAct-mCherry into embryonic rat brains using in utero electroporation at embryonic day 16 (E16). In organotypic slices prepared from the offspring between postnatal day 4 and 6 (P4–P6), numerous corticofugal F-actin-rich growth cones from layer II–III pyramidal neurons could be visualized by video microscopy at 48 hr

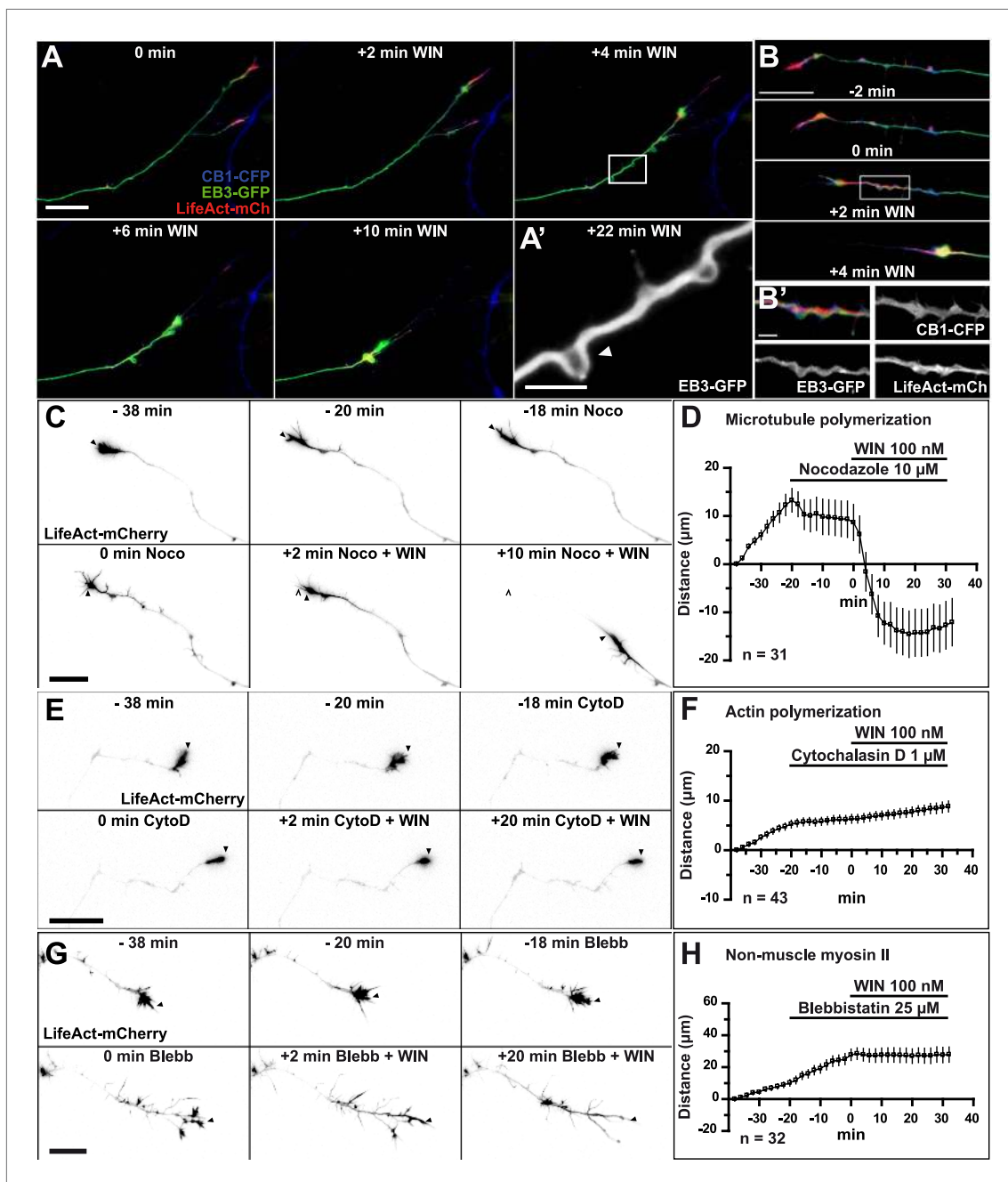


Figure 2. CB1R-induced retraction is mediated by non-muscle myosin II dependent actomyosin contraction. Cultured hippocampal neurons co-expressing Flag-CB1R-eCFP, LifeAct-mCherry, and EB3-eGFP at DIV6 were treated by WIN (100 nM) at 0 min. **(A)** Microtubules (MT) bend and form small loops (arrowhead on **A'**) in the first 4 min **(B)** F-actin is reorganized from the growth cone tips and isolated patches to homogenous cable-like distribution in distal axonal shaft. **(C–H)** Pre-treatment with: **(C and D)** MT polymerization inhibitor nocodazole (10 µM), **(E and F)** actin polymerization inhibitor cytochalasin D (1 µM), **(G and H)** Non-muscle myosin II-inhibitor blebbistatin (25 µM). Scale bars: 5 µm on **(A')** and **(B')**, 20 µm elsewhere.

DOI: [10.7554/eLife.03159.005](https://doi.org/10.7554/eLife.03159.005)

The following figure supplements are available for figure 2:

Figure supplement 1. Averaged F-actin relocalization in the distal 60 µm in growth cones in the first 4 min after WIN treatment in five randomly chosen neurons from **Figure 1C**.

DOI: [10.7554/eLife.03159.006](https://doi.org/10.7554/eLife.03159.006)

Figure supplement 2. CB1R-induced periodic microtubule bends are not due to EB3-eGFP and LifeAct-mCherry expression.

DOI: [10.7554/eLife.03159.007](https://doi.org/10.7554/eLife.03159.007)

Figure supplement 3. Concentration-response curve for the blebbistatin effect on the growth cone retraction assay after treatment with WIN (100 nM).

DOI: [10.7554/eLife.03159.008](https://doi.org/10.7554/eLife.03159.008)



Video 1. CB1R activation induces retraction of actin-rich growth cones. Dynamic, F-actin-rich growth cone of a cultured hippocampal neuron co-expressing CB1R-eCFP, LifeAct-mCherry, and EB3-eGFP at DIV6 treated with 100 nM WIN at 10 min. Scale bar: 20 μm .

DOI: [10.7554/eLife.03159.009](https://doi.org/10.7554/eLife.03159.009)

activation of endogenous CB1Rs typically led to arrest or retraction of numerous growth cones (**Figure 4C,E**). The relatively mild averaged effect is probably due to the variable level of endogenous CB1R expression in these neurons. Importantly, pre-treatment with blebbistatin (25 μM) efficiently blocked this effect (**Figure 4E**).

In conclusion, we show that CB1R activation significantly reorganizes growth cones through MLCK/ROCK-mediated NM II activation. This large-scale actomyosin contractility ultimately leads to the remodeling of MT structure in the distal axonal segments.

In the developing brain, both activation of endogenous CB1Rs and actomyosin contractility are required for path-finding of CB1R expressing corticofugal axons

In the embryonic brain, developing corticofugal axons express high levels of CB1Rs (**Figure 5B',B''**) (**Vitalis et al., 2008**). Genetic or pharmacological ablation of CB1Rs leads to axonal fasciculation deficits (**Mulder et al., 2008; Watson et al., 2008**). In order to investigate the importance of actomyosin contractility during the embryonic development of CB1R expressing axons, we inhibited *in vivo* the ATPase activity of NM II by *in utero* intra-cerebroventricular injection of rat embryos with blebbistatin (**Figure 5A**). Notably, 100% of blebbistatin-injected embryos survived and developed without apparent gross anatomical brain defects, suggesting that neuronal NM II can be safely targeted *in vivo*. In embryos treated between E15 and E17 with active (S)-(-)-blebbistatin (**Figure 5D,D',G**), but not with the inactive (R)-(+)-stereoisomer (**Figure 5C,C',G**), Tuj1-expressing axons showed important targeting errors, by invading the sub-ventricular zone, from which CB1R-expressing corticofugal axons are usually excluded (**Figure 5B,G** and **Figure 5—figure supplement 1**). Such a representative CB1R-expressing Tuj1-positive axon invading the SVZ from an embryo treated with (S)-(-)-blebbistatin is shown on **Figure 5F**. Treatment with the CB1R-specific antagonist AM251 (1 mM) but not with its vehicle (DMSO 2.8%) led to similar developmental phenotype (**Figure 5E,E',G**).

Together with our above findings showing that activation of endogenous CB1Rs in organotypic slices leads to NM II-dependent arrest or contraction of axonal growth cones, these results suggest that both activation of endogenous CB1Rs and actomyosin contractility are required for correct path finding of corticofugal axons.

CB1R-induced rapid neuronal contraction results in cell rounding, neurite retraction, and increased cell stiffness in Neuro2A cells

Next, we asked whether the above reported CB1R-mediated effect on neuronal actomyosin contractility is restricted to growth cones, which are highly specialized mobile structures, or if we can also observe this phenomenon in other neuronal sub-compartments. The mouse neuroblastoma-derived Neuro2A cell line, a widely used model of neuronal physiology, presents simpler morphology than primary hippocampal neurons, enabling high-resolution quantitative measure of cellular structure and biomechanical characteristics. The Neuro2A cells grow neurites in culture, and we observed that F-actin accumulates in the shaft and extremity of these neurites as well as in highly dynamic filopodia and in patches of the cell cortex (**Figure 6A**). CB1R-eGFP showed a characteristic distribution between the plasma membrane and endosomes, as described previously in various non-polarized cell-types

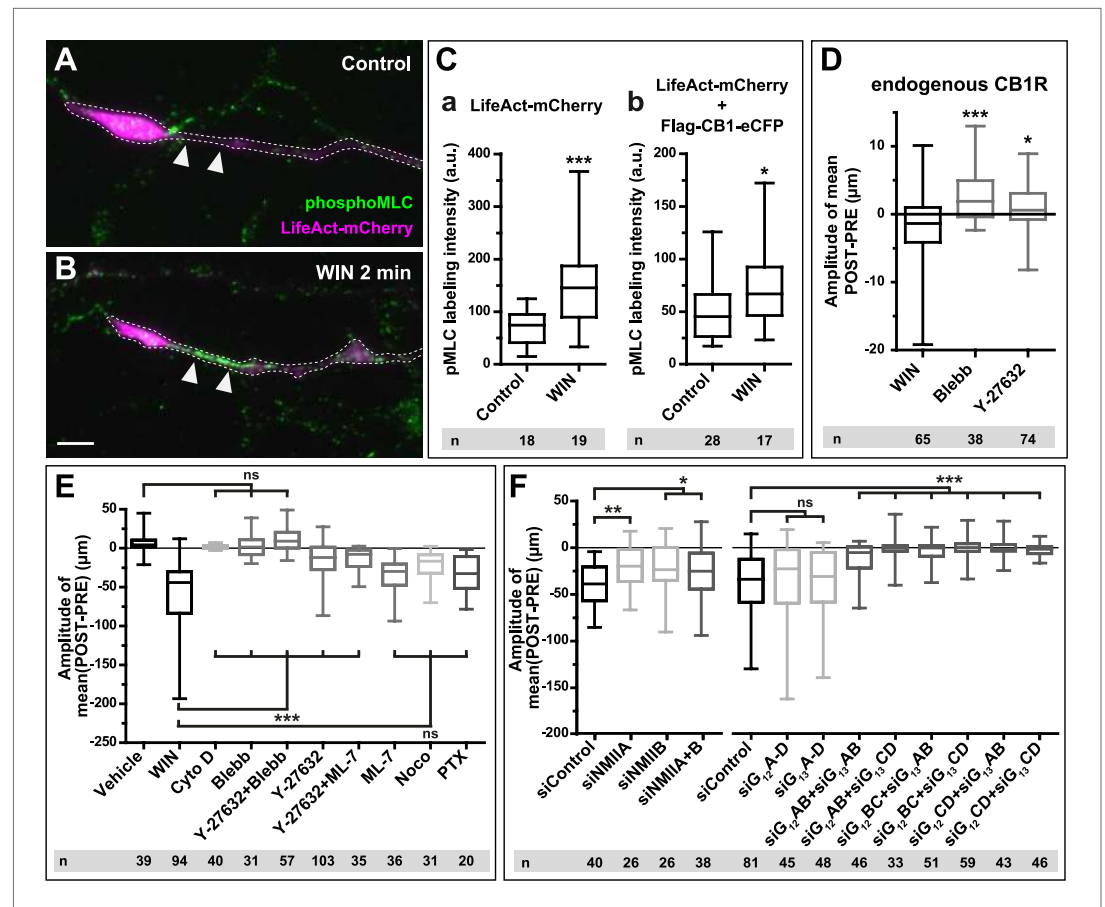


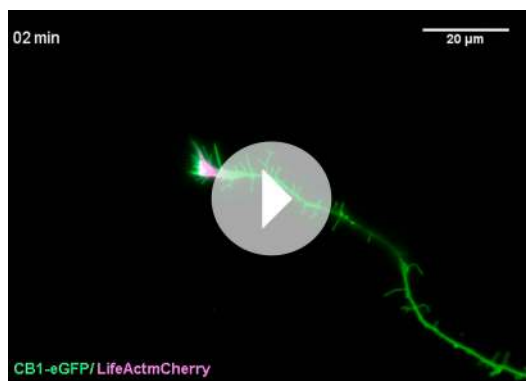
Figure 3. CB1Rs activate non-muscle myosin II through heterotrimeric G₁₂/G₁₃ proteins, Rho GTPase, and ROCK. Cultured hippocampal neurons at DIV6 co-expressing a combination of LifeAct-mCherry, Flag-CB1R-eCFP, and EB3-eGFP as indicated and treated by WIN (100 nM) at 0 min. **(A–B)** Representative LifeAct-mCherry expressing growth cones (delimited with a dotted line) at 2 min after treatment with vehicle **(A)** or WIN (100 nM, **B**), labeled with a phospho-Myosin Light Chain (phosphoMLC) antibody. Arrowheads show the distal axon adjacent to the F-actin-rich growth cone where WIN induces rapid and strong upregulation of myosin light chain phosphorylation. **(C)** pMLC labeling intensity at the distal 50–60 μm of the axon, adjacent to the actin-rich growth cone, from neurons expressing LifeAct-mCherry **(A)** or co-expressing LifeAct-mCherry and Flag-CB1R-eCFP **(B)**. The region-of-interest used to measure pMLC labeling intensity is delimited with a dotted line on a representative growth cone on **Figure 3—figure supplement 1**. **(D)** Amplitude of 100 nM WIN-induced growth cone retraction in neurons co-expressing LifeAct-mCherry and EB3-eGFP pre-treated with 25 μM blebbistatin or 10 μM Y-27632. **(E)** Amplitude of 100 nM WIN-induced growth cone retraction in neurons co-expressing LifeAct-mCherry, EB3-eGFP, and Flag-CB1R-eCFP pre-treated with: 1 μM cytochalasin D; 25 μM blebbistatin; 25 μM blebbistatin + 10 μM Y-27632; 10 μM Y-27632; 30 μM ML-7 + 10 μM Y-27632; 30 μM ML-7; 10 μM nocodazole; 100 ng/μl PTX. **(F)** Effect of siRNA-mediated knock-down of endogenous myosin IIA, IIB or of endogenous G₁₂/G₁₃ proteins on growth cone-retraction induced by 100 nM WIN in neurons co-expressing the three constructs, as compared to control (luciferase) siRNA. Results are pooled from at least two independent experiments, and outliers were removed in accordance with Grubb's test. Results are expressed as boxplots. n.s p > 0.05; *p < 0.05; **p < 0.01; ***p < 0.001 calculated using Student's t-test on **(C)**, Kruskal–Wallis one-way ANOVA followed by Dunn's post-tests on **(D)** and **(E)**, and using one-way ANOVA followed by Newman–Keuls post-tests on **(F)**. Scale bar: 10 μm.

DOI: [10.7554/eLife.03159.010](https://doi.org/10.7554/eLife.03159.010)

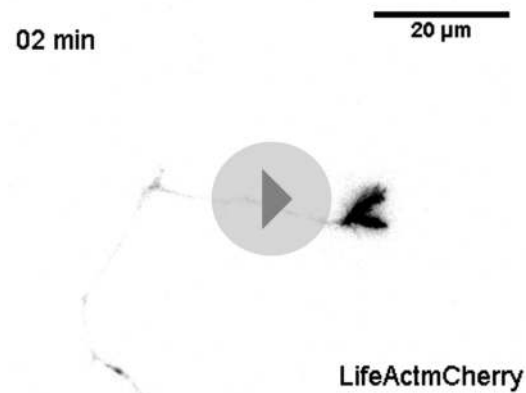
The following figure supplements are available for figure 3:

Figure supplement 1. Another representative LifeAct-mCherry expressing growth cone 2 min after treatment with WIN (100 nM), labeled with the phosphoMLC antibody, similarly to **Figure 3B**.
DOI: [10.7554/eLife.03159.011](https://doi.org/10.7554/eLife.03159.011)

Figure supplement 2. Amplitude of 100 nM WIN-induced growth cone retraction in neurons co-expressing LifeAct-mCherry, EB3-eGFP, and Flag-CB1R-eCFP with (C3T) or without (WIN) pre-treatment with 1 μg/ml C3T.
DOI: [10.7554/eLife.03159.012](https://doi.org/10.7554/eLife.03159.012)



Video 2. Effect of microtubule depolymerization on CB1R-induced growth cone retraction. Dynamic, F-actin-rich growth cone of a cultured hippocampal neuron co-expressing Flag-CB1R-eGFP and LifeAct-mCherry at DIV6, pre-treated with 10 μ M Nocodazole at 20 min before treatment with 100 nM WIN at 40 min. Scale bar: 20 μ m. DOI: [10.7554/eLife.03159.013](https://doi.org/10.7554/eLife.03159.013)



Video 3. Effect of actin depolymerization on CB1R-induced growth cone retraction. Dynamic, F-actin-rich growth cone of a cultured hippocampal neuron co-expressing CB1R-eCFP, LifeAct-mCherry, and EB3-eGFP at DIV6 pre-treated with 1 μ M cytochalasin D at 20 min before treatment with 100 nM WIN at 40 min. Scale bar: 20 μ m. DOI: [10.7554/eLife.03159.014](https://doi.org/10.7554/eLife.03159.014)

that the stiffness (Young's modulus) of unstimulated individual cells was approximately 300 Pa, close to values reported in acutely isolated hippocampal glial cells and neurons (Lu et al., 2006). For this series of experiments, cells were grown on uncoated plastic, a highly adhesive substrate, in order to minimize the displacement of Neuro2A cells during the measurement. WIN stimulation led to an overall rapid and transient increase of cell stiffness at different locations on the same cell, with the exception of the trailing edge (Figure 6C4). As the contribution of the underlying coverslip was significant in neurites (compare ordinate scale of Figure 6C1 with Figure 6C2–4), in the following experiments we have centered our force measurements on the cell bodies, corresponding to the positions 2 and 3 on Figure 6C. The important transient WIN-induced increase in cell stiffness was absent during incubation with vehicle solution and could be prevented by pre-treatment with blebbistatin (25 μ M) (Figure 6D), showing that activation of NM II is necessary to induce the measured changes.

Next, in order to follow morphological changes at the plasma membrane in detail, high-resolution time-lapse image stacks of retracting WIN-treated Neuro2A cells were acquired, deconvoluted, and

(Leterrier et al., 2004). Treatment with 100 nM WIN resulted in rapid rounding of the cell body and in retraction of neurites, leaving behind retraction-fiber-like remnants (Figure 6A,B and Video 6). F-actin was reorganized and accumulated at the end of the retraction bulb and under the plasma membrane of the cell body. This WIN-induced cell rounding could be blocked by blebbistatin treatment (25 μ M) (Figure 6B), suggesting that the observed rapid morphological changes are due to a CB1R-induced general contraction of the actomyosin cell cortex, which is the association of plasma membrane lipids and the underlying actin filament network.

Comparable large-scale contraction of the actomyosin cortex was previously characterized in detail in cells entering division (Théry and Bornens, 2008), where a regulated balance between localized actomyosin-cortex-dependent surface tension and intracellular pressure allows dividing cells to control their volume, shape, and mechanical properties (Stewart et al., 2010). When combined, these two effects result in an overall increase of cell cortex rigidity or stiffness (Stewart et al., 2010), while local and temporary detachment of the plasma membrane from the actomyosin cortex results in characteristic blebbing (Cunningham, 1995; Charras et al., 2008). Marked cell rounding, F-actin reorganization, and the presence of retraction fibers suggested that an analogous intracellular mechanism might be implicated in the above-reported cannabinoid-induced reorganization of the Neuro2A cells. We have performed two experiments to investigate this possibility.

First, in order to directly measure putative contraction of the neuronal actomyosin cortex, we measured the cell cortex rigidity of isolated CB1R-expressing Neuro2A cells before and after cannabinoid treatment, by using atomic force microscopy (AFM). Averaged AFM measurements in force mode with a 1- μ m spherical bead attached to the cantilever (Figure 6C) indicated

**LifeAct-mCherry**

Video 4. Effect of NM II inhibition on CB1R-induced growth cone retraction. Dynamic, F-actin-rich growth cone of a cultured hippocampal neuron co-expressing Flag-CB1R-eGFP and LifeAct-mCherry at DIV6 pre-treated with 25 μ M blebbistatin at 20 min before treatment with 100 nM WIN at 40 min. Only LifeAct-mCherry emission is visualized here. Scale bar: 20 μ m.

DOI: [10.7554/eLife.03159.015](https://doi.org/10.7554/eLife.03159.015)

reconstructed in three dimensions (**Figure 6E** and **Video 7**). Prior to remodeling, the shape of the cells suggested a large degree of reinforcement probably owing both to the intracellular actomyosin cortex directly beneath the plasma membrane, and to the attachment of the cell to its substrate. After CB1R agonist application, the cell changed shape drastically, acquiring a more spherical morphology. Moreover, we observed localized blebbing behavior of the cell membrane, starting at the early stages (\sim 2 min) of the contraction and ceasing after 6–8 min (**Figure 6E** and **Video 7**).

In conclusion, our results show that CB1R activation leads to rapid and NM II-dependent neurite retraction and rounding of the cell body in Neuro2A cells, which is accompanied by formation of retraction fibers and by transient increase in cell stiffness and blebbing behavior. Collectively, these findings suggest that global CB1R activation results in large-scale contraction of the neuronal cytoskeleton, which is mechanistically similar to the molecular machinery engaged in mitotic cell rounding.

Prolonged CB1R-mediated induction of actomyosin contraction reshapes somatodendritic morphology

Previously, we have reported that chronic in vitro activation of CB1Rs leads to significant inhibition of dendritic development in cultured hippocampal neurons, while genetic or pharmacological inhibition of CB1Rs leads to more numerous and longer dendrites (**Vitalis et al., 2008**). Similarly, genetic or pharmacological inhibition of CB1R leads to more complex somatodendritic morphology in septal cholinergic neurons (**Keimpema et al., 2013**). These data suggest that, in addition to axons, where CB1Rs are naturally targeted through transcytotic targeting (**Leterrier et al., 2006**), the transitory presence of CB1Rs on the somatodendritic membrane may allow efficient coupling to growth inhibitory signaling pathways. It was reported that increased NM II activity, through constitutively active MLCK or RhoA, decreases both the length and number of neurites and, consequently, delays or abolishes the development of neuronal polarity in cultured hippocampal neurons (**Kollins et al., 2009**). We thus studied whether a long-term effect of the above described rapid, CB1R-activation dependent and NM II-mediated contraction of the neuronal cytoskeleton could explain the negative regulatory effects of CB1R activation at a longer time scale (\sim 24 hr).

First, we verified the presence of the rapid structural effects of CB1R activation in the somatodendritic region. Neurons expressing CB1R-eCFP, LifeAct-mCherry, and EB3-eGFP at DIV9 responded to 100 nM WIN with rapid morphological reorganization of the somatodendritic compartment, characterized by retraction of distal dendritic regions and broadening of the proximal portion of dendrites (**Figure 7A,A'** and **Video 8**). While the overall dynamics of EB3-eGFP comets was not apparently modified, the MTs in individual dendrites often displayed a characteristic bent morphology, parallel to the appearance of straight cable-like F-actin bundles (**Figure 7A,A'** and **Video 8**) suggesting the presence of a rapid CB1R-activation-dependent actomyosin contraction. Overnight treatment with WIN (100 nM) resulted in a significant decrease in the number of dendrites of developing hippocampal neurons, expressing Flag-CB1R-eGFP and the soluble cytoplasmic marker DsRed2 at DIV4 (**Figure 7B,C**), as reported previously (**Vitalis et al., 2008**). This effect was abolished in the presence of both Y-27632 (10 μ M) or blebbistatin (25 μ M) (**Figure 7B,C**). Notably, treatment with both inhibitors led to more developed dendrites also in control conditions, confirming previous reports on the constitutive inhibition of neurite development through ROCK and NM II (**Kollins et al., 2009**).

In conclusion, our results show that the chronic activation of CB1Rs reshapes somatodendritic morphology through enhancement of the naturally present ROCK- and NM II-mediated contractile tone of neurons.

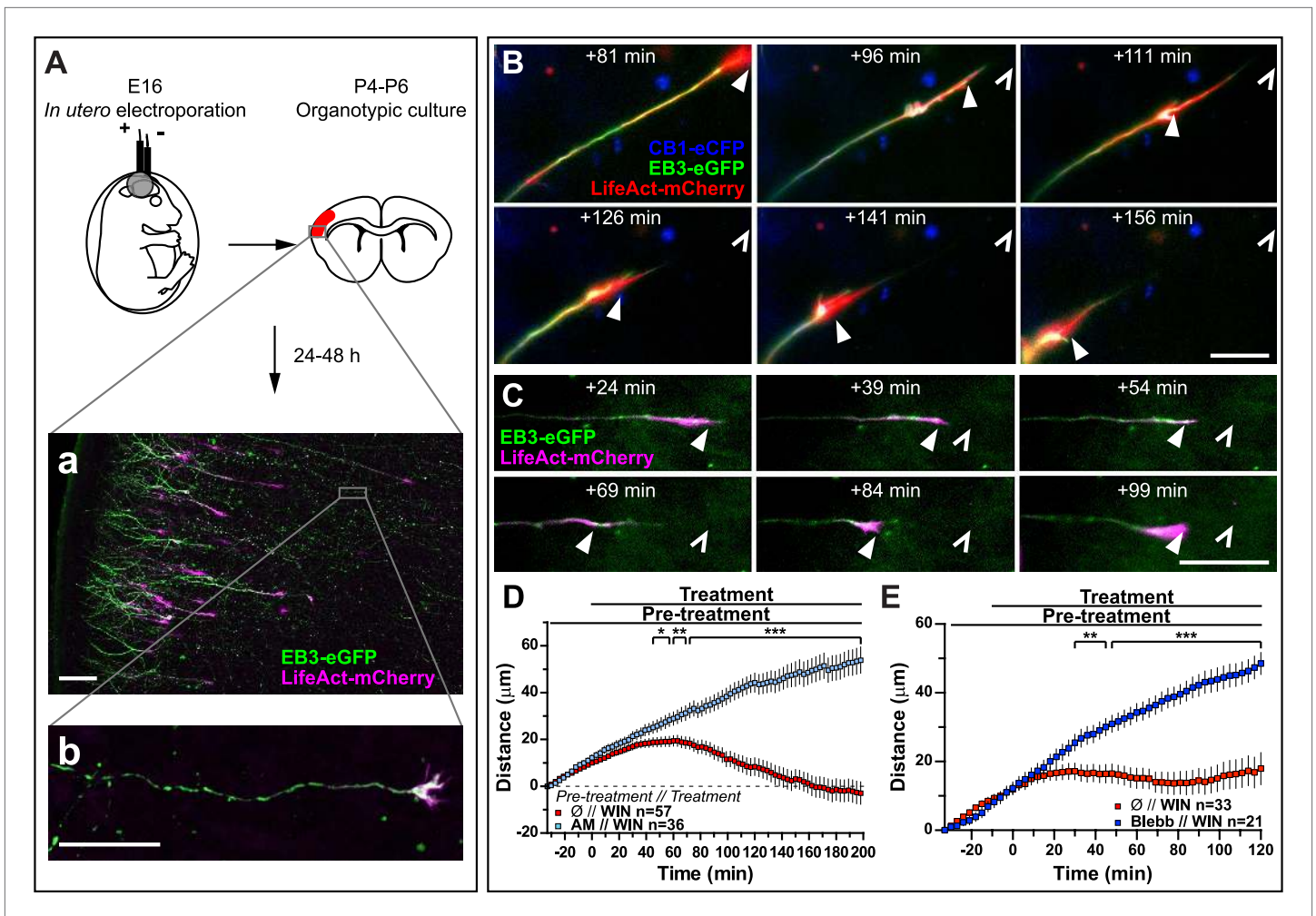


Figure 4. Activation of exogenous or endogenous CB1Rs modifies growth cone dynamics ex vivo. Progression of dynamic, F-actin-rich corticofugal growth cones from organotypic slices cultured for 24 to 48 hr, prepared from P4-6 rat brains, previously electroporated in utero at E16 to express EB3-eGFP, LifeAct-mCherry, with or without Flag-CB1R-eCFP, was followed by time-lapse imaging. (A) Experimental design and illustration of a typical transfected cortical area (A) and of a typical labeled growing axon (B). For the illustration, the organotypic section was fixed and EB3-eGFP signal was enhanced by incubation with an anti-GFP antibody. (B-E) Response to CB1R agonist WIN (1 μM , added at 0 min). The F-actin-rich growth cone is indicated by arrowheads. Open arrowheads indicate growth cone position at 0 min (B, D) WIN-induced retraction in growth cones expressing EB3-eGFP, LifeAct-mCherry, and Flag-CB1R-eCFP is abolished by pre-treatment with 5 μM CB1R-specific antagonist AM281. (C, E) WIN-induced retraction in growth cones expressing EB3-eGFP and LifeAct-mCherry is abolished by pre-treatment with blebbistatin (25 μM). Results are pooled from at least two independent experiments and are expressed as mean \pm SEM. * $p < 0.05$; ** $p < 0.01$; *** $p < 0.001$, calculated using Student's t-test. Scale bar: 100 μm on A, 20 μm elsewhere.

DOI: 10.7554/eLife.03159.016

Discussion

Our results show that acute CB1R activation results in rapid contraction of the neuronal actomyosin cytoskeleton. CB1R acts through heterotrimeric G_{12}/G_{13} proteins, Rho GTPase, and ROCK to induce the contractile interaction of NM II with F-actin. This contraction triggers the retraction of the actin-rich growth cone of the most distal 60–70 μm of the axon in cultured hippocampal neurons and in cortical neurons in organotypic slices. Pharmacological inhibition of either CB1Rs or NM II during brain development leads to excessive growth of corticofugal axons in vivo, suggesting that CB1R-induced actomyosin contractility is necessary for the correct pathfinding by mediating their repulsion from the sub-ventricular zone. This contractile behavior is not limited to the growth cone since CB1R-induced actomyosin contraction leads to neurite retraction, cell rounding, and a significant elevation in cell rigidity in the Neuro2A cells. Similarly, in the somatodendritic region of cultured



Video 5. CB1R activation induces retraction of actin-rich growth cones in organotypic slices. Dynamic, F-actin-rich corticofugal growth cones from organotypic slices were cultured for 24 to 48 hr, prepared from P4–6 rat brains, previously electroporated with EB3-eGFP, LifeAct-mCherry, and Flag-CB1R-eCFP in utero (See **Figure 3**). Treatment with 1 μ M WIN at 30 min induces retraction of the growth cone. Scale bar: 20 μ m.

DOI: [10.7554/eLife.03159.017](https://doi.org/10.7554/eLife.03159.017)

inhibition or genetic silencing of NM II leads to disorganization of the growth cone, allowing rapid axon extension over inhibitory substrates (*Hur et al., 2011*). In the present study, we report a comparable *in vivo* effect, by showing that blebbistatin treatment leads to elevated axonal invasion of the embryonic subventricular zone (SVZ). This territory, which is populated by proliferating neuronal progenitors, is typically avoided by corticofugal axons during their progression towards sub-cortical target zones. To our knowledge, these results show for the first time the existence of NM II-mediated axonal repulsion *in vivo*, suggesting that mobilization of NM II participates in the correct guidance of corticofugal axonal projections. Since pharmacological CB1R blockade has similar effects to NM II inhibition (i.e., excessive axonal growth), a likely scenario suggests that the endocannabinoid 2-AG, whose synthesizing enzyme DAGL α is specifically expressed at high levels by proliferating progenitor cells of the SVZ (*Goncalves et al., 2008*), acts through CB1Rs to repulse invading corticofugal axons through NM II-mediated growth cone retraction.

CB1Rs also rapidly modify the morphology of Neuro2A cells and cultured hippocampal neurons through enhanced actomyosin contractility, leading to large-scale reorganization of neuronal compartments that contain F-actin. Notably, CB1Rs not only alter the internal organization of the growth cone, as suggested previously (*Berghuis et al., 2007; Argaw et al., 2011*), but cause the retraction of the distal axon over several tens of microns, both in cultured hippocampal neurons and in cortical neurons in organotypic slices. This NM II-dependent contraction leads to the characteristic periodic bending of microtubules. This particular phenotype was similarly observed during strong NM II-mediated retraction in DRG neurons after the activation of the LPA receptor (*Bouquet et al., 2007*) or after treatment with Sema 3A (*Gallo et al., 2002; Wylie and Chantler, 2003; Gallo, 2006*). In addition, nitric oxide, widely recognized to induce axonal retractions during development (*Cramer et al., 1998; Ernst et al., 2000*), was reported to induce similar rapid axonal retraction accompanied by periodic bends (*He et al., 2002*).

In addition, RhoA, ROCK, and NM II are known constitutive inhibitors of neurite development (*Kollins et al., 2009*). By activating the CB1R/G $_{12}$ /G $_{13}$ /Rho GTPase/ROCK/NM II axis characterized in our study, endo- or exogenous cannabinoids are likely to mobilize a widely employed myosin-activating machinery that is involved in growth cone navigation and in the establishment and maintenance of neuronal morphology. Interestingly, similar G $_{12}$ /G $_{13}$ -dependent signaling mechanism is mobilized downstream of at least two developmentally implied neuronal GPCRs, the LPA receptor (*Katoh et al., 1998; Kranenburg et al., 1999*) and GPR55, a putative ‘atypical’ cannabinoid receptor (*Ryberg et al., 2007; Sharir and Abood, 2010*), through activation by lysophosphatidylinositols but not through genuine cannabinoid ligands (*Obara et al., 2011*). Therefore, coupling of a bona fide neurotransmitter and drug receptor, such as CB1R, to this major developmental pathway may open interesting research and therapeutic perspectives.

hippocampal neurons, distal regions of dendrites retract while proximal parts broaden. Finally, ROCK and NM II mediate the inhibitory effect of chronic CB1R activation on dendrite development, by increasing the natural contractile tone of neurons.

Owing to its position downstream of convergent signaling pathways, the NM II protein plays a pivotal role in the control of tissue architecture through its participation in processes that require cell reshaping and movement, such as cell adhesion, cell migration, and cell division (*Vicente-Manzanares et al., 2009*). In neurons, NM II is also involved in diverse aspects of cell movement, such as neuronal migration and the structural organization and efficient extension of the growth cone, which requires an intricate balance between dynein, microtubules, actin, and different myosin II isoforms (*Vallee et al., 2009*). Remarkably, previous *in vitro* results have shown that NM II is important for turning in response to boundaries of substrate-bound laminin-1 (*Turney and Bridgman, 2005*) and that pharmacological

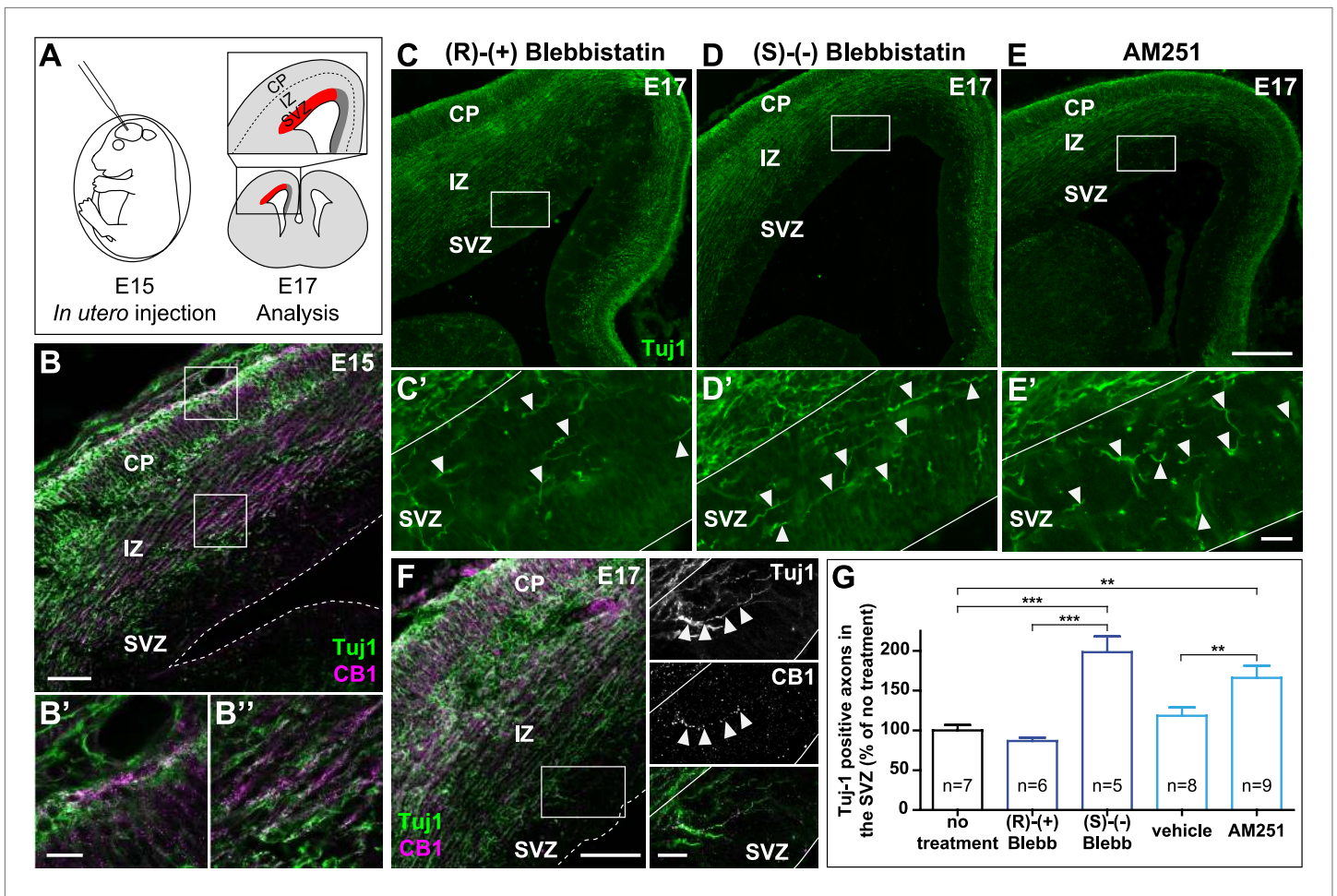


Figure 5. Actomyosin contractility is required for the correct targeting of CB1R expressing corticofugal axons. **(A)** Experimental design. Left: in utero intracerebroventricular injection of E15 rat embryos. Right: analysis of axons in the lateral sub-ventricular zone (SVZ, red). **(B)** E15 corticofugal axons starting from the cortical plate (CP) and progressing through the intermediate zone (IZ) highly co-express Tuj-1 (green) and CB1R (magenta) and mostly avoid the SVZ. **(C–G)** In embryos injected with 1 μ l of the active NM II-ATPase inhibitor (S)-(-)-blebbistatin (250 μ M) **(D, D')**, or with AM251 (1 mM) **(E, E')**, but not with the inactive (R)-(+)-stereoisomer (250 μ M) or the vehicle of AM251 (DMSO 2.8%) **(C–C')**, there is a significant increase of mistargeted corticofugal axons in the lateral SVZ (arrowheads, **G**). **(F)** Expression of endogenous CB1Rs in a representative Tuj1 positive axon invading the SVZ (arrowheads) from an embryo treated with active (S)-(-)-blebbistatin. Results are pooled from three independent experiments and are expressed as mean \pm SEM, ** $p < 0.01$, *** $p < 0.001$ calculated using one-way ANOVA followed by Newman–Keuls post-tests. Scale bars: 100 μ m on **B** and **F** (left), 250 μ m on **C, D,** and **E** and 25 μ m on **B', B'', C', D', E',** and **F** (right). DOI: 10.7554/eLife.03159.018

The following figure supplement is available for figure 5:

Figure supplement 1. Corticofugal origin of Tuj1-expressing axons in the SVZ.

DOI: 10.7554/eLife.03159.019

NM II is also involved in integrin-mediated cell adhesion; in turn, the adhesive properties of the substrate also control NM II activation (Vicente-Manzanares et al., 2009). However, CB1R-mediated morphological effects reported in the present study may not result from reduced neuronal adhesion, considering the time-scale of the rapid neuronal retraction. Instead, retracting the Neuro2A cells and growth cones of hippocampal neurons both in vitro and ex vivo leave behind thin membranous fibers, which contain F-Actin and are still attached to the adhesive substrate. The formation and morphology of these fibers are similar to those of retraction fibers reported in mitotic cells (Cramer and Mitchison, 1995) also generated by rapid contraction of the cellular actomyosin cortex (Théry and Bornens, 2008).

The ensemble of these results combined with the bulk of the available experimental data (reviewed in Gaffuri et al., 2012) suggests that endocannabinoids acting through CB1Rs exert a general negative effect on cell spreading and neurite growth. Basal cell-autonomous or paracrine activation of CB1Rs would yield relatively weak tonic inhibition of growth in the majority of developmental

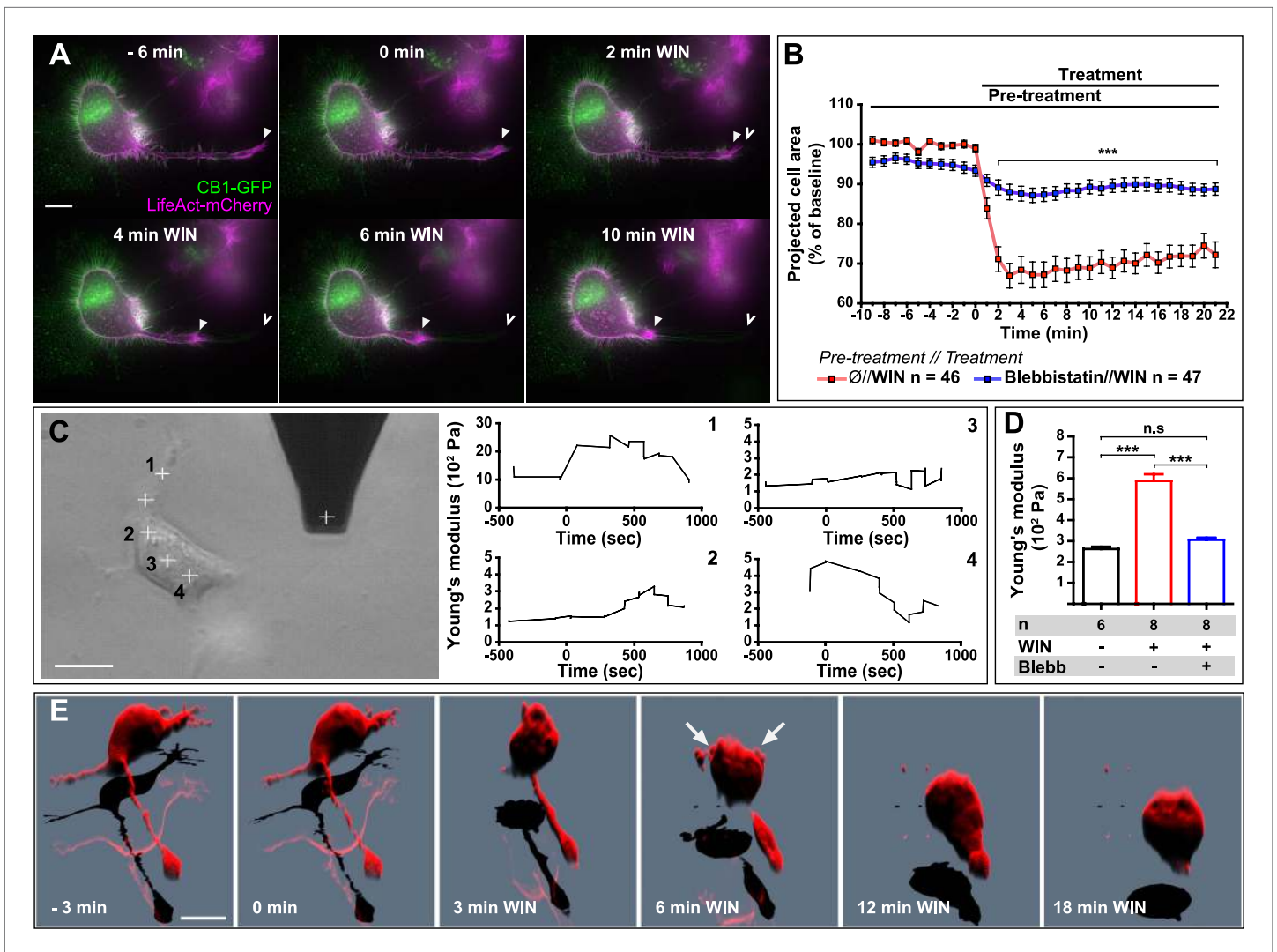


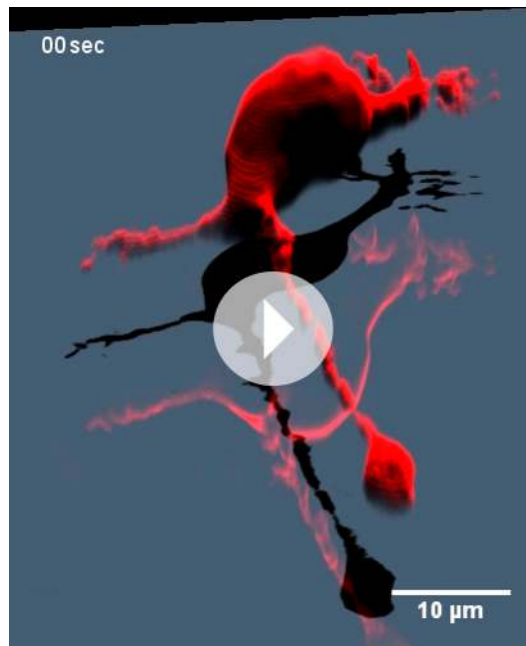
Figure 6. CB1R-induced actomyosin contraction results in neurite retraction and transiently increased cell stiffness in Neuro2A cells. **(A and B)** Cells expressing Flag-CB1R-eGFP and LifeAct-mCherry. F-actin accumulates in the extremity and shaft of neurites (arrowheads). Agonist WIN (100 nM) induces retraction of neurites. Open arrowheads: neurite tip at 0 min. **(B)** Blebbistatin (25 μ M) significantly reduces 100 nM WIN-induced cell rounding. Results are expressed as mean \pm SEM. **(C)** Phase-contrast image of a Neuro2A cell and the AFM cantilever. Stiffness response to 100 nM WIN at different cell locations (crosses). Subsequent measurements were focused on the cell bodies, corresponding to positions 2 and 3. **(D)** Blebbistatin (25 μ M) significantly reduces 100 nM WIN-induced increase of cell stiffness. Results are pooled from at least three independent experiments and are expressed as mean stiffness between 2 and 8 min after stimulation \pm SEM. **(E)** 3D reconstruction shows neurite retraction, cell rounding, and transitory blebbing (arrows) following WIN treatment (100 nM). n.s $p > 0.05$; *** $p < 0.001$, calculated using Student's t-test on B and using one-way ANOVA followed by Newman-Keuls post-tests on **(D)**. Scale bars: 10 μ m on **(A)** and **(E)**, 15 μ m on **(C)**.

DOI: 10.7554/eLife.03159.020

settings in all neuronal sub-regions where F-actin is present. Local growth-promoting effectors at the growth cone, such as the self-amplifying autocrine promoter BDNF (Cheng et al., 2011) or netrin-1 (Argaw et al., 2011), may locally surmount this weak negative tone. The resulting 'channeling' effect of widespread CB1R-mediated weak inhibition would help the neuron to focus its resources to a limited amount of growth locations, leading to more efficient polarized growth. Such weak inhibition may serve also to coordinated guidance of axonal fascicles in the brain where moderate production of eCBs by nearby axons would be used as a repulsion cue that helps axons to grow straightly towards their target. However, when growth cones reach a region highly enriched with eCBs, such as the sub-ventricular zone, enhanced eCB signaling could result in growth cone arrest, repulsion, or collapse, efficiently steering out CB1R-expressing axons from these areas. Finally, CB1R-induced actomyosin contractility may also contribute to establish functionally adequate somatodendritic



Video 6. CB1R activation induces neurite retraction and cell rounding in Neuro 2A cells. Neuro2A cell expressing Flag-CB1R-eGFP and LifeAct-mCherry. Treatment with 100 nM WIN at 30 min induces neurite retraction and cell rounding. Scale bar: 20 μm . DOI: [10.7554/eLife.03159.021](https://doi.org/10.7554/eLife.03159.021)



Video 7. CB1R activation induces neurite retraction, cell rounding, and temporary blebbing in Neuro 2A cells. 3D reconstruction of a Neuro2A cell expressing Flag-CB1R-eGFP and DsRed2. Treatment with 100 nM WIN at 7 min (420 s) induces neurite retraction, cell rounding, and transitory blebbing. Scale bar: 10 μm DOI: [10.7554/eLife.03159.022](https://doi.org/10.7554/eLife.03159.022)

Fluor-conjugated secondary antibodies were purchased from Life Technologies (Carlsbad, CA). All culture media and additives were from PAA Laboratories (Pasching, Austria).

DNA constructs

The DsRed2 encoding plasmid was produced by Clontech (Mountain View, CA). The CB1R-eCFP (Enhanced Cyan Fluorescent Protein) and Flag-CB1R-eGFP constructs have previously been described

morphology, acting as a negative regulator of dendritic growth.

In our study, we were able to characterize in detail CB1R-induced actomyosin contraction, which is rather subtle and transitory downstream of endogenous GPCRs, by using high-resolution time-lapse imaging, atomic force microscopy, and moderate over-expression of CB1Rs. Consequently, the amplitudes of reported cytoskeleton changes are likely dramatic compared to CB1R-induced remodeling in typical physiological settings. Nevertheless, the results concerning endogenous CB1Rs, obtained in cultured neurons, in organotypic slices, and in vivo suggest physiological relevance for our findings.

In conclusion, we identify NM II-mediated actomyosin contraction as a mechanism conveying a wide-ranging inhibitory role for cannabinoids in neuronal expansion and growth, downstream of CB1R coupled to G_{12}/G_{13} proteins and the Rho-associated kinase ROCK. Such modulation of the neural actomyosin cytoskeleton has not yet been reported downstream of neurotransmitter GPCRs, therefore our results open previously unexpected perspectives in the study and comprehension of brain function.

Materials and methods

Chemicals and antibodies

CB1R agonists WIN55,212-2, CP-55940, HU-210, 2-arachidonoylglycerol (2-AG), and CB1R-specific antagonist/inverse agonists AM281 and AM251 were acquired from Tocris Bioscience (Bristol, UK). Rho-associated kinase inhibitor Y-27632 and nocodazole were purchased from Calbiochem (San Diego, CA). Blebbistatin, cytochalasin D, ML-7, Δ^9 -Tetrahydrocannabinidiol solution (THC), and pertussis toxin (PTX) were brought from Sigma (Saint-Louis, MO). The Rho-GTPase inhibitor C3 transferase (C3T) was purchased from Cytoskeleton, Inc. Mouse anti-neuron-specific beta III tubulin (Tuj-1) antibody was obtained from Sigma (Catalog Number T8660), rabbit anti-myosin phospho S19/phospho S20 antibody was obtained from Rockland (Gilbertsville, PA, Cat. no. 600-401-416), rabbit anti-CB1R antibody was produced by Eurogentec (Seraing, Belgium) and described previously (Thibault *et al.*, 2013), and chicken anti-GFP antibody was from AVES (Tigard, OR). Alexa-

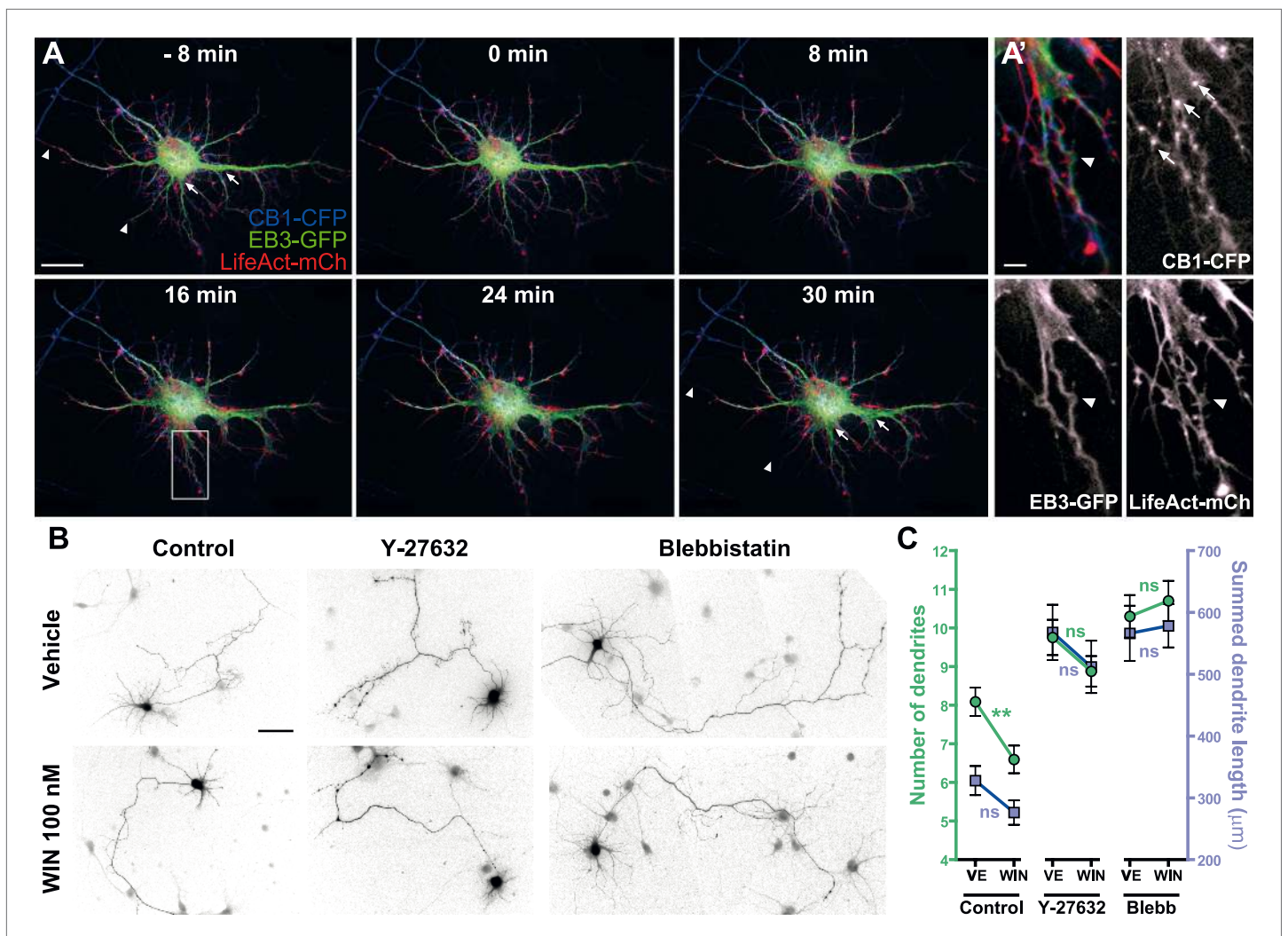


Figure 7. Acute and chronic effects of CB1R-mediated actomyosin contraction on somatodendritic morphology. **(A)** Cultured hippocampal neurons expressing CB1R-eCFP, LifeAct-mCherry, and EB3-eGFP at DIV8. Application of 100 nM WIN results in rapid and significant reorganization of somatodendritic morphology, characterized by retraction of distal dendritic parts (arrowheads), and broadening of the proximal part of dendrites (arrows). **(A')** In dendrites, characteristic microtubule bending (arrowheads) and appearance of straight cable-like F-actin bundles (arrowheads) are accompanied by CB1R endocytosis after agonist activation (arrows). **(B and C)** Chronic inhibition of ROCK or NM II abolishes CB1R-activation induced changes structure of the cultured hippocampal neurons expressing Flag-CB1R-eGFP and the structural marker DsRed2 at DIV4. Cells were fixed at 24 hr after treatment with inhibitors of ROCK (Y-27632, 10 μ M) or NM II (blebbistatin, 25 μ M) in the presence of vehicle (VE) or CB1R agonist WIN (100 nM). A representative cell is shown for each condition. **(C)** Results are pooled from at least two independent experiments and are expressed as mean \pm SEM. n.s $p > 0.05$; ** $p < 0.01$, calculated using one-way ANOVA followed by Newman-Keuls post-tests. Scale bars: 20 μ m on **(A)**, 5 μ m on **(A')**, and 50 μ m on **(B)**.

DOI: 10.7554/eLife.03159.023

elsewhere (Leterrier et al., 2004, 2006). LifeAct-mCherry was a kind gift of G Montagnac and P Chavrier (Institut Curie, Paris, France). pEGFP-N3-EB3 plasmid was a kind gift of M Piel (Institut Curie, Paris, France). pCAG-Cre and pCALNL-GFP in which GFP was replaced by Flag-CB1R-eCFP, LifeAct-mCherry, or eGFP-EB3 sequences for in utero electroporation experiments were a kind gift from T Matsuda and C Cepko (Harvard Medical School). All constructs were verified by full-length sequencing.

RNA interference

For silencing rat *non-muscle myosin IIA*, rat *non-muscle myosin IIB*, rat G_{12} and rat G_{13} specific SMARTpools were chemically synthesized by Dharmacon Research (Lafayette, CO) and siRNA targeting



Video 8. CB1R activation induces rapid remodeling of the somatodendritic region in cultured hippocampal neurons. Somatodendritic region of a cultured hippocampal neuron co-expressing CB1R-eCFP, LifeAct-mCherry, and EB3-eGFP at DIV8. The axon, whose initial segment is typically strongly labeled with EB3-GFP, exits the frame in the upper-left corner. The F-actin-rich growth cone, such as shown in **Video 1**, is at the growing end of the axon, typically hundreds of microns away from the soma at DIV8. Treatment with 100 WIN at 10 min induces retraction of distal dendrites and broadening of proximal dendrites. Scale bar: 20 μm . DOI: [10.7554/eLife.03159.024](https://doi.org/10.7554/eLife.03159.024)

19 October 1987, Ministère de l'Agriculture et de la Forêt, Service Vétérinaire de la Santé et de la Protection Animale).

Cell transfections

Neuro2A cells were transfected, in 6-well plates for ATF and deconvolution or in 12-well plates for video microscopy, with 0.8 μg of plasmid DNA using Effectene reagent (Qiagen, Venlo, NL) and processed 24 hr after transfection.

Hippocampal neurons were transfected on DIV3 (for morphometry) or DIV5-8 (for videomicroscopy) as follows: for each coverslip, plasmid DNA (2 μg) and Lipofectamine 2000 (1.25 μl , Life Technologies) in Neurobasal medium were combined and incubated for 30 min. After the addition of complete Neurobasal medium containing B27 supplement, the mix was applied onto the neuronal culture for 3 hr at 37°C. Receptor expression was allowed in growth medium for 24 to 72 hr after transfection. Immediately after transfection, DIV3 transfected hippocampal neurons were incubated with different pharmacological treatments and fixed after 24 hr. Our transfection protocol leads to moderate over-expression of CB1Rs and we imaged only low-expressing neurons in which sub-neuronal traffic and targeting of transfected receptors is similar to that of endogenous CB1Rs ([Letierrier et al., 2006](#); [Vitalis et al., 2008](#); [Thibault et al., 2013](#)).

For siRNA transfections, two different mixes were prepared: one with Lipofectamine (2 μl) and plasmid DNA (1.25 μg of Flag-CB1-eGFP and 1.25 μg of LifeAct-mCherry) in 50 μl of Neurobasal medium and one with Lipofectamine and siRNA (2.4 μl of each siRNA at 50 μM alone or combined with other siRNAs were mixed in 50 μl of Neurobasal medium). In controls, appropriate volumes of anti-luciferase siRNA (50 μM) were used to match the total amount of transfected siRNAs. After 30 min of incubation, the two mixes were combined, completed to 250 μl with conditioned complete Neurobasal medium containing B27 supplement and applied to the neuronal culture for 3 hr at 37°C. At the end of incubation, the mix was replaced by fresh complete Neurobasal medium and neurons were used 48 to 72 hr later.

Animals

Animals were housed individually with free access to food and water and maintained in a temperature-controlled environment on a 12 hr light/dark cycle. Experiments were performed in agreement with

luciferase (CGUACGCGGAAUACUUCGA, Proligo-Sigma) was used as a control, as described previously ([Miserey-Lenkei et al., 2010](#)).

Cell cultures

Neuro2A cells (ATCC CCL-131) were grown in DMEM (Life Technologies) supplemented with 4.5 g/l glucose, GlutaMAX I (Life Technologies), 10% fetal bovine serum, 10 U/ml penicillin G and 10 mg/ml streptomycin. Neuronal cultures were prepared as described previously ([Carrel et al., 2011](#)). Briefly, hippocampi of rat embryos were dissected at embryonic days 17–18. After trypsinization, tissue dissociation was achieved with a Pasteur pipette. Cells were plated on poly-D-lysine-coated coverslips at a density of 60,000–75,000 cells per 15 mm coverslip and cultivated in complete Neurobasal (Life Technologies) medium supplemented with B27 (Life Technologies), containing 0.5 mM L-glutamine, 10 U/ml penicillin G, and 10 mg/ml streptomycin containing conditioned medium obtained by incubating glial cultures (70–80% confluency) for 24 hr. Experiments were performed in agreement with the institutional guidelines for the use and care of animals and in compliance with national and international laws and policies (Council directives no. 87-848,

the institutional guidelines for the use and care of animals and in compliance with national and international laws and policies (Council directives no. 87-848, 19 October 1987, Ministère de l'Agriculture et de la Forêt, Service Vétérinaire de la Santé et de la Protection Animale).

In utero electroporation, preparation of organotypic slices, and histological procedures

Pregnant Sprague–Dawley rats at gestation day 16 were anesthetized with Ketamine/Xylazine (75/10 mixture). The abdominal cavity was opened to expose the uterine horns. 1–3 μ l of plasmids (0.5 μ g/ μ l for pCAG-Cre, 1 μ g/ μ l for pCALNL-LifeAct-mCherry and pCALNL-EB3-eGFP, and 1.5 μ g/ μ l for pCALNL-Flag-CB1R-CFP) with 1 mg/ml Fast Green (Sigma) were microinjected through the uterus into the lateral ventricles of embryos by pulled glass capillaries (Drummond Scientific, Broomall, PA). Electroporation was performed by placing the heads of the embryos between tweezer-type electrodes. Square electric pulses (65 V, 50 ms) were passed five times at 1 s intervals using a CUY21 EDIT electroporator (Nepa Gene, Chiba, Japan).

For axonal localization analysis, rat brains (E20) were dissected and fixed for 48 hr in 4% paraformaldehyde (PFA) in PBS at 4°C. Brains were then cryoprotected in 30% sucrose in PBS, frozen in OCT compound (Sakura, Tokyo, Japan), and sectioned coronally at 16 μ m using a cryostat.

For organotypic slice preparation, rats were sacrificed at P4–6 by decapitation under deep anesthesia with pentobarbital. Brains were dissected and transferred into liquid 3% low-melting agarose (38°C) and placed on ice. Embedded brains were cut coronally (300 μ m) with a VT1000S vibratome (Leica, Nussloch, Germany) at 4°C. Slices were transferred onto sterilized culture plate inserts (0.4- μ m pore size, Millicell-CM, Millipore, Billerica, MA) and cultured in semidry conditions in a humidified incubator at 37°C under 5% CO₂ atmosphere in wells containing Neurobasal medium (Life Technologies) supplemented with 1% B27 (vol/vol), 1% N2 (vol/vol), 1% GlutaMAX I (vol/vol), and 1% penicillin/streptomycin (vol/vol, Life Technologies). Slices were cultured for 24–48 hr before videomicroscopy. For illustration of electroporated cortical area, some organotypic slices cultured for 24 hr were fixed for 2 hr in 4% PFA in PBS.

In utero cerebroventricular injections and histological procedures

Pregnant Sprague–Dawley rats at gestation day 15 were prepared as for in utero electroporation. Then, 1 μ l of a solution containing active NM II ATPase inhibitor (S)-(–)-blebbistatin (250 μ M), inactive (R)-(+)-stereoisomer (250 μ M), AM251 (1 mM), or 2.8% DMSO (vehicle for AM251), mixed with 1 mg/ml Fast Green were microinjected through the uterus into the lateral ventricles of embryos by pulled glass capillaries. Embryos were allowed to develop in utero for 2 days. E17 brains were then dissected, fixed for 48 hr in 4% paraformaldehyde (PFA) in PBS at 4°C, cryoprotected in 30% sucrose in PBS, frozen in OCT compound, and sectioned coronally at 20 μ m using a cryostat.

Immunofluorescence

For immunohistochemical staining of brain sections or fixed organotypic brain slices, sections were incubated with a combination of mouse anti-Tuj1 antibody, C-Ter rabbit antibody, and chicken anti-GFP antibody (each diluted at 1:1000) overnight at room temperature in PBS (0.02 M) containing 0.3% Triton and 0.02% sodium azide (PBS-T-azide). For immunofluorescence detection of phosphoMLC, cultured neurons were fixed for 15 min in 4% PFA with 4% sucrose, permeabilized with PBS-T-azide and incubated for 90 min with the anti-phosphoMLC antibody (1:1000) diluted in 2% Bovin Serum Albumin and 3% Normal Goat Serum.

Following washes, sections or coverslips were incubated with the appropriate secondary antibodies for 2 hr at room temperature and coverslipped with Mowiol mounting medium.

Microscopy

For time-lapse microscopy, coverslips were placed in a Ludin chamber (Life Imaging Services, Basel, Switzerland) filled with imaging buffer (120 mM NaCl, 3 mM KCl, 2 mM CaCl₂, 2 mM MgCl₂, 10 mM glucose, 10 mM HEPES, and 2% B27, pH 7.35, 250 mOsm to match culture growth medium) (Lu *et al.*, 2007). Wide-field images were taken on a motorized Nikon Eclipse Ti-E/B inverted microscope with the Perfect Focus System (PFS) in a 37°C chamber, using an oil immersion CFI Plan APO VC 60x, NA 1.4 objective (Nikon, Melville, NY), equipped with a Polychrome V monochromator (Till Photonics, Gräfelfing, Germany) and an Intensilight light source (Nikon), a CoolSnap HQ2 camera (Photometrics, Tucson, AZ), and piloted by Metamorph 7.7 (Molecular Devices, Sunnyvale, CA). All filter sets were

purchased from Semrock (Rochester, NY) and the absence of cross-talk between different channels was checked with selectively labeled preparations.

For the evaluation of neurite retraction *in vitro*, neurons or Neuro2A cells co-expressing CB1R-eCFP/EB3-eGFP/LifeAct-mCherry or Flag-CB1R-eGFP/LifeAct-mCherry or expressing LifeAct-mCherry alone were imaged every 2 min in each corresponding detection channel, and the mCherry detection channel was used for quantification. Treatments with inhibitors were applied on transfected cells 20 min before stimulation with the agonist. Blebbistatin treated cells were only illuminated through the mCherry excitation channel, in order to avoid phototoxic effects of lower illumination wavelengths. For the evaluation of axon retraction *ex vivo*, neurons co-expressing Flag-CB1-CFP/EB3-eGFP/LifeAct-mCherry or expressing LifeAct-mCherry were imaged every 3 min for 150–240 min, and inhibitor treatments were applied 30 min before agonist stimulation. For pharmacological treatments, ligands dissolved in dimethylsulfoxide were added directly to the culture medium. The highest final concentration reached was 0.2% DMSO; control experiments with up to 0.5% DMSO have shown the absence of effects on neuronal morphology and on the cellular distribution of CB1Rs.

For the analysis of corticofugal axon development, images of labeled rat brain sections were taken on a Zeiss AxioImager M1 microscope using a 40× 0.75 numerical aperture (NA) objective. In each experiment, all acquisitions were performed using strictly identical exposure conditions. For the analysis of the images the SVZ was delimited and the corticofugal axons present in it were counted in blind. Between 5 and 9 embryos were employed per condition analyzing a mean of 9 brain slices per animal.

For morphological analysis, widefield images were taken on a Zeiss Imager M1 microscope with dry 20× NA 0.75 and 40× NA 0.75 and oil-immersion 100× NA 1.3 objectives (Zeiss, Oberkochen, Germany). In all cases, emission and excitation filters proper to each fluorophore were used sequentially and the absence of cross-talk between different channels was checked with selectively labeled preparations. Neurites were outlined and measured using an assisted semiautomatic method (NeuronJ) (Meijering *et al.*, 2004). For neurons at DIV4, primary and secondary dendrites were outlined and their number and length were measured. Retraction of neurites was determined using Metamorph.

For the CB1/Tuj1 and Tuj1/GFP co-localization experiments, and for illustration of the electroporated cortical area, images were taken on a Nikon A1 laser-scanning confocal microscope with dry 10× NA 0.30 and 20× NA 0.75 and oil-immersion 60×, NA 1.4 objectives.

Atomic force microscopy measurement and processing

Novascan (Ames, IA) cantilevers with attached SiO₂ spherical beads (1-μm diameter) and nominal spring constant 0.06 N/m were used. Photodiode sensitivities of each cantilever were calibrated before and after measurements on the stiff surface region of culture dishes. The cantilever spring constant was determined using the thermal fluctuations method implemented in the Nanoscope 8 software (Hutter, 1993).

Measurements were carried out 1 day after seeding Neuro2A cells at 37°C on a commercial AFM (Catalyst, Bruker, Billerica, MA) mounted on an inverted optical microscope (Olympus, Tokyo, Japan). We obtained force–distance (F–z) curves of ~3 μm peak-to-peak amplitude at 0.5 Hz, ~3 μm/s. The maximum relative deflection (d) was controlled to reach an indentation depth of <400 nm. We placed the cantilever tip around the center of the cells with the help of optical images of the tip and samples acquired with a CCD camera (Hamamatsu, Shizuoka Pref., Japan).

Three different cells were probed in a single AFM session by acquiring force curves at time intervals of <1 min. The same spherical tip was used in all measurements. Measurements were carried out before and after addition of vehicle or 100 nM of WIN at time point 0. Blebbistatin was applied 20 min before time point 0.

Each experiment approaching F–z curve was fitted by the Hertz model of a sphere indenting an elastic half space (Rico *et al.*, 2005): $F = \frac{4}{3} \frac{E}{1-\nu^2} \sqrt{R\delta^{3/2}}$, where E being the Young's modulus, ν the Poisson ratio (0.5), R, the radius of the sphere, and, δ the indentation, which was calculated in terms of the point of contact (z_c) and deflection offset (d₀) as $\delta = z - z_c - (d - d_0)$.

Deconvolution and surface reconstruction

To follow shape change of retracting Neuro2A cells co-expressing Flag-CB1R-eGFP and the structural marker DsRed2, high-resolution images were acquired as a three-dimensional time series. For 61 time

frames separated by 30 s, 51 z-slices of dimensions 149.64 μm \times 111.8 μm (1392 pixels \times 1040 pixels) and separated by 0.5 μm in height were captured. The signal to noise ratio of the images was improved by deconvoluting the z-stacks at each time frame by iteratively computing the maximum-likelihood deconvolved image using the Richardson–Lucy algorithm (Huygens Professional, Huygens, Inc., Hilversum, Netherlands). The stopping criteria for the algorithm was determined using a conservative estimate of the image quality improvement at each iteration, and approximately 60 iterations of the algorithm were required in order to significantly improve the image quality without introducing artefacts into the deconvolved image. The surface of the deconvolved image stacks was computed at each time frame using a surface-rendering algorithm (FreeSFP, Huygens, Inc.).

Statistical analysis

Data were analyzed using Prism (GraphPad Software, La Jolla, CA). Kolmogorov–Smirnov and Shapiro–Wilk tests were used to verify the normal distribution of the data. If the hypothesis of normality was confirmed, the significance of differences in mean was calculated using Student's t-test or one-way ANOVA followed by Newman–Keuls post-tests for p-value adjustment, elsewhere Kruskal–Wallis one-way ANOVA followed by Dunn's post-tests was used. For significance symbols, 'ns' means $p \geq 0.05$, one symbol means $p \leq 0.05$, two symbols mean $p \leq 0.01$, and three symbols mean $p \leq 0.001$. Outliers were removed when appropriate by applying Grubbs's test (ESD method [extreme studentized deviate]) available at the GraphPad QuickCalcs website: <http://www.graphpad.com/quickcalcs/ConflInterval1.cfm> (April 2014) or at NIST/SEMATECH e-Handbook of Statistical Methods, <http://www.itl.nist.gov/div898/handbook/eda/section3/eda35h1.htm>, April 2014.

Acknowledgements

We thank Mathieu Piel, Ana-Maria Lennon-Duménil, and Stéphanie Miserey-Lenkei (Institut Curie, Paris France), Christophe Letierrier (Laboratoire de Neurobiologie des Canaux Ioniques, INSERM UMR641, Marseille, France), and Arpiar Saunders (Harvard Medical School, Boston) for their insightful discussions, important technical advice, and comments on the manuscript. We thank Natalia Velez-Alicea (MIT, Boston) for her comments on the English syntax. ABR was supported by a doctoral fellowship from Fondation pour la Recherche Médicale, AR was supported by a postdoctoral fellowship from the Basque Country Government, DC was supported by a postdoctoral fellowship from the AXA Research Fund, AS was supported by a fellowship from the Fondation ARC. This work was supported by a grant to ZL from the French Agence Nationale de la Recherche (ANR-09-MNPS-004-01). The research in Dr SS' lab is supported by the Institut National de la Santé et Recherche Médicale (INSERM), the Aix-Marseille Université, and the French Agence Nationale de la Recherche (ANR).

Additional information

Funding

Funder	Grant reference number	Author
Agence Nationale de la Recherche	ANR-09-MNPS-004-01	Zsolt Lenkei
Institut national de la santé et de la recherche médicale		Simon Scheuring, Zsolt Lenkei

The funders had no role in study design, data collection and interpretation, or the decision to submit the work for publication.

Author contributions

ABR, AR, DC, Conception and design, Acquisition of data, Analysis and interpretation of data, Drafting or revising the article; BMJ, FR, SS, Conception and design, Acquisition of data, Analysis and interpretation of data; AS, MH-C, JF, MHMF, Acquisition of data, Analysis and interpretation of data; ZL, Conception and design, Analysis and interpretation of data, Drafting or revising the article

Ethics

Animal experimentation: Experiments were performed in agreement with the institutional guidelines for the use and care of animals and in compliance with national and international laws and policies

(Council directives no. 87-848, 19 October 1987, Ministère de l'Agriculture et de la Forêt, Service Vétérinaire de la Santé et de la Protection Animale). All surgery was performed under Ketamine/Xylazine anesthesia, and every effort was made to minimize suffering.

References

- Argaw A**, Duff G, Zabouri N, Cécyre B, Chainé N, Cherif H, Tea N, Lutz B, Ptito M, Bouchard JF. 2011. Concerted action of CB1 cannabinoid receptor and deleted in colorectal cancer in axon guidance. *Journal of Neuroscience* **31**:1489–1499. doi: [10.1523/JNEUROSCI.4134-09.2011](https://doi.org/10.1523/JNEUROSCI.4134-09.2011).
- Berghuis P**, Rajniecek AM, Morozov YM, Ross RA, Mulder J, Urbán GM, Monory K, Marsicano G, Matteoli M, Canty A, Irving AJ, Katona I, Yanagawa Y, Rakic P, Lutz B, Mackie K, Harkany T. 2007. Hardwiring the brain: endocannabinoids shape neuronal connectivity. *Science* **316**:1212–1216. doi: [10.1126/science.1137406](https://doi.org/10.1126/science.1137406).
- Bouquet C**, Ravaille-Veron M, Propst F, Nothias F. 2007. MAP1B coordinates microtubule and actin filament remodeling in adult mouse Schwann cell tips and DRG neuron growth cones. *Molecular and Cellular Neurosciences* **36**:235–247. doi: [10.1016/j.mcn.2007.07.002](https://doi.org/10.1016/j.mcn.2007.07.002).
- Carrel D**, Simon A, Emerit MB, Rivals I, Leterrier C, Biard M, Hamon M, Darmon M, Lenkei Z. 2011. Axonal targeting of the 5-HT1B serotonin receptor relies on structure-specific constitutive activation. *Traffic* **12**:1501–1520. doi: [10.1111/j.1600-0854.2011.01260.x](https://doi.org/10.1111/j.1600-0854.2011.01260.x).
- Charras GT**, Coughlin M, Mitchison TJ, Mahadevan L. 2008. Life and times of a cellular bleb. *Biophysical Journal* **94**:1836–1853. doi: [10.1529/biophysj.107.113605](https://doi.org/10.1529/biophysj.107.113605).
- Cheng PL**, Song AH, Wong YH, Wang S, Zhang X, Poo MM. 2011. Self-amplifying autocrine actions of BDNF in axon development. *Proceedings of the National Academy of Sciences of USA* **108**:18430–18435. doi: [10.1073/pnas.1115907108](https://doi.org/10.1073/pnas.1115907108).
- Cramer KS**, Leamey CA, Sur M. 1998. Nitric oxide as a signaling molecule in visual system development. *Progress in Brain Research* **118**:101–114. doi: [10.1016/S0079-6123\(08\)63203-3](https://doi.org/10.1016/S0079-6123(08)63203-3).
- Cramer LP**, Mitchison TJ. 1995. Myosin is involved in postmitotic cell spreading. *The Journal of Cell Biology* **131**:179–189. doi: [10.1083/jcb.131.1.179](https://doi.org/10.1083/jcb.131.1.179).
- Cunningham CC**. 1995. Actin polymerization and intracellular solvent flow in cell surface blebbing. *The Journal of Cell Biology* **129**:1589–1599. doi: [10.1083/jcb.129.6.1589](https://doi.org/10.1083/jcb.129.6.1589).
- Dent EW**, Tang F, Kalil K. 2003. Axon guidance by growth cones and branches: common cytoskeletal and signaling mechanisms. *The Neuroscientist* **9**:343–353. doi: [10.1177/1073858403252683](https://doi.org/10.1177/1073858403252683).
- Ernst AF**, Gallo G, Letourneau PC, McLoon SC. 2000. Stabilization of growing retinal axons by the combined signaling of nitric oxide and brain-derived neurotrophic factor. *The Journal of Neuroscience* **20**:1458–1469.
- Etienne-Manneville S**, Hall A. 2002. Rho GTPases in cell biology. *Nature* **420**:629–635. doi: [10.1038/nature01148](https://doi.org/10.1038/nature01148).
- Forscher P**, Smith SJ. 1988. Actions of cytochalasins on the organization of actin filaments and microtubules in a neuronal growth cone. *The Journal of Cell Biology* **107**:1505–1516. doi: [10.1083/jcb.107.4.1505](https://doi.org/10.1083/jcb.107.4.1505).
- Gaffuri AL**, Ladarre D, Lenkei Z. 2012. Type-1 cannabinoid receptor signaling in neuronal development. *Pharmacology* **90**:19–39. doi: [10.1159/000339075](https://doi.org/10.1159/000339075).
- Gallo G**, Yee HF Jr, Letourneau PC. 2002. Actin turnover is required to prevent axon retraction driven by endogenous actomyosin contractility. *The Journal of Cell Biology* **158**:1219–1228. doi: [10.1083/jcb.200204140](https://doi.org/10.1083/jcb.200204140).
- Gallo G**. 2006. RhoA-kinase coordinates F-actin organization and myosin II activity during semaphorin-3A-induced axon retraction. *Journal of Cell Science* **119**:3413–3423. doi: [10.1242/jcs.03084](https://doi.org/10.1242/jcs.03084).
- Goncalves MB**, Suetterlin P, Yip P, Molina-Holgado F, Walker DJ, Oudin MJ, Zentar MP, Pollard S, Yáñez-Muñoz RJ, Williams G, Walsh FS, Pangalos MN, Doherty P. 2008. A diacylglycerol lipase-CB2 cannabinoid pathway regulates adult subventricular zone neurogenesis in an age-dependent manner. *Molecular and Cellular Neuroscience* **38**:526–536. doi: [10.1016/j.mcn.2008.05.001](https://doi.org/10.1016/j.mcn.2008.05.001).
- Hall A**, Lalli G. 2010. Rho and Ras GTPases in axon growth, guidance, and branching. *Cold Spring Harbor Perspectives in Biology* **2**:a001818. doi: [10.1101/cshperspect.a001818](https://doi.org/10.1101/cshperspect.a001818).
- Harkany T**, Keimpema E, Barabás K, Mulder J. 2008. Endocannabinoid functions controlling neuronal specification during brain development. *Molecular and Cellular Endocrinology* **286**:S84–S90. doi: [10.1016/j.mce.2008.02.011](https://doi.org/10.1016/j.mce.2008.02.011).
- He Y**, Yu W, Baas PW. 2002. Microtubule reconfiguration during axonal retraction induced by nitric oxide. *Journal of Neuroscience* **22**:5982–5991.
- Howlett AC**. 2005. Cannabinoid receptor signaling. (Cannabinoids).
- Hur EM**, Yang IH, Kim DH, Byun J, Sajjilafu, Xu WL, Nicovich PR, Cheong R, Levchenko A, Thakor N, Zhou FQ. 2011. Engineering neuronal growth cones to promote axon regeneration over inhibitory molecules. *Proceedings of the National Academy of Sciences of USA* **108**:5057–5062. doi: [10.1073/pnas.1011258108](https://doi.org/10.1073/pnas.1011258108).
- Hutter JLAB**. 1993. Calibration of atomic-force microscope tips. *Review of Scientific Instruments* **64**:6.
- Ishii I**, Chun J. 2002. Anandamide-induced neuroblastoma cell rounding via the CB1 cannabinoid receptors. *Neuroreport* **13**:593–596. doi: [10.1097/00001756-200204160-00011](https://doi.org/10.1097/00001756-200204160-00011).
- Kaibuchi K**, Kuroda S, Amano M. 1999. Regulation of the cytoskeleton and cell adhesion by the Rho family GTPases in mammalian cells. *Annual Review of Biochemistry* **68**:459–486. doi: [10.1146/annurev.biochem.68.1.459](https://doi.org/10.1146/annurev.biochem.68.1.459).

- Katoh H**, Aoki J, Yamaguchi Y, Kitano Y, Ichikawa A, Negishi M. 1998. Constitutively active Galpha12, Galpha13, and Galphaq induce Rho-dependent neurite retraction through different signaling pathways. *Journal of Biological Chemistry* **273**:28700–28707. doi: [10.1074/jbc.273.44.28700](https://doi.org/10.1074/jbc.273.44.28700).
- Keimpema E**, Tortoriello G, Alpár A, Capsoni S, Arisi I, Calvigioni D, Hu SS, Cattaneo A, Doherty P, Mackie K, Harkany T. 2013. Nerve growth factor scales endocannabinoid signaling by regulating monoacylglycerol lipase turnover in developing cholinergic neurons. *Proceedings of the National Academy of Sciences of USA* **110**:1935–1940. doi: [10.1073/pnas.1212563110](https://doi.org/10.1073/pnas.1212563110).
- Kollins KM**, Hu J, Bridgman PC, Huang YQ, Gallo G. 2009. Myosin-II negatively regulates minor process extension and the temporal development of neuronal polarity. *Developmental neurobiology* **69**:279–298. doi: [10.1002/dneu.20704](https://doi.org/10.1002/dneu.20704).
- Kovács M**, Tóth J, Hetényi C, Málnási-Csizmadia A, Sellers JR. 2004. Mechanism of blebbistatin inhibition of myosin II. *Journal of Biological Chemistry* **279**:35557–35563. doi: [10.1074/jbc.M405319200](https://doi.org/10.1074/jbc.M405319200).
- Kranenburg O**, Poland M, van Horck FP, Drechsel D, Hall A, Moolenaar WH. 1999. Activation of RhoA by lysophosphatidic acid and Galpha12/13 subunits in neuronal cells: induction of neurite retraction. *Molecular Biology of the Cell* **10**:1851–1857. doi: [10.1091/mbc.10.6.1851](https://doi.org/10.1091/mbc.10.6.1851).
- Letierrier C**, Bonnard D, Carrel D, Rossier J, Lenkei Z. 2004. Constitutive endocytic cycle of the CB1 cannabinoid receptor. *The Journal of Biological Chemistry* **279**:36013–36021. doi: [10.1074/jbc.M403990200](https://doi.org/10.1074/jbc.M403990200).
- Letierrier C**, Lainé J, Darmon M, Boudin H, Rossier J, Lenkei Z. 2006. Constitutive activation drives compartment-selective endocytosis and axonal targeting of type 1 cannabinoid receptors. *The Journal of Neuroscience* **26**:3141–3153. doi: [10.1523/JNEUROSCI.5437-05.2006](https://doi.org/10.1523/JNEUROSCI.5437-05.2006).
- Lu J**, Helton TD, Blanpied TA, Rácz B, Newpher TM, Weinberg RJ, Ehlers MD. 2007. Postsynaptic positioning of endocytic zones and AMPA receptor cycling by physical coupling of dynamin-3 to Homer. *Neuron* **55**:874–889. doi: [10.1016/j.neuron.2007.06.041](https://doi.org/10.1016/j.neuron.2007.06.041).
- Lu YB**, Franze K, Seifert G, Steinhäuser C, Kirchhoff F, Wolburg H, Guck J, Janmey P, Wei EQ, Käs J, Reichenbach A. 2006. Viscoelastic properties of individual glial cells and neurons in the CNS. *Proceedings of the National Academy of Sciences of USA* **103**:17759–17764. doi: [10.1073/pnas.0606150103](https://doi.org/10.1073/pnas.0606150103).
- Meijering E**, Jacob M, Sarria JC, Steiner P, Hirling H, Unser M. 2004. Design and validation of a tool for neurite tracing and analysis in fluorescence microscopy images. *Cytometry Part A* **58**:167–176. doi: [10.1002/cyto.a.20022](https://doi.org/10.1002/cyto.a.20022).
- Miserey-Lenkei S**, Chalancon G, Bardin S, Formstecher E, Goud B, Echard A. 2010. Rab and actomyosin-dependent fission of transport vesicles at the Golgi complex. *Nature Cell Biology* **12**:645–654. doi: [10.1038/ncb2067](https://doi.org/10.1038/ncb2067).
- Mulder J**, Aguado T, Keimpema E, Barabas K, Ballester Rosado CJ, Nguyen L, Monory K, Marsicano G, Di Marzo V, Hurd YL, Guillemot F, Mackie K, Lutz B, Guzmán M, Lu HC, Galve-Roperh I, Harkany T. 2008. Endocannabinoid signaling controls pyramidal cell specification and long-range axon patterning. *Proceedings of the National Academy of Sciences of USA* **105**:8760–8765. doi: [10.1073/pnas.0803545105](https://doi.org/10.1073/pnas.0803545105).
- Obara Y**, Ueno S, Yanagihata Y, Nakahata N. 2011. Lysophosphatidylinositol causes neurite retraction via GPR55, G13 and RhoA in PC12. Cells. *PLOS ONE* **6**:e24284. doi: [10.1371/journal.pone.0024284](https://doi.org/10.1371/journal.pone.0024284).
- Rico F**, Roca-Cusachs P, Gavara N, Farré R, Rotger M, Navajas D. 2005. Probing mechanical properties of living cells by atomic force microscopy with blunted pyramidal cantilever tips. *Physical review E, Statistical, Nonlinear, and Soft Matter Physics* **72**:021914. doi: [10.1103/PhysRevE.72.021914](https://doi.org/10.1103/PhysRevE.72.021914).
- Riedl J**, Crevenna AH, Kessenbrock K, Yu JH, Neukirchen D, Bista M, Bradke F, Jenne D, Holak TA, Werb Z, Sixt M, Wedlich-Soldner R. 2008. Lifeact: a versatile marker to visualize F-actin. *Nature methods* **5**:605–607. doi: [10.1038/nmeth.1220](https://doi.org/10.1038/nmeth.1220).
- Rosner H**, Möller W, Wassermann T, Mihatsch J, Blum M. 2007. Attenuation of actinomyosin contractile activity in growth cones accelerates filopodia-guided and microtubule-based neurite elongation. *Brain Research* **1176**:1–10. doi: [10.1016/j.brainres.2007.07.081](https://doi.org/10.1016/j.brainres.2007.07.081).
- Ryberg E**, Larsson N, Sjögren S, Hjorth S, Hermansson NO, Leonova J, Elebring T, Nilsson K, Drmota T, Greasley PJ. 2007. The orphan receptor GPR55 is a novel cannabinoid receptor. *British Journal of Pharmacology* **152**:1092–1101. doi: [10.1038/sj.bjp.0707460](https://doi.org/10.1038/sj.bjp.0707460).
- Sharir H**, Abood ME. 2010. Pharmacological characterization of GPR55, a putative cannabinoid receptor. *Pharmacology & Therapeutics* **126**:301–313. doi: [10.1016/j.pharmthera.2010.02.004](https://doi.org/10.1016/j.pharmthera.2010.02.004).
- Stepanova T**, Slemmer J, Hoogenraad CC, Lansbergen G, Dortland B, De Zeeuw CI, Grosveld F, van Cappellen G, Akhmanova A, Galjart N. 2003. Visualization of microtubule growth in cultured neurons via the use of EB3-GFP (end-binding protein 3-green fluorescent protein). *Journal of Neuroscience* **23**:2655–2664.
- Stewart MP**, Helenius J, Toyoda Y, Ramanathan SP, Muller DJ, Hyman AA. 2010. Hydrostatic pressure and the actomyosin cortex drive mitotic cell rounding. *Nature* **469**:226–230. doi: [10.1038/nature09642](https://doi.org/10.1038/nature09642).
- Théry M**, Bornens M. 2008. Get round and stiff for mitosis. *HFSP Journal* **2**:65–71. doi: [10.2976/1.2895661](https://doi.org/10.2976/1.2895661).
- Thibault K**, Carrel D, Bonnard D, Gallatz K, Simon A, Biard M, Pezet S, Palkovits M, Lenkei Z. 2013. Activation-dependent subcellular distribution patterns of CB1 cannabinoid receptors in the rat forebrain. *Cerebral Cortex* **23**:2581–2591. doi: [10.1093/cercor/bhs240](https://doi.org/10.1093/cercor/bhs240).
- Turney SG**, Bridgman PC. 2005. Laminin stimulates and guides axonal outgrowth via growth cone myosin II activity. *Nature Neuroscience* **8**:717–719. doi: [10.1038/nn1466](https://doi.org/10.1038/nn1466).
- Vallee RB**, Seale GE, Tsai JW. 2009. Emerging roles for myosin II and cytoplasmic dynein in migrating neurons and growth cones. *Trends in Cell Biology* **19**:347–355. doi: [10.1016/j.tcb.2009.03.009](https://doi.org/10.1016/j.tcb.2009.03.009).
- Vicente-Manzanares M**, Ma X, Adelstein RS, Horwitz AR. 2009. Non-muscle myosin II takes centre stage in cell adhesion and migration. *Nature* **10**:778–790.

- Vitalis T**, Lainé J, Simon A, Roland A, Leterrier C, Lenkei Z. 2008. The type 1 cannabinoid receptor is highly expressed in embryonic cortical projection neurons and negatively regulates neurite growth in vitro. *European Journal of Neuroscience* **28**:1705–1718. doi: [10.1111/j.1460-9568.2008.06484.x](https://doi.org/10.1111/j.1460-9568.2008.06484.x).
- Watson S**, Chambers D, Hobbs C, Doherty P, Graham A. 2008. The endocannabinoid receptor, CB1, is required for normal axonal growth and fasciculation. *Molecular and Cellular Neuroscience* **38**:89–97. doi: [10.1016/j.mcn.2008.02.001](https://doi.org/10.1016/j.mcn.2008.02.001).
- Williams EJ**, Walsh FS, Doherty P. 2003. The FGF receptor uses the endocannabinoid signaling system to couple to an axonal growth response. *The Journal of Cell Biology* **160**:481–486. doi: [10.1083/jcb.200210164](https://doi.org/10.1083/jcb.200210164).
- Wu CS**, Zhu J, Wager-Miller J, Wang S, O'Leary D, Monory K, Lutz B, Mackie K, Lu HC. 2010. Requirement of cannabinoid CB1 receptors in cortical pyramidal neurons for appropriate development of corticothalamic and thalamocortical projections. *European Journal of Neuroscience* **32**:693–706. doi: [10.1111/j.1460-9568.2010.07337.x](https://doi.org/10.1111/j.1460-9568.2010.07337.x).
- Wylie SR**, Chantler PD. 2003. Myosin IIA drives neurite retraction. *Molecular Biology of the Cell* **14**:4654–4666. doi: [10.1091/mbc.E03-03-0187](https://doi.org/10.1091/mbc.E03-03-0187).

Results

5 Results Part1: Actomyosin dynamics mediate CB1R-induced inhibition of vesicle release in culture

Given our previous findings that CB1R activation induced retraction of growth cones through a $G_{12/13}$ /RhoA/ROCK pathway, and the unknown nature of the mechanisms driving the established function of CB1R in LTD, we pursued to test the role of actomyosin contraction on CB1R-LTD.

In collaboration with the teams of Vivien Chevaleyre and Laurent Venance, we indeed found that inhibiting actomyosin contractility with blebbistatin prevented CB1R-induced LTD without affecting eCB-STD. This effect was further found to be mediated by ROCK. The results are presented in the ensuing article (McFadden et al., in submission).

These results pointed to a role of actomyosin contraction in CB1R-induced LTD, implying a structural modulation of the presynaptic compartment under CB1R. Given previous findings for a role of actomyosin in synaptic vesicle recycling (described previously) and the evidence that CB1R induces a depletion of vesicles from the presynaptic active zone (AZ) (Ramírez-Franco et al. 2014; García-Morales, Montero, and Moreno-López 2015), we chose to test the hypothesis that actomyosin contraction may lead to a redistribution of synaptic vesicles under CB1R.

First, we tested the direct effect of CB1R on vesicle exocytosis in hippocampal cultures by using the probe synaptophysin-pHluorin (SpH), a sensitive indicator of vesicle exocytosis. Through this method we found that CB1R activation indeed reduced exocytosis at axonal boutons, an effect which was blocked by inhibiting both NMII and ROCK. These results will be detailed below. Second, we tested the effect of CB1R activation on vesicle distribution within the presynaptic compartment in hippocampal cultures using the superresolution STORM method. Through this method we find a reduction of synaptic vesicles at the AZ as well as an increased clustering of the total pool under CB1R activation. The methods employed as well as the preliminary data obtained from these experiments will be described in the next section before presenting my main results in our article in submission.

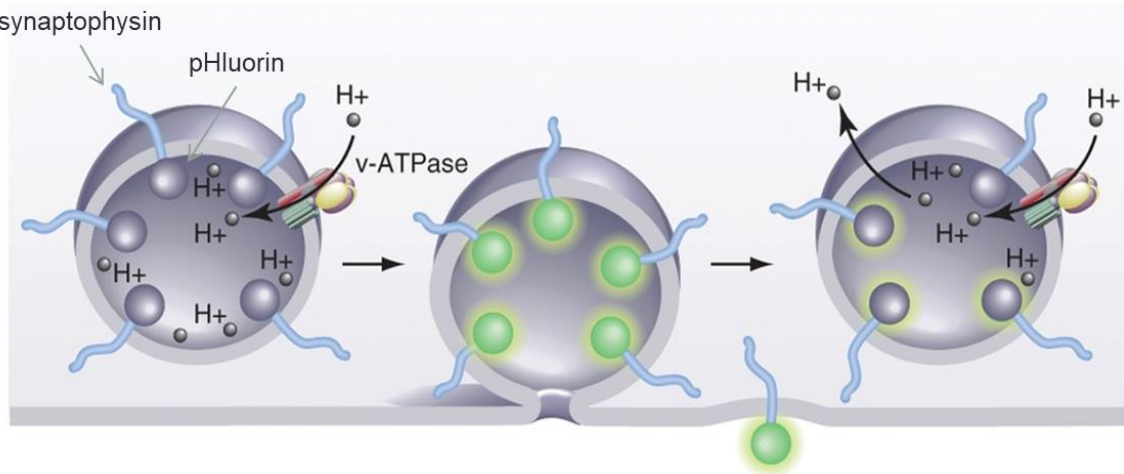


Figure 11. Function of synaptophysin-pHluorin probe in reporting exocytosis

(adapted from Kavalali and Jorgensen (2014)).

5.1 Imaging exocytosis in culture with synaptophluorin

To accomplish this, we first tested the effect of actomyosin contraction on CB1R-induced synaptic effects in a hippocampal culture model. We used a synaptophysin-pHluorin probe to image vesicle exocytosis. This probe has extensively been used in culture as well as in *in vivo* models to study vesicle recycling (Kavalali and Jorgensen 2014). The probe is a construct of synaptophysin, one of the most concentrated synaptic vesicle membrane proteins (Wilhelm et al., 2014; Takamori et al., 2006), and the pH sensitive GFP pHluorin, located on the intraluminal side of synaptophysin (**Figure 11**).

At rest, the pH in the synaptic vesicle lumen is maintained at around 5.5 through proton pumps. Upon membrane fusion, the intraluminal pH increases due to transfer with the extracellular medium, which is at a pH of around 7.4. The pHluorin probe is sensitive to this pH change, going from an inactive to a fluorescent state upon contact with the extracellular medium (**Figure 11**) (Matz et al. 2010). This property makes it a sensitive indicator of vesicle exocytosis.

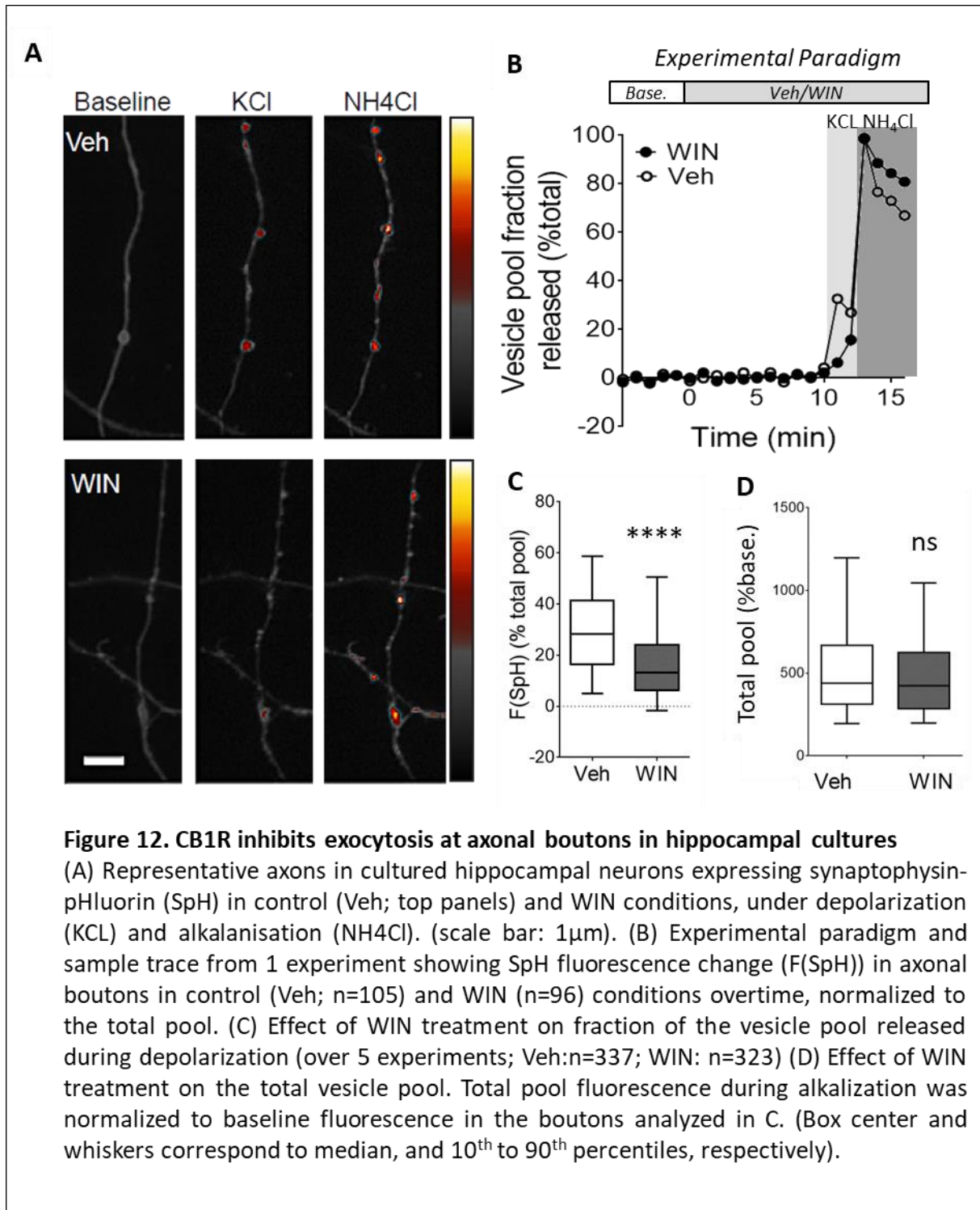
By transfecting our hippocampal cultures with this construct, I was successfully able to image vesicle exocytosis upon depolarization. Indeed, sustained depolarization (2 minutes) of mature neurons (DIV 17-20) with high concentrations of KCL (50mM) induced a significant increase in fluorescence as compared to baseline (**Figure 12**). Furthermore, alkalizing

intracellular compartments with NH₄Cl (50mM) induced a compounded increase in fluorescence, relating to the total pool of vesicles within the axonal bouton. Measuring the fluorescence increase upon depolarization as a percentage of the fluorescence peak upon alkalisation therefore gives us a measure of the fraction of vesicles released upon sustained depolarization. In our model, this fraction was on average about 30% of the total pool (29.47%±1.81), which scales well with other studies having used similar paradigms (Ramírez-Franco et al. 2013; Kavalali and Jorgensen 2014), as well as measures of recycling pool sizes (Annette Denker and Rizzoli 2010).

5.2 CB1R-activation induces a decrease in synaptic vesicle exocytosis

Using this paradigm, I then tested the effect of the CB1R selective agonist WIN55,212-2 (WIN). Bath application of WIN (1µM) for 10 min before depolarization significantly reduced the fraction of vesicles released upon depolarization (**Figure 12BC**) (16.94%±1.67; $p < 0.0001$). Importantly, this effect was not a result of a decrease in the size of the total pool as peak fluorescence increase during alkalization as a percentage of baseline did not differ between vehicle and sWIN treated boutons (**Figure 12D**) (Veh: 528.7%±31.9; WIN:499.6%±32.5; $p = 0.715$), indicating WIN treatment did not affect total pool size by vesicle recycling specifically.

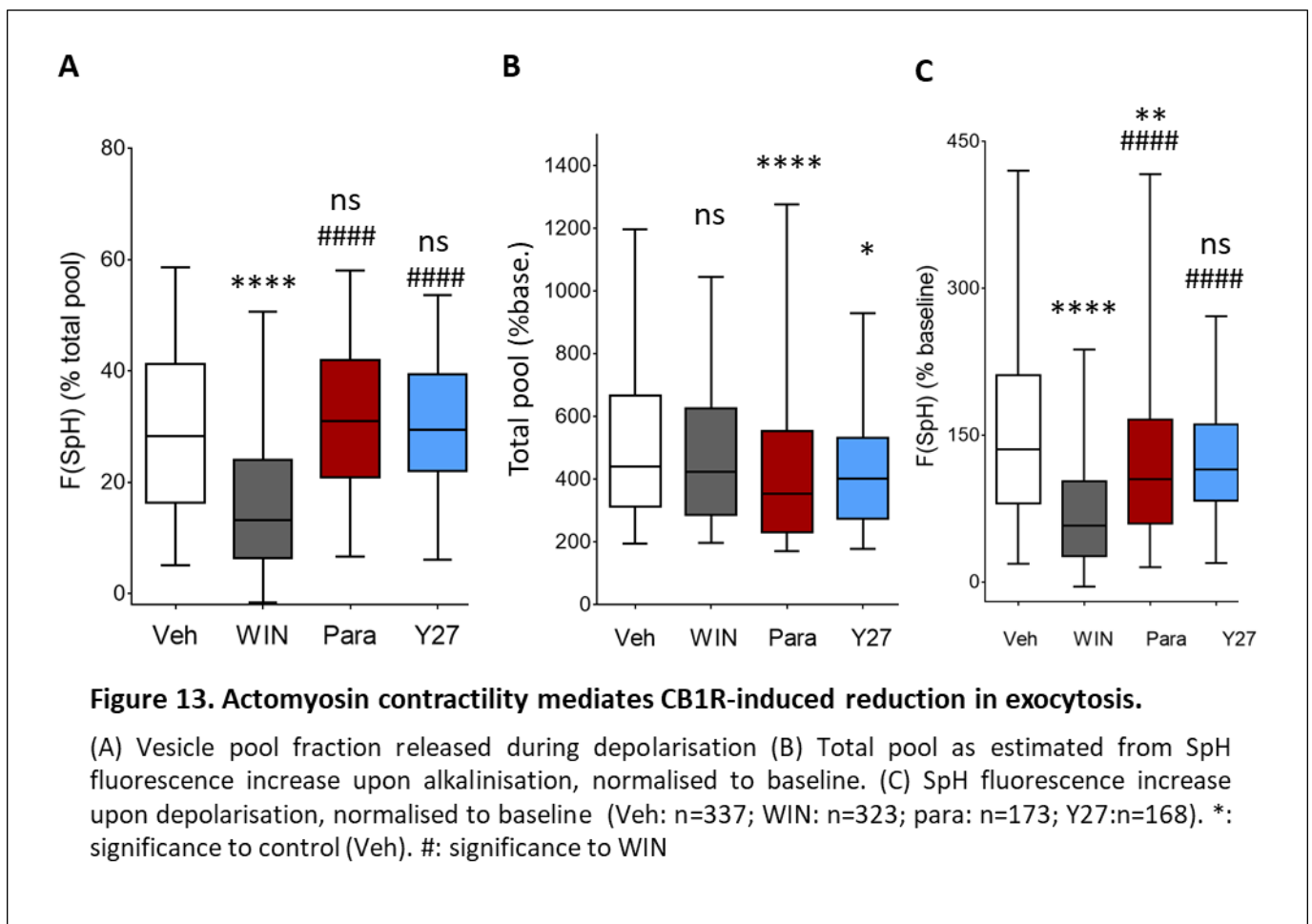
To test the specificity of the effect to CB1R, another set of experiments were conducted by pretreating neurons with CB1R selective inverse agonist AM251. These experiments were conducted with the help of Lea Anselin (Master 2 student). Pretreatment with AM251 for 20 minutes prior to WIN treatment successfully blocked the effect of WIN on exocytosis (AM: 17.67%±1.33; Veh: 14.58%±1.1; WIN: 9.47%±0.838; Veh vs. WIN: $p < 0.0001$; AM vs WIN: $p < 0.0001$). However, in these experiments, control values were significantly different compared to previous experiments.



5.3 Actomyosin contractility through ROCK mediates the effects of CB1R on vesicle exocytosis

Using this paradigm, I tested the effect of actomyosin contractility on CB1R-induced inhibition of exocytosis using both the blue light-resistant variant of blebbistatin, paranitroblebbistatin, as well as the specific ROCK inhibitor Y-27632. As presented in the following article (McFadden et al., in submission) both of these drugs prevented the CB1R-induced inhibition of exocytosis (**Figure 13A**).

Interestingly, in these experiments pretreatment with either paranitroblebbistatin or Y-27632 significantly decreased the fluorescence of the total pool of vesicles as compared to control (**Figure 13B**) (Veh: 528.7%±31.9; WIN:499.6%±32.5; para: 462.2%±50.5; Y27: 439%±32.3) (vs. Veh: WIN: p=0.715; para: p<0.0001; Y27p=0.029). As this could influence the measurement of vesicle fraction released upon depolarization, I therefore verified that the prevention effect of these drugs remained without normalization to the total pool. Indeed



when the fluorescence increase upon depolarization was normalized to baseline levels (Veh:164.6%±11.4; WIN: 81.35%±10.12; para:135.8%±16.3; Y27:126.4%±11.1), the previously described effect remained for all conditions (**Figure13C**) (vs. WIN: Veh: $p < 0.0001$; para: $p < 0.0001$; Y27: $p < 0.0001$), indicating that both paranitroblebbistatin and Y-27632 successfully prevented the effect of CB1R activation on exocytosis.

6 Results Part2: STORM imaging reveals actomyosin-induced synaptic vesicle redistribution under CB1R activation

In the results obtained in electrophysiology through our collaborations, as well as the results obtained using synaptophysin-pHluorin described previously, we show through pharmacological means that CB1R activation leads to a presynaptic suppression of transmission through NMII and ROCK recruitment. As the role of NMII at the actin cytoskeleton is primarily structural, inducing contraction and/or stabilization of actin filaments, we surmised that NMII activation under CB1R would have structural consequences at the presynaptic compartment. Previous studies have shown that CB1R activation could induce a depletion of synaptic vesicles from the docked pool using electron microscopy (García-Morales, Montero, and Moreno-López 2015; Ramírez-Franco et al. 2014). We therefore decided to test the hypothesis that NMII might mediate the redistribution of synaptic vesicles under CB1R.

To test this hypothesis, we decided to use a superresolution microscopy technique known as stochastic optical reconstruction microscopy (STORM). We chose to use this technique rather than EM as it presents several advantages. While the spatial resolution of STORM is much lower than that of EM, it is much better than that of conventional microscopy, and sufficient to image the principal structures of the presynaptic compartment, with some reporting a resolution down to 10nm. Furthermore, STORM requires less sample preparation than EM and allows for greater sample sizes. Finally, importantly, quantitative analyses developed in STORM can translate in the future into dynamic imaging of live samples, through live-imaging superresolution techniques such as PALM.

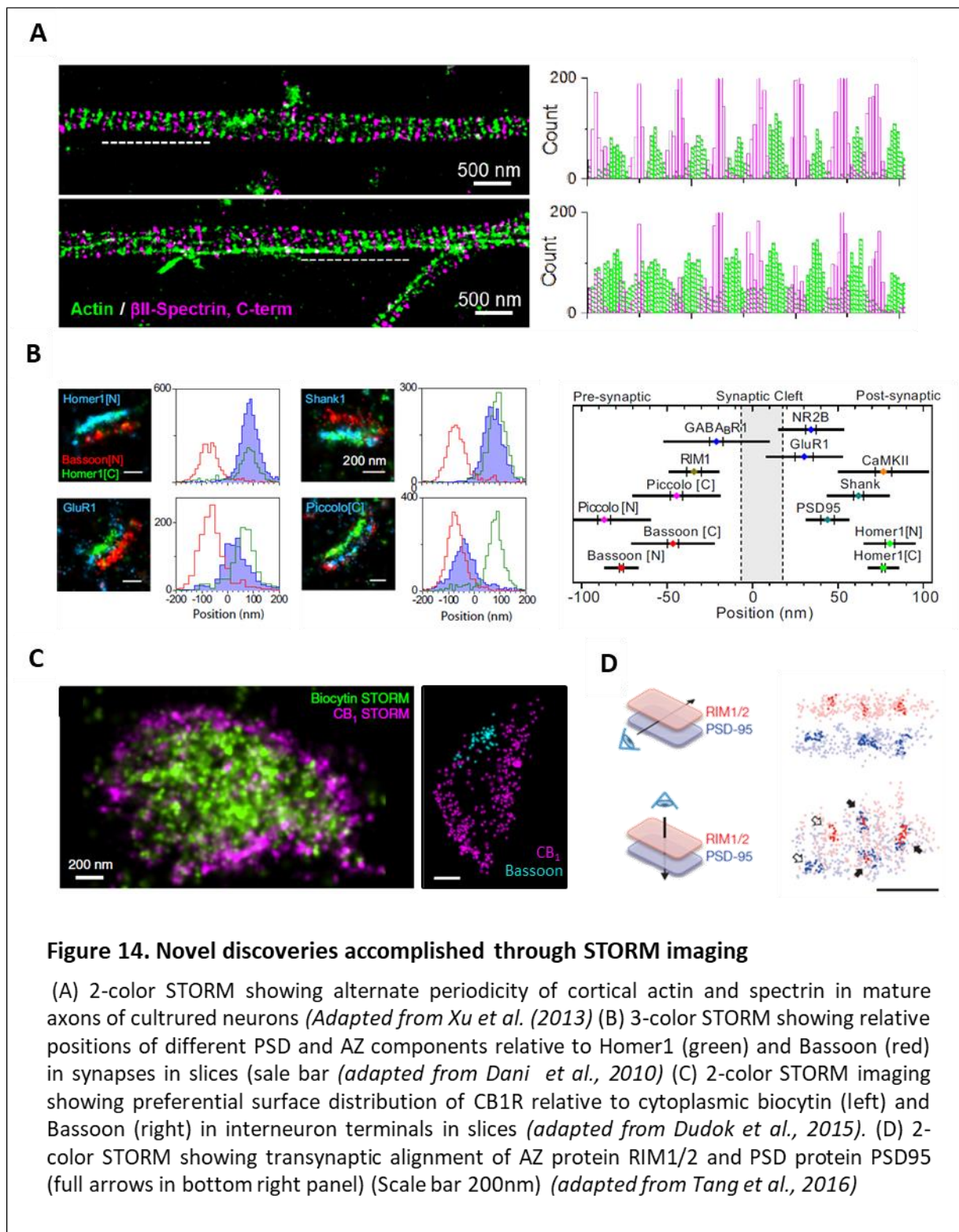
A further advantage of the technique is that the data produced comes in the form of spatial coordinates, as will be explained in the next section, meaning that protein locations and relationships can be precisely quantified in 3 dimensions using coordinate-based analyses which are not applicable to pixel-based images. Part of my thesis has therefore been in applying coordinate-based methods to our STORM data to both identify synaptic vesicles as well as quantify their relative distribution under CB1R activation. In the process I further developed a method by which to predict the 3D active zone location based on PSD properties,

to avoid cross-talk artifacts due to imaging closely located AZ proteins and synaptic vesicle proteins through STORM.

Using this technique, I show through my results that the AZ and PSD may be accurately predicted one from the other based on the sizes of pre and post synaptic protein clusters at individual synapses. Furthermore, taking advantage of this property, I show that there are fewer synaptic vesicles proximal to the active zone under CB1R activation, and that synaptic vesicles within the axonal bouton are more clustered. Importantly, I find that both of these effects are abolished under inhibition of either NMII or ROCK. The following section will outline the methods used to identify AZ and PSD appositions and synaptic vesicles in my STORM images, as well as the structural properties they presented and how they may have changed under WIN treatment.

6.1 Stochastic Optical Reconstruction Microscopy (STORM)

Imaging the presynaptic compartment is difficult with conventional microscopy as the limited resolution of 200nm does not allow the imaging of the small presynaptic structures such as the synaptic vesicles, which are typically around 45nm in diameter (Takamori et al. 2006). Development of superresolution microscopy techniques in the past decade has therefore revolutionized the field, combining higher resolution with the benefits of immunocytochemistry and transgenic fluorescence techniques, both in fixed as well as live samples, which are difficult in EM. Already a number of studies have discovered new properties of neuronal structures that had not been observed previously using stochastic optical reconstruction microscopy (STORM). Using this method, studies have discovered the ring-like structure of cortical actin along neurites (**Figure 14A**) (Xu, Zhong, and Zhuang 2013). At the synapse, STORM microscopy has allowed studies to uncover the relative distribution of presynaptic AZ and postsynaptic PSD proteins (**Figure 14B**) (Dani et al. 2010), as well as the surface distribution and density of membrane proteins such as CB1R (**Figure 14C**) (Dudok et al. 2015). Furthermore, a recent study using STORM has uncovered the precise alignment of presynaptic and postsynaptic proteins into nanocolumns, further showing that the integrity of these nanocolumns defines the efficiency of synaptic transmission (**Figure 14D**) (Tang et al. 2016).



The principles of STORM involve the blinking properties of certain fluorophores in a permissive buffer. When in this buffer, activation of certain fluorophores with a high powered laser will put these fluorophores into a dark state, a high energy state during which the fluorophore does not emit any light. The duration of this dark state is seemingly arbitrary,

meaning that different fluorophores will decrease their energy by emitting photons at different times. STORM takes advantage of this arbitrary property. As fluorophores will fluoresce at different time points, high speed imaging can capture these isolated emissions through time. By fitting Gaussian functions to these isolated spots based on predetermined point spread functions (PSF), a full image of all fluorophore locations can then be reconstructed (Zhong, 2015).

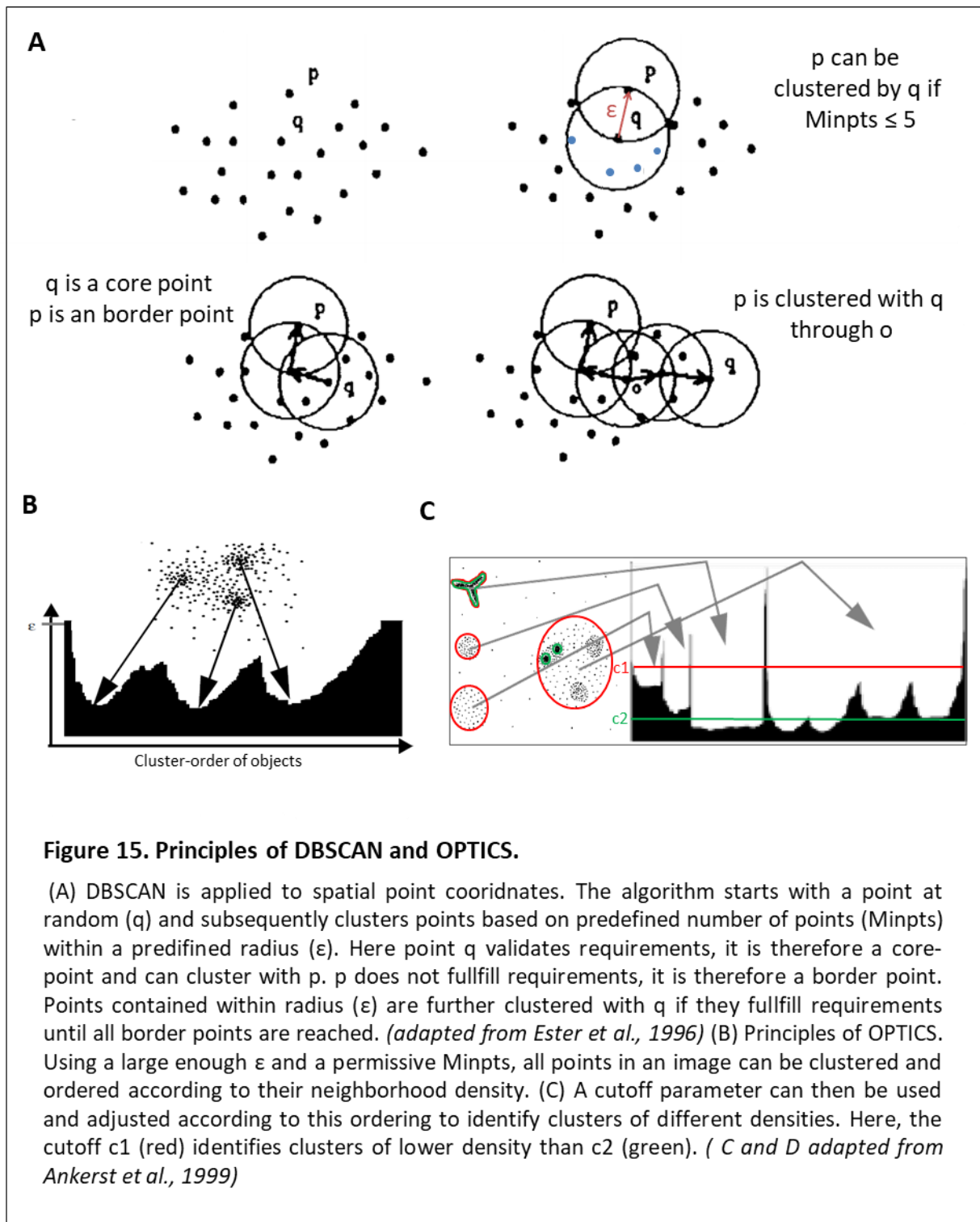
This data comes in the form of spatial coordinates. This comes at an advantage as different types of spatial analyses can therefore be applied to STORM data that cannot be with conventional images. However, as the field is relatively in its infancy, not many tools are available to easily conduct these analyses.

6.2 Clustering analysis for STORM images

Part of my thesis has therefore been in developing a clustering algorithm adequate enough in identifying protein clusters in STORM imaging. This was accomplished by learning how to program in R, a programming language and environment similar to Matlab designed specifically for statistical computing.

To perform this analysis I chose to use a variant of the DBSCAN clustering algorithm, OPTICS (Ankerst et al. 1999). DBSCAN, or Density-Based Spatial Clustering of Applications with Noise, was specifically developed for the clustering of spatial localizations (Ester et al. 1996). It works by assigning clusters into points based on two parameters: ϵ , the maximum distance allowed between two points of the same cluster, and $Minpts$, the minimum number of points necessary to form a cluster (**Figure 15A**). This algorithm is useful in separating localization clusters from non-specific noise based on cluster density, and its simple foundations make it fast and easy to implement.

However, as with most other clustering algorithms, the success of the algorithm is dependent on user defined parameters, in this case ϵ and $Minpts$. The OPTICS variant (Ankerst et al. 1999) uses the same principles as DBSCAN but complements it by ordering points hierarchically based on their nearest neighbors (**Figure 15B**). Given this structure, a single cutoff point can be used to delimit clusters depending on global image density (**Figure 15C**), as will be described below.



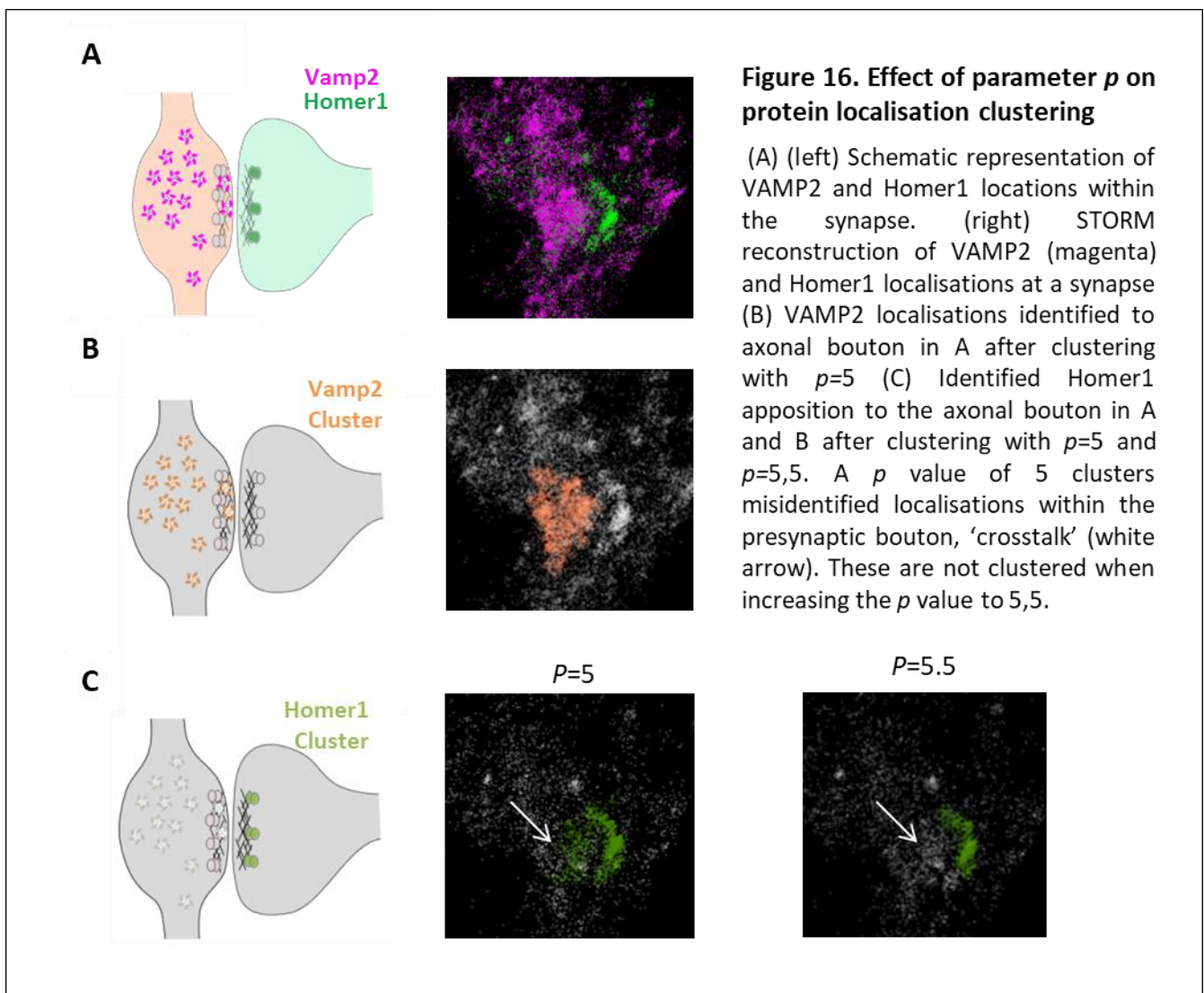
6.2.1.1 Identifying protein clusters

As STORM images are based on immunocytochemistry, a lot of variability in the density of localisations can ensue from quality of staining between experiments. Furthermore, added variability will arise from the quality of the imaging itself, which may vary greatly depending on TIRF angle and buffer oxidation among others. To overcome these differences in

localization density therefore, the parameters of the clustering algorithm were automated based on image density. Specifically, the OPTICS algorithm calculates the distance to each point's Mpts neighbor, named the core-distance. This core-distance decreases the denser the neighborhood of a point, and thus can be used as a measure of density. I therefore based a cutoff point for the algorithm based on median image core-distance and variance:

$$\text{Cutoff} = \text{median}(\text{rcd}) + p * \text{mad}(\text{rcd})$$

rcd corresponds to randomized core-distance, which indicates the core-distance of each point in the image after uniform randomization. This randomization was done so as to avoid variability caused by local assemblies. The mad, or median absolute deviation, was used as a measure of variance. $p=5$ was selected as an initial factor as the 5% significance cutoff of normal distributions is at $4.2 * \text{mad}$. This type of factor determination has been used previously in similar clustering paradigms (Tang et al. 2016). It is a good starting point for cluster



identification as it identifies clusters whose median density is significantly higher than the ambient noise. This parameter was generally sufficient to differentiate separate axonal boutons (**Figure 16 AB**).

For Homer1 and Bassoon appositions however, ‘crosstalk’ caused by misidentified localizations would sometimes cause the algorithm to overshoot the apposition limits (**Figure 16C**), this was therefore corrected by refining the p parameter manually.

6.3 Predicting the Active zone location from the post synaptic density

In order to be able to measure the relative distribution of synaptic vesicles relative to the AZ under CB1R, we needed an AZ reference. As Bassoon stainings imaged conjointly with VAMP2 stainings rendered an important amount of cross-talk, too confounding to differentiate Bassoon and VAMP2 clusters, we wanted to see if we could estimate the AZ location based on a marker disentangled from synaptic vesicles, that would produce less cross-talk. For this purpose we chose to image the post synaptic density protein Homer1.

6.3.1 Properties of Homer1 and Bassoon appositions

As mentioned previously, PSD and AZ size are tightly correlated, suggesting one can be predicted from the other. We tested this in our model by measuring the sizes of Homer1 and Bassoon appositions. The details of the methods used are described in the following article (McFadden et al., in submission). We found that Bassoon and Homer1 appositions were highly correlated both in width and length (**Figure 17ABC**) (width: Spearman’s $r=0.557$, $p<0.0001$; length: $r=0.616$, $p<0.0001$). Although significant, the Spearman’s r correlation coefficient between the depths of Homer1 and Bassoon was relatively low ($r=0.347$, $p=0.0003$) (**Figure 17C**). However, the measured distances between Homer1 and Bassoon appositions was strongly robust between synapses, with a median of 124.3nm and only a 29.2nm difference between the 25th and 75th percentiles.

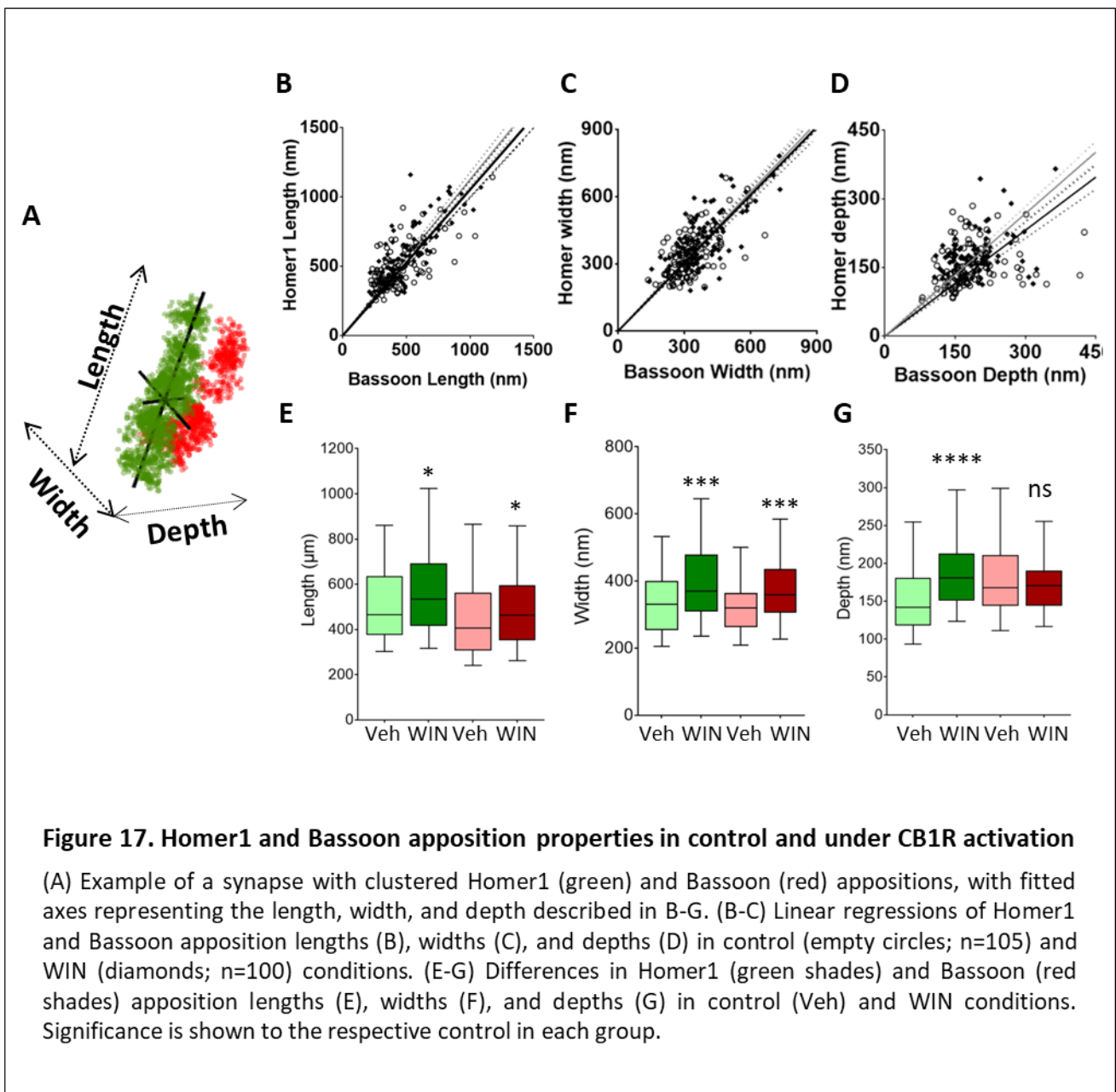
6.3.2 Predicting the AZ

Taking these properties into account, I therefore wrote an algorithm to predict the 3D location of the AZ based on Homer1 properties. The details are described in the Supplementary Methods of the following article. Briefly, an active zone prediction box volume (AZ_v) scaled to the length and width of the Homer1 cluster was projected 125nm along its depth axis towards the presynaptic site. As a control, Bassoon localizations contained within this projection were counted as a percentage of the total Bassoon localizations within the

apposition. Doing this on an independent sample of 55 synapses yielded a median accuracy of 95% (+3.38%), indicating a robust prediction of the 3-dimensional AZ location based on Homer1.

6.3.2.1 CB1R effects on Bassoon and Homer1 properties

I further tested the properties of Bassoon and Homer1 in WIN treated synapses to verify that the AZ prediction would still be valid in WIN treated conditions. Interestingly, both lengths and widths of appositions were significantly increased as compared to control conditions in WIN treated



synapses both for Homer1 (length: Veh: 505.5nm \pm 33.3; WIN: 575.1nm \pm 41.3; p=0.0145)(width: Veh: 341.9nm \pm 19.6; WIN:400.9nm \pm 24.3; p=0.0004) and Bassoon appositions (length: Veh:448.5nm \pm 36.2; WIN:496.6nm \pm 37; p=0.0224) (**Figure 17EF**). Importantly, however, this did not affect the length and width correlations between Bassoon and Homer1 (length: r=0.755, p<0.0001; width: r=0.5941; p<0.0001). Furthermore, distances between Homer1 and Bassoon appositions were strikingly similar to control conditions (120.3nm \pm 15, p=0.361). Taken together these results indicate that the AZ prediction as described would hold true for WIN treated synapses.

Interestingly the median depth of Homer1 clusters was significantly increased in WIN treated synapses as opposed to control (Veh: 153.7nm \pm 9; WIN: 188.2nm \pm 9.8; p<0.0001) (**Figure 17G**), which was not reflected in Bassoon appositions. This would not affect the prediction, however, as the prediction depth is based on the average Bassoon depth in control conditions, which does not change in treated synapses.

6.4 Synaptic vesicle identification

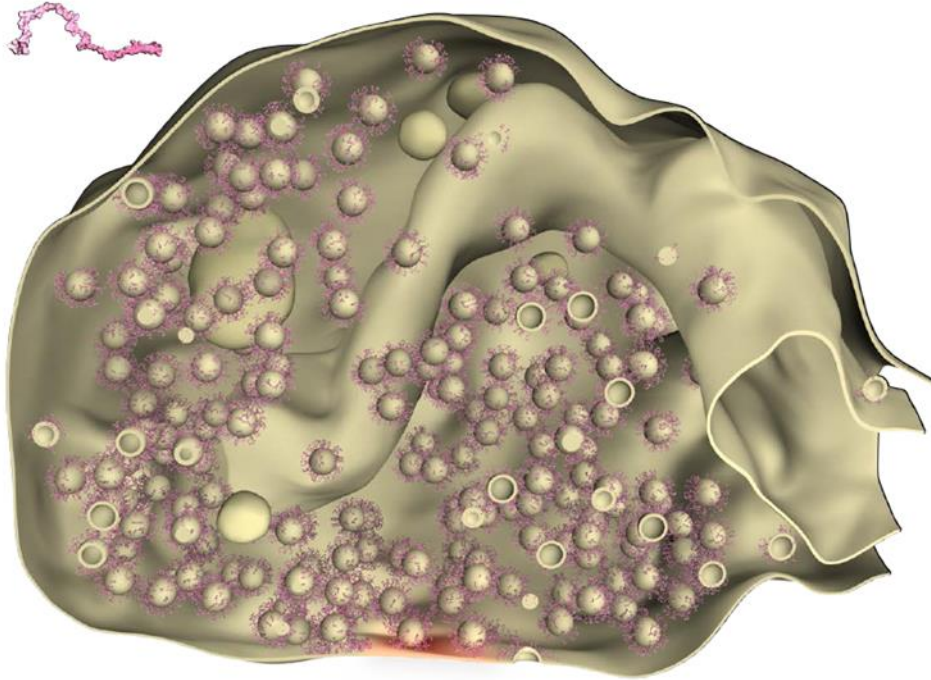
6.4.1 Identifying Synaptic Vesicles

To identify synaptic vesicles, we chose to stain the SNARE protein VAMP2 as it is one of the most abundant synaptic vesicles proteins, with an estimated 60-80 copies per SV (Wilhelm et al., 2014; Takamori et al., 2006). Using VAMP2 as a vesicle marker therefore ensures that there would be enough antibodies surrounding the synaptic vesicles to identify and cluster the vesicles themselves rather than isolated proteins (**Figure 18**).

A

VAMP 2

Category	% of total protein	Molecules/Synapse	Molarity [μM]
SNARE	0.554	26448.00 \pm 661.62	176.59



B

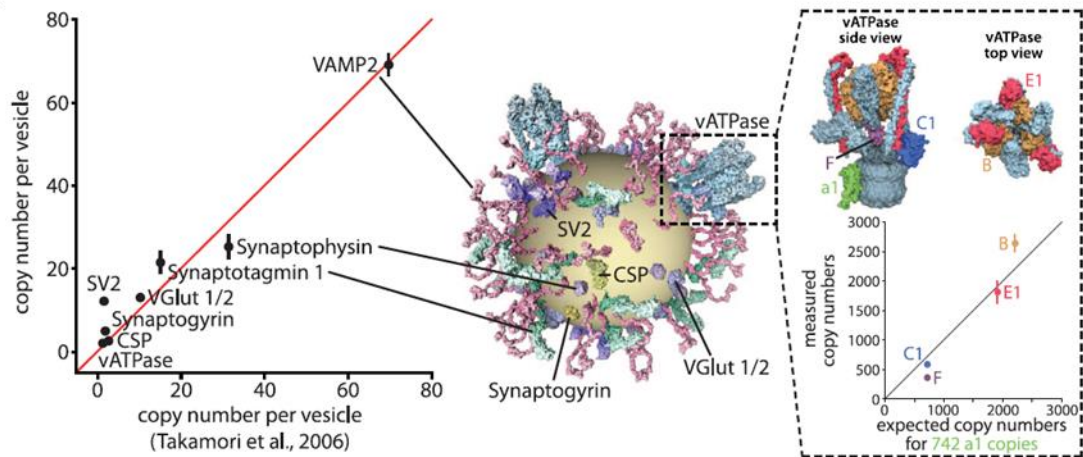


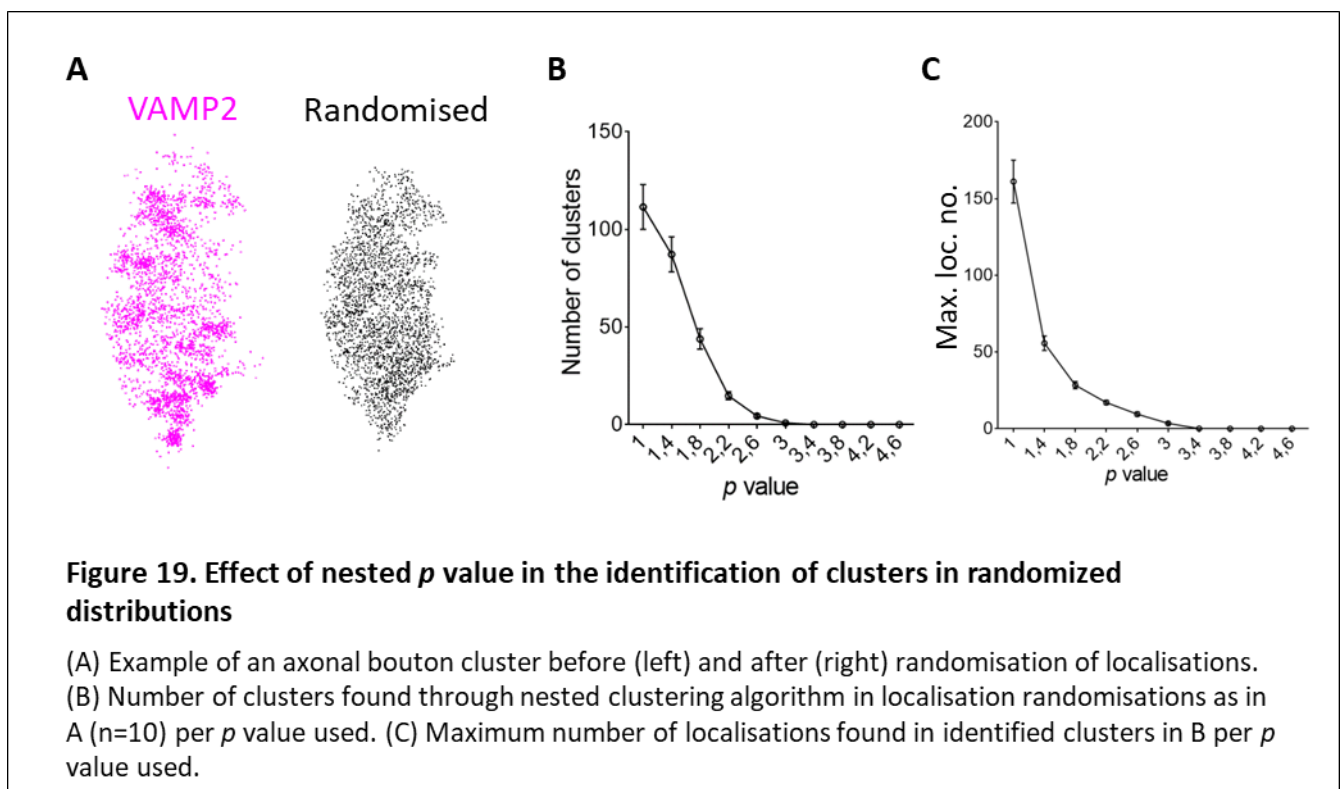
Figure 18. Distribution of Vamp2 within the presynaptic compartment and at synaptic vesicles

(A) Properties of VAMP2 at synaptosomes (top) and simulated distribution within the synapse (bottom). Although VAMP2 is a membrane protein, it is remarkably restricted to synaptic vesicle membranes, as well as fused vesicle protein clusters at the active zone (red area). (B) Copy number of various synaptic vesicle proteins. VAMP2 is the most abundant (*adapted from Wilhelm et al, 2014*)

Identification of synaptic vesicles was performed through a nested clustering algorithm. Axonal boutons were identified by clustering of Vamp2 localizations as described previously. These clusters were further put through a second clustering step. In order to ensure complete automation of the synaptic vesicle identification, to avoid experimenter bias, I further optimized the nested p parameter to ensure no artifacts would be identified. I therefore tested the optimal p cutoff point in axonal bouton clusters where localizations had been randomized along a uniform distribution (**Figure 19A**).

As can be seen from (**Figure 19B**), p values between 1 and 2.2 produced significant amounts of clusters in randomized boutons. Starting at a p of 3, the median number of clusters found over 19 randomizations was 0. Furthermore, looking at the maximum number of localizations found per cluster (**Figure 19C**), we find that starting at $p=3$, the clustering algorithm does not produce clusters of over 12 localizations.

Parameter values were further tested in automatically generated sphere simulations. Spheres were generated by randomizing points within spheres of 60nm in diameter to simulate synaptic vesicles. These spheres were further randomized within a volume of $1\mu\text{m}^3$ to simulate an axonal bouton, with 20 spheres generated per volume. To test the effect of staining density on the accuracy of clustering, I further varied the number of points generated



per sphere (ppS). As can be seen from (Figure 20), the clustering algorithm was more robust at identifying the accurate number of spheres the higher the sphere density. This was also the case with lower ppS numbers for p values between 2.6 and 4.2. Importantly, the number of points localized per identified cluster decreased with higher p values, particularly with lower

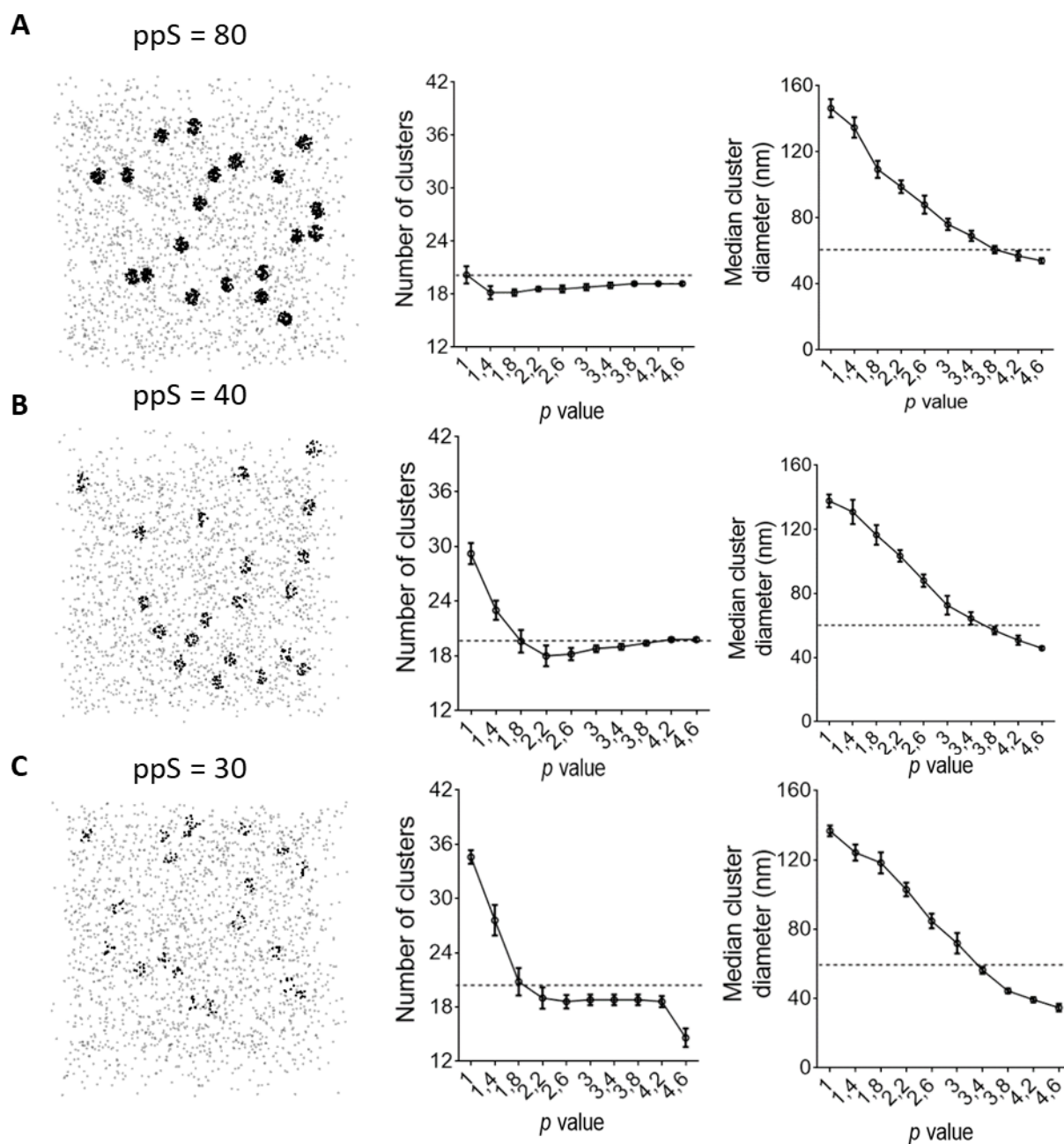


Figure 20. p value effect on simulated spheres of different densities

(A-C) (left) example of randomised sphere simulation (center) number of clusters identified per p value tested for given ppS simulation (right) median diameter of clusters identified per p value tested for given ppS simulation. Dotted line represents input value for sphere generation (20 spheres of 60nm in diameter)

ppS values, with about half and two thirds of the points identified on average at p values of 4.6 and 3.4 respectively. For this reason I chose to use a p value of 3 for further clustering of VAMP2 stainings, with a lower threshold of 15 minimum points per cluster so as to avoid clustering artifacts.

6.4.1.1 Identified Synaptic Vesicle properties

Using the parameters described above, we find an average of 23.29 vesicles per bouton (± 2.35 ; 59 boutons over 3 exp.). As the live experiments showed a decrease in total pool under NMII inhibition, I checked if this could be replicated by this method. There was no difference in to control in the number of vesicle identified, in either WIN (26.99 \pm 2.38; $p=0.079$) or paranitroblebbistatin (25.78 \pm 2.21; $p=0.611$) pretreated synapses (**Figure 21B**). As this difference could also have arisen from a difference in bouton volume I also decided to test this. Here neither, there was no difference between control (0.0997 $\mu\text{m}^3\pm$ 0.012) and WIN (0.108 $\mu\text{m}^3\pm$ 0.01; $p=0.525$) or paranitroblebbistatin (0.099 $\mu\text{m}^3\pm$ 0.009; $p>0.999$) pretreated synapses(**Figure 21C**).

The identified vesicle diameter (67.18nm \pm 2.21) was slightly higher than reported diameters through EM studies, which is around 40nm (Takamori et al., 2006). This discrepancy can be explained by the length added by the primary and secondary antibodies. Furthermore, some added length could be expected due to the clustering algorithm, as the parameter chosen for vesicle clustering tended to produce clusters of slightly larger diameter than those simulated.

Additionally, by applying the same nested clustering algorithm to Bassoon and Homer1 clusters, we find that nested clusters identified for VAMP2 staining have a significantly higher diameter than those identified for Homer1 (opposed to Vamp2: 55.11nm \pm 3.76; $p<0.0001$; opposed to Bassoon: 48.09 \pm 2.25; $p<0.0001$) or Bassoon (42.28nm \pm 1.84; $p<0.0001$) (**Figure 21A**), indicating that the staining is most likely specific to synaptic vesicles.

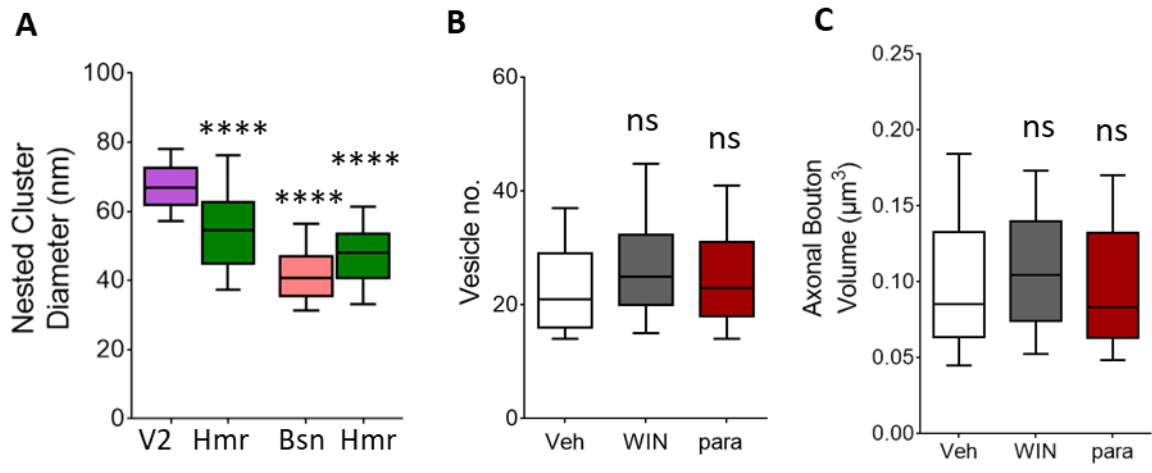


Figure 21. Nested cluster diameters and axonal bouton properties

(A) Difference in the median diameters found using nested clustering algorithm on different synaptic proteins (V2: VAMP2; Hmr: Homer1; Bsn: Bassoon) each Homer1 group is apposed to the protein it was imaged with. Significance is represented to Vamp2 (B) Number of synaptic vesicles identified in different treatment conditions. (C) Axonal bouton volume as represented as estimated by initial Vamp2 clustering in different treatment conditions. In B and C, significance is represented to control (Veh).

7 Results Part 3: Thesis article

Through the methodology presented previously, we therefore tested our working hypothesis developed from the previously presented article, that recruitment of actomyosin contractility would be conserved under CB1R in its synaptic effects, namely LTD. Furthermore, using the method presented above we further tested the hypothesis that CB1R activation would redistribute synaptic vesicles within the presynaptic compartment.

Article 2 (in submission): Actomyosin-mediated nanostructural remodeling of the presynaptic vesicle pool by cannabinoids induces long-term depression

Actomyosin-mediated nanostructural remodeling of the presynaptic vesicle pool by cannabinoids induces long-term depression

Maureen H. McFadden^{1,2,#}, Hao Xu^{3,4,#}, Yihui Cui^{3,4}, Rebecca A. Piskorowski¹, Christophe Letierrier⁵, Diana Zala^{1,2}, Laurent Venance^{3,}, Vivien Chevalerey^{1*} and Zsolt Lenkei^{1,2,*}*

#co-first authors

**co-senior authors*

¹Center of Psychiatry and Neuroscience, INSERM U894, 75014, Paris, France

²Brain Plasticity Unit, CNRS UMR8249, ESPCI-Paris, Paris Sciences et Lettres Research University, 75005, Paris, France

³Center for Interdisciplinary Research in Biology, College de France, INSERM U1050, CNRS UMR7241, Labex Memolife, 75005 Paris, France

⁴University Pierre et Marie Curie, ED 158, Paris, France

⁵Aix-Marseille Université, CNRS UMR 7286, Marseille, France

Corresponding author Zsolt Lenkei, Center of Neuroscience and Psychiatry, INSERM U894, rue de la Santé 102-108, 75015, Paris, France, email: zsolt.lenkei@inserm.fr, phone: +33 6 40 79 51 84

Conflict of Interest The authors declare no competing financial interests.

Acknowledgements This work was supported by the MyoSynapse grant of Paris Sciences et Lettres Research University and the Ecole des Neurosciences de Paris.

Author Contributions *MHM, CL, LV, VC and LZ designed research, MHM, HX, YC, SP, RAP, AMC, DZ and VC realized the experiments, MHM, RAP, LV, VC and LZ wrote the article.*

Endo- and exocannabinoids, such as the psychoactive component of marijuana, exert their effects on brain function by inducing several forms of synaptic plasticity through the modulation of presynaptic vesicle release¹⁻³. However, the molecular mechanisms underlying the widely expressed endocannabinoid-mediated long-term depression³ (eCB-LTD), are poorly understood. Here, we reveal that eCB-LTD depends on the contractile properties of the pre-synaptic actomyosin cytoskeleton. Preventing this contractility, both directly by inhibiting non-muscle myosin II NMII ATPase and indirectly by inhibiting the upstream Rho-associated kinase ROCK, abolished long-term, but not short-term forms of cannabinoid-induced functional plasticity in both inhibitory hippocampal and excitatory cortico-striatal synapses. Furthermore, using 3D superresolution microscopy, we find an actomyosin contractility-dependent redistribution of synaptic vesicle pools within the presynaptic compartment following cannabinoid receptor activation, leading to vesicle clustering and depletion from the pre-synaptic active zone. These results suggest that cannabinoid-induced functional plasticity is mediated by a nanoscale structural reorganization of the presynaptic compartment produced by actomyosin contraction. By introducing the contractile NMII as an important actin binding/structuring protein in the dynamic regulation of synaptic function, our results open new perspectives in the understanding of cognitive function, marijuana intoxication and psychiatric pathogenesis.

Brain connectivity patterns arise through protracted developmental events that lead to assembly, activity-based selection and stabilization of synapses in the mature brain, through precise regulation of cytoskeletal dynamics. Importantly, synapses retain important functional plasticity, a critical component for experience-dependent adjustments of brain function. In the adult brain, both axons and presynaptic terminals undergo long-term experience and activity-dependent structural plasticity⁴, similar to postsynaptic dendritic spines, but molecular mechanisms are not well known. Several established and widespread forms of functional presynaptic plasticity throughout the mammalian brain are retrograde and endocannabinoid-mediated¹⁻³. Activity-dependent release of endocannabinoids (eCBs) by the postsynaptic cell, followed by the activation of the presynaptic type-1 cannabinoid receptor (CB₁R), mediates either a short-term depression (STD) of transmitter release, such as depolarization-induced suppression of inhibition (DSI) or excitation (DSE), or a long-term plasticity, such as eCB-mediated long-term depression (eCB-LTD)³. Although the mechanisms underlying DSI and

DSE have been well established, the presynaptic mechanisms mediating eCB-LTD, much like other forms of long-term presynaptic plasticity, remain poorly understood.

Recently, we described a novel molecular mechanism through which the type-1 cannabinoid receptor (CB₁R), an abundant and well-known mediator of synaptic plasticity in the adult brain, exerts neurodevelopmental effects in the embryonic brain⁵. In this mechanism, endo- and exo-cannabinoids, such as Δ^9 THC, the psychoactive compound of marijuana, act through CB₁R to induce non-muscle myosin II (NMII) contractility, downstream of the small GTPase RhoA and Rho-associated kinase (ROCK). This leads to axonal growth cone retraction and to rapid and lasting changes in the morphology of developing neurons⁵. Because mediators of neuronal development and neurite growth have been proposed to retain their structural roles in the mature brain, albeit on a smaller spatial scale⁶, we investigated here the possible involvement of this molecular mechanism in CB₁R functions regulating synaptic plasticity in the mature brain by combining single-cell patch-clamp recordings with a novel quantitative analysis of presynaptic nanoarchitecture.

First, we inhibited actomyosin contractility in acute brain slices from two different brain regions (**Fig. 1a, 2a**), during well-established forms of eCB-mediated STD and LTD, by preincubating slices for 20 minutes with blebbistatin (10 μ M), a selective NMII ATPase inhibitor⁷. In hippocampal slices, DSI, a STD of GABA release triggered by depolarization of pyramidal cells, was not affected by this treatment (**Fig. 1b**); however, application of blebbistatin, but not of its inactive enantiomer, strikingly abolished the eCB-mediated LTD of inhibitory post-synaptic currents (IPSCs) (**Fig. 1c**). ROCK inhibition with the selective inhibitor Y-27632 (10 μ M) also fully blocked eCB-LTD induction (**Fig. 1h**). Blebbistatin application also abolished the change in release probability following eCB-LTD induction (as indirectly measured by the paired-pulse ratio PPR) (**Fig. 1d**), but did not affect the initial PPR (**Fig. 1d**). This indicates that blebbistatin prevented the eCB-mediated decrease in presynaptic vesicle release without altering basal transmission. In the hippocampus, induction of eCB-LTD requires not only CB₁R activation, but also spontaneous firing of GABAergic interneurons. We therefore tested whether blebbistatin might indirectly alter eCB-LTD by reducing interneuron firing. We found that blebbistatin did not change the amplitude or the frequency of spontaneous IPSCs (**Fig. 1e**). Furthermore, by applying a protocol capable of rescuing eCB-LTD when interneuron firing is blocked, using trains of stimulation following tetanus⁸, we found that eCB-LTD was still not induced in the presence of blebbistatin (**Fig. 1f**). These data strongly indicate that blebbistatin is acting at presynaptic inhibitory terminals

and is not altering interneuron activity. Finally, because eCB-LTD induction requires glutamate release, mGluR activation and eCB release, we bypassed all these steps and directly looked at the effect of CB₁R activation with the high affinity agonist WIN55,212-2⁹ on action potential-independent IPSCs, i.e. miniature IPSCs (mIPSCs). We found that WIN55,212-2 induced a significant decrease in the frequency but not the amplitude of mIPSCs, confirming the presynaptic origin of CB₁R activation (**Fig. 1g**). Strikingly, in the presence of blebbistatin, WIN55,212-2 had no effect on mIPSC frequency (**Fig. 1g**).

While in the hippocampus eCB-induced plasticity is mostly present at inhibitory synapses, it is also widely expressed at excitatory synapses throughout the brain¹⁻³. We therefore investigated the molecular mechanism of eCB-STD and LTD at an excitatory glutamatergic synapse: the corticostriatal synapse at medium-sized spiny neurons (MSNs) of the dorsolateral striatum (**Fig. 2a**). MSNs express eCB-mediated and CB₁R-dependent STD, namely a DSE, and LTD^{10,11}. Here, a sustained depolarization of MSNs induced a DSE (**Fig. 2b**), which, similar to hippocampal DSI, was not significantly affected by blebbistatin (10µM) treatment (**Fig. 2b**). We then tested the striatal eCB-LTD induced after cortical low frequency stimulation (LFS)^{10,12}. This LTD was indeed CB₁R-mediated as it was prevented by treatment with the CB₁R specific inhibitor AM251 (3µM) (**Fig. 2c**). As for hippocampal synapses, actomyosin contraction was found to be necessary for corticostriatal eCB-LTD, which was prevented by treatment with blebbistatin, but not with the inactive blebbistatin enantiomer (**Fig. 2d**). This effect was not due to alterations in basal transmission as we found no significant change in PPR for 50ms intervals inter-stimuli in any tested condition (**Fig. 2e**). We further evaluated whether the effect of blebbistatin on eCB-LTD was pre- or postsynaptic by measuring the PPF ratio before and after LFS ($PPF_{\text{plasticity/baseline}}$). We found a significant increase in PPF in control conditions whereas no significant variation of PPF was found following treatment with active blebbistatin (**Fig. 3f**), indicating presynaptic action of actomyosin contraction under eCB-LTD. The specific ROCK inhibitor Y-27632 (10µM) also impaired eCB-LTD induction (**Fig. 2g**). Therefore, similarly to hippocampal GABAergic synapses, activation of CB₁R by eCBs in corticostriatal excitatory synapses induces LTD, but not STD, through ROCK-mediated presynaptic actomyosin contraction.

As blebbistatin directly inhibits the contractility of the actomyosin cytoskeleton, the effects described above suggest that cannabinoid-mediated LTD may be elicited through actomyosin-contraction-induced cytoskeletal remodeling of the presynaptic compartment. In order to evaluate this hypothesis, we chose to directly image the nanoscale presynaptic architecture in

dissociated cultures of rat hippocampal neurons. First, we confirmed that actomyosin contractility is involved in cannabinoid-induced synaptic plasticity in this experimental model by measuring the effect of CB₁R activation on synaptic vesicle release at individual axonal boutons¹³, by using synaptophysin-pHluorin (SpH), which increases in green fluorescence intensity upon vesicle fusion¹⁴. Neuronal depolarization (KCl; 2min; 50mM) induced an average release of around 30% of total bouton vesicle pool under control conditions (**Fig. 3**), as estimated through maximal bouton fluorescence upon terminal alkaline incubation (NH₄Cl; 2min, 50mM). Importantly, vesicle release under WIN55,212-2 (1μM; 10min) was significantly lower as compared to control (**Fig. 3**) and this effect was prevented both by pretreating neurons with para-nitroblebbistatin (25μM, **Fig. 3c**), a C15 derivative of blebbistatin⁷ with reduced blue-light sensitivity¹⁵ and neuronal cytotoxicity (Extended Data Fig. 1), as well as through pretreatment with Y-27632 (10μM, **Fig. 3c**). Therefore, as in acute slices, activation of endogenous CB₁R decreases vesicle release via ROCK-mediated NMII activation at individual axonal boutons *in vitro*.

We next assessed the nanoarchitecture of the presynaptic compartment and the potential influence of actomyosin dynamics by testing the spatial relationship between synaptic vesicles and the synaptic active zone (AZ) by using the activator/reporter pairing method of multicolor 3D Stochastic Optical Reconstruction Microscopy (STORM)¹⁶, which allows imaging proteins of interest simultaneously through the same optical path, reducing spatial differences that may arise through optical aberrations. Furthermore, to avoid any artifacts resulting from cross-talk of closely localized fluorophores, we used as a closely apposed but spatially separated spatial AZ reference Homer1, a major protein of the postsynaptic scaffold (PSD, **Fig. 4a**). As pre- and post- synaptic compartments have to be precisely aligned in order to ensure sensitive and efficient detection of synaptic events, AZ and PSD synaptic scaffoldings are highly correlated¹⁷ (**Fig. 4b**), suggesting that AZ localization may be precisely predicted from the localization of the PSD scaffold. In order to verify this empirically, we measured the length, width, and depth of Homer1 and Bassoon (a major AZ scaffolding protein) appositions (Supp. Methods). All parameters were significantly correlated between corresponding appositions (n=140 over 3 independent experiments; Spearman's R for length: r=0.61, p<0.0001; width: r=0.55, p<0.0001; depth: r=0.34, p<0.0003). Furthermore, distances between Homer1 and Bassoon protein clusters varied very little between synapses and were not affected under CB₁R activation (**Fig. 4c-e**). Based on these properties, we were successfully able to predict the 3D location of the presynaptic AZ volume (AZv, **Fig. 4f**)

based on postsynaptic Homer1 clusters. Indeed, on an independent sample 95% of Bassoon locations were contained within our predicted AZv (**Fig. 4g**).

We next immunolabeled synaptic vesicles for the SNARE protein VAMP2 (**Fig. 4h**), and developed a nested clustering algorithm to identify synaptic vesicles within VAMP2 localisation clusters (**Fig.4j**; Supp. Methods), to assess the spatial organization of the synaptic vesicles pool. We found strikingly fewer synaptic vesicles in the predicted AZv under WIN55,212-2 treatment (1 μ M, 10min), whereas pretreatment with para-nitroblebbistatin (25 μ M, 20min) significantly prevented this effect. (**Fig.4k**). Furthermore, synaptic vesicles were significantly more clustered to each other within the total pool under WIN55,212-2 treatment compared to either control conditions or para-nitroblebbistatin pretreatment (**Fig.4l**). These results imply that CB₁R activation induces a significant redistribution of synaptic vesicles within the presynaptic compartment following CB₁R activation, leading to depletion of synaptic vesicles from the AZ. Inhibition of actomyosin contraction prevents both CB₁R-induced vesicle redistribution and presynaptic silencing, suggesting that cannabinoid-induced changes in synaptic efficiency depend on the contractile properties of the presynaptic actomyosin cytoskeleton (**Fig.4m**).

In conclusion, in this study we have combined patch-clamp recordings with super resolution microscopy and functional imaging to establish the link between presynaptic architecture and synapse function at two archetypal CNS synapses. By showing that CB₁R dynamically controls presynaptic organization through actomyosin contractility, our results provide both a mechanism and a functional relevance to recent electron microscopy studies that reported fewer synaptic vesicles near the presynaptic active zone following cannabinoid treatment both *in vitro* and *in vivo*^{13,18}. Our results significantly extend the suggested roles for the presynaptic actin cytoskeleton, hopefully advancing toward a more complete model of regulation of vesicle release¹⁹. Structurally, synaptic vesicles are reversibly tethered to the actin cytoskeleton by synapsin, particularly vesicles of the recycling and/or resting pool²⁰. Actin cytoskeleton dynamics also have an important role in the preferential distribution of recycling vesicles close to the AZ²¹. Our findings now identify another major actin binding/structuring protein, the contractile NMII, mechanistically explaining through dynamic redistribution of vesicles, the generation of a widespread form of long-term presynaptic plasticity. Notably, we did not find an effect of either NMII or ROCK inhibition on short-term forms of eCB-induced synaptic plasticity, neither on DSI nor DSE. Indeed, eCB-STD occur very rapidly (<1sec), following brief activation of CB₁Rs, possibly effecting only already

docked vesicles, while a longer CB₁R activation (>5min) is necessary for eCB-LTD induction²². This longer activation period may be needed to engage actomyosin contraction, a molecular mechanism leading to actin cytoskeleton remodeling over several minutes in non-muscular cells²³. Our results, by reporting a conceptually novel molecular mechanism of synaptic plasticity downstream of an important recreational drug target and known risk factor in schizophrenia²⁴ open novel perspectives in the understanding of cognitive function, the pathogenesis of marijuana intoxication and neuro-psychiatric disease.

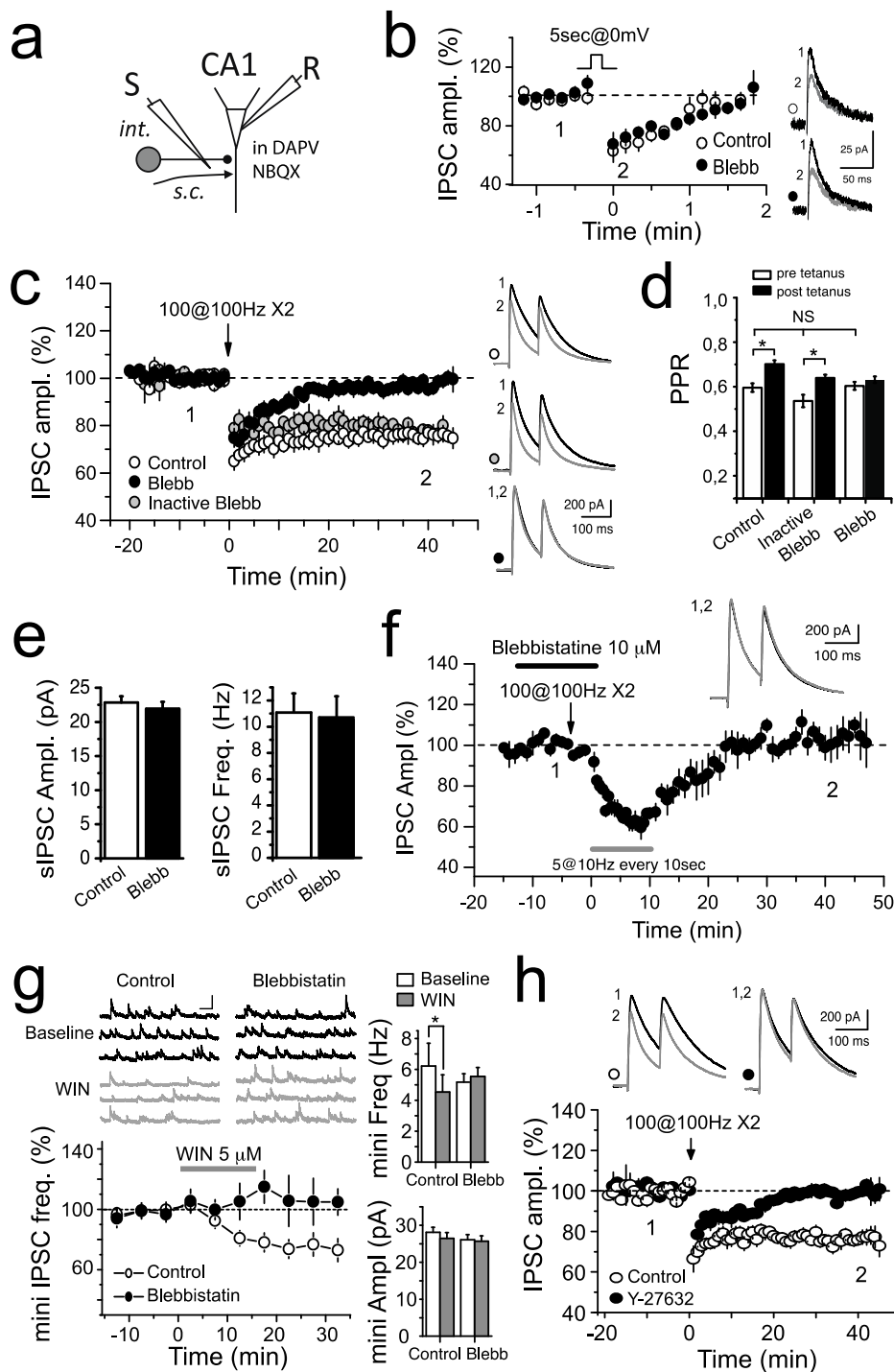


Figure 1: Presynaptic actomyosin contractility mediates eCB-LTD at inhibitory synapses in the CA1 area of the hippocampus (a) Schematic of recording paradigm. CA1: whole-cell recorded pyramidal neuron; int: inhibitory interneuron fibers, activated by a stimulating electrode in the stratum radiatum. Fast excitatory transmission from Schaffer collateral inputs (s.c.) was blocked by the AMPA/NMDA/KA receptor antagonists D-APV and NBQX. (b) The transient depression of inhibitory transmission following a 5 second

depolarization at 0 mV (white circles) was unaffected by blebbistatin (Blebb, 10 μ M, black circles). In control: 65.2 \pm 6.5% of baseline, n=7. In blebbistatin: 69 \pm 5% of baseline, n=6, p=0.63. **(c)** The long-term depression following high frequency stimulation (white circles) was completely abolished in the presence of blebbistatin (black circles) but not by the inactive blebbistatin enantiomer (10 μ M, grey circles). Average sample traces are shown on top for time points (1) and (2). Control: 75 \pm 3% of baseline, n=9; blebbistatin: 97 \pm 2%, n=8, p=0.00002, inactive blebbistatin 79 \pm 2%, n=5, p=0.27. **(d)** Tetanic stimulation resulted in a significant increase (p = 0.003) in the paired pulse ratio (PPR), in accordance with the decrease in GABA release during LTD. This increase in PPR was not affected in presence of inactive blebbistatine but was abolished in presence of blebbistatine. Note that Blebbistatine did not induced any change in PPR before the tetanus (compared to the initial PPR in control), indicating that basal release probability was not altered by Blebbistatine. **(e)** Blebbistatin did not change the amplitude or the frequency of spontaneous IPSCs. Amplitude: baseline: 22.8 \pm 0.9pA, after blebbistatin: 21.9 \pm 1.0pA, n=7, p=0.18; frequency: baseline: 11.1 \pm 1.4Hz, after blebbistatin: 10.7 \pm 1.6Hz, p=0.59. **(f)** Trains of stimulation following tetanus do not result in eCB-LTD in the presence of blebbistatin. 104 \pm 6% of baseline, n=5. **(g)** The decrease in miniature IPSC frequency mediated by WIN55,212-2 (WIN, 5 μ M, white circles) was abolished by blebbistatin (black circles). Sample traces are shown on top. Right: Average mIPSC frequencies and amplitudes. Control: 1.22 \pm 0.03 of baseline, p = 0.0029 Frequency: from 6.2 \pm 1.4 to 4.5 \pm 1.1Hz, p=0.03; Amplitude: from 28. \pm 1.4 to 26.5 \pm 1.6pA, p=0.46, n=5; blebbistatin: 1.05 \pm 0.01%, p=0.08, Frequency: from 5.2 \pm 0.5 to 5.6 \pm 0.6Hz, p=0.6; inactive blebbistatin: 1.21 \pm 0.04 p=0.02. **(h)** The LTD evoked by high frequency stimulation (white circles) was abolished in the presence of the ROCK inhibitor Y-27632 (10 μ M, black circles). Average sample traces are shown on top for time points (1) and (2). 99 \pm 1% of baseline, n=5, p=0.37 with baseline and p=0.0004 with control LTD, n=6. Student's t-test. Values: mean \pm SEM.

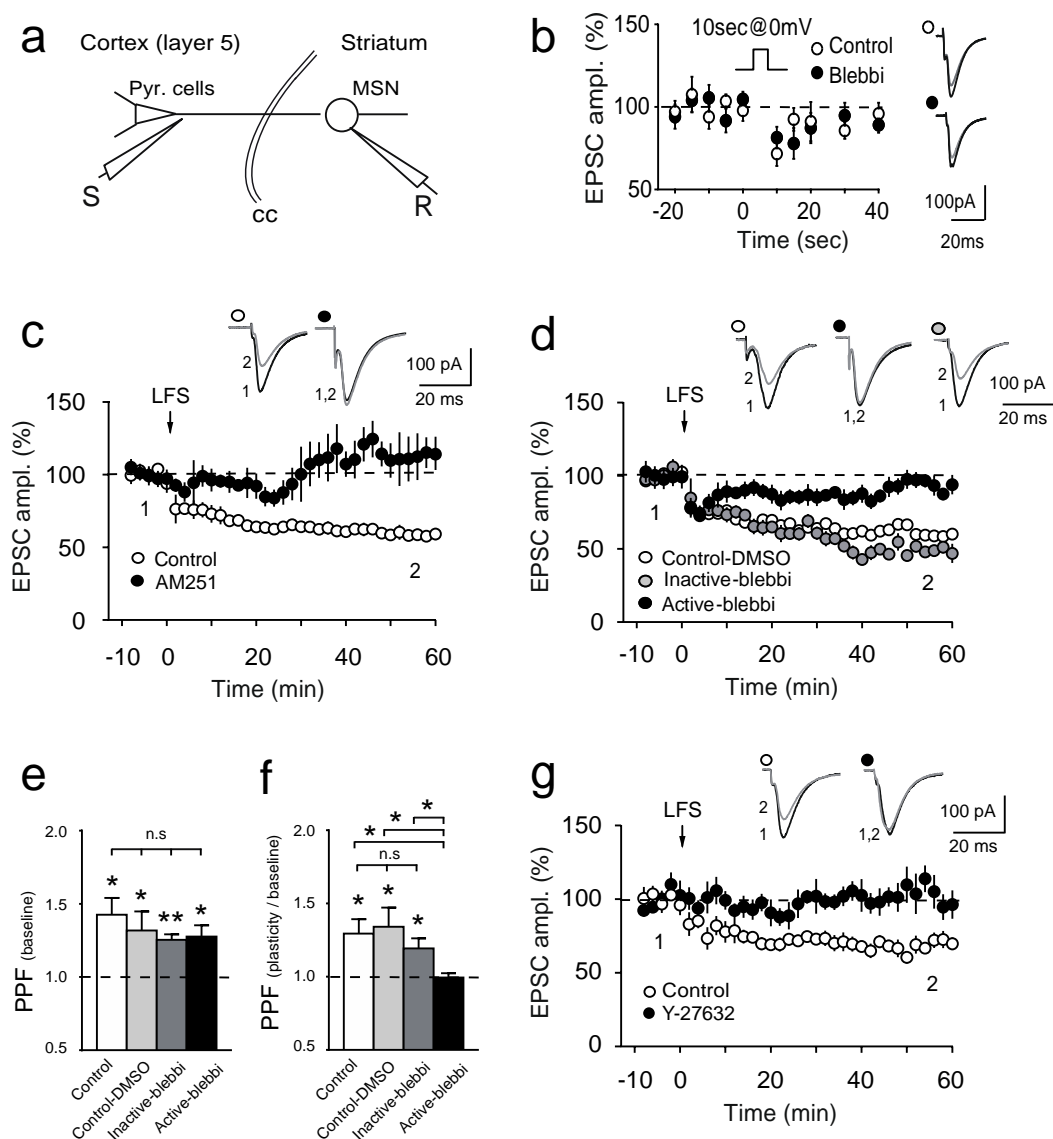


Figure 2: Presynaptic actomyosin contractility mediates eCB-LTD at excitatory corticostriatal synapses (a) Schematic of whole-cell recording of a MSN and stimulation in the somatosensory cortical layer V. MSN: medium-sized spiny neurons (b) The transient depression of excitatory transmission following a 10 second depolarization at 0mV (white circles, $81 \pm 4\%$ of baseline, $n=13$, $p=0.0003$) was unaffected by blebbistatin (black circles, $79 \pm 3\%$ of baseline, $n=11$, $p=0.0001$ with baseline; $p=0.8039$ with control DSE, $n=13$). Average sample traces before and 10sec after the depolarization are shown on the right. (c) LTD induced with LFS (control: $58 \pm 2\%$ of baseline, $n=7$, $p<0.0001$ with baseline) was CB₁R-mediated because prevented with AM251 ($107 \pm 10\%$ of baseline, $n=5$, $p=0.5244$ with

baseline, $p < 0.0001$ with control). **(d)** The eCB-LTD following a LFS (white circles, control-DMSO: $56 \pm 7\%$ of baseline, $n=9$, $p=0.0002$, $p=0.8217$ with control without DMSO) was abolished in the presence of blebbistatin (black circles, $95 \pm 3\%$ of baseline, $n=10$, $p=0.1201$ with baseline, $p < 0.0001$ with control LTD) but was unaffected by the inactive enantiomer of blebbistatin (grey circles, $10 \mu\text{M}$, $52 \pm 4\%$ of baseline, $n=11$, $p < 0.0001$ with baseline, $p=0.0556$ with control LTD). Average sample traces are shown on top at the time point before (1) and after the stimulation protocol (2). **(e)** 50ms inter-stimuli intervals induced significant PPR in control ($p=0.0203$, $n=5$), control-DMSO ($p=0.0120$, $n=8$), inactive blebbistatin ($p=0.0023$, $n=5$) and active blebbistatin ($p=0.0375$, $n=4$) conditions (Anova: $p=0.6291$ and $F(3, 18)=0.5905$). **(f)** $\text{PPR}_{\text{plasticity/baseline}}$ displayed significant increase in control ($\text{PPR}_{\text{plasticity/baseline}}=1.30 \pm 0.10$, $p=0.0397$, $n=5$) control-DMSO: inactive blebbistatin: control, control-DMSO ($\text{PPR}_{\text{plasticity/baseline}}=1.34 \pm 0.13$, $p=0.0335$, $n=8$) and inactive blebbistatin ($\text{PPR}_{\text{plasticity/baseline}}=1.19 \pm 0.07$, $p=0.0493$, $n=5$; Anova: $p=0.6630$ and $F(2, 15)=0.4225$) but not for active blebbistatin ($\text{PPR}_{\text{plasticity/baseline}}=1.00 \pm 0.03$, $p=0.8697$, $n=4$). **(g)** The ROCK inhibitor Y-27632 abolishes the eCB-LTD (black circles, $98 \pm 11\%$ of baseline, $n=7$, $p=0.7204$ with baseline, $p=0.0038$ with control LTD, $n=6$). Average sample traces are shown on top for time points (1) and (2). Student's t-test. Values: mean \pm SEM.

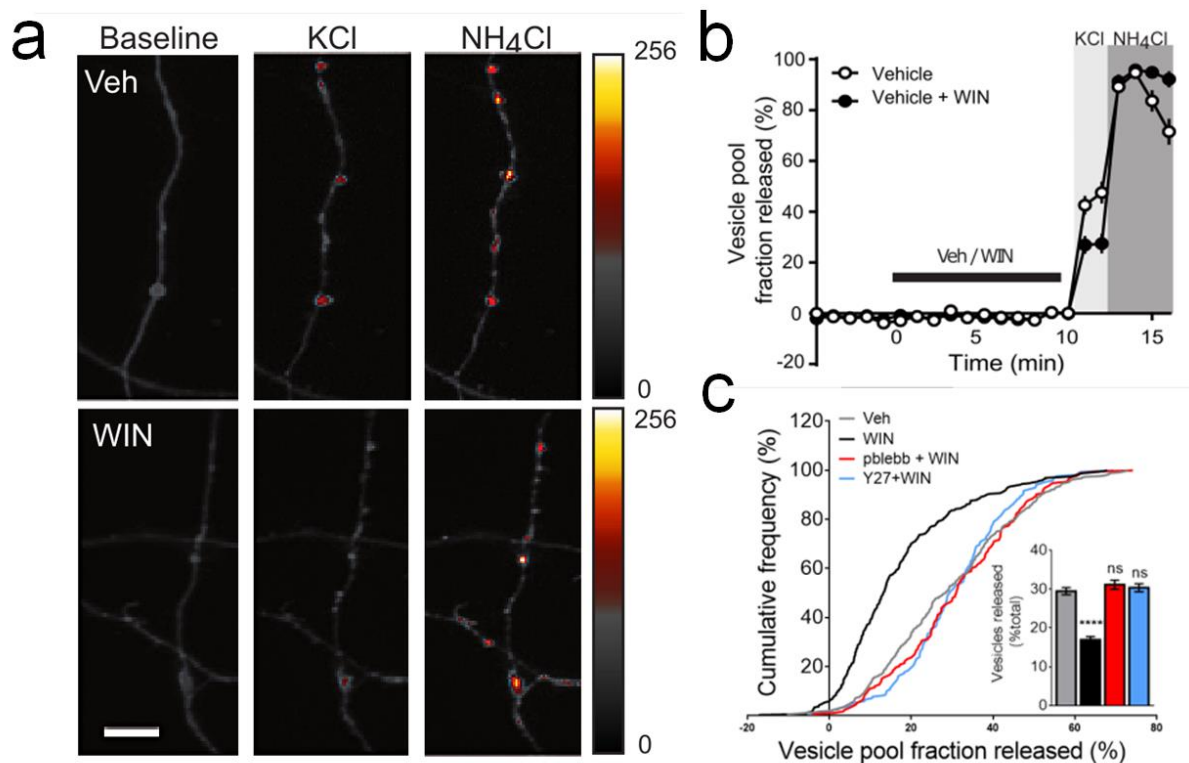


Figure 3. Actomyosin contractility mediates cannabinoid-induced suppression of vesicle release, as shown by pretreatment with the NMII inhibitor para-nitroblebbistatin (pBlebb), or the ROCK inhibitor Y-27632 (Y27). (a) Neuron expressing the vesicle release marker SpH. Example SpH fluorescence levels in a control (Veh) and a WIN55,212-2-treated (WIN, 1 μ M; 10min) axon before stimulation (Baseline), after stimulation (KCL, 50mM, 2min), and after terminal superfusion with NH₄Cl (50mM, 2min). Fluorescence intensity (arbitrary units) increases during stimulation in control conditions while WIN decreases this effect. (b) Experimental paradigm and example traces of normalized axonal bouton SpH fluorescence (c) Cumulative probability distributions of the released vesicle pool fractions under control conditions (\pm 0.92%; n=337 over 4 independent experiments), or after treatment with WIN: (16.94 \pm 0.84%; n=323 over 4 independent experiments; P <0.0001), pBleb+WIN: (25 μ M; 20min; 31.14 \pm 1.15%; n=173 over 3 independent experiments; P <0.0001); Y-27632+WIN (10 μ M; 20min; 30.35 \pm 1.03%; n=168 over 3 independent experiments; P <0.0001;. ****: p < 0.001; ns: not significant as compared to vehicle, Kruskal-Wallis test. Scale bar: 5 μ m

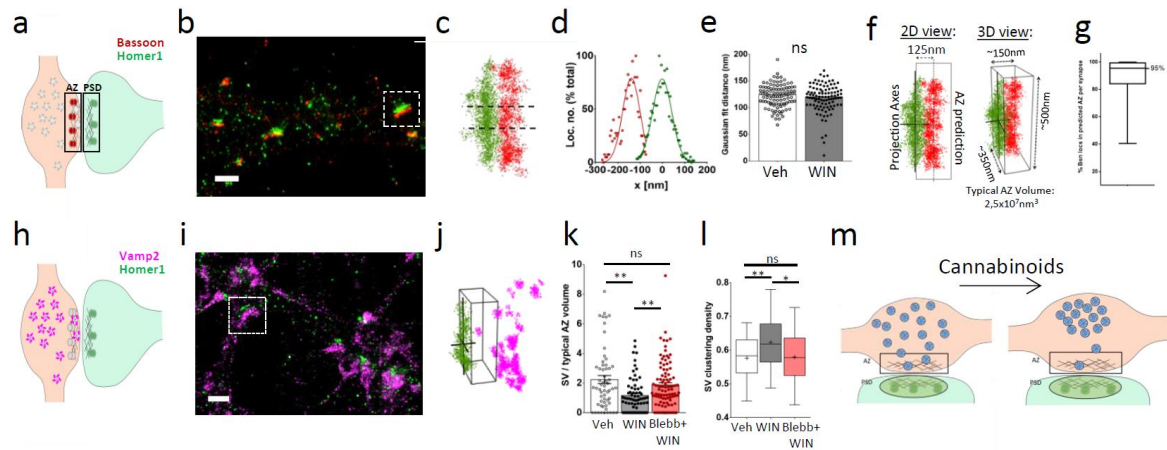


Figure 4: 3D STORM reveals synaptic vesicle redistribution with actomyosin contraction under CB₁R activation (a) Representation of Bassoon and Homer1 distributions within the pre-synaptic active zone (AZ) and post-synaptic density (PSD), respectively. (b) STORM reconstruction of Bassoon and Homer1 localizations (c). Boxed synapse in (b) after clustering analysis. Dotted lines enclose the localisations averaged over the x-axis for Gaussian fitting in d. (d) Averaged localisations and Gaussian fit of synapse in (c). Distance between Gaussian peaks represents the measured distance between Homer1 and Bassoon appositions. (e) Measured distances between pre- and post-synaptic appositions under control conditions (Veh) and CB₁R activation (WIN). (Veh: n=105, 122.3±2.0nm, WIN: n=100, 117.9±2.6nm) (f) Prediction of the AZ based on both PSD axes and the median apposition distances measured in e. Side values in the 3D view represent average measures obtained from predictions over 105 synapses for the AZ volume (AZv). (g) Percentage of Bassoon localisations per synapse contained within the predicted AZv in an independent sample (n=55, 25thpercentile: 84.3%; 75thpercentile: 99.4%). (h) Representation of Vamp2 and Homer1 distributions within the synapse. (i). STORM reconstruction of Vamp2 and Homer1 (j) Synapse boxed in (h) after identification of synaptic vesicles through nested clustering analysis. The 3D box shows the predicted AZv for this synapse, enclosing one identified vesicle. (k) Fewer vesicles are found within the predicted AZv under CB₁R activation (Veh: 87.8±10.6/μm³, n=59 over 3 independent experiments; WIN: 45.4±5.5/μm³, n=70 over 3 independent experiments, p<0.003). This depletion is prevented by inhibiting actomyosin contraction with para-nitroblebbistatin (73.2±6.2/μm³, n=98 over 3 independent experiments, p<0.004). (l) Vesicle clustering found under CB₁R activation is prevented by blocking

actomyosin contraction. **(m)** Putative mechanisms of CB₁R activation on vesicle redistribution during CB₁R -induced plasticity. Scale bars in STORM images: 1µm

Methods

Animals

Experiments were performed in accordance with local animal welfare committee (Center for Interdisciplinary Research in Biology and EU guidelines; directive 2010/63/EU). Rats and mice (Charles River, L'Arbresle, France) were housed in standard 12 hours light/dark cycles and food and water were available *ad libitum*.

Antibodies and Chemicals

Rabbit polyclonal Homer1 (Cat. No. 160 003) and mouse monoclonal VAMP2 (Cat. No. 104 211) antibodies were obtained from Synaptic Systems (Goettingen, Germany). Bassoon mouse monoclonal antibody (Cat. No. ab82958) was obtained from Abcam (Paris, France). Paired fluorophore-conjugated secondary antibodies were made as previously described²⁵. WIN55,212-2 and (RS)-3,5-DHPG were from Tocris. Carbachol, Y-27632, active (S)-(-)-blebbistatin and inactive (R)-(+)-blebbistatin enantiomers and para-nitroblebbistatin were from Calbiochem, Sigma and Optopharma. None of the bath-applied drugs had a significant effect on basal IPSC and EPSC amplitudes, in our experimental conditions.

Time-lapse microscopy of primary cultured neurons

Dissociated neurons obtained from hippocampi of day 17-18 Sprague-Dawley rat embryos were plated on Poly-D-Lysine-coated coverslips at a density of approximately 100,000 cells per coverslip and subsequently cultivated at 37°C, 5% CO₂ in NeurobasalTM (LifeTech) medium supplemented with 2% B27 (LifeTech), 0.5mM L-glutamine, 10U/mL penicillin G and 10mg/mL streptomycin containing conditioned medium, obtained by incubation with glial cultures (70-80% confluence) for 24 h as described previously⁵. Neurons were transfected either with Synaptophysin-pHluorin (SpH), a kind gift from Dr. Stefan Krueger (Dalhousie University, Halifax, NS, Canada), and LifeAct-mCherry⁵, or with SpH alone. Transfections and time-lapse microscopy were performed at 37°C at 7-9 days after plating, as described previously⁵. Briefly, coverslips were placed in a Ludin chamber (Life Imaging Services,

Basel, Switzerland) filled with imaging buffer (120 mM NaCl, 3 mM KCl, 2 mM CaCl₂, 2 mM MgCl₂, 10 mM glucose, and 10 mM HEPES, pH 7.35). Neurons were depolarized by adding 50mM KCl for 2min, followed by NH₄Cl treatment. Pretreatments and treatments were applied at 30min and 10min before KCl, respectively. Dimethylsulfoxide vehicle concentrations ranged from 0.02% to 0.1%.

Image stacks were realigned using ImageJ. SpH fluorescence intensity was measured in round ROIs of approximately 3x3µm, placed manually around visually identified axonal boutons, with mean basal axonal fluorescence intensity subtracted for each timepoint. Axonal boutons were selected for analysis if SpH response to NH₄Cl was superior to that of KCl and if baseline fluorescence was within 2x the standard deviation around baseline population mean. Statistical analyses used Kruskal-Wallis test with Dunn's post-hoc Multiple Comparison Test, n indicates the number of axonal boutons analyzed. Values are mean± SEM.

Electrophysiological recordings and analysis from hippocampal slices

400 µM transverse hippocampal vibratome slices were prepared from 6- to 8-week-old C57BL6 male mice in ice-cold extracellular solution containing (in mM): 10 NaCl, 195 sucrose, 2.5 KCl, 15 glucose, 26 NaHCO₃, 1.25 NaH₂PO₄, 1 CaCl₂ and 2 MgCl₂). The slices were then transferred to 30°C ACSF (in mM: 125 NaCl, 2.5 KCl, 10 glucose, 26 NaHCO₃, 1.25 NaH₂PO₄, 2 Na Pyruvate, 2 CaCl₂ and 1 MgCl₂) for 30min and kept at room temperature for at least 1.5 hours before recording at 33°C. Cutting and recording solutions were both saturated with 95% O₂ and 5% CO₂ (pH 7.4).

Whole-cell recordings were obtained using Axograph X software from CA1 PNs in voltage clamp mode in the continuous presence of the NMDA receptor antagonist d(-)-2-amino-5-phosphonopentanoic acid (d-APV; 50 µM) and the AMPA/kainate receptor antagonist 2,3-dihydroxy-6-nitro-7-sulfonyl-benzo[f]quinoxaline (NBQX; 10 µM) Inhibitory currents were recorded at +10 mV with a patch pipette (3–5 MΩ) containing (in mM): 135 CsMethylSulfate, 5 KCl, 0.1 EGTA-Na, 10 HEPES, 2 NaCl, 5 ATP, 0.4 GTP, 10 phosphocreatine (pH 7.2; 280–290 mOsm). Series resistance (typically 12–18MΩ) was monitored throughout each experiment; cells with more than 15% change in series resistance were excluded from analysis. Synaptic potentials were evoked by monopolar stimulation with a patch pipette filled with ACSF and positioned in the middle of CA1 SR. A HFS (100 pulses at 100Hz repeated twice) was applied following 15 – 20min of stable baseline. The amplitudes of the IPSCs were normalized to the baseline amplitude. The magnitude of LTD was estimated by comparing averaged responses at 30-40min after the induction protocol with

baseline-averaged responses 0–10min before the induction protocol.

Electrophysiological recordings and analysis from corticostriatal slices

330 μ m horizontal brain slices containing the somatosensory cortex and the corresponding corticostriatal projection field in the dorsolateral striatum were prepared from P₂₅₋₃₅ male rats as previously described^{12,26}. Brains were sliced in a 95% CO₂/5% O₂-bubbled, ice-cold cutting solution containing (in mM) 125 NaCl, 2.5 KCl, 25 glucose, 25 NaHCO₃, 1.25 NaH₂PO₄, 2 CaCl₂, 1 MgCl₂, 1 pyruvic acid, and then transferred into the same solution at 34°C for one hour and then moved to room temperature before patch-clamp whole-cell recordings (at 34°C).

Patch-clamp recordings were performed as previously described^{12,26}. Briefly, borosilicate glass pipettes of 4-6M Ω resistance contained for whole-cell recordings (in mM): 105 K-gluconate, 30 KCl, 10 HEPES, 10 phosphocreatine, 4 ATP-Mg, 0.3 GTP-Na, 0.3 EGTA (adjusted to pH 7.35 with KOH). The composition of the extracellular solution was (mM): 125 NaCl, 2.5 KCl, 25 glucose, 25 NaHCO₃, 1.25 NaH₂PO₄, 2 CaCl₂, 1 MgCl₂, 10mM pyruvic acid bubbled with 95% O₂ and 5% CO₂. Signals were amplified using EPC10-2 amplifier (HEKA Elektronik, Lambrecht, Germany). All recordings were performed at 34°C and slices were continuously superfused at 2-3ml/min with the extracellular solution. Slices were visualized on an Olympus BX51WI microscope (Olympus, Rungis, France) using a 4x/0.13 objective for the placement of the stimulating electrode and a 40x/0.80 water-immersion objective for localizing cells for whole-cell recordings. Series resistance was not compensated. Current-clamp recordings were filtered at 2.5kHz and sampled at 5kHz and voltage-clamp recordings were filtered at 5kHz and sampled at 10kHz using the Patchmaster v2x32 program (HEKA Elektronik). Electrical stimulations were performed with a bipolar electrode (Phymep) placed in the layer 5 of the somatosensory cortex and were monophasic at constant current (ISO-Flex stimulator)^{10,12,26}. Currents were adjusted to evoke striatal EPSCs ranging in amplitude from 50 to 200pA. Repetitive control stimuli were applied at a frequency of 0.1Hz for 60min after LFS protocol. Recordings on neurons were made over a period of 10 minutes at baseline, and for at least 60 minutes after the LFS protocols; long-term changes in synaptic efficacy were measured from 45 to 55 minutes. We individually measured and averaged 60 successive EPSCs, comparing the last 10 minutes of the recording with the 10-minute baseline recording. Series resistance was monitored for each sweep and a variation above 20% led to the rejection of the experiment. LTD was induced with low frequency stimulation protocol consisting in 600 cortical stimulations at 1Hz paired with postsynaptic

concomitant depolarization of the MSN during 50ms^{10,12}. For DSE induction, MSN was depolarized from RMP to 0mV during 10sec (with bath-applied carbachol, 10μM, and DHPG, 50μM)¹⁰. Off-line analysis was performed using Fitmaster (Heka Elektronik) and Igor-Pro 6.0.3 (Wavemetrics, Lake Oswego, OR, USA). Statistical analysis was performed using Prism 5.0 software (San Diego, CA, USA). “n” refers to a single cell experiment from a single slice.

Immunocytochemistry and STORM imaging

Neurons used for STORM imaging underwent the same treatment protocol as for videomicroscopy, with the exception that instead of depolarization with KCl after treatment, neurons were fixed with a preheated solution of 4% PFA and 4% sucrose in 0.1 M phosphate buffered saline (PBS) for 15 minutes at room temperature (RT), permeabilized after wash for 5 min at RT with 0.1% Triton X in PBS, and blocked for 1h at RT with blocking buffer (4% BSA in PBS). Primary and secondary antibodies were applied in blocking buffer, primary antibodies being applied overnight at 4°C and secondary antibodies being applied for 2h at RT. After washing out the secondary antibody, neurons were post-fixed with 4% PFA and 4% sucrose in PBS for 5min, washed and stored in PBS at 4°C before imaging.

STORM images were acquired on a N-STORM microscope (Nikon Instruments), outfitted with 405 nm, 561 nm, and 647 nm solid-state lasers, a 100X NA 1.49 objective and an Ixon DU-897 camera. Imaging was performed as previously described²⁵. Briefly, visually identified dendrites labelled with activator-reporter fluorophore pairs (Alexa Fluor 405 – Alexa Fluor 647 and Cy3-Alexa Fluor 647) were imaged using sequences of one activator frame (405 or 561 nm) followed by three reporter frames (647 nm)¹⁶. A cylindrical lens was placed across the optical path in order to acquire 3D information (Huang et al. 2008), and the N-STORM software (Nikon Instruments) was used for the localization of single fluorophores.

References

1. Ohno-Shosaku, T. & Kano, M. Endocannabinoid-mediated retrograde modulation of synaptic transmission. *Current Opinion in Neurobiology* **29C**, 1–8 (2014).
2. Wilson, R. I. & Nicoll, R. A. Endogenous cannabinoids mediate retrograde signalling at hippocampal synapses. *Nature* **410**, 588–592 (2001).
3. Castillo, P. E., Younts, T. J., Chávez, A. E. & Hashimoto, Y. Endocannabinoid Signaling and Synaptic Function. *Neuron* **76**, 70–81 (2012).
4. Monday, H. R. & Castillo, P. E. Closing the gap: long-term presynaptic plasticity in

- brain function and disease. *Current Opinion in Neurobiology* **45**, 106–112 (2017).
5. Roland, A. B. *et al.* Cannabinoid-induced actomyosin contractility shapes neuronal morphology and growth. *Elife* **3**, e03159–e03159 (2014).
 6. Holtmaat, A., Randall, J. & Cane, M. Optical imaging of structural and functional synaptic plasticity in vivo. *European Journal of Pharmacology* **719**, 128–136 (2013).
 7. Kovacs, M., Toth, J., Hetenyi, C., Malnasi-Csizmadia, A. & Sellers, J. R. Mechanism of blebbistatin inhibition of myosin II. *Journal of Biological Chemistry* **279**, 35557–35563 (2004).
 8. Heifets, B. D. & Castillo, P. E. Endocannabinoid Signaling and Long-Term Synaptic Plasticity. *Annu. Rev. Physiol.* **71**, 283–306 (2009).
 9. Chevaleyre, V. *et al.* Endocannabinoid-mediated long-term plasticity requires cAMP/PKA signaling and RIM1alpha. *Neuron* **54**, 801–812 (2007).
 10. Puente, N. *et al.* Polymodal activation of the endocannabinoid system in the extended amygdala. *Nature Neuroscience* **14**, 1542–1547 (2011).
 11. Atwood, B. K. & Lovinger, D. M. in *Endocannabinoids and Lipid Mediators in Brain Functions* **27**, 109–153 (Springer International Publishing, 2017).
 12. Fino, E., Glowinski, J. & Venance, L. Bidirectional activity-dependent plasticity at corticostriatal synapses. *Journal of Neuroscience* **25**, 11279–11287 (2005).
 13. Ramírez-Franco, J., Bartolomé-Martín, D., Alonso, B., Torres, M. & Sánchez-Prieto, J. Cannabinoid type 1 receptors transiently silence glutamatergic nerve terminals of cultured cerebellar granule cells. *PLoS ONE* **9**, e88594–e88594 (2013).
 14. Miesenböck, G., De Angelis, D. A. & Rothman, J. E. Visualizing secretion and synaptic transmission with pH-sensitive green fluorescent proteins. *Nature* **394**, 192–195 (1998).
 15. Képiró, M. *et al.* para-Nitroblebbistatin, the Non-Cytotoxic and Photostable Myosin II Inhibitor. *Angew. Chem. Int. Ed.* **53**, 8211–8215 (2014).
 16. Bates, M., Huang, B., Dempsey, G. T. & Zhuang, X. Multicolor super-resolution imaging with photo-switchable fluorescent probes. *Science* **317**, 1749–1753 (2007).
 17. Tang, A.-H. *et al.* A trans-synaptic nanocolumn aligns neurotransmitter release to receptors. *Nature* **536**, 210–214 (2016).
 18. García-Morales, V., Montero, F. & Moreno-López, B. Cannabinoid agonists rearrange synaptic vesicles at excitatory synapses and depress motoneuron activity in vivo. *Neuropharmacology* (2015).
 19. Rust, M. B. & Maritzen, T. Relevance of presynaptic actin dynamics for synapse function and mouse behavior. *Experimental Cell Research* **335**, 165–171 (2015).
 20. Cesca, F., Baldelli, P., Valtorta, F. & Benfenati, F. The synapsins: key actors of synapse function and plasticity. *Progress in Neurobiology* **91**, 313–348 (2010).
 21. Marra, V. *et al.* A Preferentially Segregated Recycling Vesicle Pool of Limited Size Supports Neurotransmission in Native Central Synapses. *Neuron* **76**, 579–589 (2012).
 22. Chevaleyre, V., Takahashi, K. A. & Castillo, P. E. Endocannabinoid-mediated synaptic plasticity in the CNS. *Annu. Rev. Neurosci.* **29**, 37–76 (2006).
 23. Li, D. *et al.* ADVANCED IMAGING. Extended-resolution structured illumination imaging of endocytic and cytoskeletal dynamics. *Science* **349**, aab3500–aab3500 (2015).
 24. Large, M. The need for health warnings about cannabis and psychosis. - PubMed - NCBI. *The Lancet Psychiatry* **3**, 188–189 (2016).
 25. Leterrier, C. *et al.* Nanoscale Architecture of the Axon Initial Segment Reveals an Organized and Robust Scaffold. *Cell Rep* **13**, 2781–2793 (2015).
 26. Cui, Y. *et al.* Endocannabinoid dynamics gate spike-timing dependent depression and potentiation. *Elife* **5**, e13185 (2016).

Supplementary Methods

Clustering analysis of pre- and post-synaptic appositions

To simplify analysis, reconstructed images were divided into $2 \times 2 \mu\text{m}$ ROIs around visually identified synaptic appositions. Subsequently, per ROI, pre- and post-synaptic appositions were identified visually based on pre- and post-synaptic localization clusters. In all cases, the experimenter performing the analysis was blind to the experimental conditions. Clustering was performed automatically through custom R scripts using a modified OPTICS algorithm (Ankerst et al. 1999). Briefly, ROI localizations were randomized based on a uniform distribution function. The median core-distance of this distribution after OPTICS (epsilon=500nm, minimum points=10) was used as a distance cutoff to identify staining clusters, whereby:

$$\text{Cutoff} = \text{median randomized coredistance} + p * \text{median absolute deviation of randomized coredistance}$$

$p=5$ was selected as an initial factor as the 5% significance cutoff of normal distributions is at $4.2 * \text{mad}$. This ensured that clusters were identified based on staining clustering rather than localization density, which may vary considerably between images. Clustering could be further refined by the experimenter by increasing p where clearly separate clusters were joined by several localizations.

Cluster identification was further limited for analysis by cluster volume. For Homer1 and Bassoon clusters, cluster volume was limited to a minimum of $2\,000\,000\text{ nm}^3$, while Vamp2 clusters were limited to a minimum of $10\,000\,000\text{ nm}^3$.

Crosstalk removal

To remove localizations that had been identified to the wrong activator, cluster localizations were filtered based on their neighborhood density. For each localization, the 10th nearest neighbor distance for each activator was calculated. Localizations whose 10th nearest neighbor distance for the opposing activator was closer than for its own activator were removed.

Homer1 and Bassoon scaffolding measurements

The width, depth and length of Homer1 and Bassoon appositions were measured by fitting ellipsoids to the identified Homer1 and Bassoon clusters with the *ellipsoidhull* R function (tol=1000). The fitted ellipsoid principal axes were used as width, depth and length measurements, with:

$$\text{length} > \text{width} > \text{depth}$$

and the depth axis perpendicular to the synaptic cleft. The resulting median measurements were 465.7nm (+/-46.4nm) for Homer1 length, 405.4nm (+/-50.5nm) for Bassoon length, 330.7nm (+/-28.6nm) for Homer1 width, 319.7nm (+/-22.9nm) for Bassoon width, 141.9nm (+/-8.2nm) for Homer1 depth, and 168.2nm (+/-8.4nm) for Bassoon width.

Distance between Homer1 and Bassoon clusters

Distance measurements between Homer1 and Bassoon were performed similarly to Dani et al. (Dani et al. 2010). Per ROI, after ellipsoid fitting, the identified depth axis of the Homer1 cluster was used as the x axis along which a Gaussian fit of both Homer1 cluster localizations and Bassoon cluster localizations was produced. Localizations within a 200nm range around the x axis were used for fitting, with a 5nm bin width along the axis. The distance between the peaks of the fitted Gaussian functions was used as the cluster separation distance.

Synaptic vesicle identification

Synaptic vesicles were identified based on VAMP2 localizations through a nested clustering algorithm similar to that described for clustering of appositions. First clustering of localizations as mentioned above was produced to identify synaptic boutons. The outer limits of the bouton were then identified using the `ashape3D` function of the `alpha R` package. Localizations within the bouton were then put through the clustering algorithm again using a p of 3, determined as the best parameter cutoff based on randomized simulations. Vesicles identified through this method were taken for further analysis only if they had a minimum of 15 localizations.

Identified boutons with fewer than 12 vesicles were used for quantification.

Counting vesicles within the predicted AZ

The AZ prediction was produced using length, width and depth of Homer1 measurements. Briefly, to account for variability, length, width, and depth of the AZ prediction were increased by 10% of the Homer1 measurements, equivalent to a median increase of 46nm, 33nm, and 14nm respectively. A bounding box produced with these measurements and the `ashape3D` function was then projected towards the centroid of VAMP2 localizations, at 125nm, the average measured distance between Bassoon and Homer1 appositions. Identified synaptic vesicles whose centroids were contained within the prediction were counted as being docked.

Clustering of synaptic vesicles

To measure the relative clustering of synaptic vesicles, the median expected distance between vesicles was calculated based on vesicle number and bouton volume. This value was divided by the median per bouton of the median distance of each vesicle to its 12 nearest neighbors, giving a ratio of the relative clustering of vesicles per bouton.

References

R Core Team (2017). R: A language and environment for statistical computing. R Foundation for Statistical Computing, Vienna, Austria. URL <https://www.R-project.org/>.

Thomas Lafarge and Beatriz Pateiro-Lopez (2016). alphashape3d: Implementation of the 3D Alpha-Shape for the Reconstruction of 3D Sets from a Point Cloud. R package version 1.2. <https://CRAN.R-project.org/package=alphashape3d>

Maechler, M., Rousseeuw, P., Struyf, A., Hubert, M., Hornik, K.(2017). cluster: Cluster Analysis Basics and Extensions. R package version 2.0.6.

Michael Hahsler and Matthew Piekenbrock (2017). dbscan: Density Based Clustering of Applications with Noise (DBSCAN) and Related Algorithms. R package version 1.1-1. <https://CRAN.R-project.org/package=dbscan>

8 Discussion: Actomyosin contractility through ROCK mediates CB1R induced LTD

Through this article we were able to provide evidence towards our initial hypothesis: that the signaling pathway observed under CB1R in neuronal development (Roland et al. 2014) is conserved in CB1R induced LTD. We find that, in classical eCB-LTD induction paradigms in slices, both actomyosin contractility and ROCK activity are necessary for plasticity in hippocampal inhibitory synapses (collaboration with the group of Viven Chevaleyre) as well as in excitatory corticostriatal synapses (collaboration with the group of Laurent Venance). Importantly neither actomyosin contractility nor ROCK inhibition were found to affect eCB short-term forms DSI and DSE. We further find in hippocampal cultures that a 10min application of the CB1R agonist WIN induces a depression of exocytosis that is prevented by inhibiting actomyosin contractility as well as by inhibiting ROCK. Finally, by using STORM superresolution microscopy, we find that hippocampal culture synapses treated with a CB1R agonist present fewer synaptic vesicles at the active zone, and vesicles contained within the center of the boutons are more clustered than in control groups. Furthermore, both of these effects are prevented by pretreatments with either the NMII ATPase inhibitor paranitroblebbistatin (para), or the ROCK inhibitor Y-27632 (Y27).

These results suggest a novel target underlying CB1R-induced long-term plasticity, which may potentially tie in the multitude of pathways that have previously been found to underlie this form of LTD. These will be discussed below.

8.1 Actomyosin in LTD versus DSI/DSE

One important finding presented in our results is that while actomyosin contractility affects CB1R-LTD it does not affect the short term forms of cannabinoid mediated plasticity. As mentioned in the introduction it has not yet been established why a stimulus might induce a short term depression rather than a long-term depression under the activation of the same receptor, especially considering that activation of a receptor should in principle recruit the same signaling pathways. In this context, previous studies have found that CB1R induction of LTD requires a longer activation of the receptor (>10min) than for DSI/DSE (Chevaleyre and Castillo 2003; Ronesi 2004), which would induce a higher number of G-proteins activated. One possibility that arises here given our results is that a longer activation period is required to recruit the necessary kinases for non-muscle myosin II activation. In contradiction to this

theory however, we have shown in our previous article (Roland et al. 2014) that recruitment of actomyosin contraction under CB1R can be extremely rapid, as early as 2 minutes after bath application.

Another possibility is the necessity for increased presynaptic Ca^{2+} that has been found to be necessary for CB1R-LTD induction in certain synapses (Atwood, Lovinger, and Mathur 2014). Calcium influx has previously been found to be necessary for RhoA/ROCK pathway mediation of myosin contraction in smooth muscle (Uehata et al. 1997; Fernandez-Tenorio et al. 2011). Such a concerted action of elevated Ca^{2+} and ROCK activation could therefore explain the selective recruitment of actomyosin contraction in LTD rather than STD. This hypothesis would have to be tested however as we have not tested the calcium sensitivity of actomyosin-mediated LTD in our models.

8.2 Signaling pathway to actomyosin contractility in CB1R-LTD

Another possibility is that a different G-protein is required to induce the signaling pathways necessary for LTD rather than DSI/DSE. As mentioned in the introduction, DSI/DSE have been established to occur mostly through the inhibition of certain VGCCs by $G_{\beta\gamma}$ subunits (Castillo et al. 2012). A number of studies have shown CB1R-LTD to be sensitive to pertussis toxin and cAMP/PKA activation (Chevaleyre et al. 2007), suggesting $G_{i/o}$ recruitment. Furthermore, it has been shown that CB1R co-precipitates preferentially with $G_{\alpha i}$ subunits (Mukhopadhyay and Howlett 2001). However, a direct link between the $G_{i/o}$ /cAMP/PKA pathway and the inhibition of neurotransmitter release has not been established, with some studies contesting the necessity of the pathway in LTD (Azad et al. 2003; Daniel, Rancillac, and Crepel 2004; Robbe et al. 2002).. It can therefore be suggested that recruitment of $G_{i/o}$ may not be sufficient for LTD induction. In this context, 10min of activation may be sufficient for saturation of $G_{i/o}$ protein activation within the terminal and the subsequent recruitment of other G-proteins by CB1R activation. Indeed, as mentioned previously, CB1R has been found to associate with a number of different proteins both in neurons and in non-neuronal cells (reviewed in the introduction). Furthermore, it has been shown in cultured striatal neurons that saturation of $G_{i/o}$ recruitment by co-activating CB1R with the $G_{i/o}$ -coupled dopamine receptor D2 would induce recruitment of a G_s type protein, as estimated through the concurrent increase in cAMP levels and the sensitivity of the effect to cholera toxin (Glass and Felder 1997). Furthermore, we show in our previous article (Roland et al. 2014), that inhibiting $G_{12/13}$ activity through siRNA interference blocks CB1R effects on

growth cone retraction. Taken together these findings suggest that the preferential recruitment of actomyosin in LTD might occur through saturation of $G_{i/o}$ recruitment over prolonged CB1R activation and subsequent recruitment of $G_{12/13}$. Lending credence to this hypothesis is our finding that CB1R-LTD was dependent on ROCK activation in all three of our models, and ROCK is preferentially recruited under the $G_{12/13}$ pathway.

Nonetheless, this hypothesis does not explain the studies that have found the necessity of $G_{i/o}$ or PKA inhibition in CB1R-induced LTD (Chevaleyre et al. 2007). One hypothesis that could be emitted is that CB1R-LTD might require conjoint activation of both $G_{12/13}$ and $G_{i/o}$. For example, the effects of actomyosin contractility in LTD might require permissive action of PKA inhibition to enact its effects on vesicle recycling. Indeed it has been shown that PKA can phosphorylate RIM1 α to increase neurotransmitter release (Lonart et al. 2003), potentially by increasing vesicle docking and priming for fusion. Thus, inhibition of PKA through $G_{i/o}$ might decrease the phosphorylated state of RIM1 α and therefore prevent vesicle docking and fusion. There is some evidence for this hypothesis as RIM1 α has been implicated in CB1R-LTD previously (Chevaleyre et al. 2007; Grueter, Brasnjo, and Malenka 2010), and our results suggest a depletion of docked vesicles at the active zone during CB1R-LTD, as has been previously reported (García-Morales, Montero, and Moreno-López 2015; Ramírez-Franco et al. 2014). Furthermore, PKA has been found to phosphorylate synapsin (Hirokawa et al. 1989), which blocks its vesicle binding properties. Inhibition of PKA may therefore strengthen the tethering of vesicles to the actomyosin cytoskeleton by preventing synapsin phosphorylation, potentially reducing RRP refilling at the AZ.

Although we have not tested here the potential role of either $G_{i/o}$ or $G_{12/13}$, we have shown in our previous article the actomyosin-dependent growth cone retraction under CB1R activation was sensitive to siRNA inhibition of $G_{12/13}$ and not to pertussis toxin (Roland et al. 2014), suggesting its potential recruitment in this paradigm. However, it has been shown in macrophages that CB1R activation could induce cell shape changes through RhoA/ROCK in a pertussis toxin dependent manner (Mai et al. 2015), implying involvement of $G_{i/o}$. Furthermore, a number of studies in non-neuronal cells have shown that PKA can inhibit RhoA/ROCK activity, either through direct phosphorylation of RhoA (Dong et al. 1998) or through phosphorylation of RhoGDI α and the formation of a RhoA-GTP-RhoGDI α complex (Oishi et al. 2012). It is possible therefore that the recruitment of ROCK in CB1R-LTD may occur through an increase in RhoA activity after inhibition of cAMP/PKA signaling under

$G_{i/o}$. Future experiments will therefore have to uncover the specific G-protein subunit linking CB1R activation to actomyosin recruitment in CB1R-LTD.

8.3 Actomyosin and vesicle recycling under CB1R

One of our original findings is the increased clustering of synaptic vesicles within the presynaptic compartment under cannabinoid treatment. Both this effect and the reduced number of vesicles at the AZ are sensitive to both paranitroblebbistatin and Y27, suggesting mediation by the actomyosin cytoskeleton. As reviewed in the introduction, two recurring effects found under actin cytoskeleton manipulation are the inhibition of endocytosis and synaptic vesicle tethering. Both of these functions taken conjointly can explain our findings here. Indeed, inhibition of endocytosis would prevent the preferential recycling of newly endocytosed vesicles to the RRP, preventing RRP refilling and causing a reduced RRP size, as seen under cannabinoid treatment. Furthermore, increased tethering of vesicles to the actomyosin cytoskeleton may further prevent RRP refilling, as well as increase the clustering of vesicles within the total pool.

How these functions might be put into effect in our model of CB1R-LTD is unclear however. While we do show a direct inhibition of exocytosis under CB1R activation in our cultures, we have not tested the hypothesis that it might result from an inhibition of endocytosis, the two being tightly linked. As ROCK activation would lead to increased MLC phosphorylation and therefore an increase in the formation of stable actomyosin filaments, it is possible that activation of ROCK under CB1R might inhibit endocytosis, as it has been shown that increasing F-actin stability through stabilizing agents blocks endocytosis in certain paradigms (Shupliakov et al., 2002; Bleckert et al., 2012).

However, both RRP size decrease and vesicle clustering are also prevented under paranitroblebbistatin treatment. This molecule is a specific inhibitor of NMII ATPase (Képiró et al. 2014), and preferentially binds to NMII in an actin free state. Pretreatment with paranitroblebbistatin should therefore not affect the actin filament polymerization/depolymerization thought to be needed for actin's effects on endocytosis (Shupliakov et al. 2002; Bloom et al. 2003). The effect of both ROCK inhibition and paranitroblebbistatin may however be explained through a potential effect on synaptic vesicle tethering. Indeed, by preventing actomyosin filament formation, both the inhibition of ROCK and paranitroblebbistatin may induce destabilization of the actin cytoskeleton, which has been found to reduce synaptic vesicle clustering (Shtrahman et al. 2005; R. Jordan, Lemke, and

Klingauf 2005). Therefore, activation of ROCK under CB1R may increase the stability of the actomyosin cytoskeleton, which may increase the tethering of vesicles through molecules such as synapsin, resulting in the clustering of synaptic vesicles during CB1R-LTD. Increased vesicle clustering may then prevent refilling of the RRP, resulting in fewer vesicles docked at the active zone, as seen under CB1R activation.

Perspectives

Given the conserved recruitment of actomyosin cytoskeleton under CB1R from development to adulthood, is it possible that chronic recruitment of actomyosin under CB1R might dismantle the synapse in such a way as to induce synapse loss. Indeed actomyosin has been found to be recruited in a nitric oxide (NO) model of synapse loss at motoneurons (Sunico et al. 2010). This study found that NO treatment induced a loss of excitatory synapses in motoneurons in a ROCK dependent manner. Furthermore they show that this loss is preceded by an increase in phosphorylated MLC in synaptic puncta (Sunico et al. 2010), suggesting prolonged MLC phosphorylation by long-term treatment with NO (6h) may induce retraction of axonal boutons from postsynaptic sites, and eventual synapse loss. Furthermore, similarly to CB1R activation, nitric oxide has been shown to induce presynaptic long-term depression (Reyes-Harde et al. 1999; Reynolds and Hartell 2001), as well as axonal retraction during development (Cramer, Leamey, and Sur 1998; Ernst et al. 2000). It is possible therefore that a similarly conserved mechanism under CB1R may lead to synapse loss in certain conditions, such as excessive cannabinoid consumption.

Indeed, this model might explain some of the pathological symptoms tied to excessive marijuana consumption. A number of studies have now established that excessive consumption in adolescence and early adulthood is a high risk factor for pervasive cognitive impairments in later life, including decreased affect, memory impairments, and the development of psychosis (Karila et al. 2014). Concerning psychosis particularly, a number of studies have shown a decrease in cortical mass and grey matter loss in association with schizophrenia (Vyas, Patel, and Puri 2011). Furthermore, a recent study has found that this could be exacerbated by the excessive expression of the complement component 4 (C4) found in certain schizophrenic patients (Sekar et al. 2016). The study shows that as for other complement cascade components, C4 regulates synaptic pruning in developing mice (Sekar et al. 2016), suggesting excessive pruning through increased expression of C4 may be a mediating factor in psychosis. Therefore, an increased synapse loss through excessive

activation of CB1R may explain the increased incidence of psychosis in early cannabis users. Current projects of the team are aimed at better understanding the role of actomyosin contractility in synaptic remodeling, and its putative behavioral consequences.

Annexes: R scripts

1. Blinding of ROI files for protein apposition identification

```

#Libraries
library(svDialogs)
library(readr)
library(data.table)
library(caroline)

#Method
ROIdirs=vector()
Randnames=vector()
export=vector()
Rd=vector()
Rtot=vector()

folderdir="D:/Maureen/STORM/2colorBsnHmr/BHSD414RECsp1"
blinddir=paste(folderdir,"Blinded",sep = "/")
dirrename=dir.exists(blinddir)

while (dirrename==TRUE) {
  blinddir=paste0(blinddir,"New")
  dirrename=dir.exists(blinddir)
}

dir.create(blinddir)

fno=dlgInput(message="Indicate number of ROI folders to blind", default="6")$res
fno=as.numeric(fno)

for(i in 1:fno){
  ROIdir=dlgDir(default = folderdir, "Select ROI directory")$res
  ROIdirs=c(ROIdirs,ROIdir)
  Randname=paste0("Blind",i)
  Randnames=c(Randnames,Randname)
  export=c(export,"NaN")
  Rd=c(Rd,"Nan")
  Rtot=c(Rtot,"Nan")
}

rand=runif(fno,min = 1, max=fno)
ord=order(rand)
ROIdirsx=ROIdirs[ord]
Blindres=cbind(Randnames,ROIdirsx,export,Rd,Rtot)
brespath=paste(blinddir,"Blindtable.xls",sep="/")
write.delim(Blindres,brespath, sep ="\t")
print(ROIdirs)

```

2. 3D identification of protein appositions

```

##Libraries
library(dbscan)
library(rgl)
library(alphashape3d)
library(FNN)
library(geometry)
library(data.table)
library(heplots)
library(cluster)
library(readr)
library(svDialogs)
library(caroline)
library(stats)
#Variables
set.seed(23)
iname="ST001"
mpts=10
epsi=500
steepcut=0.0001
epcut=50
alpha=30
rad=125
totroi=0
skipp=0

#Functions
getmode <- function(v) {
  uniqv <- unique(v)
  uniqv[which.max(tabulate(match(v, uniqv)))]
}

#Method
#ROIidir=dlgDir(default= "C:/Users/Maureen/Documents/STORM", "Select ROI directory")

Btabledir="D:/Navid/SD481p1RECs/Blinded"
Btablefile=paste(Btabledir,"Blindtable.xls",sep = "/")
Btable=read.delim(Btablefile)
Bno=nrow(Btable)

Clusterdone=0
clusttype=dlgList(c("Vamp2","Bassoon"),title = "Select the type of staining to cluster:")$res

blindn=as.numeric(dlgInput(message = "Enter a folder number to analyse", default="1")$res)
if(clusttype=="Vamp2") vollim=10000000 else vollim=2000000
if(is.na(Btable[blindn,4])==FALSE) {if(Btable[blindn,4]==Btable[blindn,5]) Clusterdone=1}

bfolder=paste(Btabledir,Btable[blindn,1],sep = "/")
bstat=dir.exists(bfolder)
if(bstat==FALSE) dir.create(bfolder)
fstart=Btable[blindn,4]
if(is.na(Btable[blindn,4])==TRUE) fstart=1 else fstart=fstart+1

ROIidir=as.character(Btable[blindn,2])
FileVamp=list.files(ROIidir,pattern = "405_TS3D", all.files = FALSE, full.names = TRUE, include.dirs = FALSE)
FileCy3=list.files(ROIidir,pattern = "Cy3_TS3D", all.files = FALSE, full.names = TRUE, include.dirs = FALSE)
NameVamp=list.files(ROIidir,pattern = "405_TS3D", all.files = FALSE, full.names = FALSE, include.dirs = FALSE)
NameHomer=list.files(ROIidir,pattern = "Cy3_TS3D", all.files = FALSE, full.names = FALSE, include.dirs = FALSE)
modnameV=gsub(iname, "file", NameVamp,fixed = TRUE)
modnameV=gsub("405_TS3D", "file",modnameV,fixed = TRUE)
modnameV=gsub(".csv", ".xls",modnameV,fixed = TRUE)
modnameH=gsub(iname, "file", NameHomer,fixed = TRUE)
modnameH=gsub("Cy3_TS3D", "file",modnameH,fixed = TRUE)
modnameH=gsub(".csv", ".xls",modnameH,fixed = TRUE)
flength=length(modnameV)
bfoldername=basename(bfolder)
Clusterdir=paste0(bfoldername,"Clusters")
Clusterdir=paste(bfolder,Clusterdir,sep = "/")
dir.create(Clusterdir)
Btable[blindn,3]=Clusterdir
Btable[blindn,5]=flength

for(file in fstart:flength) { ##start file loop
  if(Clusterdone==1) break
  # file=1
  Resclusters=vector()
  channelinfo=vector()
  mydatVo=read.csv(FileVamp[file])
  nameh=grep(modnameV[file], modnameH, value=FALSE)
  mydatHo=read.csv(FileCy3[nameh])
  mydatV=mydatVo[,2:4]
  mydatH=mydatHo[,2:4]
  open3d()
  rgl.bg(color="black")
  rgl.points(mydatV[,1:3],col="Red", alpha=0.3)
  rgl.points(mydatH[,1:3],col="Green", alpha=0.3)

  ##Vamp2 Cluster determination
  op=optics(mydatV, epsi, minPts = mpts)

  ###Randomized distribution
  Vn=nrow(mydatV)
  Vx=mydatV[,1]
  Vy=mydatV[,2]
  Vz=mydatV[,3]
  randx=runif(Vn, min = min(Vx), max= max(Vx) )
  randy=runif(Vn, min = min(Vy), max= max(Vy) )
  randz=runif(Vn, min = min(Vz), max= max(Vz) )
}

```

```

randdist=cbind(randx,randy,randz)

oprand=optics(randdist, epsi, minPts = mpts)
randreachmed=median(oprand$coredist[which(oprand$coredist!=Inf)])
if(is.na(randreachmed)==TRUE) next
randreachmad=mad(oprand$coredist[which(oprand$coredist!=Inf)])

##Bassoon preliminary cluster
simfact=5
refine=1

while(refine==1){
  maincut=randreachmed-(simfact*randreachmad)
  resrand=extractDBSCAN(oprand,maincut)
  resrandclust=cbind(randdist,resrand$cluster)
  res=extractDBSCAN(op, maincut)
  concatV=cbind(mydatV, res$cluster, res$order,res$reachdist,res$coredist)
  setnames(concatV, "res$coredist", "CoreDist")
  setnames(concatV, "res$reachdist","ReachDist")
  setnames(concatV, "res$order", "Order")
  setnames(concatV, "res$cluster", "Cluster")
  maxCV=max(concatV$Cluster)
  concatVtemp=concatV[which(concatV$Cluster!=0),]
  centVm=vector()
  clids=vector()
  concatVtemp=as.matrix(concatVtemp)
  cvpoints=1

  for(i in 1:maxCV){
    nr=length(concatVtemp[which(concatVtemp[,4]==i),4])
    if(nr>50){
      aV=ashape3d(concatVtemp[which(concatVtemp[,4]==i),1:3],alpha=1)
      calpha=2*mean(aV$triang[,6])
      aV=ashape3d(concatVtemp[which(concatVtemp[,4]==i),1:3],alpha=calpha)
      VolV=volume_ashape3d(aV)
      #concatVtemp=concatVtemp[which(concatVtemp[,4]!=i),]
      if(VolV>vollim){
        open3d()
        rgl.bg(color="black")
        rgl.points(concatVtemp[which(concatVtemp[,4]==i),1:3], col="coral",alpha=0.3)
        rgl.points(mydatV[,1:3],col="Gray", alpha=0.2)
        rgl.points(mydatH[,1:3],col="White", alpha=0.2)
        title3d(main = i, col="White")

centv=c(mean(concatV[which(concatV$Cluster==i),1]),mean(concatV[which(concatV$Cluster==i),2]),mean(concatV[which(concatV$Cluster==i),3]),
i, VolV)
        centVm=rbind(centVm,centv)
        clids[cvpoints]=i
        cvpoints=cvpoints+1
      }
    }
  }

  Vclustchoice=dlgList(c("Unrefine",clids,"Refine","None"), multiple=FALSE, title="Select Bassoon cluster")
  Mainclust=Vclustchoice$res
  if(Mainclust=="Unrefine") simfact=simfact-0.4
  if(Mainclust!="Refine"& Mainclust!="Unrefine") refine=0
  if(Mainclust=="Refine") simfact=simfact+0.2
  dlist=rgl.dev.list()
  dlistl=length(dlist)
  if(dlistl>0){
    for(i in 1:dlistl){
      rgl.close()
    }
  }
}

if(Mainclust!="None"){
  #if(Mainclust=="None") next()
  Mainclust=as.numeric(Vclustchoice$res)
  mainVclust=concatV[which(concatV$Cluster==Mainclust),]

  ##Homer1 main clusters
  op=optics(mydatH, epsi, minPts = mpts)

  ###Randomized distribution for Homer1 main cluster
  Hn=nrow(mydatH)
  Hx=mydatH[,1]
  Hy=mydatH[,2]
  Hz=mydatH[,3]
  randx=runif(Hn, min = min(Hx), max= max(Hx) )
  randy=runif(Hn, min = min(Hy), max= max(Hy) )
  randz=runif(Hn, min = min(Hz), max= max(Hz) )
  randdist=cbind(randx,randy,randz)
  oprand=optics(randdist, epsi, minPts = mpts)

  randreachmed=median(oprand$coredist[which(oprand$coredist!=Inf)])
  randreachmad=mad(oprand$coredist[which(oprand$coredist!=Inf)])

  ###Homer1 preliminary main cluster
  simfact=5
  refine=1

  while(refine==1){
    maincut=randreachmed-(simfact*randreachmad)
    resrand=extractDBSCAN(oprand,maincut)
    resrandclust=cbind(randdist,resrand$cluster)
    res=extractDBSCAN(op, maincut)

```

```

concatH=cbind(mydatH, res$cluster, res$order, res$reachdist, res$coredist)
setnames(concatH, "res$coredist", "Coredist")
setnames(concatH, "res$reachdist", "ReachDist")
setnames(concatH, "res$order", "Order")
setnames(concatH, "res$cluster", "Cluster")
maxCH=max(concatH$Cluster)
concatHtemp=concatH[which(concatH$Cluster!=0),]
concatHtemp=as.matrix(concatHtemp)
centHm=vector()
clids=vector()
cvpoints=1

for(i in 1:maxCH){
  nr=length(concatHtemp[which(concatHtemp[,4]==i),4])
  if(nr>50){
    aH=ashape3d(concatHtemp[which(concatHtemp[,4]==i),1:3],alpha=1)
    calpha=2*mean(aH$Striang[,6])
    aH=ashape3d(concatHtemp[which(concatHtemp[,4]==i),1:3],alpha=calpha)
    VolH=volume_ashape3d(aH)
    #concatHtemp=concatHtemp[which(concatHtemp[,4]!=i),]
    if(VolH>2000000){
      open3d()
      rgl.bg(color="black")
      rgl.points(concatHtemp[which(concatHtemp[,4]==i),1:3], col="chartreuse4",alpha=0.3)
      rgl.points(mydatH[,1:3],col="Gray", alpha=0.2)
      rgl.points(mainVclust[,1:3],col="red", alpha=0.2)
      title3d(main = i, col="White")
      clids[cvpoints]=i
      cvpoints=cvpoints+1
    }
  }
}
Hclustchoice=dlgList(c("Unrefine",clids,"Refine","None"), multiple=FALSE, title="Select Homer1 cluster")
Mainclust=Hclustchoice$res
#if(Mainclust=="None") next()
if(Mainclust=="Unrefine") simfact=simfact-0.4
if(Mainclust!="Refine"& Mainclust!="Unrefine") refine=0
if(Mainclust=="Refine") simfact=simfact+0.2
dlist=rgl.dev.list()
dlistl=length(dlist)
if(dlistl>0){
  for(i in 1:dlistl){
    rgl.close()
  }
}
dlist=rgl.dev.list()
dlistl=length(dlist)
if(dlistl>0){
  for(i in 1:dlistl){
    rgl.close()
  }
}
if(Mainclust!="None"){
  Mainclust=as.numeric(Hclustchoice$res)
  mainHclust=concatH[which(concatH$Cluster==Mainclust),]
  mainHclustx=mainHclust
  mainVclustx=mainVclust
  #Homer1 vesicle cluster determination
  # mainHclust=as.matrix(mainHclust)
  mainHclust=mainHclust[,1:3]
  mainVclust=mainVclust[,1:3]
  bluech=nrow(mainVclust)
  redch=nrow(mainHclust)
  channelinfo[1:bluech]=1
  channelinfo[(bluech+1):(bluech+redch)]=2
  Resclusters=rbind(mainVclust,mainHclust)
  Resclusters=cbind(Resclusters,channelinfo)
  Respath=paste0("Clustertable",filen,bfoldername,".xls")
  Respath=paste(Clusterdir,Respath, sep = "/")
  write.delim(Resclusters,Respath, sep = "\t")
}
}
Btable[blindn,4]=filen
write.delim(Btable,Btablefile,sep = "\t")
# filen=filen+1
} ##end file loop

print(filn-1)

```

3. Clustering of Homer1-Bassoon appositions and property measurement

```

##Libraries
library(dbscan)
library(rgl)
library(alphashape3d)
library(FNN)
library(geometry)
library(data.table)
library(heplots)
library(cluster)
library(readr)
library(svDialogs)
library(caroline)
library(stats)
library(bda)
library(xlsx)

#Variables
set.seed(23)
iname="ST003"
mpts=10
epsi=500
steepcut=0.0001
epcut=50
alpha=30
rad=124
totroi=0
skipp=0

#Functions
sqr=function(x){
  y=x*x
  return(y)
}
RsqrGauss=function(x,mn,param){#param are parameters of gaussian function (mean, sd, and variance)
  valx=x[,2]-mn
  valfity=(param[3]*exp(-1/2*(x[,1]-param[1])^2/param[2]^2))-mn
  y=sum(sqr(valfity))/sum(sqr(valx))
  return(y)
}

Bdir="D:/Maureen/STORM/2colorBsnHmr/Blinded directories.xlsx"
BlindDirs=as.vector(read.xlsx(Bdir,1,header = FALSE))
blength=length(BlindDirs[,1])
Btabledir=as.character(BlindDirs[,])

pb=winProgressBar(title=paste0("Blind directory ",1,"of",blength),label =paste0("0% of 0"), min=0, max=100,initial=0)

for(bd in 1:blength) {
  #Method
  Btablefile=paste(Btabledir[bd],"Blindtable.xls",sep = "/" )
  Btable=read.delim(Btablefile)
  Bno=nrow(Btable)

  exportdir=paste(Btabledir[bd],"Analysis", sep="/")

  dirrename=dir.exists(exportdir)

  while(dirrename==TRUE){
    exportdir=paste0(exportdir,"New")
    dirrename=dir.exists(exportdir)
  }
  dir.create(exportdir)

  Clusterdir=paste(exportdir,"ClusterInfo", sep="/")
  dir.create(Clusterdir)

  for(blindfold in 1:Bno){ #start ROI folder loop

    Objsumm=vector()
    Anasumm=vector()

    ROIIdir=as.character(Btable[blindfold,1])
    ROIIdir=paste0(Btabledir[bd],"/",ROIIdir,"/",ROIIdir,"Clusters")
    Clusterfiles=list.files(ROIIdir, all.files = FALSE, full.names = TRUE, include.dirs = FALSE)
    nofull=length(grep("full.xls",Clusterfiles))
    if(nofull!=0) Clusterfiles=Clusterfiles[-grep("full.xls",Clusterfiles)]
    flength=length(Clusterfiles)

    expname=basename(as.character(Btable[blindfold,2]))
    clusterexp=paste0(Clusterdir,"/", expname,"Clusters")
    dir.create(clusterexp)

    for(filen in 1:flength) { ##start file loop
      # filen=1
      mydat=read.delim(Clusterfiles[filen],sep="\t")
      mydatV=as.matrix(mydat[which(mydat[,4]==1),1:3])
      mydatH=as.matrix(mydat[which(mydat[,4]==2),1:3])

      #Cross-talk subtraction
      Hdist=knn.dist(mydatH, k=10)[,10]
      Bdist=knn.dist(mydatV, k=10)[,10]

      Hcut=median(Hdist)+mad(Hdist)
      Vcut=median(Bdist)+mad(Bdist)

      BtH=knnx.dist(mydatH[,1:3],mydatV[,1:3],k=10)[,10]
      HtB=knnx.dist(mydatV[,1:3],mydatH[,1:3],k=10)[,10]

      Hxt=HtB/Hdist
      Bxt=BtH/Bdist
    }
  }
}

```

```

mydatH=mydatH[which(Hxt>1),]
mydatV=mydatV[which(Bxt>1),]

Hdb=dbscan(mydatH,Hcut,minPts = 10)
maxref=max(Hdb$cluster)
num=0
for(i in 1:maxref){
  no=length(which(Hdb$cluster==i))
  stat=no-num
  if(stat>0){
    num=no
    clust=i
  }
}
mydatH=mydatH[which(Hdb$cluster==clust),]

Vdb=dbscan(mydatV,Vcut,minPts = 10)
maxref=max(Vdb$cluster)
num=0
for(i in 1:maxref){
  no=length(which(Vdb$cluster==i))
  stat=no-num
  if(stat>0){
    num=no
    clust=i
  }
}
mydatV=mydatV[which(Vdb$cluster==clust),]

#Vamp2 main cluster info
centv=c(mean(mydatV[,1]),mean(mydatV[,2]),mean(mydatV[,3]))
aV=ashape3d(mydatV[,1:3],alpha=1)
calpha=2*mean(aV$triang[,6])
aV=ashape3d(mydatV[,1:3],alpha=calpha)
VolmainV=volume_ashape3d(aV)

#Bsn nc cluster determination
Vn=nrow(mydatV)
Vx=mydatV[,1]
Vy=mydatV[,2]
Vz=mydatV[,3]
randx=runif(Vn*20, min = min(Vx), max= max(Vx) )
randy=runif(Vn*20, min = min(Vy), max= max(Vy) )
randz=runif(Vn*20, min = min(Vz), max= max(Vz) )
randdist=cbind(randx,randy,randz)
inaV=inashape3d(aV, indexAlpha = 1, randdist[,1:3])
randdist=cbind(randdist,inaV)
randdist=randdist[which(randdist[,4]==TRUE),]
if(length(randdist[,1])<Vn) next
randdist=randdist[1:Vn,]
oprand=optics(randdist, epsi, minPts = mpts)
randreachmed=median(oprand$coredist[which(oprand$coredist!=Inf)])
randreachmad=mad(oprand$coredist[which(oprand$coredist!=Inf)])
vcutlow=randreachmed-(3*randreachmad)
opvrandlow=extractDBSCAN(oprand, vcutlow)
opv=optics(mydatV[,1:3], epsi, minPts = mpts)
resvlow=extractDBSCAN(opv, vcutlow)
mydatV=cbind(mydatV, resvlow$cluster, resvlow$order, resvlow$reachdist, resvlow$coredist)

centroidsV=vector()
ckeepv=vector()
locnov=vector()
cnndv=vector()
diav=vector()
vno=max(mydatV[,4])

for(i in 1:vno){
  nclust=length(mydatV[which(mydatV[,4]==i),2])
  if(nclust>16){
    diax=c(max(mydatV[which(mydatV[,4]==i),1])-min(mydatV[which(mydatV[,4]==i),1]))
    diay=c(max(mydatV[which(mydatV[,4]==i),2])-min(mydatV[which(mydatV[,4]==i),2]))
    cnnd=knn.dist(mydatV[which(mydatV[,4]==i),1:3],k=1)
    cnndv=c(cnndv,median(cnnd))
    locnov=c(locnov,nclust)
    cv=c(i,mean(mydatV[which(mydatV[,4]==i),1]),mean(mydatV[which(mydatV[,4]==i),2]),mean(mydatV[which(mydatV[,4]==i),3]))
    diav=c(diav,median(diax,diay))
    centroidsV=rbind(centroidsV,cv)
    ckeepv=c(ckeevp,i)
  }
}

c2keepv=mydatV[,4][in%ckeevp]
ConcatVcout=mydatV[-which(c2keepv==TRUE),1:3]
outcno=nrow(ConcatVcout)
outcnnd=knnx.dist(mydatV[,1:3],ConcatVcout,k=2)

outcnnd=median(outcnnd[,2])
locrat=locnov/Vn
cnndrat=outcnnd/cnndv

vclustno=length(ckeevp)

#Homer1 main Cluster info
centH=c(mean(mydatH[,1]),mean(mydatH[,2]),mean(mydatH[,3]))
aH=ashape3d(mydatH[,1:3],alpha=1)
calpha=2*mean(aH$triang[,6])
aH=ashape3d(mydatH[,1:3],alpha=calpha)
VolH=volume_ashape3d(aH)

#Homer1 vesicle cluster determination

```

```

Hn=nrow(mydatH)
Hx=mydatH[,1]
Hy=mydatH[,2]
Hz=mydatH[,3]
randx=runif(Hn*20, min = min(Hx), max= max(Hx) )
randy=runif(Hn*20, min = min(Hy), max= max(Hy) )
randz=runif(Hn*20, min = min(Hz), max= max(Hz) )
randdist=cbind(randx,randy,randz)
inaH=inashape3d(aH, indexAlpha = 1, randdist[,1:3])
randdist=cbind(randdist,inaH)
randdist=randdist[which(randdist[,4]==TRUE),]
randdist=randdist[1:Hn,]
oprand=optics(randdist, epsi, minPts = mpts)
randreachmed=median(oprand$reachdist[-which(oprand$reachdist==Inf)])
randreachmad=mad(oprand$reachdist[-which(oprand$reachdist==Inf)])
Hcutlow=randreachmed-(3*randreachmad)
opH=optics(mydatH[,1:3], epsi, minPts = mpts)
resHlow=extractDBSCAN(opH, Hcutlow)
mydatH=cbind(mydatH[,1:3], resHlow$order, resHlow$reachdist, resHlow$scoredist)
Halphap=aH$triang[which(aH$triang[,9]==2),]
Halphapt=t(Halphap[,1:3])

centroidsVv=vector()
locnoh=vector()
cnndh=vector()
ckeepp=vector()
diaH=vector()

hclustno=unique(mydatH[,4])
hcno=max(mydatH[,4])

clusthno=0
if(hcno>0){
  for(i in 1:hcno){
    nclusth=length(mydatH[which(mydatH[,4]==i),1])
    if(nclusth>16){
      diax=c(max(c(mydatH[which(mydatH[,4]==i),1]))-min(c(mydatH[which(mydatH[,4]==i),1])))
      diay=c(max(c(mydatH[which(mydatH[,4]==i),2]))-min(c(mydatH[which(mydatH[,4]==i),2])))
      diaH=c(diaH,median(diax,diay))
      cnnd=knn.dist(mydatH[which(mydatH[,4]==i),1:3],k=1)
      cnndh=c(cnndh,median(cnnd))
      locnoh=c(locnoh,nclusth)
    }
  }
  chinfo=c(paste0("Homer",i),median(mydatH[which(mydatH[,4]==i),1]),median(mydatH[which(mydatH[,4]==i),2]),median(mydatH[which(mydatH[,4]==i),3]))

  centroidsVv=rbind(centroidsVv,chinfo)
  clusthno=clusthno+1
  ckeepp=c(ckeepp,i)
}

c2keep=mydatH[,4]%in%ckeepp
ConcatHcout=mydatH[-which(c2keep==TRUE),1:3]
outcnoh=nrow(ConcatHcout)
outcnndh=knnx.dist(mydatH[,1:3],ConcatHcout,k=2)
outcnndh=median(outcnndh[,2])

locnohtrat=locnoh/Hn
cnndhtrat=outcnndh/cnndh

#ROI Bsn and Homer1 nanocluster info
bno=length(ckeeppv)
hcno=length(ckeepp)
if(hcno>0){
  hna=vector()
  hna[hcno]=NA
  centroidsVv=cbind(centroidsVv,locnoh,diaH,locnohtrat,cnndh,cnndhtrat,hna,hna)
} else {
  centroidsVv=c("Homer", centH,NA,NA,NA,NA,NA,NA,NA)
}
if(bno>0){
  bna=vector()
  bna[bno]=NA
  centroidsV=cbind(centroidsV,locnov,diav,locrat,cnndv,cnndrat,bna,bna)
} else {
  centroidsV=c("Bassoon", centH,NA,NA,NA,NA,NA,NA,NA)
}

centroidsVr=rbind(centroidsV,centroidsVv)
centroidsVr=as.data.table(centroidsVr)
names=c("Cluster","x [nm]","y [nm]","z [nm]","Loc. no.", "NC diameter [nm]","Loc NC/out ratio","NC nnd [nm]", "NC/out nnd ratio", "SV
nnd [nm]", "SV dist. to Hmr node [nm]")
setnames(centroidsVr,names)
centroidsVtable=paste0(clusterexp,"/","Info",basename(Clusterfiles[filen]))
write.delim(centroidsVr,centroidsVtable, sep ="/t")

#Homer1 ellipse
Hellihull=ellipsoidhull(mydatH[,1:3],tol = 1000)
Haxes=ellipse3d.axes(Hellihull$cov, centre = Hellihull$loc)
rgl.close()

#translation to origin
mydatVx=rbind(cbind(mydatV[,1]-Hellihull$loc[1],mydatV[,2]-Hellihull$loc[2],mydatV[,3]-Hellihull$loc[3]),c(centv[1]-
Hellihull$loc[1],centv[2]-Hellihull$loc[2],centv[3]-Hellihull$loc[3]))
mydatHx=cbind(mydatH[,1]-Hellihull$loc[1],mydatH[,2]-Hellihull$loc[2],mydatH[,3]-Hellihull$loc[3])
Haxesx=cbind(Haxes[,1]-Hellihull$loc[1],Haxes[,2]-Hellihull$loc[2],Haxes[,3]-Hellihull$loc[3])

##rotation around z axis (xycoordinat rotation)
vAC=as.vector(0-Haxesx[6,1:2])

```

```

vCO=as.vector(c(1,0))
if(Haxesx[6,2]<0){
  angle=2*pi-acos(dot(vAC,vCO)/(knn.dist(rbind(c(0,0),vAC),k=1)[1]*knn.dist(rbind(c(0,0),vCO),k=1)[1]))
} else {
  angle=acos(dot(vAC,vCO)/(knn.dist(rbind(c(0,0),vAC),k=1)[1]*knn.dist(rbind(c(0,0),vCO),k=1)[1]))
}

mydatVx1=mydatVx
mydatVx1[,1]=mydatVx[,1]*cos(angle)-mydatVx[,2]*sin(angle)
mydatVx1[,2]=mydatVx[,2]*cos(angle)+mydatVx[,1]*sin(angle)

mydatHx1=mydatHx
mydatHx1[,1]=mydatHx[,1]*cos(angle)-mydatHx[,2]*sin(angle)
mydatHx1[,2]=mydatHx[,2]*cos(angle)+mydatHx[,1]*sin(angle)

Haxesx1=Haxesx
Haxesx1[,1]=Haxesx[,1]*cos(angle)-Haxesx[,2]*sin(angle)
Haxesx1[,2]=Haxesx[,2]*cos(angle)+Haxesx[,1]*sin(angle)

mydatVx=mydatVx1
mydatHx=mydatHx1
Haxesx=Haxesx1

##rotation around y axis (xz coordinate rotation)
vAC=as.vector(0-c(Haxesx[6,1],Haxesx[6,3]))
vCO=as.vector(c(1,0))
if(Haxesx[6,3]<0){
  angle=2*pi-acos(dot(vAC,vCO)/(knn.dist(rbind(c(0,0),vAC),k=1)[1]*knn.dist(rbind(c(0,0),vCO),k=1)[1]))
} else {
  angle=acos(dot(vAC,vCO)/(knn.dist(rbind(c(0,0),vAC),k=1)[1]*knn.dist(rbind(c(0,0),vCO),k=1)[1]))
}
mydatVx1=mydatVx
mydatVx1[,1]=(mydatVx[,1]*cos(angle)-mydatVx[,3]*sin(angle))
mydatVx1[,3]=(mydatVx[,3]*cos(angle)+mydatVx[,1]*sin(angle))

mydatHx1=mydatHx
mydatHx1[,1]=mydatHx[,1]*cos(angle)-mydatHx[,3]*sin(angle)
mydatHx1[,3]=mydatHx[,3]*cos(angle)+mydatHx[,1]*sin(angle)

Haxesx1=Haxesx
Haxesx1[,1]=Haxesx[,1]*cos(angle)-Haxesx[,3]*sin(angle)
Haxesx1[,3]=Haxesx[,3]*cos(angle)+Haxesx[,1]*sin(angle)

mydatVx=mydatVx1
mydatHx=mydatHx1
Haxesx=Haxesx1

##rotation around x axis (yz coordinate rotation)
vAC=as.vector(0-c(Haxesx[2,2],Haxesx[2,3]))
vCO=as.vector(c(1,0))

if(Haxesx[2,3]<0){
  angle=2*pi-acos(dot(vAC,vCO)/(knn.dist(rbind(c(0,0),vAC),k=1)[1]*knn.dist(rbind(c(0,0),vCO),k=1)[1]))
} else {
  angle=acos(dot(vAC,vCO)/(knn.dist(rbind(c(0,0),vAC),k=1)[1]*knn.dist(rbind(c(0,0),vCO),k=1)[1]))
}

mydatVx1=mydatVx
mydatVx1[,2]=(mydatVx[,2]*cos(angle)-mydatVx[,3]*sin(angle))
mydatVx1[,3]=(mydatVx[,3]*cos(angle)+mydatVx[,2]*sin(angle))

mydatHx1=mydatHx
mydatHx1[,2]=mydatHx[,2]*cos(angle)-mydatHx[,3]*sin(angle)
mydatHx1[,3]=mydatHx[,3]*cos(angle)+mydatHx[,2]*sin(angle)

Haxesx1=Haxesx
Haxesx1[,2]=Haxesx[,2]*cos(angle)-Haxesx[,3]*sin(angle)
Haxesx1[,3]=Haxesx[,3]*cos(angle)+Haxesx[,2]*sin(angle)

mydatVx=mydatVx1
mydatHx=mydatHx1
Haxesx=Haxesx1

xval=abs(mydatVx[length(mydatVx[,1]),1])
centrvrot=mydatVx[length(mydatVx[,1]),]
mydatVx=mydatVx[1:length(mydatVx[,1])-1,]

#loc chunk for gaussian analysis
datchunkV=mydatVx[which(-100<mydatVx[,2]&mydatVx[,2]<100),1]
if(length(datchunkV)<2)next()
datchunkH=mydatHx[which(-100<mydatHx[,2]&mydatHx[,2]<100),1]
if(length(datchunkH)<2)next()
chunkinfo=rbind(cbind(datchunkV,1),cbind(datchunkH,2))

#Gaussian fitting
Hbin=binning(datchunkH[order(datchunkH)],bw=5)
Vbin=binning(datchunkV[order(datchunkV)],bw=5)

#hmr peak fit
x <- Hbin$mids
f <- function(par)
{
  m <- par[1]
  sd <- par[2]
  k <- par[3]
  rhat <- k * exp(-0.5 * ((x - m)/sd)^2)
  sum((Hbin$counts - rhat)^2)
}

resfith=optim(c(mean(datchunkH), 20, 10), f, method="BFGS", control=list(reltol=1e-9))
v=resfith$par
Rhmr=RsqrGauss(cbind(Hbin$mids,Hbin$counts),mean(Hbin$counts),v)
if(Rhmr>1)Rhmr=2-Rhmr

```

```

if (Rhm<0.75) next()

#bsn peak fit
x <- Vbin$mids
f <- function(par)
{
  m <- par[1]
  sd <- par[2]
  k <- par[3]
  rhat <- k * exp(-0.5 * ((x - m)/sd)^2)
  sum((Vbin$counts - rhat)^2)
}
resfitb=optim(c(mean(datchunkV), 20, 10), f, method="BFGS", control=list(reltol=1e-9))
v=resfitb$par
Rbsn=RsqrGauss(cbind(Vbin$mids,Vbin$counts),mean(Vbin$counts),v)
if (Rbsn>1) Rbsn=2-Rbsn

clusteriexp=paste0(clusterexp,"/", "gausslocs",filen,".xls")
write_delim(as.data.frame(chunkinfo),clusteriexp,delim = "\t")

ptop=abs(resfitb$par[1]-resfith$par[1])
plot(x=c(Vbin$mids,Hbin$mids),y=c(Vbin$counts,Hbin$counts),main = ptop)
newhlen=max(mydatHx[,2])-min(mydatHx[,2])
newhdepth=4.71*resfith$par[2]
newhwidth=max(mydatHx[,3])-min(mydatHx[,3])

newblen=max(mydatVx[,2])-min(mydatVx[,2])
newbdepth=4.71*resfitb$par[2]
newbwidth=max(mydatVx[,3])-min(mydatVx[,3])

#Homer1 alpha translation along ellipse axes

#Homer1 bbox projection
if(centvrot[1]>0) rad=124 else rad=-124
EBSn=rbind(c(rad,max(mydatHx[,2]),0),c(rad,min(mydatHx[,2]),0),c(rad,0,max(mydatHx[,3])),c(rad,0,min(mydatHx[,3])),c(rad+
(newhdepth/2)+20,0,0),c(rad-(newhdepth/2)-20,0,0))
plengthax=dist(EBSn[1:2,])*0.05
pwidthax=dist(EBSn[3:4,])*0.05
pdepthax=dist(EBSn[5:6,])*0.05
EBSn=rbind(c(rad,max(mydatHx[,2])+plengthax,0),c(rad,min(mydatHx[,2])-
plengthax,0),c(rad,0,max(mydatHx[,3])+pwidthax),c(rad,0,min(mydatHx[,3])-pwidthax),c(rad+(newhdepth/2)+20,0,0),c(rad-(newhdepth/2)-20,0,0))

#Bounding box
centaxes=c(rad, 0, 0)
AxeX=EBSn[1:2,]
projtop=EBSn[3:6,]
Boxpoints=vector()
Boxproj=vector()
interpoints=vector()

#AxeX point projection to Axes plane
for(i in 1:2) {
  Norm=c((centaxes[1]-projtop[i,1]),(centaxes[2]-projtop[i,2]),(centaxes[3]-projtop[i,3]))
  dplane=Norm[1]*projtop[i,1] + Norm[2]*projtop[i,2] + Norm[3]*projtop[i,3]
  plane=c(Norm, dplane)
  t=as.numeric((dplane-(AxeX[1,1]*Norm[1])-(AxeX[1,2]*Norm[2])-(AxeX[1,3]*Norm[3]))/((Norm[1]^2)+(Norm[2]^2)+(Norm[3]^2)))
  bpoint1=c((AxeX[1,1]+t*Norm[1]),(AxeX[1,2]+t*Norm[2]),(AxeX[1,3]+t*Norm[3]))
  bpoint2=c((AxeX[2,1]+t*Norm[1]),(AxeX[2,2]+t*Norm[2]),(AxeX[2,3]+t*Norm[3]))
  Boxproj=rbind(Boxproj,bpoint1,bpoint2)
}
Boxpoints=Boxproj

#Bbox area
lengthax=as.numeric(dist(EBSn[1:2,]))/1000
widthax=as.numeric(dist(EBSn[3:4,]))/1000
depthax=as.numeric(dist(EBSn[5:6,]))/1000
hmrarea=lengthax*widthax
bboxvol=lengthax*widthax*depthax

for(i in 3:4){
  bpoints=Boxproj
  Norm=c((centaxes[1]-projtop[i,1]),(centaxes[2]-projtop[i,2]),(centaxes[3]-projtop[i,3]))
  dplane=Norm[1]*projtop[i,1] + Norm[2]*projtop[i,2] + Norm[3]*projtop[i,3]
  plane=c(Norm, dplane)
  t=as.numeric((dplane-(AxeX[1,1]*Norm[1])-(AxeX[1,2]*Norm[2])-(AxeX[1,3]*Norm[3]))/((Norm[1]^2)+(Norm[2]^2)+(Norm[3]^2)))
  trans=c(t*Norm[1],t*Norm[2],t*Norm[3])
  bpoints[,1]=Boxproj[,1]+trans[1]
  bpoints[,2]=Boxproj[,2]+trans[2]
  bpoints[,3]=Boxproj[,3]+trans[3]
  interpoints=rbind(interpoints,bpoints)
  Boxpoints=rbind(Boxpoints,bpoints)
}
# Boxpoints=rbind(Boxpoints,EBSn)
boxa=ashape3d(Boxpoints,alpha=10000, pert = TRUE)
btri=boxa$triang
btrit=t(btri[which(btri[,9]==2),1:3])

#Test of Bsn locs within bbox
cinBa=inashape3d(boxa,indexAlpha = 1, mydatVx[,1:3])
cinBano=(length(cinBa)-length(cinBa[which(cinBa==FALSE)]))*100/length(cinBa)

open3d()
rgl.points(mydatVx[,1:3],col="red",alpha=0.4,size=5)
rgl.points(mydatHx[,1:3],col="chartreuse4",alpha=0.4,size=5)
rgl.triangles(Boxpoints[btrit,],col="black",alpha=0.3)
segments3d(Haxesx)

#Summary of Homer and Vamp2 object metrics
Objdat=c(basename(Clusterfiles[filen]),Rhm,Rbsn,cinBano,ptop,knn.dist(rbind(centH,centv),k=1)[1],xval, VolmainV, Vn, VolH,Hn,lengthax,
widthax, depthax,bboxvol,newhlen,newwidth,newhdepth,newblen,newbwidth,newbdepth)
if (bno==0) Objdat=c(Objdat,0, NA,outcnnd, NA,NA) else Objdat=c(Objdat,bno, median(diav),median(loccrat),outcnnd, median(cnndrat))

```

```

if(hcno==0)  Objdat=c(Objdat,0, NA,outcnndh, NA,NA) else Objdat=c(Objdat,hcno, median(diaH),median(locnohrat),outcnndh, median(cnndhrat))

Objsumm=rbind(Objsumm,Objdat)

ijstat=trunc(filen*100/flength)
setWinProgressBar(pb,ijstat, title=paste0("Blind directory ",bd,"of",blength),label = paste0(ijstat,"% of ",blindfold,"/",Bno))

} ##end file loop

Objsumm=as.data.table(Objsumm)
names=c("ROI","Hmr fit R2","Bsn fit R2","Bsn locs in bbox", "peak to peak distance","centroid distances","centroid xval dist", "Bassoon
Volume", "Bassoon Loc no.", "Homer1 Volume", "Hmr Loc. no.", "Homer bbox length (nm)", "Homer bbox width (nm)", "Homer Bbox depth (nm)", "Homer
bbox volume (µm3)", "newhlen", "newhwidth", "newhdepth", "newblen", "newbwidth", "newbdepth", "Bsn nc no.", "median Bnc diameter", "median
Bncloc.no./total", "extra Bnc nnd", "median Bnc extrannd/ncnnd", "Homer1 cluster no.", "median Hmr nc diameter", "median Hmr ncloc.no./total",
"Hmr extra nc nnd", "median Hmr extrannd/ncnnd")
setnames(Objsumm,names)
objexp=paste0(exportdir,"/", "Objects",basename(as.character(Btable[blindfold,2])), ".xls")
write.delim(Objsumm,objexp, sep ="\t")
}#end blind folder loop
}#end Blind directory loop

cpb=close(pb)
print("Done")

```

4. Clustering of Vamp2-Homer1 appositions and synaptic vesicle identification

```

##Libraries
library(dbscan)
library(rgl)
library(alphashape3d)
library(FNN)
library(geometry)
library(data.table)
library(heplots)
library(cluster)
library(readr)
library(svDialogs)
library(caroline)
library(stats)
library(bda)
library(xlsx)

#Variables
set.seed(23)
mpts=10
epsi=500
# alpha=30

#Functions
sqr=function(x){
  y=x*x
  return(y)
}
RsqrGauss=function(x,mn,param){#param are parameters of gaussian function (mean, sd, and variance)
  valx=x[,2]-mn
  valfity=(param[3]*exp(-1/2*(x[,1]-param[1])^2/param[2]^2))-mn
  y=sum(sqr(valfity))/sum(sqr(valx))
  return(y)
}

Bdir="D:/Maureen/STORM/2colorVamp2Hmr/Vamp2-Homer1 DZcal/BlindedDirectories.xlsx"
BlindDirs=as.vector(read.xlsx(Bdir,1,header = FALSE))
blength=length(BlindDirs[,1])
Btabledir=as.character(BlindDirs[,])

pb=winProgressBar(title=paste0("Blind directory ",1,"of",blength),label =paste0("%0% of 0"), min=0, max=100,initial=0)

for(bd in 1:blength){
  #Method
  Btablefile=paste(Btabledir[bd],"Blindtable.xls",sep = "/" )
  Btable=read.delim(Btablefile)
  Bno=nrow(Btable)

  exportdir=paste(Btabledir[bd],"Analysis", sep="/")

  dirrename=dir.exists(exportdir)

  while(dirrename==TRUE){
    exportdir=paste0(exportdir,"New")
    dirrename=dir.exists(exportdir)
  }
  dir.create(exportdir)

  Clusterdir=paste(exportdir,"ClusterInfo", sep="/")
  dir.create(Clusterdir)

  for(blindfold in 1:Bno){ #start ROI folder loop

    Objsumm=vector()
    Anasumm=vector()

    ROIIdir=as.character(Btable[blindfold,1])
    ROIIdir=paste0(Btabledir[bd],"/",ROIIdir,"/",ROIIdir,"Clusters")
    Clusterfiles=list.files(ROIIdir, all.files = FALSE, full.names = TRUE, include.dirs = FALSE)
    nofull=length(grep("full.xls",Clusterfiles))
    if(nofull!=0) Clusterfiles=Clusterfiles[-grep("full.xls",Clusterfiles)]
    flength=length(Clusterfiles)

    expname=basename(as.character(Btable[blindfold,2]))
    clusterexp=paste0(Clusterdir,"/", expname,"Clusters")
    dir.create(clusterexp)

    for(filen in 1:flength) { ##start file loop

      mydat=read.delim(Clusterfiles[filen],sep="\t")
      mydatV=as.matrix(mydat[which(mydat[,4]==1),1:3])
      mydatH=as.matrix(mydat[which(mydat[,4]==2),1:3])

      #Cross-talk subtraction
      Hdlist=knn.dist(mydatH, k=10)[,10]
      Bdlist=knn.dist(mydatV,k=10)[,10]

      Hcut=median(Hdlist)+mad(Hdlist)
      Vcut=median(Bdlist)+mad(Bdlist)

      BtH=knnx.dist(mydatH[,1:3],mydatV[,1:3],k=10)[,10]
      HtB=knnx.dist(mydatV[,1:3],mydatH[,1:3],k=10)[,10]

      Hxt=BtH/Hdlist
      Bxt=BtH/Bdlist

      mydatH=mydatH[which(Hxt>1),]
      mydatV=mydatV[which(Bxt>1),]

      Hdb=dbscan(mydatH,Hcut,minPts = 10)
      maxref=max(Hdb$cluster)
      num=0
      for(i in 1:maxref){

```

```

no=length(which(Hdb$cluster==i))
stat=no-num
if(stat>0){
  num=no
  clust=i
}
}
mydatH=mydatH[which(Hdb$cluster==clust),]

Vdb=dbscan(mydatV,Vcut,minPts = 10)
maxref=max(Vdb$cluster)
num=0
for(i in 1:maxref){
  no=length(which(Vdb$cluster==i))
  stat=no-num
  if(stat>0){
    num=no
    clust=i
  }
}
mydatV=mydatV[which(Vdb$cluster==clust),]

centv=c(mean(mydatV[,1]),mean(mydatV[,2]),mean(mydatV[,3]))
centH=c(mean(mydatH[,1]),mean(mydatH[,2]),mean(mydatH[,3]))

#Homer1 ellipse
Hellihull=ellipsoidhull(mydatH[,1:3],tol = 1000)
Haxes=ellipse3d.axes(Hellihull$cov, centre = Hellihull$loc)
rgl.close()

#translation to origin
mydatVx=rbind(cbind(mydatV[,1]-Hellihull$loc[1],mydatV[,2]-Hellihull$loc[2],mydatV[,3]-Hellihull$loc[3]),c(centv[1]-
Hellihull$loc[1],centv[2]-Hellihull$loc[2],centv[3]-Hellihull$loc[3]))
mydatHx=cbind(mydatH[,1]-Hellihull$loc[1],mydatH[,2]-Hellihull$loc[2],mydatH[,3]-Hellihull$loc[3])
Haxesx=cbind(Haxes[,1]-Hellihull$loc[1],Haxes[,2]-Hellihull$loc[2],Haxes[,3]-Hellihull$loc[3])

##rotation around z axis (xycoordinate rotation)
vAC=as.vector(0-Haxesx[6,1:2])
vCO=as.vector(c(1,0))
if(Haxesx[6,2]<0){
  angle=2*pi-acos(dot(vAC,vCO)/(knn.dist(rbind(c(0,0),vAC),k=1)[1]*knn.dist(rbind(c(0,0),vCO),k=1)[1]))
} else {
  angle=acos(dot(vAC,vCO)/(knn.dist(rbind(c(0,0),vAC),k=1)[1]*knn.dist(rbind(c(0,0),vCO),k=1)[1]))
}

mydatVx1=mydatVx
mydatVx1[,1]=mydatVx[,1]*cos(angle)-mydatVx[,2]*sin(angle)
mydatVx1[,2]=mydatVx[,2]*cos(angle)+mydatVx[,1]*sin(angle)

mydatHx1=mydatHx
mydatHx1[,1]=mydatHx[,1]*cos(angle)-mydatHx[,2]*sin(angle)
mydatHx1[,2]=mydatHx[,2]*cos(angle)+mydatHx[,1]*sin(angle)

Haxesx1=Haxesx
Haxesx1[,1]=Haxesx[,1]*cos(angle)-Haxesx[,2]*sin(angle)
Haxesx1[,2]=Haxesx[,2]*cos(angle)+Haxesx[,1]*sin(angle)

mydatVx=mydatVx1
mydatHx=mydatHx1
Haxesx=Haxesx1

##rotation around y axis (xz coordinate rotation)
vAC=as.vector(0-c(Haxesx[6,1],Haxesx[6,3]))
vCO=as.vector(c(1,0))
if(Haxesx[6,3]<0){
  angle=2*pi-acos(dot(vAC,vCO)/(knn.dist(rbind(c(0,0),vAC),k=1)[1]*knn.dist(rbind(c(0,0),vCO),k=1)[1]))
} else {
  angle=acos(dot(vAC,vCO)/(knn.dist(rbind(c(0,0),vAC),k=1)[1]*knn.dist(rbind(c(0,0),vCO),k=1)[1]))
}

mydatVx1=mydatVx
mydatVx1[,1]=(mydatVx[,1]*cos(angle)-mydatVx[,3]*sin(angle))
mydatVx1[,3]=(mydatVx[,3]*cos(angle)+mydatVx[,1]*sin(angle))

mydatHx1=mydatHx
mydatHx1[,1]=mydatHx[,1]*cos(angle)-mydatHx[,3]*sin(angle)
mydatHx1[,3]=mydatHx[,3]*cos(angle)+mydatHx[,1]*sin(angle)

Haxesx1=Haxesx
Haxesx1[,1]=Haxesx[,1]*cos(angle)-Haxesx[,3]*sin(angle)
Haxesx1[,3]=Haxesx[,3]*cos(angle)+Haxesx[,1]*sin(angle)

mydatVx=mydatVx1
mydatHx=mydatHx1
Haxesx=Haxesx1

##rotation around x axis (yz coordinate rotation)
vAC=as.vector(0-c(Haxesx[2,2],Haxesx[2,3]))
vCO=as.vector(c(1,0))

if(Haxesx[2,3]<0){
  angle=2*pi-acos(dot(vAC,vCO)/(knn.dist(rbind(c(0,0),vAC),k=1)[1]*knn.dist(rbind(c(0,0),vCO),k=1)[1]))
} else {
  angle=acos(dot(vAC,vCO)/(knn.dist(rbind(c(0,0),vAC),k=1)[1]*knn.dist(rbind(c(0,0),vCO),k=1)[1]))
}

mydatVx1=mydatVx
mydatVx1[,2]=(mydatVx[,2]*cos(angle)-mydatVx[,3]*sin(angle))
mydatVx1[,3]=(mydatVx[,3]*cos(angle)+mydatVx[,2]*sin(angle))

mydatHx1=mydatHx
mydatHx1[,2]=mydatHx[,2]*cos(angle)-mydatHx[,3]*sin(angle)
mydatHx1[,3]=mydatHx[,3]*cos(angle)+mydatHx[,2]*sin(angle)

```

```

Haxesx1=Haxesx
Haxesx1[,2]=Haxesx[,2]*cos(angle)-Haxesx[,3]*sin(angle)
Haxesx1[,3]=Haxesx[,3]*cos(angle)+Haxesx[,2]*sin(angle)

mydatVx=mydatVx1
mydatHx=mydatHx1
Haxesx=Haxesx1

xval=abs(mydatVx[length(mydatVx[,1]),1])
centvrot=mydatVx[length(mydatVx[,1]),]
mydatVx=mydatVx[1:length(mydatVx[,1])-1,]

#loc chunk for gaussian analysis
datchunkH=mydatHx[which(-100<mydatHx[,2]&mydatHx[,2]<100),1]
chunkinfo=datchunkH

#Gaussian fitting
Hbin=binning(datchunkH[order(datchunkH)],bw=5)

#hmr peak fit
x <- Hbin$mid
f <- function(par)
{
  m <- par[1]
  sd <- par[2]
  k <- par[3]
  rhat <- k * exp(-0.5 * ((x - m)/sd)^2)
  sum((Hbin$counts - rhat)^2)
}

resfith=optim(c(mean(datchunkH), 20, 10), f, method="BFGS", control=list(reltol=1e-9))
v=resfith$par
Rhrmr=Rsqrgauss(cbind(Hbin$mid,Hbin$counts),mean(Hbin$counts),v)
if(Rhrmr>1)Rhrmr=2-Rhrmr

if(Rhrmr<0.75) next()

newhlen=max(mydatHx[,2])-min(mydatHx[,2])
newhdepth=4.71*resfith$par[2]
newhwidth=max(mydatHx[,3])-min(mydatHx[,3])

mydatH=mydatHx
mydatV=mydatVx
Haxes=Haxesx

#Vamp2 main cluster info
aV=ashape3d(mydatV[,1:3],alpha=1)
calpha=2*mean(aV$triang[,6])
aV=ashape3d(mydatV[,1:3],alpha=calpha)
VolmainV=volume_ashape3d(aV)
Vn=nrow(mydatV)
Vdens=Vn/(VolmainV/1000000000)
# if(Vdens<30000) next()
# if(Vdens>50000) next()

#Homer1 main Cluster info
aH=ashape3d(mydatH[,1:3],alpha=1)
calpha=2*mean(aH$triang[,6])
aH=ashape3d(mydatH[,1:3],alpha=calpha)
VolH=volume_ashape3d(aH)
Hn=nrow(mydatH)
Hdens=Hn/(VolH/1000000000)

#Vamp2 nc cluster determination
Vx=mydatV[,1]
Vy=mydatV[,2]
Vz=mydatV[,3]
lrand=0
repeat{
  if(lrand>=Vn)break
  randx=runif(Vn*20, min = min(Vx), max= max(Vx) )
  randy=runif(Vn*20, min = min(Vy), max= max(Vy) )
  randz=runif(Vn*20, min = min(Vz), max= max(Vz) )
  randdist=cbind(randx,randy,randz)
  inaV=inashape3d(aV, indexAlpha = 1, randdist[,1:3])
  randdist=cbind(randdist,inaV)
  randdist=randdist[which(randdist[,4]==TRUE),]
  lrand=length(randdist[,1])
}
randdist=randdist[1:Vn,]
oprand=optics(randdist, epsi, minPts = mpts)
randreachmed=median(oprand$scoredist[which(oprand$scoredist!=Inf)])
randreachmad=mad(oprand$scoredist[which(oprand$scoredist!=Inf)])
vcutlow=randreachmed-(3*randreachmad)
opvrandlow=extractDBSCAN(oprand, vcutlow)
opv=optics(mydatV[,1:3], epsi, minPts = mpts)
resvlow=extractDBSCAN(opv, vcutlow)
mydatV=cbind(mydatV, resvlow$cluster, resvlow$order, resvlow$reachdist, resvlow$scoredist)

centroidsV=vector()
ckeeppv=vector()
locnov=vector()
cnndv=vector()
diav=vector()
vno=max(mydatV[,4])

for(i in 1:vno){
  nclust=length(mydatV[which(mydatV[,4]==i),2])
  if(nclust>15){
    diax=c(max(mydatV[which(mydatV[,4]==i),1])-min(mydatV[which(mydatV[,4]==i),1]))
    diay=c(max(mydatV[which(mydatV[,4]==i),2])-min(mydatV[which(mydatV[,4]==i),2]))
  }
}

```

```

cnnd=knn.dist(mydatV[which(mydatV[,4]==i),1:3],k=1)
cnndv=c(cnndv,median(cnnd))
locnov=c(locnov,nclust)
cV=c(i,mean(mydatV[which(mydatV[,4]==i),1]),mean(mydatV[which(mydatV[,4]==i),2]),mean(mydatV[which(mydatV[,4]==i),3]))
diav=c(diav,median(diax,diay))
centroidsV=rbind(centroidsV,cV)
ckeepv=c(ckeepv,i)
}
}
if(length(ckeepv)<13) next()

c2keepv=mydatV[,4]%in%ckeepv
ConcatVcout=mydatV[-which(c2keepv==TRUE),1:3]
outcno=nrow(ConcatVcout)
outcnnd=knnx.dist(mydatV[,1:3],ConcatVcout,k=2)

outcnnd=median(outcnnd[,2])
locrat=locnov/Vn
cnndrat=outcnnd/cnndv
centroidsdist=knn.dist(centroidsV[,2:4],k=12)
centroidsdist=apply(centroidsdist,MARGIN=1,FUN=function(x) median(x))

vclustno=length(ckeepv)
medcentdist=median(centroidsdist)

#Homer1 nanocluster determination
Hx=mydatH[,1]
Hy=mydatH[,2]
Hz=mydatH[,3]
lrand=0
repeat{
  if(lrand>=Hn)break
  randx=runif(Hn*20,min=min(Hx),max=max(Hx))
  randy=runif(Hn*20,min=min(Hy),max=max(Hy))
  randz=runif(Hn*20,min=min(Hz),max=max(Hz))
  randdist=cbind(randx,randy,randz)
  inaH=inashape3d(aH,indexAlpha=1,randdist[,1:3])
  randdist=cbind(randdist,inaH)
  randdist=randdist[which(randdist[,4]==TRUE),]
  lrand=length(randdist[,1])
}
randdist=randdist[1:Hn,]
oprand=optics(randdist,epsi,minPts=mpts)
randreachmed=median(oprand$reachdist[-which(oprand$reachdist==Inf)])
randreachmad=mad(oprand$reachdist[-which(oprand$reachdist==Inf)])
Hcutlow=randreachmed-(3*randreachmad)
opH=optics(mydatH[,1:3],epsi,minPts=mpts)
resHlow=extractDBSCAN(opH,Hcutlow)
mydatH=cbind(mydatH[,1:3],resHlow$order,resHlow$reachdist,resHlow$score)
Halphap=aH$triang[which(aH$triang[,9]==2),]
Halphapt=t(Halphap[,1:3])

centroidsVv=vector()
locnoh=vector()
cnndh=vector()
ckeep=vector()
diaH=vector()

hclustno=unique(mydatH[,4])
hcno=max(mydatH[,4])

clusthno=0
if(hcno>0){
  for(i in 1:hcno){
    nclusth=length(mydatH[which(mydatH[,4]==i),1])
    if(nclusth>15){
      diax=c(max(c(mydatH[which(mydatH[,4]==i),1]))-min(c(mydatH[which(mydatH[,4]==i),1])))
      diay=c(max(c(mydatH[which(mydatH[,4]==i),2]))-min(c(mydatH[which(mydatH[,4]==i),2])))
      diaH=c(diaH,median(diax,diay))
      cnnd=knn.dist(mydatH[which(mydatH[,4]==i),1:3],k=1)
      cnndh=c(cnndh,median(cnnd))
      locnoh=c(locnoh,nclusth)
    }
  }
  chinfo=c(paste0("Homer",i),median(mydatH[which(mydatH[,4]==i),1]),median(mydatH[which(mydatH[,4]==i),2]),median(mydatH[which(mydatH[,4]==i),3]))
  centroidsVv=rbind(centroidsVv,chinfo)
  clusthno=clusthno+1
  ckeep=c(ckeep,i)
}
}

c2keep=mydatH[,4]%in%ckeep
ConcatHcout=mydatH[-which(c2keep==TRUE),1:3]
outcnoh=nrow(ConcatHcout)
outcnndh=knnx.dist(mydatH[,1:3],ConcatHcout,k=2)
outcnndh=median(outcnndh[,2])

locnohrat=locnoh/Hn
cnndhrat=outcnndh/cnndh
}

#Homer1 bbox projection
if(centvrot[1]>0) rad=125 else rad=-125
EBSn=rbind(c(rad,max(mydatHx[,2]),0),c(rad,min(mydatHx[,2]),0),c(rad,0,max(mydatHx[,3])),c(rad,0,min(mydatHx[,3])),c(rad+(newhdepth/2)+20,0,0),c(rad-(newhdepth/2)-20,0,0))
plengthax=dist(EBSn[1:2,])*0.05
pwidthax=dist(EBSn[3:4,])*0.05
pdepthax=dist(EBSn[5:6,])*0.05
EBSn=rbind(c(rad,max(mydatHx[,2])+plengthax,0),c(rad,min(mydatHx[,2])-plengthax,0),c(rad,0,max(mydatHx[,3])+pwidthax),c(rad,0,min(mydatHx[,3])-pwidthax),c(rad+((newhdepth+pdepthax)/2)+20,0,0),c(rad-((newhdepth+pdepthax)/2)-20,0,0))

#Bounding box

```

```

centaxes=c(rad, 0, 0)
AxeX=EBsn[1:2,]
projtop=EBsn[3:6,]
Boxpoints=vector()
Boxproj=vector()
interpoints=vector()

#AxeX point projection to Axes plane
for(i in 1:2) {
  Norm=c((centaxes[1]-projtop[i,1]), (centaxes[2]-projtop[i,2]), (centaxes[3]-projtop[i,3]))
  dplane=Norm[1]*projtop[i,1] + Norm[2]*projtop[i,2] + Norm[3]*projtop[i,3]
  plane=c(Norm, dplane)
  t=as.numeric((dplane-(AxeX[1,1]*Norm[1])-(AxeX[1,2]*Norm[2])-(AxeX[1,3]*Norm[3]))/((Norm[1]^2)+(Norm[2]^2)+(Norm[3]^2)))
  bpoint1=c((AxeX[1,1]+t*Norm[1]), (AxeX[1,2]+t*Norm[2]), (AxeX[1,3]+t*Norm[3]))
  bpoint2=c((AxeX[2,1]+t*Norm[1]), (AxeX[2,2]+t*Norm[2]), (AxeX[2,3]+t*Norm[3]))
  Boxproj=rbind(Boxproj,bpoint1,bpoint2)
}
Boxpoints=Boxproj

#Bbox area
lengthax=as.numeric(dist(EBsn[1:2,]))/1000
widthax=as.numeric(dist(EBsn[3:4,]))/1000
depthax=as.numeric(dist(EBsn[5:6,]))/1000
hmrarea=lengthax*widthax
bboxvol=lengthax*widthax*depthax

for(i in 3:4){
  bpoints=Boxproj
  Norm=c((centaxes[1]-projtop[i,1]), (centaxes[2]-projtop[i,2]), (centaxes[3]-projtop[i,3]))
  dplane=Norm[1]*projtop[i,1] + Norm[2]*projtop[i,2] + Norm[3]*projtop[i,3]
  plane=c(Norm, dplane)
  t=as.numeric((dplane-(AxeX[1,1]*Norm[1])-(AxeX[1,2]*Norm[2])-(AxeX[1,3]*Norm[3]))/((Norm[1]^2)+(Norm[2]^2)+(Norm[3]^2)))
  trans=c(t*Norm[1],t*Norm[2],t*Norm[3])
  bpoints[,1]=Boxproj[,1]+trans[1]
  bpoints[,2]=Boxproj[,2]+trans[2]
  bpoints[,3]=Boxproj[,3]+trans[3]
  interpoints=rbind(interpoints,bpoints)
  Boxpoints=rbind(Boxpoints,bpoints)
}
# Boxpoints=rbind(Boxpoints,EBsn)
boxa=ashape3d(Boxpoints,alpha=10000, pert = TRUE)
btri=boxa$triang
btrit=t(btri[which(btri[,9]==2),1:3])

#Test of SV within bbox
cinBa=inashape3d(boxa,indexAlpha = 1, centroidsV[,2:4])
cinBano=(length(cinBa)-length(cinBa[which(cinBa==FALSE)]))

#SV randomization
randseeds=trunc(runif(10,min=1,max=100))
randinterdist=vector()
randinbbox=vector()
for(rn in 1:10){
  set.seed(randseeds[rn])
  Vx=mydatVx[,1]
  Vy=mydatVx[,2]
  Vz=mydatVx[,3]
  lrand=0
  repeat{
    if(lrand>=vclustno)break
    randx=runif(vclustno*20, min = min(Vx), max= max(Vx) )
    randy=runif(vclustno*20, min = min(Vy), max= max(Vy) )
    randz=runif(vclustno*20, min = min(Vz), max= max(Vz) )
    randdist=cbind(randx,randy,randz)
    inaV=inashape3d(aV, indexAlpha = 1, randdist[,1:3])
    randdist=randdist[which(inaV==TRUE),]
    randknn=knn.dist(randdist,k=1)
    randdist=randdist[which(randknn>35),]
    lrand=length(randdist[,1])
  }
  randdist=randdist[1:vclustno,]
  randknn=knn.dist(randdist,k=10)
  randknn=apply(randknn, MARGIN = 1, FUN = function(x) median(x))
  randknn=median(randknn)
  randinterdist=c(randinterdist, randknn)

  randinBa=inashape3d(boxa,indexAlpha = 1, randdist)
  randinBano=(length(randinBa)-length(randinBa[which(randinBa==FALSE)]))
  randinbbox=c(randinbbox, randinBano)
}
medrandinterdist=median(randinterdist)
medrandinbbox=median(randinbbox)
maxrandinbbox=max(randinbbox)
if(maxrandinbbox==0) next()

#ROI Vamp2 and Homer1 nanocluster info
centroidsV=cbind(centroidsV,locnov,diaV,locrat,cnndv,cnndrat,centroidsdist)
hcno=length(ckkeep)
if(hcno>0){
  hna=vector()
  hna[hcno]=NA
  centroidsVv=cbind(centroidsVv,locnoh,diaH,locnohrat,cnndh,cnndhrat,hna)
} else {
  centroidsVv=c("Homer", centH,NA,NA,NA,NA,NA,NA,NA)
}
centroidsVr=rbind(centroidsV,centroidsVv)
centroidsVr=as.data.table(centroidsVr)
names=c("Cluster","x [nm]", "y [nm]", "z [nm]", "Loc. no.", "NC diameter [nm]","Loc NC/out ratio","NC nnd [nm]", "NC/out nnd ratio", "SV
nnd [nm]")
setnames(centroidsVr,names)
centroidsVtable=paste0(clusterexp,"/", "Info",basename(Clusterfiles[filen]))

```

```

write.delim(centroidsVr,centroidsVtable, sep ="\t")

clusteriexp=paste0(clusterexp,"/", "gausslocs",filen,".xls")
write_delim(as.data.frame(chunkinfo),clusteriexp,delim = "\t")

#Summary of Homer and Vamp2 object metrics
Objdat=c(basename(Clusterfiles[filen]),Rhr,cinBano,cinBano/bboxvol, vclustno, VolmainV, Vn,Vdens,
VolH,Hn,Hdens,bboxvol,newhlen,newhwidth,newhdepth,median(diav),median(lochrat),outcnnd,
median(cnndrat),medcentdist,medrandinterdist,medrandinbbox,maxrandinbbox)
if(hcno==0) Objdat=c(Objdat,0, NA,outcnndh, NA,NA) else Objdat=c(Objdat,length(ckeep), median(diaH),median(lochnohrat),outcnndh,
median(cnndhrat))

Objsumm=rbind(Objsumm,Objdat)
ijstat=trunc(filn*100/flength)
setWinProgressBar(pb,ijstat, title=paste0("Blind directory ",bd,"of",blength),label = paste0(ijstat,"% of ",blindfold,"/",Bno))
} ##end file loop

if(length(Objsumm)<2)next()
Objsumm=as.data.table(Objsumm)
names=c("ROI","Hmr fit R2","SV no. per bbox","SV no. per bbox  $\mu\text{m}^3$ ","SV no.,""Vamp2 Volume", "Vamp2 Loc no.,""Vamp2 loc. density [ $\mu\text{m}^3$ ]",
"Homer1 Volume","Hmr Loc. no.,""Hmr loc. density [ $\mu\text{m}^3$ ]"",Homer1 volume ( $\mu\text{m}^3$ )","newhlen","newhwidth","newhdepth","median SV
diameter","median SVloc.no./total","extra SV nnd","median SV extrannd/ncnnd", "median SV k10 dist","med. rand. k10 dist","med. rand. inbbox",
"max rand. inbbox", "Homer1 cluster no.", "median Hmr nc diameter", "median Hmr ncloc.no./total", "Hmr extra nc nnd","median Hmr
extrannd/ncnnd")
setnames(Objsumm,names)
objexp=paste0(exportdir,"/", "Objects",basename(as.character(Btable[blindfold,2])), ".xls")
write.delim(Objsumm,objexp, sep ="\t")

}#end blind folder loop

}#end Blind directory loop

cpb=close(pb)
print("Done")

```

Bibliography

- Aburima, Ahmed, Katie S Wraith, Zaher Raslan, Robert Law, Simbarashe Magwenzi, and Khalid M Naseem. 2013. "cAMP Signaling Regulates Platelet Myosin Light Chain (MLC) Phosphorylation and Shape Change through Targeting the RhoA-Rho Kinase-MLC Phosphatase Signaling Pathway." *Blood* 122 (20). American Society of Hematology: 3533–45. doi:10.1182/blood-2013-03-487850.
- Adermark, Louise, Giuseppe Talani, and David M. Lovinger. 2009. "Endocannabinoid-Dependent Plasticity at GABAergic and Glutamatergic Synapses in the Striatum Is Regulated by Synaptic Activity." *European Journal of Neuroscience* 29 (1): 32–41. doi:10.1111/j.1460-9568.2008.06551.x.
- Aimone, James B., Yan Li, Star W. Lee, Gregory D. Clemenson, Wei Deng, and Fred H. Gage. 2014. "Regulation and Function of Adult Neurogenesis: From Genes to Cognition." *Physiological Reviews* 94 (4): 991–1026. doi:10.1152/physrev.00004.2014.
- Albertinazzi, Chiara, Daniela Gilardelli, Simona Paris, Renato Longhi, and Ivan De Curtis. 1998. "Overexpression of a Neural-Specific Rho Family GTPase, cRac1B, Selectively Induces Enhanced Neuritogenesis and Neurite Branching in Primary Neurons." *Journal of Cell Biology* 142 (3): 815–25. doi:10.1083/jcb.142.3.815.
- Albertinazzi, Chiara, Lorena Za, Simona Paris, and Ivan de Curtis. 2003. "ADP-Ribosylation Factor 6 and a Functional PIX/p95-APP1 Complex Are Required for Rac1B-Mediated Neurite Outgrowth." *Molecular Biology of the Cell* 14 (4): 1295–1307. doi:10.1091/mbc.E02-07-0406.
- Alger, Bradley E., and Jimok Kim. 2011. "Supply and Demand for Endocannabinoids." *Trends in Neurosciences*. doi:10.1016/j.tins.2011.03.003.
- Ankerst, Mihael, Mihael Ankerst, Markus M. Breunig, Hans-peter Kriegel, and Jörg Sander. 1999. "OPTICS: Ordering Points To Identify the Clustering Structure," 49--60. <http://citeseerx.ist.psu.edu/viewdoc/summary?doi=10.1.1.129.6542>.
- Argaw, A., G. Duff, N. Zabouri, B. Cecyre, N. Chaine, H. Cherif, N. Tea, B. Lutz, M. Ptito, and J.-F. Bouchard. 2011. "Concerted Action of CB1 Cannabinoid Receptor and Deleted

- in Colorectal Cancer in Axon Guidance.” *Journal of Neuroscience* 31 (4): 1489–99. doi:10.1523/JNEUROSCI.4134-09.2011.
- Atwood, Brady K, David M Lovinger, and Brian N Mathur. 2014. “Presynaptic Long-Term Depression Mediated by Gi/o-Coupled Receptors.” *Trends in Neurosciences* 37 (11). NIH Public Access: 663–73. doi:10.1016/j.tins.2014.07.010.
- Atwood, Brady K, and Ken Mackie. 2010. “CB2: A Cannabinoid Receptor with an Identity Crisis.” *British Journal of Pharmacology* 160 (3): 467–79. doi:10.1111/j.1476-5381.2010.00729.x.
- Azad, Shahnaz Christina, Matthias Eder, Giovanni Marsicano, Beat Lutz, Walter Zieglgänsberger, and Gerhard Rammes. 2003. “Activation of the Cannabinoid Receptor Type 1 Decreases Glutamatergic and GABAergic Synaptic Transmission in the Lateral Amygdala of the Mouse.” *Learning & Memory* 10 (2): 116–28. doi:10.1101/lm.53303.
- Bacci, Alberto, John R. Huguenard, and David A. Prince. 2004. “Long-Lasting Self-Inhibition of Neocortical Interneurons Mediated by Endocannabinoids.” *Nature* 431 (7006): 312–16. doi:10.1038/nature02913.
- Baker, David, Gareth Pryce, Wayne L. Davies, and C. Robin Hiley. 2006. “In Silico Patent Searching Reveals a New Cannabinoid Receptor.” *Trends in Pharmacological Sciences*. doi:10.1016/j.tips.2005.11.003.
- Bamji, Shernaz X., Kazuhiro Shimazu, Nikole Kimes, Joerg Huelsken, Walter Birchmeier, Bai Lu, and Louis F. Reichardt. 2003. “Role of β -Catenin in Synaptic Vesicle Localization and Presynaptic Assembly.” *Neuron* 40 (4): 719–31. doi:10.1016/S0896-6273(03)00718-9.
- Bates, Mark, Bo Huang, Graham T Dempsey, and Xiaowei Zhuang. 2007. “Multicolor Super-Resolution Imaging with Photo-Switchable Fluorescent Probes.” *Science (New York, N.Y.)* 317 (5845): 1749–53. doi:10.1126/science.1146598.
- Berghuis, P., M. B. Dobszay, X. Wang, S. Spano, F. Ledda, K. M. Sousa, G. Schulte, et al. 2005. “Endocannabinoids Regulate Interneuron Migration and Morphogenesis by Transactivating the TrkB Receptor.” *Proceedings of the National Academy of Sciences* 102 (52): 19115–20. doi:10.1073/pnas.0509494102.

- Berghuis, P., A. M. Rajniecek, Y. M. Morozov, R. A. Ross, J. Mulder, G. M. Urban, K. Monory, et al. 2007. "Hardwiring the Brain: Endocannabinoids Shape Neuronal Connectivity." *Science* 316 (5828): 1212–16. doi:10.1126/science.1137406.
- Bernstein, B W, M DeWit, and J R Bamburg. 1998. "Actin Disassembles Reversibly during Electrically Induced Recycling of Synaptic Vesicles in Cultured Neurons." *Brain Research. Molecular Brain Research* 53 (1–2): 236–51.
<http://www.ncbi.nlm.nih.gov/pubmed/9473683>.
- Betke, Katherine M., Christopher A. Wells, and Heidi E. Hamm. 2012. "GPCR Mediated Regulation of Synaptic Transmission." *Progress in Neurobiology* 96 (3): 304–21. doi:10.1016/j.pneurobio.2012.01.009.
- Bidaut-Russell, M, W A Devane, and A C Howlett. 1990. "Cannabinoid Receptors and Modulation of Cyclic AMP Accumulation in the Rat Brain." *Journal of Neurochemistry* 55 (1): 21–26. doi:10.1111/j.1471-4159.1990.tb08815.x.
- Birnbaumer, Lutz, Joel Abramowitz, and Arthur M. Brown. 1990. "Receptor-Effector Coupling by G Proteins." *BBA - Reviews on Biomembranes*. doi:10.1016/0304-4157(90)90007-Y.
- Bisogno, Tiziana, Fiona Howell, Gareth Williams, Alberto Minassi, Maria Grazia Cascio, Alessia Ligresti, Isabel Matias, et al. 2003. "Cloning of the First sn1-DAG Lipases Points to the Spatial and Temporal Regulation of Endocannabinoid Signaling in the Brain." *The Journal of Cell Biology* 163 (3): 463–68. doi:10.1083/jcb.200305129.
- Bisogno, Tiziana, Alessia Ligresti, and Vincenzo Di Marzo. 2005. "The Endocannabinoid Signalling System: Biochemical Aspects." In *Pharmacology Biochemistry and Behavior*, 81:224–38. doi:10.1016/j.pbb.2005.01.027.
- Bleckert, Adam, Huzefa Photowala, and Simon Alford. 2012. "Dual Pools of Actin at Presynaptic Terminals." *Journal of Neurophysiology* 107 (12): 3479–92. doi:10.1152/jn.00789.2011.
- Bloom, Ona, Emma Evergren, Nikolay Tomilin, Ole Kjaerulff, Peter Löw, Lennart Brodin, Vincent A. Pieribone, Paul Greengard, and Oleg Shupliakov. 2003. "Colocalization of Synapsin and Actin during Synaptic Vesicle Recycling." *Journal of Cell Biology* 161 (4): 737–47. doi:10.1083/jcb.200212140.

- Bodor, A. L., István Katona, Gábor Nyíri, Ken Mackie, Catherine Ledent, Norbert Hájos, and Tamás F Freund. 2005. "Endocannabinoid Signaling in Rat Somatosensory Cortex: Laminar Differences and Involvement of Specific Interneuron Types." *Journal of Neuroscience* 25 (29): 6845–56. doi:10.1523/JNEUROSCI.0442-05.2005.
- Bonhaus, D W, L K Chang, J Kwan, and G R Martin. 1998. "Dual Activation and Inhibition of Adenylyl Cyclase by Cannabinoid Receptor Agonists: Evidence for Agonist-Specific Trafficking of Intracellular Responses." *The Journal of Pharmacology and Experimental Therapeutics* 287 (3): 884–88. <http://www.jpnet.org>.
- Bouaboula, M, M Rinaldi, P Carayon, C Carillon, B Delpech, D Shire, G Le Fur, and P Casellas. 1993. "Cannabinoid-Receptor Expression in Human Leukocytes." *European Journal of Biochemistry / FEBS* 214 (1): 173–80. doi:10.1111/j.1432-1033.1993.tb17910.x.
- Branco, Tiago, Vincenzo Marra, and Kevin Staras. 2010. "Examining Size-Strength Relationships at Hippocampal Synapses Using an Ultrastructural Measurement of Synaptic Release Probability." *Journal of Structural Biology* 172 (2): 203–10. doi:10.1016/j.jsb.2009.10.014.
- Cabral, Guy A., Peter J. McNERNEY, and Eric M. Mishkin. 1987. "Interaction of Delta-9-Tetrahydrocannabinol with Rat B103 Neuroblastoma Cells." *Archives of Toxicology* 60 (6): 438–49. doi:10.1007/BF00302387.
- Calixto, Eduardo, Edda Thiels, Eric Klann, and Germán Barrionuevo. 2003. "Early Maintenance of Hippocampal Mossy Fiber--Long-Term Potentiation Depends on Protein and RNA Synthesis and Presynaptic Granule Cell Integrity." *The Journal of Neuroscience : The Official Journal of the Society for Neuroscience* 23 (12): 4842–49.
- Cannizzaro, C., M. D'Amico, P. Preziosi, and M. Martire. 2006. "Presynaptic Effects of Anandamide and WIN55,212-2 on Glutamatergic Nerve Endings Isolated from Rat Hippocampus." *Neurochemistry International* 48 (3): 159–65. doi:10.1016/j.neuint.2005.10.009.
- Carlisle, S. J., F. Marciano-Cabral, A. Staab, C. Ludwick, and G. A. Cabral. 2002. "Differential Expression of the CB2 Cannabinoid Receptor by Rodent Macrophages and Macrophage-like Cells in Relation to Cell Activation." *International*

Immunopharmacology 2 (1): 69–82. doi:10.1016/S1567-5769(01)00147-3.

Castillo, Pablo E., Susanne Schoch, Frank Schmitz, Thomas C. Südhof, and Robert C. Malenka. 2002. “RIM1 α Is Required for Presynaptic Long-Term Potentiation.” *Nature* 415 (6869). Nature Publishing Group: 327–30. doi:10.1038/415327a.

Castillo, Pablo E., Thomas J. Younits, Andrés E. Chávez, and Yuki Hashimoto. 2012. “Endocannabinoid Signaling and Synaptic Function.” *Neuron* 76 (1): 70–81. doi:10.1016/j.neuron.2012.09.020.

Chapman, Edwin R. 2008. “How Does Synaptotagmin Trigger Neurotransmitter Release?” *Annual Review of Biochemistry* 77 (1): 615–41. doi:10.1146/annurev.biochem.77.062005.101135.

Chemin, Jean, Joël Nargeot, and Philippe Lory. 2002. “Neuronal T-Type Alpha 1H Calcium Channels Induce Neurogenesis and Expression of High-Voltage-Activated Calcium Channels in the NG108-15 Cell Line.” *The Journal of Neuroscience : The Official Journal of the Society for Neuroscience* 22 (16): 6856–62. doi:20026671.

Chevaleyre, Vivien, and Pablo E. Castillo. 2003. “Heterosynaptic LTD of Hippocampal GABAergic Synapses: A Novel Role of Endocannabinoids in Regulating Excitability.” *Neuron* 38 (3): 461–72. doi:10.1016/S0896-6273(03)00235-6.

Chevaleyre, Vivien, Boris D. Heifets, Pascal S. Kaeser, Thomas C. Südhof, Dominick P. Purpura, and Pablo E. Castillo. 2007. “Endocannabinoid-Mediated Long-Term Plasticity Requires cAMP/PKA Signaling and RIM1 α .” *Neuron* 54 (5): 801–12. doi:10.1016/j.neuron.2007.05.020.

Chevaleyre, Vivien, Kanji A. Takahashi, and Pablo E. Castillo. 2006. “Endocannabinoid-Mediated Synaptic Plasticity in the Cns.” *Annual Review of Neuroscience* 29 (1): 37–76. doi:10.1146/annurev.neuro.29.051605.112834.

Childers, S. R., and S. A. Deadwyler. 1996. “Role of Cyclic AMP in the Actions of Cannabinoid Receptors.” *Biochemical Pharmacology*. doi:10.1016/0006-2952(96)00419-4.

Cingolani, Lorenzo A., and Yukiko Goda. 2008. “Actin in Action: The Interplay between the Actin Cytoskeleton and Synaptic Efficacy.” *Nature Reviews Neuroscience*.

doi:10.1038/nrn2373.

- Cole, Andy A, Xiaobing Chen, and Thomas S Reese. 2016. "A Network of Three Types of Filaments Organizes Synaptic Vesicles for Storage, Mobilization, and Docking." *The Journal of Neuroscience : The Official Journal of the Society for Neuroscience* 36 (11). Society for Neuroscience: 3222–30. doi:10.1523/JNEUROSCI.2939-15.2016.
- Cole, J C, B R Villa, and R S Wilkinson. 2000. "Disruption of Actin Impedes Transmitter Release in Snake Motor Terminals." *The Journal of Physiology* 525 Pt 3 (June): 579–86. <http://www.ncbi.nlm.nih.gov/pubmed/10856113>.
- Colicelli, J. 2004. "Human RAS Superfamily Proteins and Related GTPases." *Science Signaling* 2004 (250): re13-re13. doi:10.1126/stke.2502004re13.
- Coutts, A A, S Anavi-Goffer, R A Ross, D J MacEwan, K Mackie, R G Pertwee, and A J Irving. 2001. "Agonist-Induced Internalization and Trafficking of Cannabinoid CB1 Receptors in Hippocampal Neurons." *The Journal of Neuroscience : The Official Journal of the Society for Neuroscience* 21 (7): 2425–33. <http://www.ncbi.nlm.nih.gov/pubmed/11264316>.
- Cramer, K. S., C. A. Leamey, and M. Sur. 1998. "Nitric Oxide as a Signaling Molecule in Visual System Development." *Prog Brain Res* 118: 101–14. doi:Review.
- Dani, Adish, Bo Huang, Joseph Bergan, Catherine Dulac, and Xiaowei Zhuang. 2010. "Superresolution Imaging of Chemical Synapses in the Brain." *Neuron* 68 (5): 843–56. doi:10.1016/j.neuron.2010.11.021.
- Daniel, Herve, A. Rancillac, and F. Crepel. 2004. "Mechanisms Underlying Cannabinoid Inhibition of Presynaptic Ca²⁺influx at Parallel Fibre Synapses of the Rat Cerebellum." *Journal of Physiology* 557 (1): 159–74. doi:10.1113/jphysiol.2004.063263.
- Darcy, Kevin J, Kevin Staras, Lucy M Collinson, and Yukiko Goda. 2006. "Constitutive Sharing of Recycling Synaptic Vesicles between Presynaptic Boutons." *Nature Neuroscience* 9 (3): 315–21. doi:10.1038/nn1640.
- Davis, Margaret I., Jennifer Ronesi, and David M. Lovinger. 2003. "A Predominant Role for Inhibition of the Adenylate Cyclase/protein Kinase A Pathway in ERK Activation by Cannabinoid Receptor 1 in N1E-115 Neuroblastoma Cells." *The Journal of Biological*

Chemistry 278 (49): 48973–80. doi:10.1074/jbc.M305697200.

De La Torre, José R., Veit H. Höpker, Guo Li Ming, Mu Ming Poo, Marc Tessier-Lavigne, Ali Hemmati-Brivanlou, and Christine E. Holt. 1997. “Turning of Retinal Growth Cones in a Netrin-1 Gradient Mediated by the Netrin Receptor DCC.” *Neuron* 19 (6): 1211–24. doi:10.1016/S0896-6273(00)80413-4.

De Paola, Vincenzo, Anthony Holtmaat, Graham Knott, Sen Song, Linda Wilbrecht, Pico Caroni, and Karel Svoboda. 2006. “Cell Type-Specific Structural Plasticity of Axonal Branches and Boutons in the Adult Neocortex.” *Neuron* 49 (6): 861–75. doi:10.1016/j.neuron.2006.02.017.

Deng, Lunbin, Pascal S. Kaeser, Wei Xu, and Thomas C. Südhof. 2011. “RIM Proteins Activate Vesicle Priming by Reversing Autoinhibitory Homodimerization of munc13.” *Neuron* 69 (2): 317–31. doi:10.1016/j.neuron.2011.01.005.

Denker, A., I. Bethani, K. Krohnert, C. Korber, H. Horstmann, B. G. Wilhelm, S. V. Barysch, T. Kuner, E. Neher, and S. O. Rizzoli. 2011. “A Small Pool of Vesicles Maintains Synaptic Activity in Vivo.” *Proceedings of the National Academy of Sciences* 108 (41): 17177–82. doi:10.1073/pnas.1112688108.

Denker, A., K. Krohnert, J. Buckers, E. Neher, and S. O. Rizzoli. 2011. “The Reserve Pool of Synaptic Vesicles Acts as a Buffer for Proteins Involved in Synaptic Vesicle Recycling.” *Proceedings of the National Academy of Sciences* 108 (41): 17183–88. doi:10.1073/pnas.1112690108.

Denker, Annette, and Silvio O. Rizzoli. 2010. “Synaptic Vesicle Pools: An Update.” *Frontiers in Synaptic Neuroscience*. doi:10.3389/fnsyn.2010.00135.

Dent, Erik W, Stephanie L Gupton, and Frank B Gertler. 2011. “The Growth Cone Cytoskeleton in Axon Outgrowth and Guidance.” *Cold Spring Harbor Perspectives in Biology* 3 (3). Cold Spring Harbor Laboratory Press. doi:10.1101/cshperspect.a001800.

Derkinderen, P, C Ledent, M Parmentier, and J a Girault. 2001. “Cannabinoids Activate p38 Mitogen-Activated Protein Kinases through CB1 Receptors in Hippocampus.” *Journal of Neurochemistry* 77 (3): 957–60. doi:10.1046/j.1471-4159.2001.00333.x.

Devane, W., L Hanus, A Breuer, R. Pertwee, L. Stevenson, G Griffin, D Gibson, A

- Mandelbaum, A Etinger, and R Mechoulam. 1992. "Isolation and Structure of a Brain Constituent That Binds to the Cannabinoid Receptor." *Science* 258 (5090): 1946–49. doi:10.1126/science.1470919.
- Devane, W A, F A Dysarz, M R Johnson, L S Melvin, and A C Howlett. 1988. "Determination and Characterization of a Cannabinoid Receptor in Rat Brain." *Molecular Pharmacology* 34 (5): 605–13. doi:88/050605-09\$02.00/O.
- Dong, Jing Ming, Thomas Leung, Edward Manser, and Louis Lim. 1998. "cAMP-Induced Morphological Changes Are Counteracted by the Activated RhoA Small GTPase and the Rho Kinase ROK α ." *Journal of Biological Chemistry* 273 (35): 22554–62. doi:10.1074/jbc.273.35.22554.
- Dudok, Barna, László Barna, Marco Ledri, Szilárd I Szabó, Eszter Szabadits, Balázs Pintér, Stephen G Woodhams, et al. 2015. "Cell-Specific STORM Super-Resolution Imaging Reveals Nanoscale Organization of Cannabinoid Signaling." *Nature Neuroscience* 18 (1). Nature Publishing Group: 75–86. doi:10.1038/nn.3892.
- Ernst, A F, G Gallo, P C Letourneau, and S C McLoon. 2000. "Stabilization of Growing Retinal Axons by the Combined Signaling of Nitric Oxide and Brain-Derived Neurotrophic Factor." *The Journal of Neuroscience* 20 (4): 1458–69.
- Ester, Martin, Hans-Peter Kriegel, Jörg Sander, and Xiaowei Xu. 1996. "A Density-Based Algorithm for Discovering Clusters a Density-Based Algorithm for Discovering Clusters in Large Spatial Databases with Noise." *Proceedings of the Second International Conference on Knowledge Discovery and Data Mining*. AAAI Press. <https://dl.acm.org/citation.cfm?id=3001507>.
- Fasshauer, D., R. B. Sutton, A. T. Brunger, and R. Jahn. 1998. "Conserved Structural Features of the Synaptic Fusion Complex: SNARE Proteins Reclassified as Q- and R-SNAREs." *Proceedings of the National Academy of Sciences* 95 (26): 15781–86. doi:10.1073/pnas.95.26.15781.
- Fernández-Alfonso, Tomás, Ricky Kwan, and Timothy A. Ryan. 2006. "Synaptic Vesicles Interchange Their Membrane Proteins with a Large Surface Reservoir during Recycling." *Neuron* 51 (2): 179–86. doi:10.1016/j.neuron.2006.06.008.
- Fernández-Busnadiego, Rubén, Benoît Zuber, Ulrike Elisabeth Maurer, Marek Cyrklaff,

- Wolfgang Baumeister, and Vladan Lučić. 2010. “Quantitative Analysis of the Native Presynaptic Cytomatrix by Cryoelectron Tomography.” *Journal of Cell Biology* 188 (1): 145–56. doi:10.1083/jcb.200908082.
- Fernández-Ruiz, Javier, F Berrendero, Mari Luz Hernández, J Romero, and J A Ramos. 1999. “Role of Endocannabinoids in Brain Development.” *Life Sciences* 65 (iii): 725–36. doi:10.1017/CBO9781107415324.004.
- Fernandez-Tenorio, M., C. Porrás-Gonzalez, A. Castellano, A. del Valle-Rodríguez, J. López-Barneo, and J. Urena. 2011. “Metabotropic Regulation of RhoA/Rho-Associated Kinase by L-Type Ca²⁺ Channels: New Mechanism for Depolarization-Evoked Mammalian Arterial Contraction.” *Circulation Research* 108 (11): 1348–57. doi:10.1161/CIRCRESAHA.111.240127.
- Foord, Steven M, T O M I Bonner, Richard R Neubig, Edward M Rosser, Jean-phillipe Pin, Anthony P Davenport, Michael Spedding, and Anthony J Harmar. 2005. “International Union of Pharmacology. XLVI. G Protein-Coupled Receptor List.” *Pharmacological Reviews* 57 (2): 279–88. doi:10.1124/pr.57.2.5.2.
- Fornasiero, E. F., A. Raimondi, F. C. Guarnieri, M. Orlando, R. Fesce, F. Benfenati, and F. Valtorta. 2012. “Synapsins Contribute to the Dynamic Spatial Organization of Synaptic Vesicles in an Activity-Dependent Manner.” *Journal of Neuroscience* 32 (35): 12214–27. doi:10.1523/JNEUROSCI.1554-12.2012.
- Fowler, Milena Wagner, and Kevin Staras. 2015a. “Synaptic Vesicle Pools: Principles, Properties and Limitations.” *Experimental Cell Research* 335 (2): 150–56. doi:10.1016/j.yexcr.2015.03.007.
- . 2015b. “Synaptic Vesicle Pools: Principles, Properties and Limitations.” *Experimental Cell Research* 335 (2): 150–56. doi:10.1016/j.yexcr.2015.03.007.
- Fu, Min, Xinzhu Yu, Ju Lu, and Yi Zuo. 2012. “Repetitive Motor Learning Induces Coordinated Formation of Clustered Dendritic Spines in Vivo.” *Nature* 483 (7387): 92–96. doi:10.1038/nature10844.
- Gaffield, Michael A., Silvio O. Rizzoli, and William J. Betz. 2006. “Mobility of Synaptic Vesicles in Different Pools in Resting and Stimulated Frog Motor Nerve Terminals.” *Neuron* 51 (3): 317–25. doi:10.1016/j.neuron.2006.06.031.

- Gaffuri, Anne-Lise, Delphine Ladarre, and Zsolt Lenkei. 2012. "Type-1 Cannabinoid Receptor Signaling in Neuronal Development." *Pharmacology* 90 (1–2): 19–39. doi:10.1159/000339075.
- Galiègue, S, S Mary, J Marchand, D Dussosoy, D Carrière, P Carayon, M Bouaboula, D Shire, G Le Fur, and P Casellas. 1995. "Expression of Central and Peripheral Cannabinoid Receptors in Human Immune Tissues and Leukocyte Subpopulations." *European Journal of Biochemistry* 232 (1): 54–61. <http://www.ncbi.nlm.nih.gov/pubmed/7556170>.
- Galve-Roperh, Ismael, Valerio Chiurchiù, Javier Díaz-Alonso, Monica Bari, Manuel Guzmán, and Mauro Maccarrone. 2013. "Cannabinoid Receptor Signaling in Progenitor/stem Cell Proliferation and Differentiation." *Progress in Lipid Research* 52 (4): 633–50. doi:10.1016/j.plipres.2013.05.004.
- Gao, Ying, Dmitry V Vasilyev, Maria Beatriz Goncalves, Fiona V Howell, Carl Hobbs, Melina Reisenberg, Ru Shen, et al. 2010. "Loss of Retrograde Endocannabinoid Signaling and Reduced Adult Neurogenesis in Diacylglycerol Lipase Knock-out Mice." *The Journal of Neuroscience : The Official Journal of the Society for Neuroscience* 30 (6): 2017–24. doi:10.1523/JNEUROSCI.5693-09.2010.
- Gaoni, Y., and R. Mechoulam. 1964. "Isolation, Structure, and Partial Synthesis of an Active Constituent of Hashish." *Journal of the American Chemical Society* 86 (8): 1646–47. doi:10.1021/ja01062a046.
- García-Morales, Victoria, Fernando Montero, David González-Forero, Guillermo Rodríguez-Bey, Laura Gómez-Pérez, María Jesús Medialdea-Wandossell, Germán Domínguez-Vías, José Manuel García-Verdugo, and Bernardo Moreno-López. 2015. "Membrane-Derived Phospholipids Control Synaptic Neurotransmission and Plasticity." *PLoS Biology* 13 (5). Public Library of Science: e1002153. doi:10.1371/journal.pbio.1002153.
- García-Morales, Victoria, Fernando Montero, and Bernardo Moreno-López. 2015. "Cannabinoid Agonists Rearrange Synaptic Vesicles at Excitatory Synapses and Depress Motoneuron Activity in Vivo." *Neuropharmacology* 92C: 69–79. doi:10.1016/j.neuropharm.2014.12.036.
- Gaspar, Patricia, Olivier Cases, and Luc Maroteaux. 2003. "The Developmental Role of

- Serotonin: News from Mouse Molecular Genetics.” *Nature Reviews Neuroscience* 4 (12): 1002–12. doi:10.1038/nrn1256.
- Gebremedhin, D, a R Lange, W B Campbell, C J Hillard, and D R Harder. 1999. “Cannabinoid CB1 Receptor of Cat Cerebral Arterial Muscle Functions to Inhibit L-Type Ca²⁺ Channel Current.” *The American Journal of Physiology* 276 (6 Pt 2): H2085–93.
- Gerard, C M, C Mollereau, G Vassart, Marc Parmentier, and C M Gérard. 1991. “Molecular Cloning of a Human Cannabinoid Receptor Which Is Also Expressed in Testis.” *The Biochemical Journal* 279 (Pt 1): 129–34.
<http://www.pubmedcentral.nih.gov/articlerender.fcgi?artid=1151556&tool=pmcentrez&rendertype=abstract>.
- Glass, M, and C C Felder. 1997. “Concurrent Stimulation of Cannabinoid CB1 and Dopamine D2 Receptors Augments cAMP Accumulation in Striatal Neurons: Evidence for a Gs Linkage to the CB1 Receptor.” *The Journal of Neuroscience : The Official Journal of the Society for Neuroscience* 17 (14): 5327–33.
<http://www.ncbi.nlm.nih.gov/pubmed/9204917>.
- Goddard, Alan D., and Anthony Watts. 2012. “Regulation of G Protein-Coupled Receptors by Palmitoylation and Cholesterol.” *BMC Biology*. doi:10.1186/1741-7007-10-27.
- Granseth, Björn, Benjamin Odermatt, Stephen J Royle, and Leon Lagnado. 2006. “Clathrin-Mediated Endocytosis Is the Dominant Mechanism of Vesicle Retrieval at Hippocampal Synapses.” *Neuron* 51 (6): 773–86. doi:10.1016/j.neuron.2006.08.029.
- Granseth, Björn, Benjamin Odermatt, Stephen J Royle, and Leon Lagnado. 2009. “Comment on ‘The Dynamic Control of Kiss-and-Run and Vesicular Reuse Probed with Single Nanoparticles’.” *Science (New York, N.Y.)* 325 (5947): 1499; author reply 1499. doi:10.1126/science.1175790.
- Greenhough, Alexander, Helena A. Patsos, Ann C. Williams, and Christos Paraskeva. 2007. “The Cannabinoid Δ^9 -Tetrahydrocannabinol Inhibits RAS-MAPK and PI3K-AKT Survival Signalling and Induces BAD-Mediated Apoptosis in Colorectal Cancer Cells.” *International Journal of Cancer* 121 (10): 2172–80. doi:10.1002/ijc.22917.
- Grueter, Brad A., Gabor Brasnjo, and Robert C. Malenka. 2010. “Postsynaptic TRPV1

- Triggers Cell Type-Specific Long-Term Depression in the Nucleus Accumbens.” *Nature Neuroscience* 13 (12): 1519–26. doi:10.1038/nn.2685.
- Hall, Alan, and Giovanna Lalli. 2010. “Rho and Ras GTPases in Axon Growth, Guidance, and Branching.” *Cold Spring Harbor Perspectives in Biology*. doi:10.1101/cshperspect.a001818.
- Han, Yunyun, Pascal S. Kaeser, Thomas C. Südhof, and Ralf Schneggenburger. 2011. “RIM Determines Ca²⁺-channel Density and Vesicle Docking at the Presynaptic Active Zone.” *Neuron* 69 (2): 304–16. doi:10.1016/j.neuron.2010.12.014.
- Harata, N, T A Ryan, S J Smith, J Buchanan, and R W Tsien. 2001. “Visualizing Recycling Synaptic Vesicles in Hippocampal Neurons by FM 1-43 Photoconversion.” *Proceedings of the National Academy of Sciences of the United States of America* 98 (22): 12748–53. doi:10.1073/pnas.171442798.
- Harris, K M, and P Sultan. 1995. “Variation in the Number, Location and Size of Synaptic Vesicles Provides an Anatomical Basis for the Nonuniform Probability of Release at Hippocampal CA1 Synapses.” *Neuropharmacology* 34 (11): 1387–95. <http://www.ncbi.nlm.nih.gov/pubmed/8606788>.
- Haucke, Volker, Erwin Neher, and Stephan J. Sigrist. 2011. “Protein Scaffolds in the Coupling of Synaptic Exocytosis and Endocytosis.” *Nature Reviews Neuroscience* 12 (3): 127–38. doi:10.1038/nrn2948.
- He, John Cijiang, Ivone Gomes, Tracy Nguyen, Gomathi Jayaram, Prahlad T. Ram, Lakshmi A. Devi, and Ravi Iyengar. 2005. “The G_{αo}/i-Coupled Cannabinoid Receptor-Mediated Neurite Outgrowth Involves Rap Regulation of Src and Stat3.” *Journal of Biological Chemistry* 280 (39): 33426–34. doi:10.1074/jbc.M502812200.
- Heifets, B. D., V. Chevaleyre, and P. E. Castillo. 2008. “Interneuron Activity Controls Endocannabinoid-Mediated Presynaptic Plasticity through Calcineurin.” *Proceedings of the National Academy of Sciences* 105 (29): 10250–55. doi:10.1073/pnas.0711880105.
- Herkenham, M, A B Lynn, M R Johnson, L S Melvin, B R de Costa, and K C Rice. 1991. “Characterization and Localization of Cannabinoid Receptors in Rat Brain: A Quantitative in Vitro Autoradiographic Study.” *The Journal of Neuroscience : The Official Journal of the Society for Neuroscience* 11 (2): 563–83.

<http://www.ncbi.nlm.nih.gov/pubmed/1992016>.

Herkenham, M, A B Lynn, M D Little, M R Johnson, L S Melvin, B R de Costa, and K C Rice. 1990. "Cannabinoid Receptor Localization in Brain." *Proceedings of the National Academy of Sciences of the United States of America* 87 (5): 1932–36.

<http://www.ncbi.nlm.nih.gov/pubmed/2308954>.

Heuser, J. E., T. S. Reese, M. J. Dennis, Y. Jan, L. Jan, and L. Evans. 1979. "Synaptic Vesicle Exocytosis Captured by Quick Freezing and Correlated with Quantal Transmitter Release." *Journal of Cell Biology* 81 (2): 275–300. doi:10.1083/jcb.81.2.275.

Heuser, J E, and T S Reese. 1981. "Structural Changes after Transmitter Release at the Frog Neuromuscular Junction." *The Journal of Cell Biology* 88 (3): 564–80. doi:10.1083/jcb.88.3.564.

Hill, E. L., T. Gallopin, I. Ferezou, B. Cauli, J. Rossier, P. Schweitzer, and B. Lambolez. 2007. "Functional CB1 Receptors Are Broadly Expressed in Neocortical GABAergic and Glutamatergic Neurons." *Journal of Neurophysiology* 97 (4): 2580–89. doi:10.1152/jn.00603.2006.

Hirokawa, N., K. Sobue, K. Kanda, A. Harada, and H. Yorifuji. 1989. "The Cytoskeletal Architecture of the Presynaptic Terminal and Molecular Structure of Synapsin 1." *Journal of Cell Biology* 108 (1): 111–26. doi:10.1083/jcb.108.1.111.

Hoopmann, P., A. Punge, S. V. Barysch, V. Westphal, J. Buckers, F. Opazo, I. Bethani, M. A. Lauterbach, S. W. Hell, and S. O. Rizzoli. 2010. "Endosomal Sorting of Readily Releasable Synaptic Vesicles." *Proceedings of the National Academy of Sciences* 107 (44): 19055–60. doi:10.1073/pnas.1007037107.

Howlett, A C, and R M Fleming. 1984. "Cannabinoid Inhibition of Adenylate Cyclase. Pharmacology of the Response in Neuroblastoma Cell Membranes." *Molecular Pharmacology* 26 (3): 532–38.

<http://molpharm.aspetjournals.org/content/26/3/532.abstract>
<http://molpharm.aspetjournals.org/content/26/3/532.full.pdf>.

Howlett, Allyn C., and Somnath Mukhopadhyay. 2000. "Cellular Signal Transduction by Anandamide and 2-Arachidonoylglycerol." *Chemistry and Physics of Lipids*. doi:10.1016/S0009-3084(00)00187-0.

- Hua, Zhaolin, Sergio Leal-Ortiz, Sarah M. Foss, Clarissa L. Waites, Craig C. Garner, Susan M. Voglmaier, and Robert H. Edwards. 2011. "V-SNARE Composition Distinguishes Synaptic Vesicle Pools." *Neuron* 71 (3): 474–87. doi:10.1016/j.neuron.2011.06.010.
- Huang, Bo, Wenqin Wang, Mark Bates, and Xiaowei Zhuang. 2008. "Three-Dimensional Super-Resolution Imaging by Stochastic Optical Reconstruction Microscopy." *Science (New York, N.Y.)* 319 (5864): 810–13. doi:10.1126/science.1153529.
- Huang, Yan You, Xiao Ching Li, and Eric R. Kandel. 1994. "cAMP Contributes to Mossy Fiber LTP by Initiating Both a Covalently Mediated Early Phase and Macromolecular Synthesis-Dependent Late Phase." *Cell* 79 (1): 69–79. doi:10.1016/0092-8674(94)90401-4.
- Hudson, Brian D, Terence E Hébert, and Melanie E M Kelly. 2010. "Ligand- and Heterodimer-Directed Signaling of the CB(1) Cannabinoid Receptor." *Molecular Pharmacology* 77 (1): 1–9. doi:10.1124/mol.109.060251.
- Ishii, I, and J Chun. 2002. "Anandamide-Induced Neuroblastoma Cell Rounding via the CB1 Cannabinoid Receptors." *Neuroreport* 13 (5): 593–96. papers://1fa4e632-4d39-4b47-95a2-5a607126d96f/Paper/p115.
- Jordan, J Dedrick, John Cijiang He, Narat J Eungdamrong, Ivone Gomes, Wasif Ali, Tracy Nguyen, Trever G Bivona, Mark R Philips, Lakshmi A Devi, and Ravi Iyengar. 2005. "Cannabinoid Receptor-Induced Neurite Outgrowth Is Mediated by Rap1 Activation through G(alpha)o/i-Triggered Proteasomal Degradation of Rap1GAPII." *The Journal of Biological Chemistry* 280 (12). American Society for Biochemistry and Molecular Biology: 11413–21. doi:10.1074/jbc.M411521200.
- Jordan, Randolph, Edward A Lemke, and Jurgen Klingauf. 2005. "Visualization of Synaptic Vesicle Movement in Intact Synaptic Boutons Using Fluorescence Fluctuation Spectroscopy." *Biophysical Journal* 89 (3): 2091–2102. doi:10.1529/biophysj.105.061663.
- Jung, Jasmin, Kristina Loy, Eva-Maria Schilling, Mareike Röther, Jan M. Brauner, Tobias Huth, Ursula Schlötzer-Schrehardt, et al. 2014. "The Antidepressant Fluoxetine Mobilizes Vesicles to the Recycling Pool of Rat Hippocampal Synapses During High Activity." *Molecular Neurobiology* 49 (2): 916–30. doi:10.1007/s12035-013-8569-5.

- Jung, K M, G Astarita, D Thongkham, and D Piomelli. 2011. "Diacylglycerol Lipase-Alpha and -Beta Control Neurite Outgrowth in Neuro-2a Cells through Distinct Molecular Mechanisms." *Mol Pharmacol* 80 (1): 60–67. doi:mol.110.070458
[pii]\r10.1124/mol.110.070458.
- Jung, Kwang Mook, Marja Sepers, Christopher M. Henstridge, Olivier Lassalle, Daniela Neuhofer, Henry Martin, Melanie Ginger, et al. 2012. "Uncoupling of the Endocannabinoid Signalling Complex in a Mouse Model of Fragile X Syndrome." *Nature Communications* 3. doi:10.1038/ncomms2045.
- Kaesler, Pascal S., Lunbin Deng, Yun Wang, Irina Dulubova, Xinran Liu, Josep Rizo, and Thomas C. Südhof. 2011. "RIM Proteins Tether Ca²⁺channels to Presynaptic Active Zones via a Direct PDZ-Domain Interaction." *Cell* 144 (2): 282–95.
doi:10.1016/j.cell.2010.12.029.
- Kaesler, Pascal S, Hyung-Bae Kwon, Jacqueline Blundell, Vivien Chevalere, Wade Morishita, Robert C Malenka, Craig M Powell, Pablo E Castillo, and Thomas C Südhof. 2008. "RIM1alpha Phosphorylation at Serine-413 by Protein Kinase A Is Not Required for Presynaptic Long-Term Plasticity or Learning." *Proceedings of the National Academy of Sciences of the United States of America* 105: 14680–85.
doi:10.1073/pnas.0806679105.
- Kamin, Dirk, Marcel A. Lauterbach, Volker Westphal, Jan Keller, Andreas Schönle, Stefan W. Hell, and Silvio O. Rizzoli. 2010. "High- and Low-Mobility Stages in the Synaptic Vesicle Cycle." *Biophysical Journal* 99 (2): 675–84. doi:10.1016/j.bpj.2010.04.054.
- Kano, Masanobu, Takako Ohno-Shosaku, Yuki Hashimotodani, Motokazu Uchigashima, and Masahiko Watanabe. 2009. "Endocannabinoid-Mediated Control of Synaptic Transmission." *Physiological Reviews* 89 (1): 309–80. doi:10.1152/physrev.00019.2008.
- Karila, Laurent, Perrine Roux, Benjamin Rolland, Amine Benyamina, Michel Reynaud, Henri-Jean Aubin, and Christophe Lançon. 2014. "Acute and Long-Term Effects of Cannabis Use: A Review." *Current Pharmaceutical Design* 20 (25): 4112–18.
<http://www.ncbi.nlm.nih.gov/pubmed/24001294>.
- Katona, I. 2006. "Molecular Composition of the Endocannabinoid System at Glutamatergic Synapses." *Journal of Neuroscience* 26 (21): 5628–37. doi:10.1523/JNEUROSCI.0309-

06.2006.

- Katona, I, E A Rancz, L Acsady, C Ledent, K Mackie, N Hajos, and T F Freund. 2001. “Distribution of CB1 Cannabinoid Receptors in the Amygdala and Their Role in the Control of GABAergic Transmission.” *The Journal of Neuroscience : The Official Journal of the Society for Neuroscience* 21 (23): 9506–18.
<http://www.ncbi.nlm.nih.gov/pubmed/11717385>.
- Katona, I, B Sperlagh, A Sık, A Kafalvi, E S Vizi, K Mackie, and T F Freund. 1999. “Presynaptically Located CB1 Cannabinoid Receptors Regulate GABA Release from Axon Terminals of Specific Hippocampal Interneurons.” *The Journal of Neuroscience : The Official Journal of the Society for Neuroscience* 19 (11): 4544–58.
<http://www.ncbi.nlm.nih.gov/pubmed/10341254>.
- Kavalali, Ege T, and Erik M Jorgensen. 2014. “Visualizing Presynaptic Function.” *Nature Neuroscience* 17 (1): 10–16. doi:10.1038/nn.3578.
- Kawamura, Y. 2006. “The CB1 Cannabinoid Receptor Is the Major Cannabinoid Receptor at Excitatory Presynaptic Sites in the Hippocampus and Cerebellum.” *Journal of Neuroscience* 26 (11): 2991–3001. doi:10.1523/JNEUROSCI.4872-05.2006.
- Keck, Tara, Volker Scheuss, R. Irene Jacobsen, Corette J. Wierenga, Ulf T. Eysel, Tobias Bonhoeffer, and Mark Hübener. 2011. “Loss of Sensory Input Causes Rapid Structural Changes of Inhibitory Neurons in Adult Mouse Visual Cortex.” *Neuron* 71 (5): 869–82. doi:10.1016/j.neuron.2011.06.034.
- Kellogg, R., K. Mackie, and A. Straiker. 2009. “Cannabinoid CB1 Receptor-Dependent Long-Term Depression in Autaptic Excitatory Neurons.” *Journal of Neurophysiology* 102 (2): 1160–71. doi:10.1152/jn.00266.2009.
- Kepiro, Miklos, Boglarka H. Varkuti, Laszlo Vegner, Gergely Voros, Gyorgy Hegyi, Mate Varga, and Andras Malnasi-Csizmadia. 2014. “Para-Nitroblebbistatin, the Non-Cytotoxic and Photostable Myosin II Inhibitor.” *Angewandte Chemie - International Edition* 53 (31): 8211–15. doi:10.1002/anie.201403540.
- Kevenaar, Josta T, and Casper C Hoogenraad. 2015. “The Axonal Cytoskeleton: From Organization to Function.” *Frontiers in Molecular Neuroscience* 8. Frontiers Media SA: 44. doi:10.3389/fnmol.2015.00044.

- Kim, Sung Hyun, and Timothy A. Ryan. 2010. "CDK5 Serves as a Major Control Point in Neurotransmitter Release." *Neuron* 67 (5): 797–809. doi:10.1016/j.neuron.2010.08.003.
- Kneussel, Matthias, and Wolfgang Wagner. 2013. "Myosin Motors at Neuronal Synapses: Drivers of Membrane Transport and Actin Dynamics." *Nature Reviews. Neuroscience* 14 (4): 233–47. doi:10.1038/nrn3445.
- Kuhlman, Sandra J., and Z. Josh Huang. 2008. "High-Resolution Labeling and Functional Manipulation of Specific Neuron Types in Mouse Brain by Cre-Activated Viral Gene Expression." Edited by Rachel O. L. Wong. *PLoS ONE* 3 (4): e2005. doi:10.1371/journal.pone.0002005.
- Kuriu, Toshihiko, Yuchio Yanagawa, and Shiro Konishi. 2012. "Activity-Dependent Coordinated Mobility of Hippocampal Inhibitory Synapses Visualized with Presynaptic and Postsynaptic Tagged-Molecular Markers." *Molecular and Cellular Neuroscience* 49 (2): 184–95. doi:10.1016/j.mcn.2011.11.002.
- Kuromi, Hiroshi, and Yoshiaki Kidokoro. 1998. "Two Distinct Pools of Synaptic Vesicles in Single Presynaptic Boutons in a Temperature-Sensitive *Drosophila* Mutant, *Shibire*." *Neuron* 20 (5): 917–25. doi:10.1016/S0896-6273(00)80473-0.
- Landis, Dennis M.D., Alison K. Hall, Lori A. Weinstein, and Thomas S. Reese. 1988. "The Organization of Cytoplasm at the Presynaptic Active Zone of a Central Nervous System Synapse." *Neuron* 1 (3): 201–9. doi:10.1016/0896-6273(88)90140-7.
- Lauckner, J. E., B. Hille, and K. Mackie. 2005. "The Cannabinoid Agonist WIN55,212-2 Increases Intracellular Calcium via CB1 Receptor Coupling to Gq/11 G Proteins." *Proceedings of the National Academy of Sciences* 102 (52): 19144–49. doi:10.1073/pnas.0509588102.
- Lebon, Guillaume, Tony Warne, Patricia C. Edwards, Kirstie Bennett, Christopher J. Langmead, Andrew G.W. Leslie, and Christopher G. Tate. 2011. "Agonist-Bound Adenosine A2A Receptor Structures Reveal Common Features of GPCR Activation." *Nature* 474 (7352): 521–26. doi:10.1038/nature10136.
- Lee, Jae Sung, Won-Kyung Ho, Erwin Neher, and Suk-Ho Lee. 2013. "Superpriming of Synaptic Vesicles after Their Recruitment to the Readily Releasable Pool." *Proceedings of the National Academy of Sciences of the United States of America* 110 (37): 15079–

84. doi:10.1073/pnas.1314427110.

Leterrier, Christophe, Jeanne Lainé, Michèle Darmon, Hélène Boudin, Jean Rossier, and Zsolt Lenkei. 2006. “Constitutive Activation Drives Compartment-Selective Endocytosis and Axonal Targeting of Type 1 Cannabinoid Receptors.” *The Journal of Neuroscience : The Official Journal of the Society for Neuroscience* 26 (12): 3141–53. doi:10.1523/JNEUROSCI.5437-05.2006.

Leterrier, Christophe, Jean Potier, Ghislaine Caillol, Claire Debarnot, Fanny Rueda Boroni, and Bénédicte Dargent. 2015. “Nanoscale Architecture of the Axon Initial Segment Reveals an Organized and Robust Scaffold.” *Cell Reports* 13 (12): 2781–93. doi:10.1016/j.celrep.2015.11.051.

Li, Chenchen, and Donald G. Rainnie. 2014. “Bidirectional Regulation of Synaptic Plasticity in the Basolateral Amygdala Induced by the D1-like Family of Dopamine Receptors and Group II Metabotropic Glutamate Receptors.” *Journal of Physiology* 592 (19): 4329–51. doi:10.1113/jphysiol.2014.277715.

Li, Lin, Xiaomei Wu, Hai Yuan Yue, Yong Chuan Zhu, and Jianhua Xu. 2016. “Myosin Light Chain Kinase Facilitates Endocytosis of Synaptic Vesicles at Hippocampal Boutons.” *Journal of Neurochemistry*, 60–73. doi:10.1111/jnc.13635.

Li, Zhiying, and Venkatesh N. Murthy. 2001. “Visualizing Postendocytic Traffic of Synaptic Vesicles at Hippocampal Synapses.” *Neuron* 31 (4): 593–605. doi:10.1016/S0896-6273(01)00398-1.

Liu, J, B Gao, F Mirshahi, A J Sanyal, A D Khanolkar, A Makriyannis, and G Kunos. 2000. “Functional CB1 Cannabinoid Receptors in Human Vascular Endothelial Cells.” *The Biochemical Journal* 346 Pt 3: 835–40. doi:10.1042/bj3460835.

Liu, Karen S.Y., Matthias Siebert, Sara Mertel, Elena Knoche, Stephanie Wegener, Carolin Wichmann, Tanja Matkovic, et al. 2011. “RIM-Binding Protein, a Central Part of the Active Zone, Is Essential for Neurotransmitter Release.” *Science* 334 (6062): 1565–69. doi:10.1126/science.1212991.

Llano, I., N. Leresche, and A. Marty. 1991. “Calcium Entry Increases the Sensitivity of Cerebellar Purkinje Cells to Applied GABA and Decreases Inhibitory Synaptic Currents.” *Neuron* 6 (4): 565–74. doi:10.1016/0896-6273(91)90059-9.

- Lonart, György, Susanne Schoch, Pascal S. Kaeser, C.Jenny Larkin, Thomas C. Südhof, and David J. Linden. 2003. “Phosphorylation of RIM1 α by PKA Triggers Presynaptic Long-Term Potentiation at Cerebellar Parallel Fiber Synapses.” *Cell* 115 (1). Elsevier: 49–60. doi:10.1016/S0092-8674(03)00727-X.
- López-Cardona, Angela Patricia, Serafín Pérez-Cerezales, Raúl Fernández-González, Ricardo Laguna-Barraza, Eva Pericuesta, Naiara Agirregoitia, Alfonso Gutiérrez-Adán, and Ekaitz Agirregoitia. 2017. “CB1cannabinoid Receptor Drives Oocyte Maturation and Embryo Development via PI3K/Akt and MAPK Pathways.” *FASEB Journal* 31 (8): 3372–82. doi:10.1096/fj.201601382RR.
- Ludányi, A., S.S.-J. Hu, M. Yamazaki, A. Tanimura, D. Piomelli, M. Watanabe, M. Kano, et al. 2011. “Complementary Synaptic Distribution of Enzymes Responsible for Synthesis and Inactivation of the Endocannabinoid 2-Arachidonoylglycerol in the Human Hippocampus.” *Neuroscience* 174 (February): 50–63. doi:10.1016/j.neuroscience.2010.10.062.
- Luján, Rafael, James Maylie, and John P. Adelman. 2009. “New Sites of Action for GIRK and SK Channels.” *Nature Reviews Neuroscience* 10 (7): 475–80. doi:10.1038/nrn2668.
- Luo, Liqun. 2002. “Actin Cytoskeleton Regulation in Neuronal Morphogenesis and Structural Plasticity.” *Annual Review of Cell and Developmental Biology* 18 (1): 601–35. doi:10.1146/annurev.cellbio.18.031802.150501.
- Lüscher, Christian, and Robert C. Malenka. 2012. “NMDA Receptor-Dependent Long-Term Potentiation and Long-Term Depression (LTP/LTD).” *Cold Spring Harbor Perspectives in Biology* 4 (6): 1–15. doi:10.1101/cshperspect.a005710.
- Lysko, D. E., M. Putt, and J. A. Golden. 2011. “SDF1 Regulates Leading Process Branching and Speed of Migrating Interneurons.” *Journal of Neuroscience* 31 (5): 1739–45. doi:10.1523/JNEUROSCI.3118-10.2011.
- Mackie, K., and B. Hille. 1992. “Cannabinoids Inhibit N-Type Calcium Channels in Neuroblastoma-Glioma Cells.” *Proceedings of the National Academy of Sciences* 89 (9): 3825–29. doi:10.1073/pnas.89.9.3825.
- Mackie, K, Y Lai, R Westenbroek, and R Mitchell. 1995. “Cannabinoids Activate an Inwardly Rectifying Potassium Conductance and Inhibit Q-Type Calcium Currents in

- AtT20 Cells Transfected with Rat Brain Cannabinoid Receptor.” *Journal of Neuroscience* 15 (10): 6552–61.
- Mai, Ping, Lei Tian, Le Yang, Lin Wang, Lin Yang, and Liying Li. 2015. “Cannabinoid Receptor 1 but Not 2 Mediates Macrophage Phagocytosis by G_{(α)i/o}/RhoA/ROCK Signaling Pathway.” *Journal of Cellular Physiology* 230 (7): 1640–50. doi:10.1002/jcp.24911.
- Malenka, Robert C., and Mark F. Bear. 2004. “LTP and LTD.” *Neuron* 44 (1): 5–21. doi:10.1016/j.neuron.2004.09.012.
- Marik, Sally A., Homare Yamahachi, Justin N. J. McManus, Gabor Szabo, and Charles D. Gilbert. 2010. “Axonal Dynamics of Excitatory and Inhibitory Neurons in Somatosensory Cortex.” Edited by Daniel Feldman. *PLoS Biology* 8 (6): e1000395. doi:10.1371/journal.pbio.1000395.
- Marra, Vincenzo, Jemima J. Burden, Julian R. Thorpe, Ikuko T. Smith, Spencer L. Smith, Michael Häusser, Tiago Branco, and Kevin Staras. 2012. “A Preferentially Segregated Recycling Vesicle Pool of Limited Size Supports Neurotransmission in Native Central Synapses.” *Neuron* 76 (3): 579–89. doi:10.1016/j.neuron.2012.08.042.
- Marrs, William R., Jacqueline L. Blankman, Eric A. Horne, Aurore Thomazeau, Yi Hsing Lin, Jonathan Coy, Agnes L. Bodor, et al. 2010. “The Serine Hydrolase ABHD6 Controls the Accumulation and Efficacy of 2-AG at Cannabinoid Receptors.” *Nature Neuroscience* 13 (8): 951–57. doi:10.1038/nn.2601.
- Marsicano, Giovanni, and Beat Lutz. 1999. “Expression of the Cannabinoid Receptor CB1 in Distinct Neuronal Subpopulations in the Adult Mouse Forebrain.” *European Journal of Neuroscience* 11 (12): 4213–25. doi:10.1046/j.1460-9568.1999.00847.x.
- Matsuda, L A, T I Bonner, and S J Lolait. 1993. “Localization of Cannabinoid Receptor mRNA in Rat Brain.” *J Comp Neurol.* 1993 Jan 22; 327(4): 535-50.
- Matsuda, Lisa A., Stephen J. Lolait, Michael J. Brownstein, Alice C. Young, and Tom I. Bonner. 1990. “Structure of a Cannabinoid Receptor and Functional Expression of the Cloned cDNA.” *Nature* 346 (6284): 561–64. doi:10.1038/346561a0.
- Mátyás, F., Y. Yanovsky, K. Mackie, W. Kelsch, U. Misgeld, and T. F. Freund. 2006.

- “Subcellular Localization of Type 1 Cannabinoid Receptors in the Rat Basal Ganglia.” *Neuroscience* 137 (1): 337–61. doi:10.1016/j.neuroscience.2005.09.005.
- Matz, Jacob, Andrew Gilyan, Annette Kolar, Terrence McCarvill, and Stefan R Krueger. 2010. “Rapid Structural Alterations of the Active Zone Lead to Sustained Changes in Neurotransmitter Release.” *Proceedings of the National Academy of Sciences of the United States of America* 107 (19). National Academy of Sciences: 8836–41. doi:10.1073/pnas.0906087107.
- McCudden, C. R., M. D. Hains, R. J. Kimple, D. P. Siderovski, and F. S. Willard. 2005. “G-Protein Signaling: Back to the Future.” *Cellular and Molecular Life Sciences*. doi:10.1007/s00018-004-4462-3.
- McDonald, Neil A., Christopher M. Henstridge, Christopher N. Connolly, and Andrew J. Irving. 2007. “Generation and Functional Characterization of Fluorescent, N-Terminally Tagged CB1 Receptor Chimeras for Live-Cell Imaging.” *Molecular and Cellular Neuroscience* 35 (2): 237–48. doi:10.1016/j.mcn.2007.02.016.
- Mechoulam, Raphael, Shimon Ben-Shabat, Lumir Hanus, Moshe Ligumsky, Norbert E. Kaminski, Anthony R. Schatz, Asher Gopher, et al. 1995. “Identification of an Endogenous 2-Monoglyceride, Present in Canine Gut, That Binds to Cannabinoid Receptors.” *Biochemical Pharmacology* 50 (1): 83–90. doi:10.1016/0006-2952(95)00109-D.
- Mechoulam, Raphael, and Yehiel Gaoni. 1967. “The Absolute Configuration of δ 1-Tetrahydrocannabinol, the Major Active Constituent of Hashish.” *Tetrahedron Letters* 8 (12): 1109–11. doi:10.1016/S0040-4039(00)90646-4.
- Meyer, Daniel, Tobias Bonhoeffer, and Volker Scheuss. 2014. “Balance and Stability of Synaptic Structures during Synaptic Plasticity.” *Neuron* 82 (2): 430–43. doi:10.1016/j.neuron.2014.02.031.
- Miki, Takafumi, Gerardo Malagon, Camila Pulido, Isabel Llano, Erwin Neher, and Alain Marty. 2016. “Actin- and Myosin-Dependent Vesicle Loading of Presynaptic Docking Sites Prior to Exocytosis.” *Neuron* 91 (4). Elsevier: 808–23. doi:10.1016/j.neuron.2016.07.033.
- Miller, T. M., and J. E. Heuser. 1984. “Endocytosis of Synaptic Vesicle Membrane at the

- Frog Neuromuscular Junction.” *Journal of Cell Biology* 98 (2): 685–98.
doi:10.1083/jcb.98.2.685.
- Ming, Guo Li, Hong Jun Song, Benedikt Berninger, Christine E. Holt, Marc Tessier-Lavigne, and Mu Ming Poo. 1997. “cAMP-Dependent Growth Cone Guidance by Netrin-1.” *Neuron* 19 (6): 1225–35. doi:10.1016/S0896-6273(00)80414-6.
- Mochida, Sumiko, Haruo Kobayashi, Yuzuru Matsuda, Yasukatsu Yuda, Kazuyo Muramoto, and Yoshiaki Nonomura. 1994. “Myosin II Is Involved in Transmitter Release at Synapses Formed between Rat Sympathetic Neurons in Culture.” *Neuron* 13 (5): 1131–42. doi:10.1016/0896-6273(94)90051-5.
- Monday, Hannah R., and Pablo E. Castillo. 2017. “Closing the Gap: Long-Term Presynaptic Plasticity in Brain Function and Disease.” *Current Opinion in Neurobiology* 45: 106–12. doi:10.1016/j.conb.2017.05.011.
- Morales, M, S D Wang, O Diaz-Ruiz, and D H Jho. 2004. “Cannabinoid CB1 Receptor and Serotonin 3 Receptor Subunit A (5-HT3A) Are Co-Expressed in GABA Neurons in the Rat Telencephalon.” *J Comp Neurol* 468 (2): 205–16. doi:10.1002/cne.10968.
- Morales, Miguel, Michael A Colicos, and Yukiko Goda. 2000. “Actin-Dependent Regulation of Neurotransmitter Release at Central Synapses.” *Neuron* 27 (3): 539–50. doi:10.1016/S0896-6273(00)00064-7.
- Morrison, Deborah K., and Roger J. Davis. 2003. “Regulation of MAP Kinase Signaling Modules by Scaffold Proteins in Mammals.” *Annual Review of Cell and Developmental Biology* 19 (1): 91–118. doi:10.1146/annurev.cellbio.19.111401.091942.
- Mukhopadhyay, Somnath, and Allyn C. Howlett. 2001. “CB₁ Receptor-G Protein Association.” *European Journal of Biochemistry* 268 (3). Blackwell Science Ltd: 499–505. doi:10.1046/j.1432-1327.2001.01810.x.
- Mulder, J., T. Aguado, E. Keimpema, K. Barabas, C. J. Ballester Rosado, L. Nguyen, K. Monory, et al. 2008. “Endocannabinoid Signaling Controls Pyramidal Cell Specification and Long-Range Axon Patterning.” *Proceedings of the National Academy of Sciences* 105 (25): 8760–65. doi:10.1073/pnas.0803545105.
- Munro, Sean, Kerrie L. Thomas, and Muna Abu-Shaar. 1993. “Molecular Characterization of

- a Peripheral Receptor for Cannabinoids.” *Nature* 365 (6441): 61–65.
doi:10.1038/365061a0.
- Murthy, Venkatesh N., and Charles F. Stevens. 1998. “Synaptic Vesicles Retain Their Identity through the Endocytic Cycle.” *Nature* 392 (6675): 497–501. doi:10.1038/33152.
- Nahir, Ben, Casie Lindsly, and Charles J. Frazier. 2010. “mGluR-Mediated and Endocannabinoid-Dependent Long-Term Depression in the Hilar Region of the Rat Dentate Gyrus.” *Neuropharmacology* 58 (4–5): 712–21.
doi:10.1016/j.neuropharm.2009.12.022.
- Navarrete, Marta, and Alfonso Araque. 2008. “Endocannabinoids Mediate Neuron-Astrocyte Communication.” *Neuron* 57 (6): 883–93. doi:10.1016/j.neuron.2008.01.029.
- Northup, J. K., P. C. Sternweis, and A. G. Gilman. 1983. “The Subunits of the Stimulatory Regulatory Component of Adenylate Cyclase. Resolution, Activity, and Properties of the 35,000-Dalton (Beta) Subunit.” *Journal of Biological Chemistry* 258 (18): 11361–68.
- Northup, John K, Paul C Sternweis, Murray D Smigel, Leonard S Schleifer, Elliott M Ross, and Alfred G Gilman. 1980. “Purification of the Regulatory Component of Adenylate Cyclase.” *Proceedings of the National Academy of Sciences of the United States of America* 77 (11): 6516–20. doi:10.1073/pnas.77.11.6516.
- Nyíri, G., C. Cserép, E. Szabadits, K. Mackie, and T. F. Freund. 2005. “CB1cannabinoid Receptors Are Enriched in the Perisynaptic Annulus and on Preterminal Segments of Hippocampal GABAergic Axons.” *Neuroscience* 136 (3): 811–22.
doi:10.1016/j.neuroscience.2005.01.026.
- Ohno-Shosaku, T, T Maejima, and M Kano. 2001. “Endogenous Cannabinoids Mediate Retrograde Signals from Depolarized Postsynaptic Neurons to Presynaptic Terminals.” *Neuron* 29 (3): 729–38. <http://www.ncbi.nlm.nih.gov/pubmed/11301031>.
- Oishi, Atsuro, Noriko Makita, Junichiro Sato, and Taroh Iiri. 2012. “Regulation of RhoA Signaling by the cAMP-Dependent Phosphorylation of RhoGDI α .” *The Journal of Biological Chemistry* 287 (46). American Society for Biochemistry and Molecular Biology: 38705–15. doi:10.1074/jbc.M112.401547.
- Opazo, Felipe, Annedore Punge, Johanna Bückers, Peer Hoopmann, Lars Kastrup, Stefan W.

- Hell, and Silvio O. Rizzoli. 2010. "Limited Intermixing of Synaptic Vesicle Components upon Vesicle Recycling." *Traffic* 11 (6): 800–812. doi:10.1111/j.1600-0854.2010.01058.x.
- Orenbuch, Ayelet, Lee Shalev, Vincenzo Marra, Isaac Sinai, Yotam Lavy, Joy Kahn, Jemima J Burden, Kevin Staras, and Daniel Gitler. 2012. "Synapsin Selectively Controls the Mobility of Resting Pool Vesicles at Hippocampal Terminals." *The Journal of Neuroscience : The Official Journal of the Society for Neuroscience* 32 (12): 3969–80. doi:10.1523/JNEUROSCI.5058-11.2012.
- Oudin, Madeleine J., Carl Hobbs, and Patrick Doherty. 2011. "DAGL-Dependent Endocannabinoid Signalling: Roles in Axonal Pathfinding, Synaptic Plasticity and Adult Neurogenesis." *European Journal of Neuroscience*. doi:10.1111/j.1460-9568.2011.07831.x.
- Pan, X, S R Ikeda, and D L Lewis. 1996. "Rat Brain Cannabinoid Receptor Modulates N-Type Ca²⁺ Channels in a Neuronal Expression System." *Molecular Pharmacology* 49 (4): 707–14.
- Parish, C. L., D. Stanic, J. Drago, E. Borrelli, D. I. Finkelstein, and Malcolm K. Horne. 2002. "Effects of Long-Term Treatment with Dopamine Receptor Agonists and Antagonists on Terminal Arbor Size." *European Journal of Neuroscience* 16 (5): 787–94. doi:10.1046/j.1460-9568.2002.02132.x.
- Parish, C L, D I Finkelstein, J Drago, E Borrelli, and M K Horne. 2001. "The Role of Dopamine Receptors in Regulating the Size of Axonal Arbors." *The Journal of Neuroscience : The Official Journal of the Society for Neuroscience* 21 (14): 5147–57. doi:21/14/5147 [pii].
- Park, Hyokeun, Yulong Li, and Richard W. Tsien. 2012. "Influence of Synaptic Vesicle Position on Release Probability and Exocytotic Fusion Mode." *Science* 335 (6074): 1362–66. doi:10.1126/science.1216937.
- Peng, Amy, Ziv Rotman, Pan-Yue Deng, and Vitaly A Klyachko. 2012. "Differential Motion Dynamics of Synaptic Vesicles Undergoing Spontaneous and Activity-Evoked Endocytosis." *Neuron* 73 (6): 1108–15. doi:10.1016/j.neuron.2012.01.023.
- Perkins, G. A., J. Tjong, J. M. Brown, P. H. Poquiz, R. T. Scott, D. R. Kolson, M. H.

- Ellisman, and G. A. Spirou. 2010. “The Micro-Architecture of Mitochondria at Active Zones: Electron Tomography Reveals Novel Anchoring Scaffolds and Cristae Structured for High-Rate Metabolism.” *Journal of Neuroscience* 30 (3): 1015–26.
doi:10.1523/JNEUROSCI.1517-09.2010.
- Peters, Alan, and Ita R. Kaiserman-Abramof. 1970. “The Small Pyramidal Neuron of the Rat Cerebral Cortex. The Perikaryon, Dendrites and Spines.” *American Journal of Anatomy* 127 (4): 321–55. doi:10.1002/aja.1001270402.
- Pickel, V M, J Chan, T L Kash, J J Rodriguez, and K MacKie. 2004. “Compartment-Specific Localization of Cannabinoid 1 (CB1) and Mu-Opioid Receptors in Rat Nucleus Accumbens.” *Neuroscience* 127 (1): 101–12. doi:10.1016/j.neuroscience.2004.05.015.
- Pitler, T.a., and B.E. Alger. 1992. “Postsynaptic Spike Firing Reduces Synaptic GABAA Responses in Hippocampal Pyramidal Cells.” *The Journal of Neuroscience : The Official Journal of the Society for Neuroscience* 12 (October): 4122–32.
- Pollard, T. D., and M. S. Mooseker. 1981. “Direct Measurement of Actin Polymerization Rate Constants by Electron Microscopy of Actin Filaments Nucleated by Isolated Microvillus Cores.” *Journal of Cell Biology* 88 (3): 654–59. doi:10.1083/jcb.88.3.654.
- Pollard, Thomas D. 1986. “Rate Constants for the Reactions of ATP-and ADP-Actin with the Ends of Actin Filaments.” *Journal of Cell Biology* 103 (6): 2747.
doi:10.1083/jcb.103.6.2747.
- . 2016. “Actin and Actin-Binding Proteins.” *Cold Spring Harbor Perspectives in Biology* 8 (8). doi:10.1101/cshperspect.a018226.
- Pollard, Thomas D., and John A. Cooper. 2009. “Actin, a Central Player in Cell Shape and Movement.” *Science*. doi:10.1126/science.1175862.
- Qiao, Qian, Lei Ma, Wei Li, Jin Wu Tsai, Guang Yang, and Wen Biao Gan. 2016. “Long-Term Stability of Axonal Boutons in the Mouse Barrel Cortex.” *Developmental Neurobiology* 76 (3): 252–61. doi:10.1002/dneu.22311.
- Ramírez-Franco, Jorge, Beatris Alonso, David Bartolomé-Martín, José Sánchez-Prieto, and Magdalena Torres. 2013. “Studying Synaptic Efficiency by Post-Hoc Immunolabelling.” *BMC Neuroscience* 14: 127. doi:10.1186/1471-2202-14-127.

- Ramírez-Franco, Jorge, David Bartolomé-Martín, Beatris Alonso, Magdalena Torres, and José Sánchez-Prieto. 2014. “Cannabinoid Type 1 Receptors Transiently Silence Glutamatergic Nerve Terminals of Cultured Cerebellar Granule Cells.” *PLoS One* 9 (2): e88594. doi:10.1371/journal.pone.0088594.
- Ratnayaka, Arjuna, Vincenzo Marra, Daniel Bush, Jemima J. Burden, Tiago Branco, and Kevin Staras. 2012. “Recruitment of Resting Vesicles into Recycling Pools Supports NMDA Receptor-Dependent Synaptic Potentiation in Cultured Hippocampal Neurons.” *Journal of Physiology* 590 (7): 1585–97. doi:10.1113/jphysiol.2011.226688.
- Reyes-Harde, M, B V Potter, Antony Galione, and Patric K Stanton. 1999. “Induction of Hippocampal LTD Requires Nitric-Oxide-Stimulated PKG Activity and Ca²⁺ Release from Cyclic ADP-Ribose-Sensitive Stores.” *Journal of Neurophysiology* 82 (3): 1569–76.
<http://eutils.ncbi.nlm.nih.gov/entrez/eutils/elink.fcgi?dbfrom=pubmed&id=10482770&retmode=ref&cmd=prlinks%5Cnpapers3://publication/uuid/EE21C71A-BB4A-4C18-96DB-1174738DBDBC>.
- Reynolds, Tracy, and Nicholas A. Hartell. 2001. “Roles for Nitric Oxide and Arachidonic Acid in the Induction of Heterosynaptic Cerebellar LTD.” *NeuroReport* 12 (1): 133–36. doi:10.1097/00001756-200101220-00034.
- Richards, Thomas A., and Thomas Cavalier-Smith. 2005. “Myosin Domain Evolution and the Primary Divergence of Eukaryotes.” *Nature* 436 (7054). Nature Publishing Group: 1113–18. doi:10.1038/nature03949.
- Rizzoli, Silvio O. 2014. “Synaptic Vesicle Recycling: Steps and Principles.” *The EMBO Journal* 33 (8): 788–822. doi:10.1002/embj.201386357.
- Robbe, D., M. Kopf, A. Remaury, J. Bockaert, and O. J. Manzoni. 2002. “Endogenous Cannabinoids Mediate Long-Term Synaptic Depression in the Nucleus Accumbens.” *Proceedings of the National Academy of Sciences* 99 (12): 8384–88. doi:10.1073/pnas.122149199.
- Roland, Alexandre B., Ana Ricobaraza, Damien Carrel, Benjamin M. Jordan, Felix Rico, Anne Simon, Marie Humbert-Claude, et al. 2014. “Cannabinoid-Induced Actomyosin Contractility Shapes Neuronal Morphology and Growth.” *eLife* 3 (September): e03159.

doi:10.7554/eLife.03159.

- Roloff, Alan M, Garret R Anderson, Kirill A Martemyanov, and Stanley A Thayer. 2010. “Homer 1a Gates the Induction Mechanism for Endocannabinoid-Mediated Synaptic Plasticity.” *The Journal of Neuroscience : The Official Journal of the Society for Neuroscience* 30 (8). Society for Neuroscience: 3072–81. doi:10.1523/JNEUROSCI.4603-09.2010.
- Romero, J., F. Berrendero, L. Garcia-Gil, P. De La Cruz, J. A. Ramos, and J. J. Fernández-Ruiz. 1998. “Loss of Cannabinoid Receptor Binding and Messenger RNA Levels and Cannabinoid Agonist-Stimulated [35S]guanylyl-5'-O-(Thio)-Triphosphate Binding in the Basal Ganglia of Aged Rats.” *Neuroscience* 84 (4): 1075–83. doi:10.1016/S0306-4522(97)00552-6.
- Romero, J., E. Garcia-Palomero, F. Berrendero, L. Garcia-Gil, M.L. Hernandez, J.A. Ramos, and J.J. Fernandez-Ruiz. 1997. “Atypical Location of Cannabinoid Receptors in White Matter Areas during Rat Brain Development.” *Synapse* 26 (3): 317–23. doi:10.1002/(SICI)1098-2396(199707)26:3<317::AID-SYN12>3.0.CO;2-S.
- Ronesi, J. 2004. “Disruption of Endocannabinoid Release and Striatal Long-Term Depression by Postsynaptic Blockade of Endocannabinoid Membrane Transport.” *Journal of Neuroscience* 24 (7): 1673–79. doi:10.1523/JNEUROSCI.5214-03.2004.
- Rosenmund, Christian, and Charles F. Stevens. 1996. “Definition of the Readily Releasable Pool of Vesicles at Hippocampal Synapses.” *Neuron* 16 (6): 1197–1207. doi:10.1016/S0896-6273(00)80146-4.
- Rueda, D, I Galve-Roperh, a Haro, and M Guzmán. 2000. “The CB(1) Cannabinoid Receptor Is Coupled to the Activation of c-Jun N-Terminal Kinase.” *Molecular Pharmacology* 58 (4): 814–20. <http://www.ncbi.nlm.nih.gov/pubmed/10999952>.
- Ryan, T A, L Li, L S Chin, P Greengard, and S J Smith. 1996. “Synaptic Vesicle Recycling in Synapsin I Knock-out Mice.” *The Journal of Cell Biology* 134 (5): 1219–27. doi:10.1083/jcb.134.5.1219.
- Ryan, Timothy A. 1999. “Inhibitors of Myosin Light Chain Kinase Block Synaptic Vesicle Pool Mobilization during Action Potential Firing.” *Journal of Neuroscience* 19 (4).

- Sakaba, Takeshi, and Erwin Neher. 2003. "Involvement of Actin Polymerization in Vesicle Recruitment at the Calyx of Held Synapse." *The Journal of Neuroscience : The Official Journal of the Society for Neuroscience* 23 (3): 837–46. doi:23/3/837 [pii].
- Sankaranarayanan, Sethuraman, Pradeep P. Atluri, and Timothy A. Ryan. 2003. "Actin Has a Molecular Scaffolding, Not Propulsive, Role in Presynaptic Function." *Nature Neuroscience* 6 (2): 127–35. doi:10.1038/nn1002.
- Santini, Emanuela, Thu N. Huynh, and Eric Klann. 2014. "Mechanisms of Translation Control Underlying Long-Lasting Synaptic Plasticity and the Consolidation of Long-Term Memory." *Progress in Molecular Biology and Translational Science* 122: 131–67. doi:10.1016/B978-0-12-420170-5.00005-2.
- Schatz, a R, M Lee, R B Condie, J T Pulaski, and N E Kaminski. 1997. "Cannabinoid Receptors CB1 and CB2: A Characterization of Expression and Adenylate Cyclase Modulation within the Immune System." *Toxicology and Applied Pharmacology* 142 (2): 278–87. doi:10.1006/taap.1996.8034.
- Schikorski, T, and C F Stevens. 1997. "Quantitative Ultrastructural Analysis of Hippocampal Excitatory Synapses." *The Journal of Neuroscience : The Official Journal of the Society for Neuroscience* 17 (15): 5858–67. <http://www.ncbi.nlm.nih.gov/pubmed/9221783>.
- Schikorski, T, C F Stevens, T. Sakurai, M. Ohara-Imaizumi, H. Misonou, S. Nakamura, Y. Matsuda, and Y. Nonomura. 1997. "Quantitative Ultrastructural Analysis of Hippocampal Excitatory Synapses." *The Journal of Neuroscience : The Official Journal of the Society for Neuroscience* 17 (15). Society for Neuroscience: 5858–67. <http://www.ncbi.nlm.nih.gov/pubmed/9221783>.
- Schumann, Anne, Agnieszka Klawiter, Tobias Bonhoeffer, and Corette J. Wierenga. 2013. "Structural Plasticity of GABAergic Axons Is Regulated by Network Activity and GABAA Receptor Activation." *Frontiers in Neural Circuits* 7: 113. doi:10.3389/fncir.2013.00113.
- Sekar, Aswin, Allison R Bialas, Heather de Rivera, Avery Davis, Timothy R Hammond, Nolan Kamitaki, Katherine Tooley, et al. 2016. "Schizophrenia Risk from Complex Variation of Complement Component 4." *Nature* 530 (7589). NIH Public Access: 177–83. doi:10.1038/nature16549.

- Shire, David, Bernard Calandra, Monique Delpech, Xavier Dumont, Mourad Kaghad, Gérard Le Fur, Daniel Caput, and Pascual Ferrara. 1996. "Structural Features of the Central Cannabinoid CB1 Receptor Involved in the Binding of the Specific CB1 Antagonist SR 141716A." *Journal of Biological Chemistry* 271 (12): 6941–46.
doi:10.1074/jbc.271.12.6941.
- Shoemaker, J. L. 2005. "The Endocannabinoid Noladin Ether Acts as a Full Agonist at Human CB2 Cannabinoid Receptors." *Journal of Pharmacology and Experimental Therapeutics* 314 (2): 868–75. doi:10.1124/jpet.105.085282.
- Shtrahman, Matthew, Chuck Yeung, David W. Nauen, Guo Qiang Bi, and Xiao Lun Wu. 2005. "Probing Vesicle Dynamics in Single Hippocampal Synapses." *Biophysical Journal* 89 (5): 3615–27. doi:10.1529/biophysj.105.059295.
- Shupliakov, O. 2009. "The Synaptic Vesicle Cluster: A Source of Endocytic Proteins during Neurotransmitter Release." *Neuroscience* 158 (1): 204–10.
doi:10.1016/j.neuroscience.2008.03.035.
- Shupliakov, O., O. Bloom, J. S. Gustafsson, O. Kjaerulff, P. Low, N. Tomilin, V. A. Pieribone, P. Greengard, and L. Brodin. 2002. "Impaired Recycling of Synaptic Vesicles after Acute Perturbation of the Presynaptic Actin Cytoskeleton." *Proceedings of the National Academy of Sciences* 99 (22): 14476–81. doi:10.1073/pnas.212381799.
- Signorello, Maria Grazia, and Giuliana Leoncini. 2014. "Effect of 2-Arachidonoylglycerol on Myosin Light Chain Phosphorylation and Platelet Activation: The Role of Phosphatidylinositol 3 kinase/AKT Pathway." *Biochimie* 105 (October): 182–91.
doi:10.1016/j.biochi.2014.07.014.
- Siksou, Léa, Philippe Rostaing, Jean-Pierre Lechaire, Thomas Boudier, Toshihisa Ohtsuka, Anna Fejtová, Hung-Teh Kao, et al. 2007. "Three-Dimensional Architecture of Presynaptic Terminal Cytomatrix." *The Journal of Neuroscience : The Official Journal of the Society for Neuroscience* 27 (26). Society for Neuroscience: 6868–77.
doi:10.1523/JNEUROSCI.1773-07.2007.
- Simon, Gabriel M, and Benjamin F Cravatt. 2010. "Characterization of Mice Lacking Candidate N-Acyl Ethanolamine Biosynthetic Enzymes Provides Evidence for Multiple Pathways That Contribute to Endocannabinoid Production in Vivo." *Molecular*

bioSystems 6 (8): 1411–18. doi:10.1039/c000237b.

Simon, Melvin I., Michael P. Strathmann, and Narasimhan Gautam. 1991. “Diversity of G Proteins in Signal Transduction.” *Science* 252 (5007): 802–8. doi:10.1126/science.1902986.

Simsek-Duran, Fatma, David J. Linden, and György Lonart. 2004. “Adapter Protein 14-3-3 Is Required for a Presynaptic Form of LTP in the Cerebellum.” *Nature Neuroscience* 7 (12): 1296–98. doi:10.1038/nn1348.

Singla, S., A. C. Kreitzer, and R. C. Malenka. 2007. “Mechanisms for Synapse Specificity during Striatal Long-Term Depression.” *Journal of Neuroscience* 27 (19): 5260–64. doi:10.1523/JNEUROSCI.0018-07.2007.

Song, Hong Jun, Guo Li Ming, and Mu Ming Poo. 1997. “cAMP-Induced Switching in Turning Direction of Nerve Growth Cones.” *Nature* 388 (6639): 275–79. doi:10.1038/40864.

Spiering, Désirée, and Louis Hodgson. 2011. “Dynamics of the Rho-Family Small GTPases in Actin Regulation and Motility.” *Cell Adhesion and Migration*. doi:10.4161/cam.5.2.14403.

Srinivasan, G., J. H. Kim, and H. von Gersdorff. 2008. “The Pool of Fast Releasing Vesicles Is Augmented by Myosin Light Chain Kinase Inhibition at the Calyx of Held Synapse.” *Journal of Neurophysiology* 99 (4): 1810–24. doi:10.1152/jn.00949.2007.

Steindel, Frauke, Raissa Lerner, Martin Häring, Sabine Ruehle, Giovanni Marsicano, Beat Lutz, and Krisztina Monory. 2013. “Neuron-Type Specific Cannabinoid-Mediated G Protein Signalling in Mouse Hippocampus.” *Journal of Neurochemistry* 124 (6): 795–807. doi:10.1111/jnc.12137.

Stella, Nephi. 2004. “Cannabinoid Signaling in Glial Cells.” *GLIA*. doi:10.1002/glia.20084.

Südhof, Thomas C. 2012. “The Presynaptic Active Zone.” *Neuron* 75 (1): 11–25. doi:10.1016/j.neuron.2012.06.012.

Sugiura, Takayuki, Sachiko Kondo, Akihiro Sukagawa, Shinji Nakane, Akira Shinoda, Kiyoko Itoh, Atsushi Yamashita, and Keizo Waku. 1995. “2-Arachidonoylglycerol: A Possible Endogenous Cannabinoid Receptor Ligand in Brain.” *Biochemical and*

Biophysical Research Communications. doi:10.1006/bbrc.1995.2437.

Sullivan, J M. 1999. "Mechanisms of Cannabinoid-Receptor-Mediated Inhibition of Synaptic Transmission in Cultured Hippocampal Pyramidal Neurons." *Journal of Neurophysiology* 82 (3): 1286–94.

Sunico, Carmen R, David González-Forero, Germán Domínguez, José Manuel García-Verdugo, and Bernardo Moreno-López. 2010. "Nitric Oxide Induces Pathological Synapse Loss by a Protein Kinase G-, Rho Kinase-Dependent Mechanism Preceded by Myosin Light Chain Phosphorylation." *The Journal of Neuroscience : The Official Journal of the Society for Neuroscience* 30 (3). Society for Neuroscience: 973–84. doi:10.1523/JNEUROSCI.3911-09.2010.

Takagishi, Yoshiko, Sugiko Futaki, Kanako Itoh, Enilza M Espreafico, Noriko Murakami, Yoshiharu Murata, and Sumiko Mochida. 2005. "Localization of Myosin II and V Isoforms in Cultured Rat Sympathetic Neurons and Their Potential Involvement in Presynaptic Function." *The Journal of Physiology* 569 (Pt 1): 195–208. doi:10.1113/jphysiol.2005.095943.

Takamori, Shigeo, Matthew Holt, Katinka Stenius, Edward A Lemke, Mads Grønborg, Dietmar Riedel, Henning Urlaub, et al. 2006. "Molecular Anatomy of a Trafficking Organelle." *Cell* 127 (4). Elsevier: 831–46. doi:10.1016/j.cell.2006.10.030.

Tang, Ai-Hui, Haiwen Chen, Tuo P. Li, Sarah R. Metzbower, Harold D. MacGillavry, and Thomas A. Blanpied. 2016. "A Trans-Synaptic Nanocolumn Aligns Neurotransmitter Release to Receptors." *Nature* 536 (7615). Nature Research: 210–14. doi:10.1038/nature19058.

Tanimura, Asami, Maya Yamazaki, Yuki Hashimoto, Motokazu Uchigashima, Shinya Kawata, Manabu Abe, Yoshihiro Kita, et al. 2010. "The Endocannabinoid 2-Arachidonoylglycerol Produced by Diacylglycerol Lipase α Mediates Retrograde Suppression of Synaptic Transmission." *Neuron* 65 (3): 320–27. doi:10.1016/j.neuron.2010.01.021.

Thibault, Karine, Damien Carrel, Damien Bonnard, Katalin Gallatz, Anne Simon, Marc Biard, Sophie Pezet, Miklos Palkovits, and Zsolt Lenkei. 2013. "Activation-Dependent Subcellular Distribution Patterns of CB1 Cannabinoid Receptors in the Rat Forebrain."

Cerebral Cortex 23 (11): 2581–91. doi:10.1093/cercor/bhs240.

Tokuoka, H, and Y Goda. 2006. “Myosin Light Chain Kinase Is Not a Regulator of Synaptic Vesicle Trafficking during Repetitive Exocytosis in Cultured Hippocampal Neurons.” *J Neurosci* 26 (45): 11606–14. doi:26/45/11606 [pii]r10.1523/JNEUROSCI.3400-06.2006.

Trifaró, J. M., T. Lejen, S. D. Rosé, T. Dumitrescu Pene, N. D. Barkar, and E. P. Seward. 2002. “Pathways That Control Cortical F-Actin Dynamics during Secretion.” *Neurochemical Research*. doi:10.1023/A:1021627800918.

Tyler, William J., Xiao Lei Zhang, Kenichi Hartman, Jochen Winterer, Wolfgang Muller, Patric K. Stanton, and Lucas Pozzo-Miller. 2006. “BDNF Increases Release Probability and the Size of a Rapidly Recycling Vesicle Pool within Rat Hippocampal Excitatory Synapses.” *Journal of Physiology* 574 (3): 787–803. doi:10.1113/jphysiol.2006.111310.

Tzounopoulos, T, R Janz, T C Südhof, R a Nicoll, and R C Malenka. 1998. “A Role for cAMP in Long-Term Depression at Hippocampal Mossy Fiber Synapses.” *Neuron* 21 (4): 837–45. <http://www.ncbi.nlm.nih.gov/pubmed/9808469>.

Uehata, Masayoshi, Toshimasa Ishizaki, Hiroyuki Satoh, Takashi Ono, Toshio Kawahara, Tamami Morishita, Hiroki Tamakawa, et al. 1997. “Calcium Sensitization of Smooth Muscle Mediated by a Rho-Associated Protein Kinase in Hypertension.” *Nature* 389 (6654): 990–94. doi:10.1038/40187.

Varma, Namita, Darrin H. Brager, Wade Morishita, Robert A. Lenz, Barry London, and Bradley Alger. 2002. “Presynaptic Factors in the Regulation of DSI Expression in Hippocampus.” *Neuropharmacology* 43 (4): 550–62. doi:10.1016/S0028-3908(02)00168-5.

Vega-Riveroll, Laura J., Steven R. Wylie, Paul T. Loughna, Simon H. Parson, and Peter D. Chantler. 2005. “Nonmuscle Myosins IIA and IIB Are Present in Adult Motor Nerve Terminals.” *NeuroReport* 16 (11): 1143–46. doi:10.1097/00001756-200508010-00002.

Vicente-Manzanares, Miguel, Xuefei Ma, Robert S Adelstein, and Alan Rick Horwitz. 2009. “Non-Muscle Myosin II Takes Centre Stage in Cell Adhesion and Migration.” *Nature Reviews. Molecular Cell Biology* 10 (11). NIH Public Access: 778–90. doi:10.1038/nrm2786.

- Vitalis, Tania, Jeanne Lainé, Anne Simon, Alexandre Roland, Christophe Leterrier, and Zsolt Lenkei. 2008. "The Type 1 Cannabinoid Receptor Is Highly Expressed in Embryonic Cortical Projection Neurons and Negatively Regulates Neurite Growth in Vitro." *European Journal of Neuroscience* 28 (9): 1705–18. doi:10.1111/j.1460-9568.2008.06484.x.
- Vyas, Nora S., Neva H. Patel, and Basant K. Puri. 2011. "Neurobiology and Phenotypic Expression in Early Onset Schizophrenia." *Early Intervention in Psychiatry*. doi:10.1111/j.1751-7893.2010.00253.x.
- Walter, Lisa, Allyn Franklin, Anke Witting, Christian Wade, Yiheng Xie, George Kunos, Ken Mackie, and Nephi Stella. 2003. "Nonpsychotropic Cannabinoid Receptors Regulate Microglial Cell Migration." *The Journal of Neuroscience : The Official Journal of the Society for Neuroscience* 23 (4): 1398–1405. doi:10.1002/glia.20813.
- Wang, X H, J Q Zheng, and M M Poo. 1996. "Effects of Cytochalasin Treatment on Short-Term Synaptic Plasticity at Developing Neuromuscular Junctions in Frogs." *The Journal of Physiology* 491 (Pt 1) (February): 187–95. <http://www.ncbi.nlm.nih.gov/pubmed/9011610>.
- Watanabe, Shigeki, Benjamin R. Rost, Marcial Camacho-Pérez, M. Wayne Davis, Berit Söhl-Kielczynski, Christian Rosenmund, and Erik M. Jorgensen. 2013. "Ultrafast Endocytosis at Mouse Hippocampal Synapses." *Nature* 504 (7479): 242–47. doi:10.1038/nature12809.
- Waters, Jack, and Stephen J. Smith. 2002. "Vesicle Pool Partitioning Influences Presynaptic Diversity and Weighting in Rat Hippocampal Synapses." *Journal of Physiology* 541 (3): 811–23. doi:10.1113/jphysiol.2001.013485.
- Wegner, Albrecht. 1976. "Head to Tail Polymerization of Actin." *Journal of Molecular Biology* 108 (1): 139–50. doi:10.1016/S0022-2836(76)80100-3.
- Wettschureck, Nina, and Stefan Offermanns. 2005. "Mammalian G Proteins and Their Cell Type Specific Functions." *Physiological Review*, 1159–1204. doi:10.1152/physrev.00003.2005.
- Wienisch, Martin, and Jurgen Klingauf. 2006. "Vesicular Proteins Exocytosed and Subsequently Retrieved by Compensatory Endocytosis Are Nonidentical." *Nature*

Neuroscience 9 (8): 1019–27. doi:10.1038/nn1739.

- Wilhelm, Benjamin G, Sunit Mandad, Sven Truckenbrodt, Katharina Kröhnert, Christina Schäfer, Burkhard Rammner, Seong Joo Koo, et al. 2014. “Composition of Isolated Synaptic Boutons Reveals the Amounts of Vesicle Trafficking Proteins.” *Science (New York, N.Y.)* 344 (6187): 1023–28. doi:10.1126/science.1252884.
- Williams, Emma Jane, Frank S. Walsh, and Patrick Doherty. 2003. “The FGF Receptor Uses the Endocannabinoid Signaling System to Couple to an Axonal Growth Response.” *Journal of Cell Biology* 160 (4): 481–86. doi:10.1083/jcb.200210164.
- Willig, Katrin I, Silvio O Rizzoli, Volker Westphal, Reinhard Jahn, and Stefan W Hell. 2006. “STED Microscopy Reveals That Synaptotagmin Remains Clustered after Synaptic Vesicle Exocytosis.” *Nature* 440 (7086): 935–39. doi:10.1038/nature04592.
- Wilson, R. I., and R. A. Nicoll. 2001a. “Endogenous Cannabinoids Mediate Retrograde Signalling at Hippocampal Synapses.” *Nature* 410 (6828): 588–92. doi:10.1038/35069076.
- Wilson, R I, G Kunos, and R A Nicoll. 2001. “Presynaptic Specificity of Endocannabinoid Signaling in the Hippocampus.” *Neuron* 31 (3): 453–62. <http://www.ncbi.nlm.nih.gov/pubmed/11516401>.
- Wilson, R I, and R A Nicoll. 2001b. “Endogenous Cannabinoids Mediate Retrograde Signalling at Hippocampal Synapses.” *Nature* 410 (6828): 588–92. doi:10.1038/35069076.
- Xiang, Yang, Yan Li, Zhe Zhang, Kai Cui, Sheng Wang, Xiao-bing Yuan, Chien-ping Wu, Mu-ming Poo, and Shumin Duan. 2002. “Nerve Growth Cone Guidance Mediated by G Protein–coupled Receptors.” *Nature Neuroscience* 5 (9): 843–48. doi:10.1038/nn899.
- Xu, K., G. Zhong, and X. Zhuang. 2013. “Actin, Spectrin, and Associated Proteins Form a Periodic Cytoskeletal Structure in Axons.” *Science* 339 (6118): 452–56. doi:10.1126/science.1232251.
- Yang, Y., and N. Calakos. 2010. “Acute In Vivo Genetic Rescue Demonstrates That Phosphorylation of RIM1 Serine 413 Is Not Required for Mossy Fiber Long-Term Potentiation.” *Journal of Neuroscience* 30 (7): 2542–46.

doi:10.1523/JNEUROSCI.4285-09.2010.

Yang, Ying, and Nicole Calakos. 2013. “Presynaptic Long-Term Plasticity.” *Frontiers in Synaptic Neuroscience* 5 (October): 8. doi:10.3389/fnsyn.2013.00008.

Yin, H H, M I Davis, J a Ronesi, and D M Lovinger. 2006. “The Role of Protein Synthesis in Striatal Long-Term Depression.” *J Neurosci* 26 (46): 11811–20. doi:26/46/11811 [pii]r10.1523/JNEUROSCI.3196-06.2006.

Younts, Thomas J., Hannah R. Monday, Barna Dudok, Matthew E. Klein, Bryen A. Jordan, István Katona, and Pablo E. Castillo. 2016. “Presynaptic Protein Synthesis Is Required for Long-Term Plasticity of GABA Release.” *Neuron* 92 (2): 479–92. doi:10.1016/j.neuron.2016.09.040.

Yuan, S., and B. D. Burrell. 2013. “Endocannabinoid-Dependent Long-Term Depression in a Nociceptive Synapse Requires Coordinated Presynaptic and Postsynaptic Transcription and Translation.” *Journal of Neuroscience* 33 (10): 4349–58. doi:10.1523/JNEUROSCI.3922-12.2013.

Yue, Hai-Yuan, and Jianhua Xu. 2014. “Myosin Light Chain Kinase Accelerates Vesicle Endocytosis at the Calyx of Held Synapse.” *The Journal of Neuroscience : The Official Journal of the Society for Neuroscience* 34 (1): 295–304. doi:10.1523/JNEUROSCI.3744-13.2014.

Zhang, Qi, Yulong Li, and Richard W. Tsien. 2009. “The Dynamic Control of Kiss-and-Run and Vesicular Reuse Probed with Single Nanoparticles.” *Science* 323 (5920): 1448–53. doi:10.1126/science.1167373.

Zhang, Ye, Kenian Chen, Steven A Sloan, Mariko L Bennett, Anja R Scholze, Sean O’Keefe, Hemali P Phatnani, et al. 2014. “An RNA-Sequencing Transcriptome and Splicing Database of Glia, Neurons, and Vascular Cells of the Cerebral Cortex.” *The Journal of Neuroscience : The Official Journal of the Society for Neuroscience* 34 (36): 11929–47. doi:10.1523/JNEUROSCI.1860-14.2014.

Zhou, Dan, and Z. H. Song. 2001. “CB1 Cannabinoid Receptor-Mediated Neurite Remodeling in Mouse Neuroblastoma N1E-115 Cells.” *Journal of Neuroscience Research* 65 (4): 346–53. doi:10.1002/jnr.1160.

Résumé

Le développement cérébral est un processus complexe qui nécessite une plasticité intrinsèque des neurones. Un grand nombre d'étapes de ce développement requièrent une adaptation morphologique des neurones au travers du cytosquelette actomyosine. De plus, les neurones nécessitent des systèmes de signalisations distincts afin de recruter différents réseaux neuronaux. Le système endocannabinoïde (ECS) est l'un de ces systèmes, et son récepteur neuronal principal, le récepteur cannabinoïde de type 1 (CB1R), régule des formes majeures de plasticité synaptique, bien que les mécanismes exacts de fonctionnement restent méconnus.

Plusieurs études ont récemment découvert l'importance de CB1R dans le développement neuronal. Notre équipe, de même, a trouvé que CB1R régule le développement neuritique par la contraction actomyosine. Plusieurs autres systèmes de signalisation connus pour leurs effets sur le développement neuronal affectent aussi la plasticité synaptique au travers de l'actomyosine. Il est donc raisonnable d'envisager un rôle potentiel de l'actomyosine dans les effets synaptiques de CB1R.

En vérifiant cette hypothèse, nous avons trouvé que la contraction actomyosine est nécessaire à la l'inhibition de l'exocytose des vésicules synaptiques et à la plasticité synaptique à long-terme induite par CB1R. De plus, en utilisant une technique de microscopie de superresolution STORM, nous observons que l'activation de CB1R induit une restructuration du pool de vésicules présynaptique par la contraction actomyosine. Ces résultats impliquent que CB1R conserve ses effets sur le cytosquelette au travers du développement neuronal et suggèrent un nouveau mécanisme d'action contrôlant la plasticité synaptique.

Mots Clés

CB1R, cannabinoïdes, actomyosine, cytosquelette, NMII, ROCK, eCB, plasticité synaptique, LTD, STORM

Abstract

Brain wiring is a multistep process requiring plastic changes of neural networks, starting at the single neuron level. Virtually all steps require morphological adaptation of neural processes through actomyosin dynamics. Moreover, neurons require distinct signaling systems to distinguish different neural networks. One such system is the endocannabinoid system (ECS), whose main neural receptor, the type-1 cannabinoid receptor (CB1R), is known to regulate major forms of synaptic plasticity, although the exact mechanisms have yet to be elucidated.

In recent years, a number of studies have uncovered CB1R's importance in various steps of neural development. One such study from our team found that CB1R regulates neurite development and axonal pathfinding by inducing the contraction of the actomyosin cytoskeleton. Additionally, other signaling systems known to affect axonal pathfinding have been tied to the recruitment of actomyosin during synaptic plasticity. This evidence lends credence to a potential role for actomyosin contraction in the synaptic effects of CB1R.

By verifying this main working hypothesis, we find that actomyosin contraction is necessary for the inhibition of synaptic vesicle exocytosis under CB1R activation in hippocampal cultures. Furthermore, we find that inhibiting actomyosin contraction virtually abolishes long-term forms of CB1R-mediated synaptic plasticity. Finally, by using STORM superresolution imaging, we find that CB1R activation induces nanoscale restructuring of the presynaptic vesicle pool in an actomyosin-dependent manner. Taken together, these results offer evidence for a specific role of presynaptic actomyosin contraction during CB1R-mediated synaptic plasticity, further implying a conserved signaling pathway downstream of CB1R throughout neural development.

Keywords

CB1R, cannabinoids, actomyosin, cytoskeleton, NMII, ROCK, eCB, synaptic plasticity, LTD, STORM